New Chemistry of Sterically-Crowded Carboranes

Brian William Hutton

Submitted for the degree of Doctor of Philosophy at Heriot-Watt University, on completion of research in the School of Engineering and Physical Sciences

November 2014

Abstract

Chapter one gives an introduction into heteroborane chemistry focussing on the areas of icosahedral and supraicosahedral (metalla)carboranes and their isomerisation mechanisms.

Chapter two describes attempts at placing bulky substituents onto a 1,7-*closo*-C_2B_{10} species so that upon reduction and subsequent oxidation the carbon atoms are unable to connect thus potentially preventing oxidation and allowing for easier capitation to form a supraicosahedral carborane. Initial efforts to synthesise such 1,7- bulky species, using tertiary alcohol substituents, did not lead to polyhedral expansion due to undesired reactivity. Compounds with bulky substituents incorporating cobaltacarborane clusters were successfully prepared but in insufficient yield for further expansion chemistry.

Chapter three discusses the synthesis and characterisation of 1,7-*closo*-C_2B_{10} species which incorporate a ferrocenyl unit on each substituent. Polyhedral expansion to form a 13-vertex carborane was unsuccessful, instead upon oxidation forming significantly sterically deformed 1,2 species with unprecedentedly elongated C-C connectivities.

Chapter four investigates the redox chemistry of the ferrocenyl 1,2 and 1,7 species. The electronic spectrum of the 1,2 species were compared to that given by TD DFT calculations which suggest a degree of charge transfer. Associated electrochemistry suggests this may be a sterically-induced charge transfer within the 1,2 species.

The steric deformation of the bis-ferrocenyl 1,2 species leads to a relatively low-temperature isomerisation to the 1,7 species. This has renewed interest in the elucidation of the isomerisation mechanism of icosahedral carboranes. Chapter five details the synthesis and characterisation of labelled species with labels which can be reliably tracked upon isomerisation. A comparison of the experimental findings to the results of theoretical studies on the subject is examined.

Chapter six contains experimental procedures and characterisation details for all the new compounds reported herein. Crystallographic data is listed in Appendices A and B (CD) along with structure solution and refinement details.

For my wife Lori, children Holly and Harry
and Mum and Dad

Love you x

“No, that’s a pharmacist.”

-Every chemist everywhere, ever.

Acknowledgements

First and foremost I would like to say a very big “Thank you” to my supervisor, Professor Alan Welch, for all his support over the last few years. His seemingly limitless patience and understanding have been invaluable to me and are greatly appreciated. It has been a privilege to work alongside such an enthusiastic and inspired chemist.

I also wish to give special thanks to Dr Dave Ellis who was very approachable and always there and to answer my (sometimes awful) questions in the lab and teach me loads especially about NMR. Cheers Dave.

I should also thank past members of the boron group who made the PhD experience far more enjoyable than it should have been, especially Drs Ross McLellan (the consummate bedfellow), Peter Abram (Missing Men?), Amelia McAnaw (I dreamed a dream) and Hugo ‘Tricky’ Tricas. Thanks also go to Drs Sergey Zlatogorksy, Elena Lopez, Gobika Sivasubramanium and Dimitry Perekalin. Thanks also go to current members of the group for letting me steal your models and textbooks whilst writing up, Dr Winnie Man, Greig Scott, Sam Powley, Laura Riley and Dipendu Mandal.

I have had the pleasure to assist project students over the years so thanks to Marie Marek, Fraser McIntosh and Laura Mitchell for all your hard work. Very special thanks also go to my good friend Michael Edie for many insightful discussions.

Thanks to Dr Georgina Rosair for her help with X-ray crystallography, Dr Alan Boyd (and Dave) for NMR experiments and Christina Graham for elemental analyses.

Thanks to collaborators Prof. Stuart Macgregor’s group and Prof. Martin Paterson for computational experiments and Prof. Piero Zanello and co-workers for electrochemistry.

Finally, I would like to thank my family for all their support during this time. My wife, Lori, has always encouraged me to keep going even during the tough times and for that I am grateful. Love you loads babes, thank you. To my kids, Holly and Harry, thanks for keeping me awake at night and giving me the time to ponder over this thesis. And special thanks to my parents for all your support. I couldn’t have done it without your help. Love you all. xXxXx.

ACADEMIC REGISTRY
Research Thesis Submission

Name*:*	Brian William Hutton		
School/PGI:	School of Engineering and Physical Sciences		
Version: *(i.e. First, Resubmission, Final)*	Final	Degree Sought (Award **and** Subject area)	PhD Chemistry

Declaration

In accordance with the appropriate regulations I hereby submit my thesis and I declare that:

1) the thesis embodies the results of my own work and has been composed by myself
2) where appropriate, I have made acknowledgement of the work of others and have made reference to work carried out in collaboration with other persons
3) the thesis is the correct version of the thesis for submission and is the same version as any electronic versions submitted*.
4) my thesis for the award referred to, deposited in the Heriot-Watt University Library, should be made available for loan or photocopying and be available via the Institutional Repository, subject to such conditions as the Librarian may require
5) I understand that as a student of the University I am required to abide by the Regulations of the University and to conform to its discipline.

* *Please note that it is the responsibility of the candidate to ensure that the correct version of the thesis is submitted.*

Signature of Candidate*:*		Date:	

Submission

Submitted By *(name in capitals):*	BRIAN HUTTON
Signature of Individual Submitting:	
Date Submitted:	

For Completion in the Student Service Centre (SSC)

Received in the SSC by *(name in capitals):*			
Method of Submission *(Handed in to SSC; posted through internal/external mail):*			
*E-thesis Submitted (**mandatory for final theses)***			
Signature:		Date:	

Please note this form should bound into the submitted thesis.

Updated February 2008, November 2008, February 2009, January 2011

Table of Contents

Chapter 5 Isomerisation Studies of Labelled Carboranes

Chapter 6 Experimental Section

Abbreviations

2c-2e	two centre two electron (bond)
3c-2e	three centre two electron (bond)
4c-2e	four centre two electron (bond)
Å	Angstrom (1.0×10^{-10} m)
A	Absorbance
app.	apparent
BNCT	Boron Neutron Capture Therapy
br.	broad
COSY	Correlation Spectroscopy
Cp	Cyclopentadienyl (C_5H_5)
CHN	Elemental analysis
d	doublet
DCM	Dichloromethane
DFT	Density Functional Theory
DSD	Diamond-Square-Diamond
δ	chemical shift
E	Energy
EI	Electron Impact
Fc	Ferrocenyl group {-(C_5H_4)Fe(Cp)}
g	grams
HMQC	Heteronuclear Multiple-Quantum Correlation
i-propyl	iso-propyl group {-CH(CH_3)$_2$}
liq.	liquid
M	moles per litre
M^+	Parent ion
Me	Methyl group (-CH_3)
MHz	megahertz
Mg	milligrams
mol	moles
mmol	millimoles
MOM	methoxymethyl group (-OCH_2OCH_3)
MS	Mass Spectrometry

m	multiplet
m/z	mass to charge ratio
nm	nanometres
NMR	Nuclear Magnetic Resonance
NOE	Nuclear Overhauser Effect
p-cymene	$CH_3C_6H_4CH(CH_3)_2$
pet. ether	fraction of petroleum ether boiling between 40 and 60 °C (unless otherwise stated)
Pm	Pentamethylene ($-C_5H_{10}$)
Ph	Phenyl group ($-C_6H_5$)
ppm	parts per million
PSE	Polyhedral Skeletal Electrons
PSEP	Polyhedral Skeletal Electron Pairs
PSEPT	Polyhedral Skeletal Electron Pair Theory
q	quartet
Redox	Reduction and oxidation
R_f	Resolution factor
RT	Room temperature
s	singlet
SCE	Saturated Calomel Electrode
SEP	Skeletal Electron Pair
sept	septet
t	triplet
TD	Time Dependent
TFR	Triangular Face Rotation
THF	Tetrahydrofuran
TLC	Thin Layer Chromatography
UV-vis	Ultraviolet-visible (spectroscopy)
V	volt (formal electrode potentials)
xs	excess

Abbreviations for Specific Compounds

1	1,7-$(CMe_2OH)_2$-1,7-*closo*-$C_2B_{10}H_{10}$
2	1-(CMe_2OH)-1,2-*closo*-$C_2B_{10}H_{11}$
3	1,7-$(CMe_2OCH_2OCH_3)$2-1,7-*closo*-$C_2B_{10}H_{10}$
4	4-(*p*-cymene)-2,6-μ-(OCH_2CMe_2)-4,1,6-*closo*-$RuC_2B_{10}H_9$
5a	1-$\{CMe_2(C_5H_5)\}$-7-$\{CMe_2[3-(C_5H_4)$-3,1,2-*closo*-$CoC_2B_9H_{11}]\}$-1,7-*closo*-$C_2B_{10}H_{10}$
5b	1,7-$\{CMe_2[3-(C_5H_4)$-3,1,2-*closo*-$CoC_2B_9H_{11}]\}_2$-1,7-*closo*-$C_2B_{10}H_{10}$
6a	1-$\{CPm(C_5H_5)\}$-7-$\{CPm[3-(C_5H_4)$-3,1,2-*closo*-$CoC_2B_9H_{11}]\}$-1,7-*closo*-$C_2B_{10}H_{10}$
6b	1,7-$\{CPm[3-(C_5H_4)$-3,1,2-*closo*-$CoC_2B_9H_{11}]\}_2$-1,7-*closo*-$C_2B_{10}H_{10}$
7a	1,7-$\{CMe_2(C_5H_5)\}_2$-1,7-*closo*-$C_2B_{10}H_{10}$
7b	1,7-$\{CPm(C_5H_5)\}_2$-1,7-*closo*-$C_2B_{10}H_{10}$
7c	1,7-$\{CPm(Me_4)(C_5H_5)\}_2$-1,7-*closo*-$C_2B_{10}H_{10}$
8a	1,7-$(CMe_2Fc)_2$-1,7-*closo*-$C_2B_{10}H_{10}$
8b	1,7-$(CPmFc)_2$-1,7-*closo*-$C_2B_{10}H_{10}$
9a	1,2-$(CMe_2Fc)_2$-1,2-*closo*-$C_2B_{10}H_{10}$
9b	1,2-$(CPmFc)_2$-1,2-*closo*-$C_2B_{10}H_{10}$
10	tentatively assigned as 4-(*p*-cym)-1,6-$(CMe_2Fc)_2$-4,1,6-*closo*-$RuC_2B_{10}H_{10}$
11	1,2-$(CMe_2Fc)_2$-4-OH-1,2-*closo*-$C_2B_{10}H_9$
12a	1-(CPmFc)-1,2-*closo*-$C_2B_{10}H_{11}$
12b	tentatively assigned as 1-ferrocenylcyclohex-1-ene
13a	8,9-Me_2-1,2-*closo*-$C_2B_{10}H_{10}$
13b	8,9-Ph_2-1,2-*closo*-$C_2B_{10}H_{10}$
14	4-(*p*-cymene)-2,11-Me_2-4,1,6-*closo*-$RuC_2B_{10}H_{10}$
15a	9,10-Me_2-1,7-$\{CPm(C_5H_5)\}_2$-1,7-*closo*-$C_2B_{10}H_8$
15b	9,10-Ph_2-1,7-$\{CPm(C_5H_5)\}_2$-1,7-*closo*-$C_2B_{10}H_8$
16a	9,10-Me_2-1,7-$(CPmFc)_2$-1,7-*closo*-$C_2B_{10}H_8$
16b	9,10-Ph_2-1,7-$(CPmFc)_2$-1,7-*closo*-$C_2B_{10}H_8$
16b′	9,10-Ph_2-1-$\{CPm(C_5H_5)\}$-7-(CPmFc)-1,7-*closo*-$C_2B_{10}H_8$
17a	8,9-Me_2-1,2-$(CPmFc)_2$-1,2-*closo*-$C_2B_{10}H_8$
17b	9,12-Me_2-1,2-$(CPmFc)_2$-1,2-*closo*-$C_2B_{10}H_8$
18	4,9-Me_2-1,7-$(CPmFc)_2$-1,7-*closo*-$C_2B_{10}H_8$

Chapter 1 Introduction

1.1 Boron

Although boron compounds have been known for hundreds of years it is only relatively recently, particularly during the development of (hetero)borane cluster chemistry, that their true uniqueness and versatility has allowed, unquestionably, for some exciting and remarkable advancements in the field.

Davy, Guy-Lussac and Thénard first discovered elemental boron in 1808 through the reduction of borates with metallic potassium.[1] Elemental boron is not found freely in nature and boron-containing compounds are relatively rare, accounting for only 0.001% of the earth's crust. Major boron-containing ores are borax ($Na_2B_4O_7$ $10H_2O$), kernite ($Na_2B_4O_7$ $4H_2O$) and sassoline (H_3BO_3) from which pure boron can be extracted. The natural isotopic ratio of boron is ^{10}B at 19.78% and ^{11}B at 80.22%. A fascinating property of ^{10}B is its high neutron capture cross section rendering it useful as a shield for nuclear radiation and as control rods in nuclear reactors. This property also gives ^{10}B a potential application in medicine as a non-invasive treatment for cancer via Boron Neutron Capture Therapy (BNCT).[2,3] This involves neutron beam irradiation of cancer cells that have been tagged by an appropriate ^{10}B-containing chemical. The capture of a low energy neutron by ^{10}B facilitates a type of nuclear fission: the boron nucleus is split into an α-particle and a lithium ion (Equation 1.1). The energy released in this process can destroy the cell to which it is attached without damage to any nearby healthy human tissue. BNCT is becoming more established and has been the subject of a number of clinical trials.

$$^{10}_{5}B + {}^{1}n \rightarrow \{ {}^{11}_{5}B \} \rightarrow {}^{4}_{2}He + {}^{7}_{3}Li + E_k$$

Equation 1.1 Radiative decay of ^{10}B following neutron capture

Boron compounds, heteroborane clusters in particular, possess exceptional solubility properties, high thermal and chemical stability and electron-delocalised frameworks. Their ability to incorporate elements spanning the periodic table makes them a unique and useful class of molecule.

These properties allow applications including homogeneous catalysis as weakly coordinating anions,[4] non-linear optical materials,[5] medicine and pharmacology[6] and metal ion extraction.[7] Many of these properties may be enhanced with larger boron content within the molecule hence effort is focussed on preparing such compounds; the results of such studies will be presented later in this chapter.

1.2 Boron Hydrides

The simplest compounds of boron are the boron hydrides, also known as boranes, and are composed solely of boron and hydrogen. Interest in these compounds grew in 1933 when Alfred Stock first synthesised and characterised a series of boranes[8] from B_2H_6 to $B_{10}H_{14}$ that fell into the two distinctive homologous series of B_nH_{n+4} and B_nH_{n+6}. Before this work diborane was a rare substance that could only be made in less than gram quantities in only two laboratories in the world. The fact that the simplest boron hydride was observed as B_2H_6 (Figure 1.1) and not BH_3 introduced problems with the recognised bonding schemes and electronic theory at the time. When comparing the alkane C_2H_6 to the analogous boron hydride B_2H_6 it became apparent that B_2H_6 must have two less electrons available for bonding due to the fact that boron has one less valence electron than neighbouring carbon. This meant that the bonding in B_2H_6 and C_2H_6 must be quite different. Longuet-Higgins hence developed the concept of the 3-centre 2-electron (3c-2e) bond in 1949 in order to account for these irregular structures.[9]

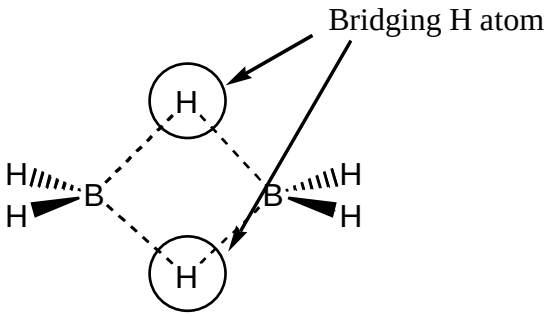

Figure 1.1 The proposed and confirmed structure of B_2H_6

Monomeric BH_3 is incredibly reactive due to the fact it is a very powerful Lewis acid and combines with itself to form the dimer. Only six valence electrons are available to

the central boron atom in BH_3, two short of a favourable octet. It can very readily accept a lone pair of electrons from Lewis bases to form a variety of adducts.

The twelve available valence electrons in B_2H_6 are distributed as follows: eight are used in conventional 2c-2e bonding forming the terminal B-H bonds and the remaining four electrons are delocalised within two bridging 3c-2e B-H-B units. Each boron atom contains four sp^3 hybrid orbitals that overlap (and thus share electrons) with the 1s orbitals of the bridging H atoms (Figure 1.2). This effectively provides each central boron atom with a stable octet of electrons.[10]

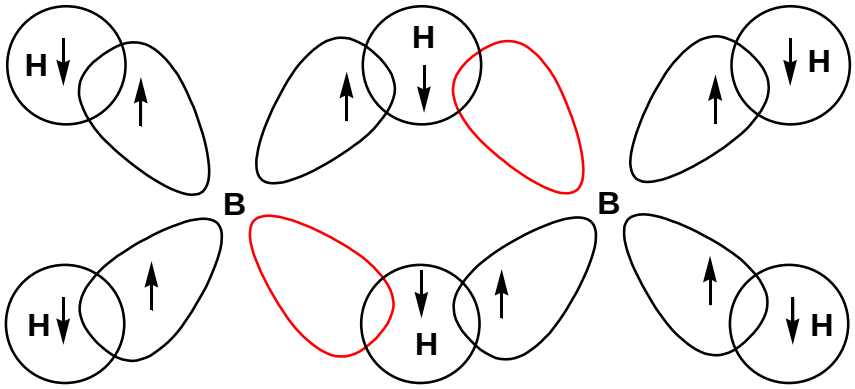

Figure 1.2 Orbital diagram of B_2H_6

Lipscomb confirmed the structure a few years later with the aid of X-ray diffraction when he successfully obtained a crystal structure[11] of B_2H_6. Larger boron hydrides soon followed and decaborane[12] ($B_{10}H_{14}$) (Figure 1.3) was also eventually characterised by X-ray diffraction. It was quickly observed that the larger boranes (e.g. $[B_{10}H_{10}]^{2-}$) were, in fact, closed polyhedra when the formula is $[B_nH_n]^{2-}$. Longuet-Higgins predicted in a 1954 paper[13] that $[B_{12}H_{12}]^{2-}$ would have an icosahedral geometry and this was indeed confirmed in 1960 by Hawthorne and Pitocelli.[14] They isolated the icosahedral $[B_{12}H_{12}]^{2-}$ dianion firstly as the copper salt followed by the potassium salt. These borane clusters are today often (incorrectly) termed 'electron deficient'. Most boron clusters show no 'deficiency' of electron density and, in fact, icosahedral structures such as $C_2B_{10}H_{12}$ and $[B_{12}H_{12}]^{2-}$ are among the most thermodynamically stable molecules known having a sufficient number of electrons needed to occupy the available bonding molecular orbitals.

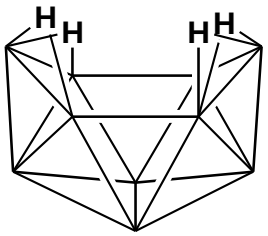

Figure 1.3 The structure of decaborane $B_{10}H_{14}$

More recent work has seen the concept of 'electron deficient' bonds extended to 4c-2e bonding.[15] An example is the $[B_6H_7]^-$ anion that is effectively a distorted octahedron consisting of a proton localised above one triangular face (Figure 1.4).

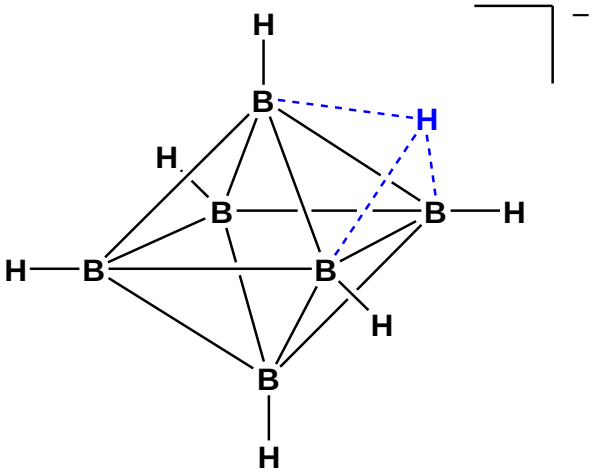

Figure 1.4 Example of 4c-2e bonding in $[B_6H_7]^-$

1.2.1 Bonding Theories

There have been various attempts to find a bonding scheme to rationalise and predict borane structures. The appreciation of 3c-2e bonds led to the development of Lipscomb's *styx* rules.[16] These rules used a combination of electron deficient B-H-B and B-B-B bonds alongside classical B-B and B-H covalent bonds to account for some borane structures. If a boron hydride has the formula B_nH_{n+m} it was noticed that the *n* boron atoms and the *m* (endo) hydrogen atoms all lie on the 'inner' pseudo-spherical surface. On an outer sphere lie the *n* (exo) hydrogen atoms that are attached to the boron atoms via normal covalent links and protrude radially outward from the sphere (Figure 1.5). The boron and the endo hydrogen atoms involve bonding with (*2n*+*m*) electrons;

two from each BH unit and one from each hydrogen atom. The number of each type of bond was allocated a letter by Lipscomb (in brackets): B-H-B (*s*) and B-B-B (*t*) from the 3-centre, 2-electron category; B-B (*y*) and BH_2 (*x*) from the 2-centre, 2-electron category. A set of equations were derived linking the values of *s,t,y* and *x* to *n* and *m*:

$$s = m - x = n - t = 2y + x$$

This gives a set of '*styx'* values for specific values of *n* and *m* allowing a prediction of likely structures for those boranes yet unknown.

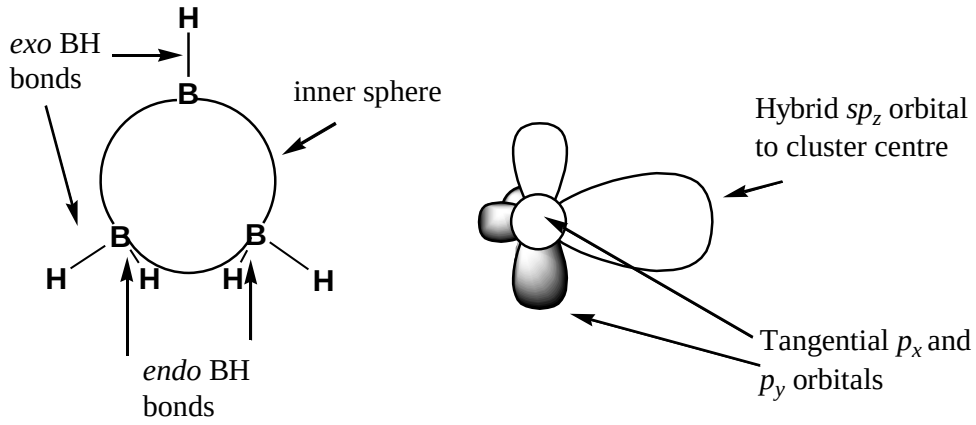

Figure 1.5 *Endo* and *exo* B-H bonds and related orbitals

This theory was acceptable for the smaller boranes but broke down when trying to predict structures of larger boron hydrides, often offering several possible structures for one formula; for example, four structures are predicted for B_5H_9.[17] Lipscomb's method was therefore limited, ambiguous and rather cumbersome.

The total number of electron pairs holding the cluster together are now referred to as skeletal electron pairs (SEPs). Wade's rules,[18] which were developed in 1971, have advantages over the *styx* method in that they are quicker and easier to apply, have a firm basis in molecular orbital theory and apply also to heteroboranes and other clusters such as main group or low valency transition metal clusters. The method simply involves counting the number of skeletal electrons in the cluster to determine its 3D geometry. The cluster is broken down into fragments of each individual vertex and the number of electrons employed in cluster bonding by each gives the total number.

For a main group vertex, the electronic input to the skeletal framework (*s*) is given by the equation:

$$\boldsymbol{s = v + x - 2}$$

v = no. of valence electrons from the vertex atom (e.g. 3 for B)

x = no. of electrons from exopolyhedral groups or atoms (e.g. 1 for H)

NB. *s* and *x* here bear no relation to *s* and *x* in Lipscomb's *styx* method.

For a transition metal vertex, due to the different orbitals used, the equation is altered slightly to:

$\boldsymbol{s = v + x - 12}$ for an 18 electron species or

$\boldsymbol{s = v + x - 10}$ for a 16 electron species.

All the *s* values are then totalled to give the total number of electrons available for skeletal bonding. The number is then halved to reveal the total number of electron pairs that govern the overall shape. This is called the number of *Polyhedral Skeletal Electron Pairs (PSEPs)*.

This is compared with the number of vertices (*n*) in the molecule and the following relationships hold:

If we have (*n*+1) PSEPs the structure is *closo*	closed polyhedron
If we have (*n*+2) PSEPs the structure is *nido*	*closo* minus one vertex
If we have (*n*+3) PSEPs the structure is *arachno*	two adjacent vertices missing

There is a geometrical similarity between *closo n* vertex, *nido* (*n*-1) vertex and *arachno* (*n*-2) vertex polyhedra due to the constant number of skeletal electrons. The vertices are lost from a *closo*-structure by removal of the highest connected vertex then the next vertex is lost by removal of the highest connected vertex in the open face. The Wade-Williams-Rudolph structural matrix[19] (Figure 1.6) shows these relationships. All the *closo*- compounds are exclusively deltahedra i.e. polyhedra with triangular faces.

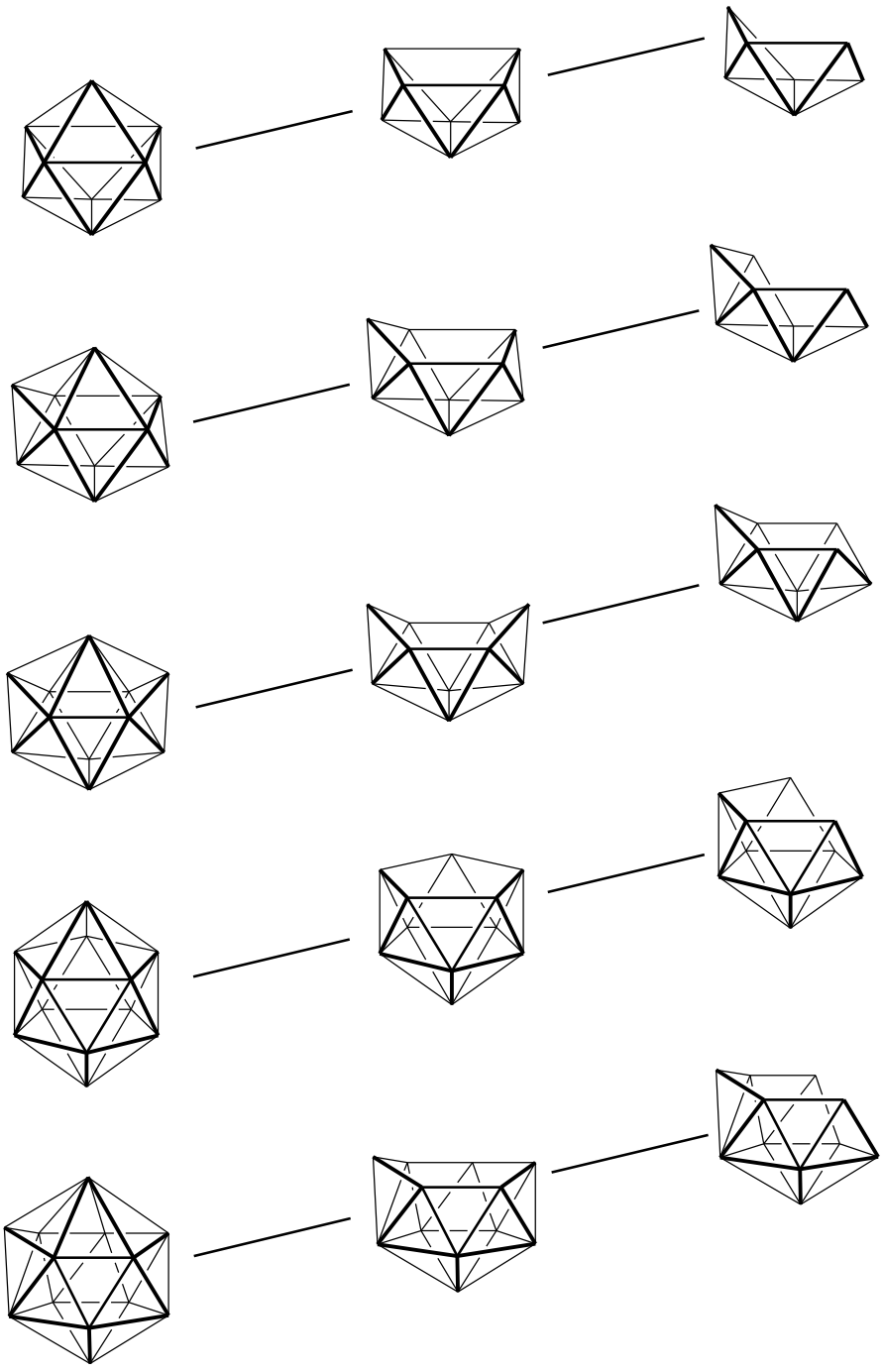

Figure 1.6 Part of the Wade-Williams-Rudolph structural matrix

1.2.2 Nomenclature

A boron cluster compound with a vertex atom other than boron is called a heteroborane. Boranes and heteroboranes have a unique system of nomenclature and numbering. A neutral molecule has the number of boron atoms stated first and with the suffix '-ane' followed by the number of hydrogen atoms shown in brackets e.g. $B_{10}H_{14}$ is called decaborane(14) (Figure 1.7). If the molecule is an anion the number of hydrogen atoms is stated first, followed by the number of boron atoms and the suffix '-ate' is used to show that it is anionic with the charge stated in brackets at the end e.g. $[B_3H_8]^-$ is called octahydridotriborate(-1).

Numbering starts at the top atom and successive belts or rings are numbered clockwise with a boron-boron connectivity being skipped when crossing from one belt to another (Figure 1.7). Heteroatoms are given the lowest possible numbers and carbon is usually given precedence over metals.

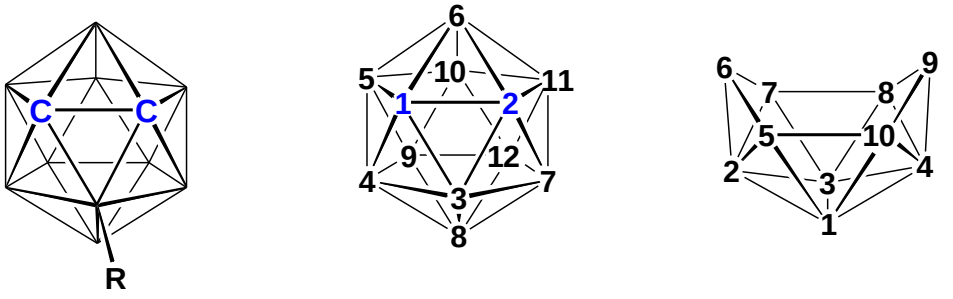

e.g. 3-R-1,2-*closo*-$C_2B_{10}H_{11}$

nido-decaborane(14)

Figure 1.7 Examples of numbered (hetero)boranes

1.3 Carboranes

Carboranes are undoubtedly the largest class of heteroboranes studied. This is where a $\{BH^-\}$ vertex fragment is replaced by {CH}. Replacement of two $\{BH^-\}$ units with the isoelectronic {CH} moiety results in neutral compounds with the general formula $C_2B_{n-2}H_n$. There are countless other fragments that are isolobal in this way with the {BH} unit many of which are transition metal based (Figure 1.8).

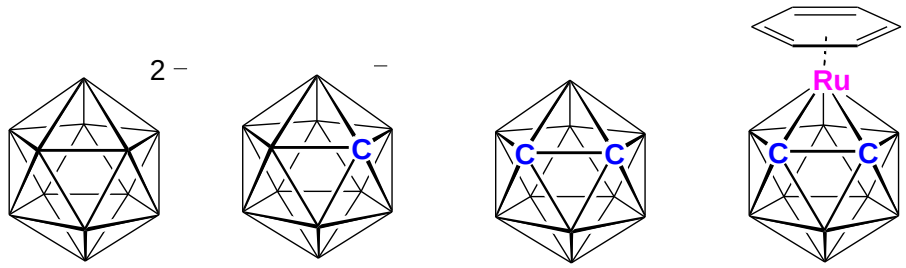

Figure 1.8 Icosahedral structures with different isolobal vertices

1.3.1 Synthesis and Reactivity

The first example of an icosahedral carborane was reported in 1963 by Heying.[20] This was prepared by inserting an alkyne into decaborane, $B_{10}H_{14}$, with the aid of a Lewis base acting as catalyst (Figure 1.9). The base forms an *arachno* species from the nido decaborane, opening up the borane to allow easier insertion of the alkyne and also dislodging two of the bridging hydrogen atoms.

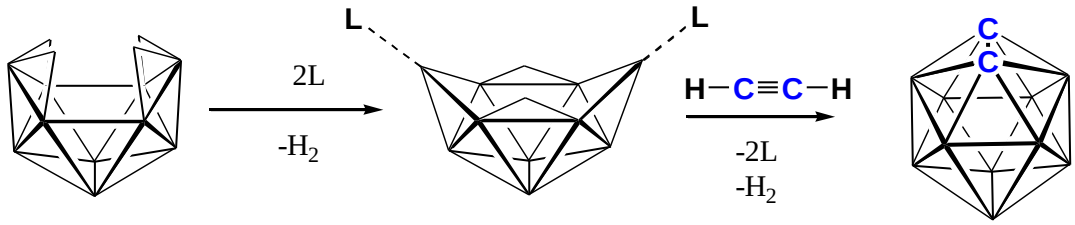

Figure 1.9 Synthesis of 1,2-*closo*-$C_2B_{10}H_{12}$ via acetylene insertion

Functional groups can be added onto the carbon atoms by using the appropriately substituted alkyne. For example diphenylcarborane can be synthesised by insertion of diphenylacetylene into decaborane.[21] If ethyne is added to decaborane in the presence of a Lewis base then the icosahedral species, 1,2-*closo*-$C_2B_{10}H_{12}$, is produced. Insertions

into *arachno* species are successful for most R groups, notable exceptions being R=CO_2H and R=$SiMe_3$.

Due to the relatively electronegative carbon atoms, the hydrogen atoms bonded to carbon are comparatively acidic and can facilitate nucleophilic substitution. Butyl lithium can remove these protons allowing substitution at the carbon atoms. The process goes through a dilithium salt intermediate which acts as a nucleophile and can react with compounds of the type RX to yield R substituted carboranes. A very useful reaction of this type is the addition of carboxyl groups[22] (Figure 1.10) as these can be modified in a variety of ways to give wide range of substituted icosahedral carboranes.[23]

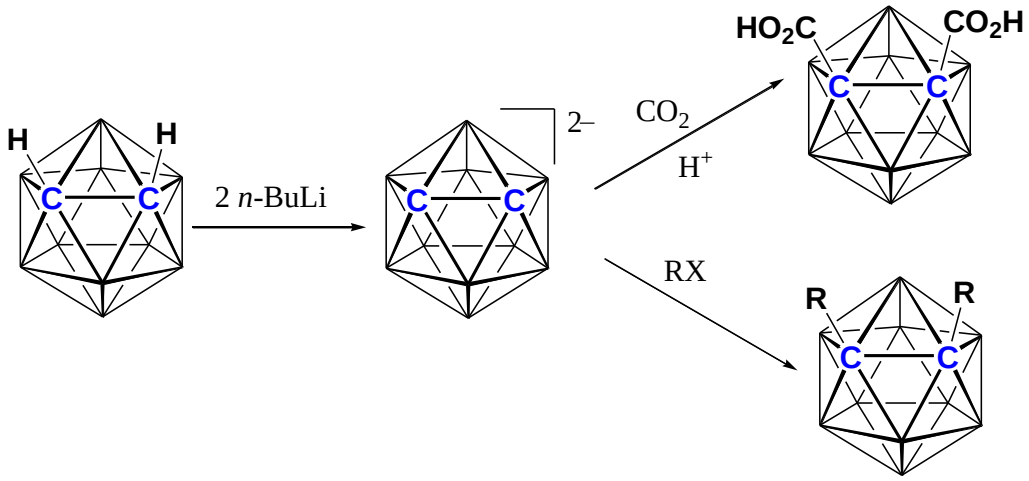

Figure 1.10 Deprotonation of 1,2-*closo*-$C_2B_{10}H_{12}$ followed by nucleophilic substitution

The cage can also be boron substituted. The electronegative carbon atoms leave the neighbouring boron atoms at positions 3 and 6 with a slight positive charge and these can be attacked by nucleophiles. A strong base can remove one of these boron atoms producing a nido deboronated or decapitated carborane[24] with an endo proton in the B(10) position (Figure 1.11).[25]

The endo proton can be easily removed using sodium hydride or butyl lithium as it is slightly acidic resulting in a dicarbollide anion [7,8-*nido*-$C_2B_9H_{11}$]$^{2-}$ which is an important precursor for many reactions. Recapitation is then possible by addition of B-X, B-R (in the form of BRX_2 etc.) or M-L fragments to complete the substitution process.[26]

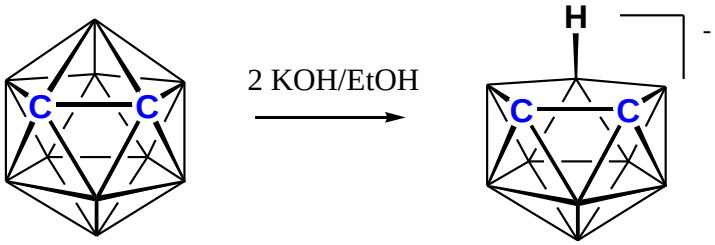

Figure 1.11 Deboronation of 1,2-*closo*-$C_2B_{10}H_{12}$

The presence of heteroatoms (carbon atoms in this case) results in overall electron density that is different to that of $[B_{12}H_{12}]^{2-}$ where it is spread evenly throughout the molecule. As already discussed, in 1,2-*closo*-$C_2B_{10}H_{12}$ the boron atoms adjacent to the electronegative carbon atoms possess a slight positive charge over the other boron atoms.[27] In contrast, the boron atoms furthest away from the carbon atoms are the most negative. The relative charges of each vertex in 1,2-*closo*-$C_2B_{10}H_{12}$ are shown below.

C (1, 2) > B (9, 12) > B (8, 10) > B (4, 5, 7, 11) > B (3, 6)

This allows electrophilic substitution to occur at various vertices allowing a variety of halogenated carboranes to be synthesised. The reaction of 1,2-*closo*-$C_2B_{10}H_{12}$ with gaseous X_2 affords a route to per-halogenation,[28] the first boron atoms to be halogenated in this process being B(9) and B(12), followed by the B(8) and B(10) positions. This is an ineffective method, however, for the preparation of singly or doubly halogenated compounds as it is difficult control the reaction to stop halogenating at the desired point.

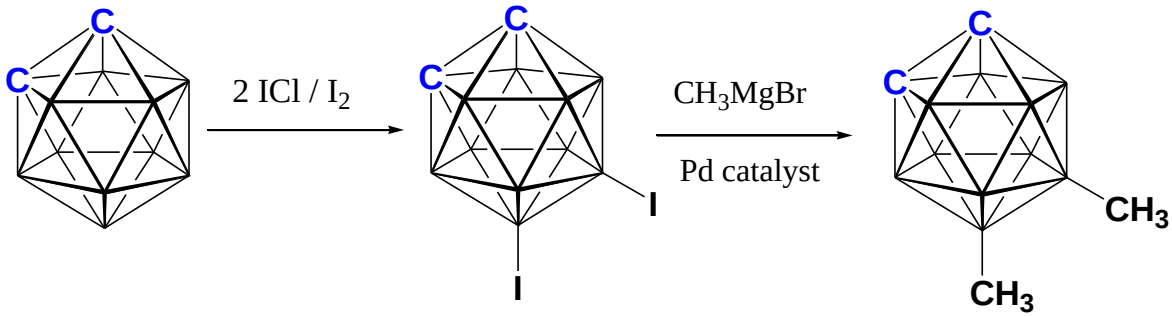

Figure 1.12 Halogenation and methylation of 1,2-*closo*-$C_2B_{10}H_{12}$

A more controlled halogenation method[29] involves the use of ICl as a source of I^+ which readily substitute onto the negative B(9) and B(12) vertices of 1,2-*closo*-$C_2B_{10}H_{12}$. One molar equivalent of I^+ gives the monosubstituted product whilst two equivalents affords the disubstituted product (Figure 1.12).

Selective iodination of B(9), B(12), B(8) and B(10) is also achievable[30] via a solvent free method whereby I_2 is reacted with 1,2-*closo*-$C_2B_{10}H_{12}$ at 270°C. Most $C_2B_{10}H_{12}$ halogenated analogues can undergo reactions with Grignard reagents yielding alkyl derivatives.[29] Direct electrophilic alkylation without the need for prior halogenation is also possible.[31]

1.4 Metallacarboranes

Metallacarboranes have a metal integrated within the cage network of a carborane. They were first synthesised in 1965 by Hawthorne[32] when he incorporated an iron atom between two dicarbollide units. He recognised that the dicarbollide anion was isolobal with the cyclopentadienide anion so his structure was analogous to ferrocene (Figure 1.13).

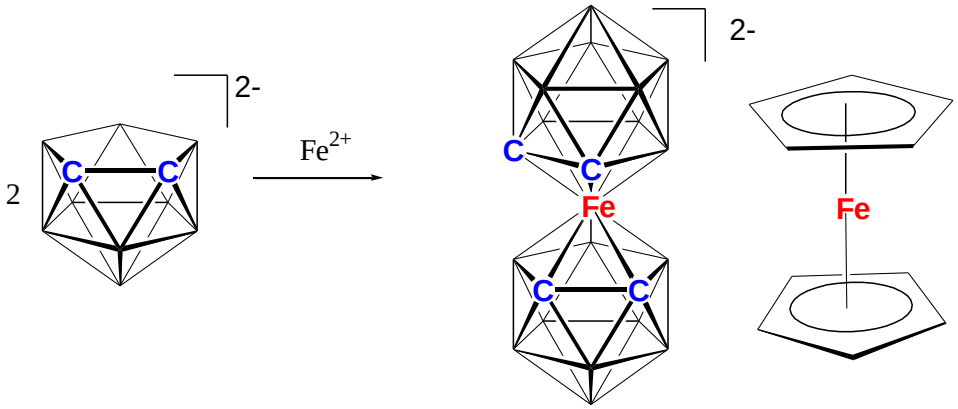

Figure 1.13 Bisdicarbollide iron sandwich and analogous metallocene (ferrocene)

The use of the dicarbollide dianion as a ligand actually adds to the overall stability of these compounds compared to that of analogous metallocenes. The frontier molecular orbitals are more favourably orientated to bind to a metal as they point inwards, due to the inclination of exo hydrogen atoms, instead of them all being parallel to each other, giving greater overlap with the metal orbitals (Figure 1.14). The isolobality between a {BH} fragment and certain metal fragments means that there are now thousands of icosahedral metallacarboranes[26, 33] in the literature using a wide variety of elements in the periodic table.

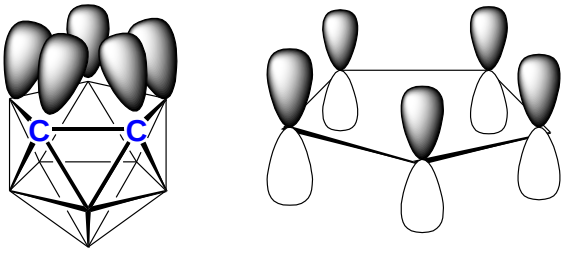

Figure 1.14 Inward pointing orbitals of dicarbollide anion

There are three broad structural types observed for metallacarboranes, depending on the manner which the metal is bonded to the cage. Class 1 metallacarboranes have the metal incorporated into the cluster as a vertex; class 2 has a bridging metal over the edge of the cluster and class 3 has a metal bonded to the cluster via a classical covalent bond (Figure 1.15).

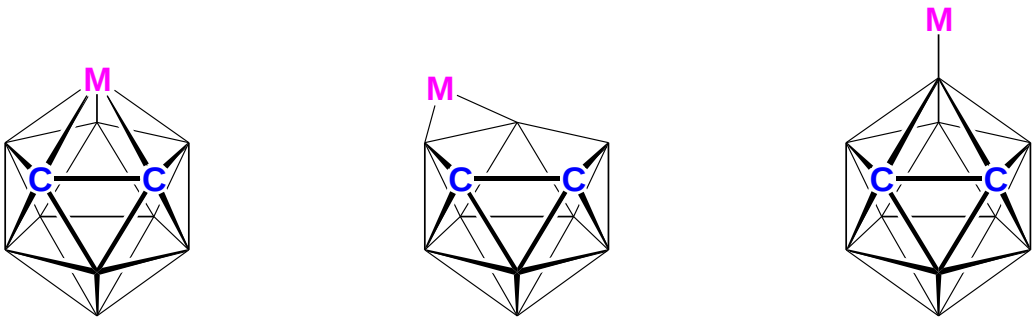

1 **2** **3**

Figure 1.15 Classes of metallacarboranes

1.5 Supraicosahedral Heteroboranes

A developing field in (hetero)borane chemistry is the study of supraicosahedral (hetero)boranes, molecules where there are more than twelve vertices present in the cage. These compounds are made by a method known as polyhedral expansion first achieved by Hawthorne[34] to create the first 13-vertex metallacarborane. This was achieved by preparing the [7,9-*nido*-$C_2B_{10}H_{12}$]$^{2-}$ ion by reduction of the corresponding *closo*-carborane with sodium naphthalenide, followed by a capitation of the species by a {CoCp}$^{2+}$ fragment (Figure 1.16). The two carbon atoms move apart upon reduction forming a 13-vertex docosahedron.

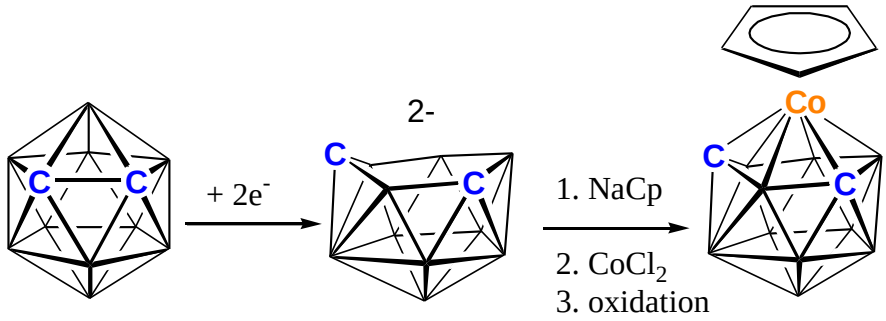

Figure 1.16 Polyhedral expansion of 1,2-*closo*-$C_2B_{10}H_{12}$

The polyhedral expansion can be taken a step further to produce 14-vertex structures with a bicapped hexagonal antiprismatic geometry. The first such compounds were prepared in 1974 by Hawthorne,[35] $(CpCo)_2C_2B_{10}H_{12}$. They were prepared by the reduction and metallation (Figure 1.17) of either 4,1,8-, or 4,1,12-monocobaltacarboranes. Since then only a handful of other 14-vertex metallacarboranes have been synthesised[36] with two metals, which can be two of the same metal or two different metals.

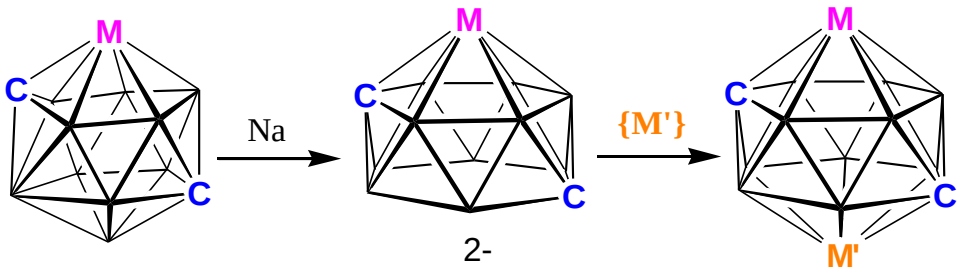

Figure 1.17 Reduction and metallation of a 13-vertex metallacarborane to form a 14-vertex bimetallacarborane

Synthetic work by Welch has seen the development of 14-vertex metallacarboranes with only one metal present prepared by reduction and metallation of a thirteen vertex tethered carborane (which will be discussed later). Presently, any attempts to reduce a 14-vertex bimetallacarborane have proved unsuccessful.

Only two examples of 15-vertex heteroboranes are known and the use of the C-C tether is employed. The first reported example, 1-(*p*-cymene)-8,14-μ-$(CH_2)_3$-1,8,14-$RuC_2B_{12}H_{12}$, was obtained by thermolysis of a monoruthenacarborane.[37] The second reported example was afforded by sodium reduction of a 14-vertex carborane followed by metallation to produce a different isomer to that given by the thermolysis route.[38]

1.5.1 Supraicosahedral Carboranes

Although lessons are being learnt about the bonding schemes and reactivity of larger cage structures by adding metals, ultimately it would be more desirable to find an easy way be able to add more boron atoms. This has proved difficult due to what has been termed the icosahedral barrier. The 12-vertex icosahedron is a very stable structure but the 13-vertex structure is considerably less stable. Starting from 1,2-*closo*-$C_2B_{10}H_{12}$ we can reduce or decapitate. Metal fragments can be inserted into both the *nido*-intermediates to form stable *closo* compounds but insertion of boron fragments is more challenging for the reduced carborane (Figure 1.18). The orbitals of a boron fragment are not diffuse enough to sit easily on a 6-atom open face whereas metals have more diffuse orbitals that are more compatible.

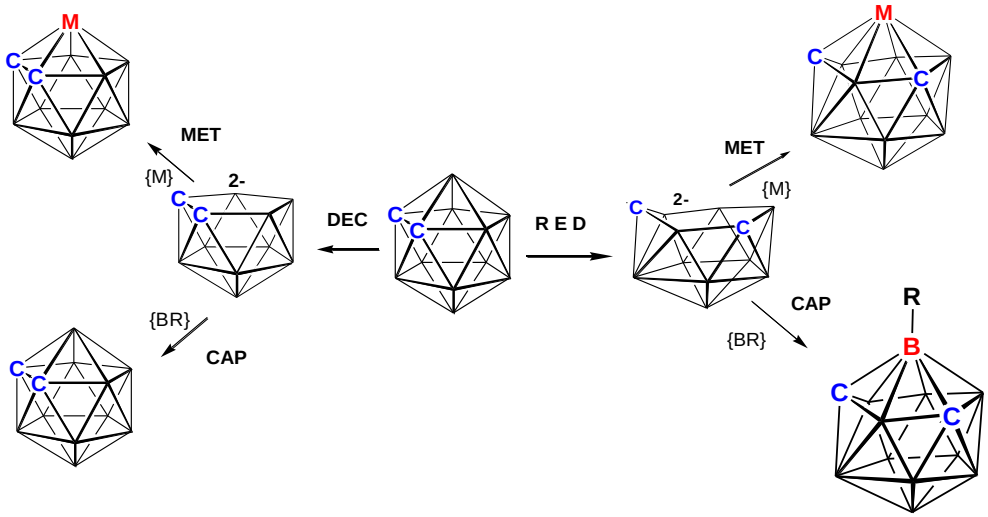

Figure 1.18 Various synthetic routes from 1,2-*closo*-$C_2B_{10}H_{12}$

In 1992, Lipscomb and Massa[39] computed the geometries of species $[B_nH_n]^{2-}$ for n = 13–24 and von Schleyer followed this with calculations[40] at a higher level of theory showing the cumulative addition energy for the addition of a boron vertex in the borane series.

The addition of a {BH} unit to icosahedral $[B_{12}H_{12}]^{2-}$ making $[B_{13}H_{13}]^{2-}$ is calculated to be a highly unfavourable endothermic reaction (Figure 1.19). The addition of two or three more vertices is also seen to be endothermic. However, additional vertices added after these should be easier to insert as these involve exothermic reactions. i.e. the addition of four {BH} units to the icosahedral $[B_{12}H_{12}]^{2-}$ is calculated to be overall exothermic, hence favourable.

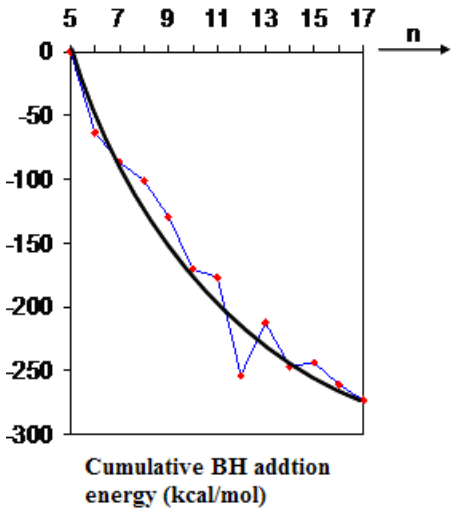

Figure 1.19 Cumulative energy additions in kcal mol^{-1} vs. number of boron atoms

The cumulative addition energy (Figure 1.19) has a general downwards slope in terms of addition of vertices which suggests high stability of, yet unknown, larger boranes. von Schleyer suggests the icosahedron is so thermodynamically stable that the synthesis of larger boranes may be hindered by degradation reactions forming icosahedral cages. On the other hand the *closo* borane clusters with twenty, thirty two, forty two and ninety two vertices are predicted to be particularly stable.[41]

The first reported experimental example of a supraicosahedral carborane was as recently as 2003, by Welch.[42] This was achieved by tethering together the two carbon atoms so

they could not move apart upon reduction. The open face of the 7,8-*nido* dianion so formed was then capitated with a {BPh} fragment (Figure 1.20) giving rise to a cage of henicosahedral geometry[43] with one trapezoidal face instead of the usual uniformity of triangular faces expected from the predicted docosahedron.

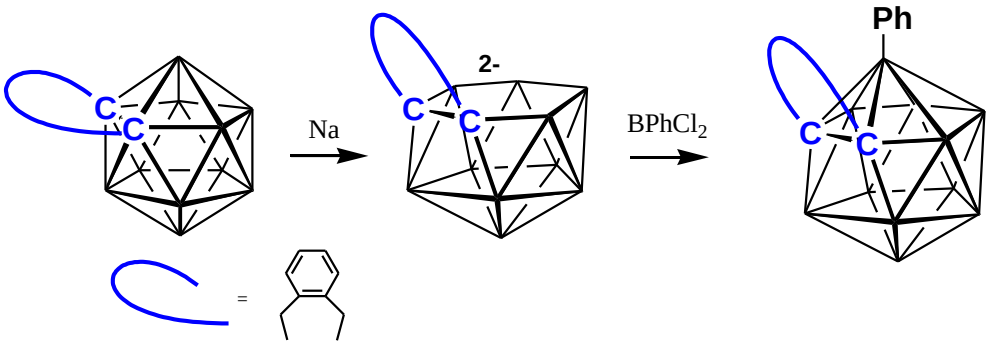

Figure 1.20 Synthesis of the first supraicosahedral carborane

The henicosahedral 13-vertex carborane has one degree-6 vertex (initially occupied by the B-Ph fragment via capitation of a six atom open face) and two degree-4 vertices (occupied by carbon atoms). Subsequent and facile isomerisation at room temperature moves the B-Ph fragment to a more favoured degree-5 vertex.

The first 14-vertex carborane was reported by Xie.[44] This was not prepared by the conventional reduction/capitation reactions but was more serendipitous (Figure 1.21). Two boron vertices were added to an *arachno* fragment containing both 5 and 6 atom open faces formed by the four-electron lithium reduction of tethered carborane. The reducing power of the nido carborane with carbon atoms apart is believed by Xie to be strong enough to reduce the incoming reagents providing the added vertex and is the main reason attempts have been have unsuccessful in past. He believes the tethered carborane with carbon atoms adjacent is less reducing and more readily accepts a vertex.

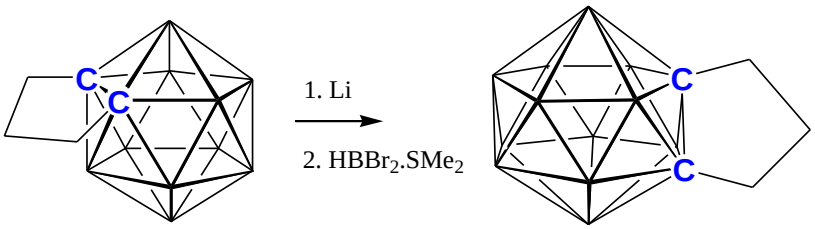

Figure 1.21 Synthesis of the first 14-vertex carborane

More recently, an untethered 13-vertex carborane with the carbon atoms separated has been prepared.[45] The carbon atoms were initially tethered together using a silyl tether to give 1,2-$Me_2Si(CH_2)_2$-1,2-*closo*-$C_2B_{10}H_{10}$ which was reduced and capitated. This resulted in a 13-vertex henicosahedral carborane (the same geometry as the first 13-vertex carborane described previously), 1,2-$Me_2Si(CH_2)_2$-1,2-*closo*-$C_2B_{11}H_{11}$, which when passed through a silica column resulted in loss of the $SiMe_2$ unit leaving only methyl groups on the carbon atoms. The carbon atoms were then separated giving a 'carbons apart' supraicosahedral isomer by heating in toluene (Figure 1.22).

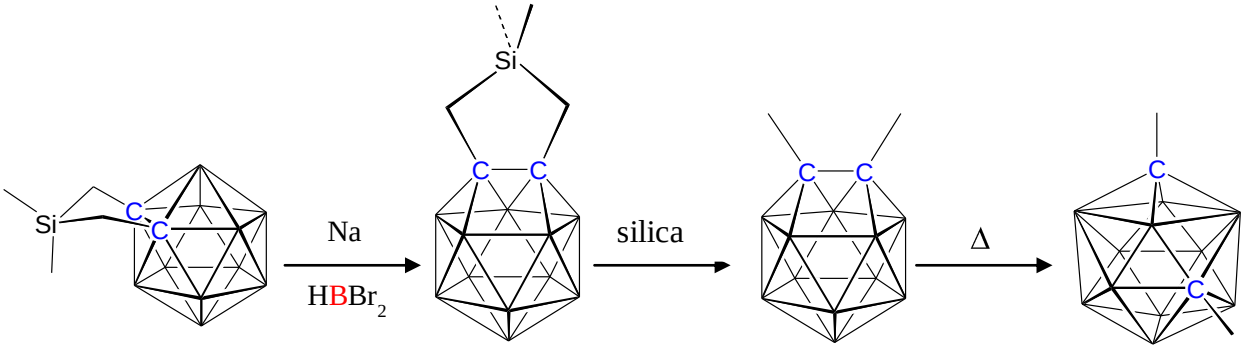

Figure 1.22 Synthesis of the first untethered supraicosahedral carborane

The increasing number of degree-6 sites as the number of vertices in the cage increases (Figure 1.23) explains why it is more challenging to prepare larger compounds. These compounds are stabilised by having metals in high-connected sites whilst boron atoms are relatively unfavoured in these sites as their orbitals are not diffuse enough to cap 6-atom open faces. However, an increasing number of metals also make the molecules more electron rich, perhaps making them more difficult to reduce, even as metallacarboranes.

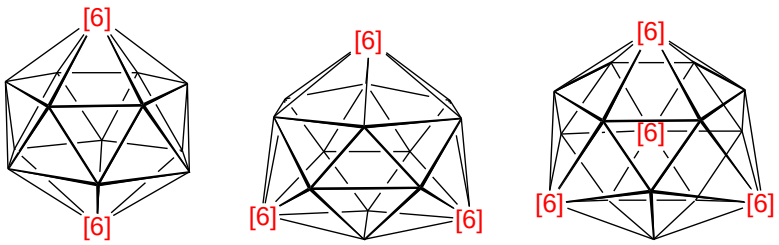

Figure 1.23 Cage sizes from 14-16 showing increased number of degree-6 sites

1.6 Isomerisations

1.6.1 Carborane Isomerisation

Grafstein and Dvorak discovered in 1963 that 1,2-*closo*-$C_2B_{10}H_{12}$ (*ortho*-carborane) quantitatively isomerised[46] at very high temperatures to 1,7-*closo*-$C_2B_{10}H_{12}$ (*meta*-carborane). One year later the 1,7-*closo*-$C_2B_{10}H_{12}$ to 1,12-*closo*-$C_2B_{10}H_{12}$ (*para*-carborane) rearrangement was also observed albeit in lower yields resulting from decomposition due to the increased temperature needed[47] (Figure 1.24). The driving force behind these rearrangements is believed to be the separation of the relatively negative carbon atoms. All three isomers are similar to each other in odour, appearance (white solids) and solubility but show significant differences in IR and NMR spectra. The reverse isomerisation was also observed soon after via successive two-electron reductions and oxidations. A two-electron reduction of the 1,12 isomer followed by reoxidation results in the 1,7 isomer being formed. Likewise, the same redox process converts the 1,7 isomer back to the 1,2 isomer[48] (Figure 1.24).

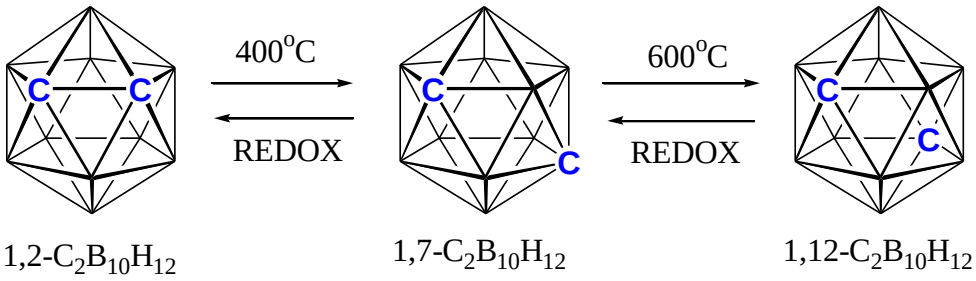

Figure 1.24 Thermal and electrochemical carborane rearrangements

The actual mechanism of these thermal isomerisations is, to date, still not fully established but many theories have been postulated and have been studied experimentally and computationally. Isolation of any intermediate species would be valuable for this task but is probably, if not certainly, impossible due to the extremely high temperatures involved. In the absence of any experimental intermediates synthetic chemists have resorted to vertex labelling whereby specific vertices of 1,2-*closo*-$C_2B_{10}H_{12}$ are labelled before being subjected to thermal isomerisation in an attempt to track these labels and seek clues as to the mechanism involved. A brief overview of these experiments and related mechanism will now be discussed.

1.6.2 Proposed Mechanisms

Lipscomb's original Diamond-Square-Diamond (DSD) mechanism[49] is one of the most well-known potential mechanisms. A common edge is broken between two triangular faces and then recreated between the other two vertices of the square (Figure 1.25).

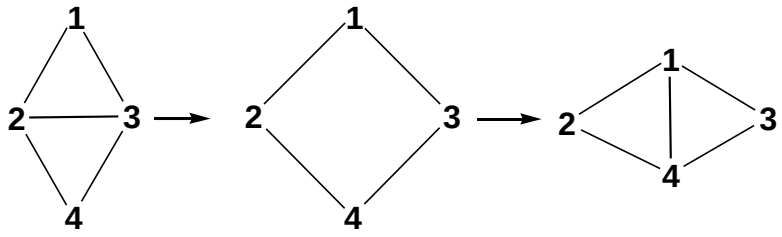

Figure 1.25 Lipscomb's Diamond-Square-Diamond mechanism

This could account for the rearrangement from 1,2-*closo*-$C_2B_{10}H_{12}$ to 1,7-*closo*-$C_2B_{10}H_{12}$ via a cubeoctahedral intermediate[50] where six DSD processes occur simultaneously (Figure 1.26)

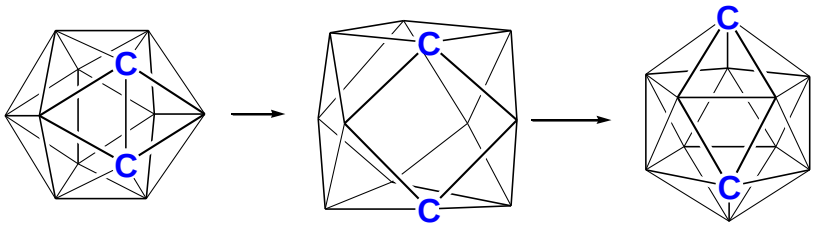

Figure 1.26 Rearrangement via a cubeoctahedral intermediate

Although an elegant idea, the feasibility of this approach was questioned when the calculated activation energy for the cubeoctahedron to form was found to be too high as it required the breaking of many bonds and a large distortion of the favoured icosahedron.[51] Lipscomb suggested that not all DSD process need occur at the same time but could happen in a sequential manner thereby lowering the activation energy for the rearrangement and eliminating the requirement for the cubeoctahedral intermediate.

However, there was still a major weakness in this idea as it did not account for the synthesis of 1,12-*closo*-$C_2B_{10}H_{12}$ starting from either 1,2- or 1,7-*closo*-$C_2B_{10}H_{12}$ irrespective of how many DSD processes take place.

Another study by Zakharkin[52] also asked questions of Lipscomb's theory. The DSD mechanism could not account for all the isomers observed in the thermal isomerisation of a series of monohalogenated carboranes. This led a modification in the DSD theory allowing the rotation of triangular faces[53] in the cubeoctahedral intermediate (DSD twist) that could account for the formation of all of the observed species and also provided a potential pathway to 1,12-*closo*-$C_2B_{10}H_{12}$ from 1,2-*closo*-$C_2B_{10}H_{12}$. 1,12-isomers produced in the halo-labelling experiments also support this.[52b]

Tantalisingly, there is an example of a cubeoctahedral carborane in the literature, however this is not an isomerisation intermediate but the product of two smaller cages fused together[54] probably formed via a transition metal sandwich intermediate.

Another proposed mechanism for rearrangement is one based on an anti-cubeoctahedral intermediate.[55] As with the cubeoctahedron theory a six-fold DSD type rearrangement needs to occur but revealing a different geometry (Figure 1.27).

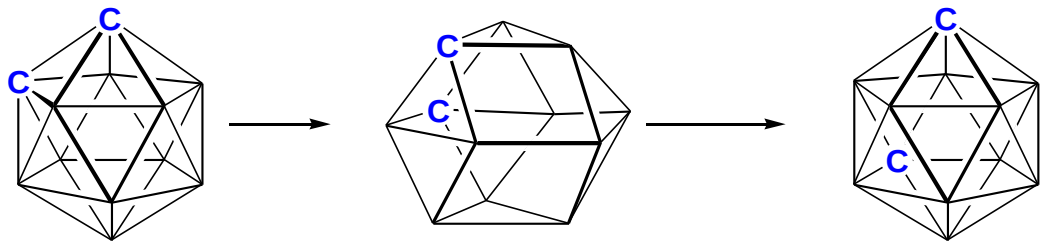

Figure 1.27 Rearrangement via an anticubeoctahedral intermediate

The advantage of this theory is that it need not undergo a second rearrangement as there are no antipodal relationships to be destroyed: one of the main weaknesses of the cubeoctahedron approach. Furthermore, it has been suggested that this mechanism involves fewer simultaneous DSD steps. It has been suggested by Wales "that the smaller the number of simultaneous DSD processes occurring in a symmetry allowed rearrangement, the more favourable it will be".[56] Unfortunately, experimental findings do little to support this intermediate. The antipodal relationships between the carbon vertices and the B-substituted vertices are maintained throughout the isomerisation of 1,2-Me_2-9,12-Cl_2-1,2-*closo*-$C_2B_{10}H_8$. This should not occur if the rearrangement goes via the anticubeoctahedron unless there is some degree of triangular face rotation.[52b] Moreover, the anticubeoctahedron route is unfavoured in that it has been calculated to

have an unfeasibly high activation energy, higher than even that of the cubeoctahedron.[57]

On the other hand, halogen labelled carborane experiments are now thought of as an unreliable means of determining mechanisms as the high temperatures required for rearrangement often result in halogen-hydrogen exchange and so the validity of these experiments has been questioned.[58]

Another theory is pentagonal face rotation[46,52a] where a whole belt of atoms rotate relative to the other. Rotation of one belt of 1,2-*closo*-$C_2B_{10}H_{12}$ by 72° gives the 1,7 isomer and a subsequent rotation yields the 1,12 isomer (Figure 1.28). However, this would give rise to too many connectivities being broken, consequently large energy barriers would need to be overcome. For this reason the mechanism is considered unlikely.

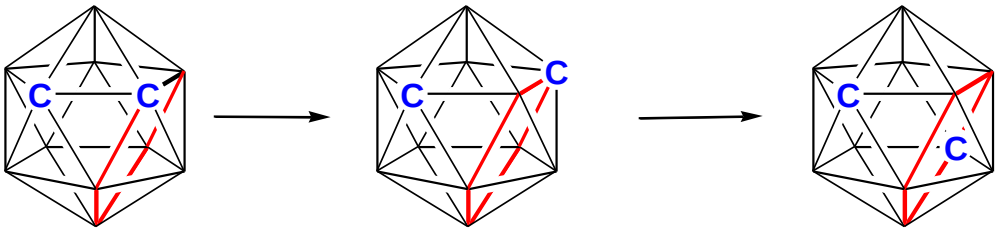

Figure 1.28 Pentagonal Face Rotation of icosahedral carboranes

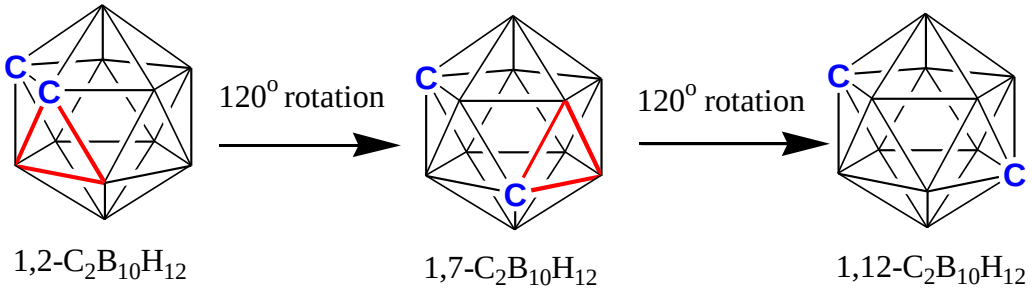

Figure 1.29 Rearrangement via Triangular Face Rotations

The ideas of triangular face rotations (TFR) have already been presented: they could occur in the cubeoctahedral or anticubeoctahedral intermediates. It has also been suggested by Muetterties and Knoth they could occur in the ground state.[53] This is currently one of the most favoured ideas and more favourable than TFRs occurring in the transition states (Figure 1.29).

Rotations of triangular faces can account for both the formation of 1,7- and 1,12-*closo*-$C_2B_{10}H_{12}$ from 1,2-*closo*-$C_2B_{10}H_{12}$ and in fact any isomer of a vertex labelled carborane. Wu and Jones[59a] investigated this idea further as DSD processes could not be used to explain many of the 1,7 isomers that formed. Their mechanism involved rotation of the middle triangles at opposite ends of the cluster which are then rotated in relation to the hexagonal framework (Figure 1.30). This approach was termed Extended TFR.

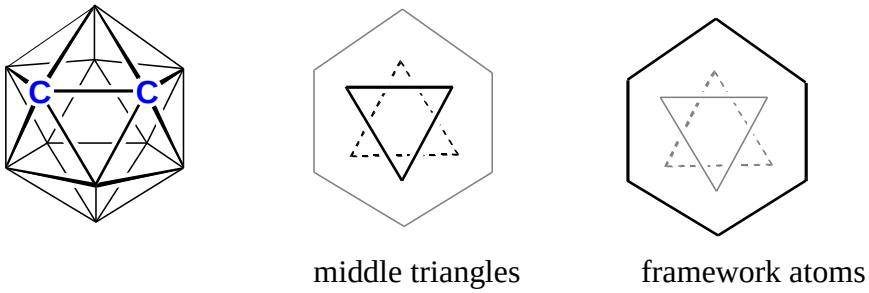

Figure 1.30 Extended TFR schematic

The ‘front’ and ‘back’ triangles can be rotated by sixty degrees in a clockwise or anticlockwise fashion forming an intermediate with a set of ‘eclipsed’ triangles. When we allow these triangles to relax back into a staggered arrangement the final vertex position of the cluster will have changed. This could give rise to many possible isomers especially when we consider there are ten pairs of triangles in the required para relationship and each pair of triangles has four possible methods of rotation. These are front side clockwise, front side anticlockwise, back side clockwise and back side anticlockwise. Each of these have four routes to a stable icosahedron making a total of 160 possible icosahedron-intermediate-icosahedron interconversions as each of the ten triangle pairs have a possible sixteen transformations.

Furthermore, the sixteen possible transformations can be consigned into four groups.

1. One triangle rotated by 120 degrees: standard TFR
2. One triangle rotated by 120 degrees: no net change in molecule
3. Con-rotation of two opposite triangles by 60 degrees
4. Dis-rotation of two opposite triangles by 60 degrees.

It was realised that con-rotation of two opposite triangles by 60 degrees (group 3) gave an equivalent transformation to that of five DSD processes and in fact all DSD transformations originally suggested by Lipscomb could be rationalised by some combination of triangle pair rotations.

However, in 1,2-*closo*-$C_2B_{10}H_{12}$ not all triangular rotations are equally favoured due to slight asymmetry caused by the presence of the carbon atoms. There are actually only three possible structural patterns for triangle rotations of a 1,2-*closo*-C_2B_{10} carborane (Figure 1.31).

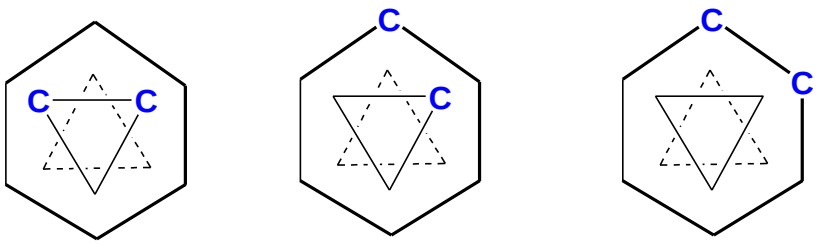

Figure 1.31 Possible structural patterns for triangle rotations of a 1,2-*closo*-C_2B_{10} carborane

Pattern A consists of a triangle where both carbon atoms are located on a common middle triangle. Pattern B has one carbon atom on a middle triangle and one on the outer framework and pattern C has both carbon atoms on the outer framework.

Edvenson and Gaines in 1990 attempted to use isotopically labelled ^{10}B in their clusters[60] to examine the theory proposed by Lipscomb and Wong[61] that the rearrangement proceeded via a *nido* intermediate. It was suggested that DSD arrangements could occur in the open face of the *nido* species. Their results gave good agreement with this concept but were considered somewhat unsatisfying due to a low

conversion to 1,7-isomers and labelled boron atoms being observed from 1,2 to 1,2 isomer rearrangements. It was soon suggested that DSD mechanisms could account for many of the previously suggested theories; TFR, pentagonal face rotation etc. and could simply be explained a combination of DSD processes.

1.6.3 Computational Studies

In 2006 a computational study by McKee examined two potential pathways of rearrangement.[62] One involved a series of TFR steps and the other went through many different DSD processes which also incorporated a *pseudonido* structure. It was calculated that the 1,2- to 1,7 isomerisation had a lower energy pathway by undergoing a series of TFRs whilst a non-TFR pathway was favourable for the 1,7 to 1,12 isomerisation.

It can often be easy to rationalise a rearrangement from starting material to product using a series of DSD and TFR steps. *Ab initio* calculations by Gimarc and Ott[63], and Wales and Stone[56] attempted to provide an overall picture of the dynamic processes involved in a rearrangement. It was found that intermediates that possess high symmetry are the most likely. Furthermore, the previously suggested cubeoctahedron and bicapped pentagonal prism species were found to be not true transition states.

Using the most plausible processes (TFR and DSD) Wales[51] carried out calculations on the potential energy surface for the isomerisation of 1,2-*closo*-$C_2B_{10}H_{12}$. His pathway consists of a number of high energy, low symmetry intermediates linked by transition states of higher energy (Figure 1.32). These transition states occur via a number of concerted DSD steps that Lipscomb proposed years earlier. Wales's calculations also took into account specific DSD steps that should be 'forbidden' under the Woodward-Hoffman rules as shown by Gimarc and Ott. The use of a double DSD process was a way of getting round this problem.

Figure 1.32 shows the three possible carborane isomers as the energy minima 1,12 I_h, 1,7 I_h and 1,2 I_h. These are all commonly linked to the lowest energy intermediate 1,2 C_2 which was believed to be a potential synthetic target. It is non-icosahedral and contains two degree-6 and two degree-4 vertices; the carbon atoms being the degree-4

sites as they prefer to be in sites of low connectivity. A metallacarborane was synthesised with the C_2 intermediate geometry[64] and this will be discussed in the next section.

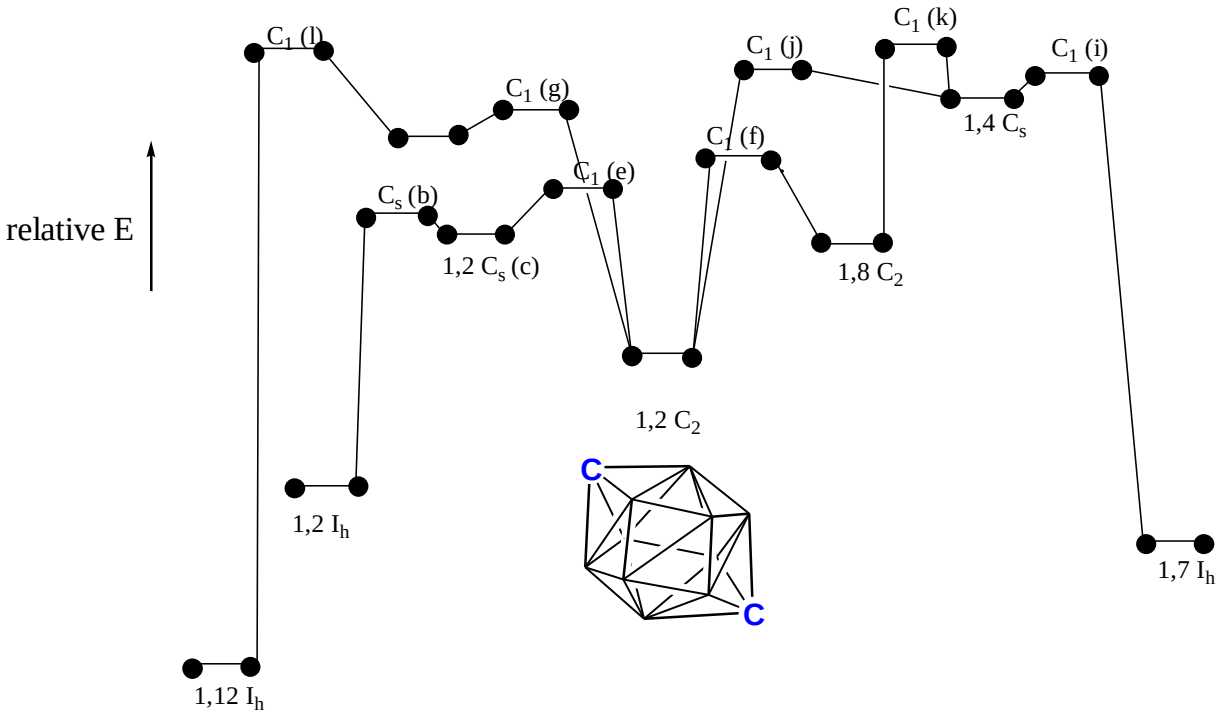

Figure 1.32 Potential energy surface diagram for isomerisation of 1,2-*closo*-$C_2B_{10}H_{12}$ and the 1,2 C_2 intermediate

1.6.4 Metallacarborane Isomerisations

It has already been shown that carboranes require extremely high temperatures to induce isomerisation. For metallacarboranes, on the other hand, the process is much more facile: some are even known to isomerise spontaneously at room temperature.[65] One study shows the formation of two supraicosahedral isomers from 4,1,6-*closo*-$MC_2B_{10}H_{12}$ (M = CpCo) with one carbon atom remaining in the 1 position and the other switching to the 8 or 12 position.[65] The red-orange 4,1,12- isomer is the thermodynamically most stable isomer. The 4,1,6-*closo*-MC_2B_{10} species is also fluxional between two enantiomers at room temperature.[66] This low temperature rearrangement is common in many supraicosahedral metallacarboranes.

It was also observed that deboronation followed by metallation of 1,2-Ph_2-*closo*-$C_2B_{10}H_{10}$ often did not yield the expected 3,1,2-metallacarborane.[67] Instead the product isolated was a 2,1,8-MC_2B_9 metallacarborane isomer which had presumably formed via facile isomerisation of a transient 3,1,2-MC_2B_9 species which could not be isolated. However, under the correct conditions and careful selection of metal-ligand fragment a *pseudocloso* species could be isolated,[68] also from deboronation and metallation of 1,2-Ph_2-*closo*-$C_2B_{10}H_{10}$. The C-C connectivities of *pseudocloso* metallacarboranes are formally broken and form opposite vertices of a trapezoidal face within the cluster. Facile room temperature isomerisation occurs to relieve the steric strain associated with the three exopolyhedral groups.

The facile nature of isomerisation of these metallacarboranes was thought to be a useful tool in elucidation of the mechanism of isomerisation of unmetallated carboranes. With appropriate labelling of specific vertices of a crowded metallacarborane followed by rearrangement, attempts were made to compare the isomerisation product's overall framework topology with that of an unmetallated carborane of the same framework topology. The B–X bonds that were previously unreliable due to the harsh conditions for carborane isomerisation can confidently be said to remain intact under the gentle conditions needed for low temperature metallacarborane isomerisation.[69]

It has been shown however that the isomerisation pathway is metal dependent.[59(c)] Studies show that 3,1,2-nickelacarboranes and 3,1,2-platinacarboranes give different products. The platinum compounds tend to give only the expected 1,2 to 1,7 products whilst the nickel compounds give both 1,2 to 1,2 and 1,2 to 1,7 products. A 1,2 to 1,2 rearrangement is one where one carbon atom may move but remains connected to its neighbouring carbon atom.[59] This cannot be observed in naked carboranes, however a metallacarborane offers a useful opportunity to see this type of rearrangement.

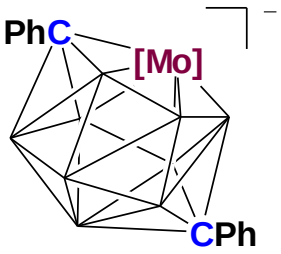

[Mo] = Mo(η^3-allyl)$(CO)_2$

Figure 1.33 Isolated molybdacarborane 1,2 C_2 intermediate

Dunn *et al*. isolated the first 12-vertex non-icosahedral structure[64] (Figure 1.33) in a reaction between $Na_2[7,8\text{-}Ph_2\text{-}nido\text{-}C_2B_9H_9]$ and $[MoBr(MeCN)_2(\eta^3\text{-}C_3H_5)(CO)_2]$. The product formed is a metallacarborane analogous to the C_2 unit predicted by Wales. This was a genuine isomerisation intermediate as gentle heating led to the 1,7 C-isomerised icosahedral compound. This work was extended by creating a labelled analogue.[70] An SMe_2 group was substituted onto the B(9) position. Two isomers formed as final isomerisation products only one of which was in agreement with Wales' predictions (Figure 1.34).

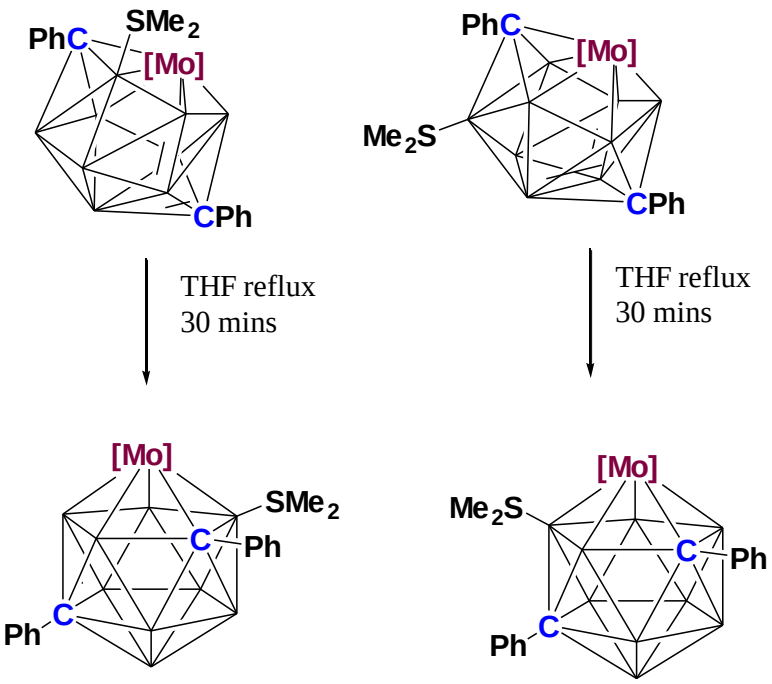

Figure 1.34 Isomerisation from C_2 intermediate to 2,1,8 isomers of a metallacarborane

In fact, isomerisation can often lead to more than one product.[69d] Three isomers are produced in the low temperature platination of $[5\text{-}I\text{-}7,8\text{-}Ph_2\text{-}7,8\text{-}nido\text{-}C_2B_9H_8]^{2-}$. The varying yields suggest some pathways are favoured over others and portray a complex picture of the overall mechanistic process. There is also a degree of uncertainty to how similar the mechanism for metallacarborane isomerisation would be to that of carboranes. The presence of a transition metal would presumably perturb the potential energy surface causing the isomerisation to be specific to that particular metallacarborane studied.

1.7 Scope of Thesis

Chapter 1 gives a summary of the pertinent literature on borane and heteroborane chemistry focussing on icosahedral and supraicosahedral species. Discussed are current theories on bonding and structure; relevant icosahedral carborane chemistry; polyhedral expansion and heteroborane isomerisation, topics upon which the work in this thesis is founded.

Polyhedral expansion of carboranes is of interest but challenging to achieve experimentally, the facile oxidation of the generated nido species formed upon reduction of a *closo* carborane and the incorporation of a relatively small boron fragment into the nido open face providing significant obstacles. It is known that both 1,2- and 1,7-*closo*-C_2B_{10} species can be subjected to 2-electron reduction with subsequent oxidation affording exclusively the 1,2-*closo*-C_2B_{10} species with the carbon atoms adjacent.

Chapter 2 introduces the concept of placing bulky substituents onto a 1,7-*closo*-C_2B_{10} species so that oxidation of the generated nido species with substituents of sufficient bulk may prevent the carbon atoms connecting thus preventing oxidation and allowing for easier capitation to form a supraicosahedral carborane. This chapter reports some initial efforts at bulky groups that did not lead to polyhedral expansion due to undesired reactivity of the substituent or products that were synthesised in insufficient yield.

Chapter 3 discusses the synthesis and characterisation of 1,7-*closo*-C_2B_{10} species which incorporate a ferrocenyl unit on each substituent. Reduction of the 1,7-species and subsequent treatment with a boron fragment did not yield a supraicosahedral carborane, instead oxidising to form significantly sterically deformed 1,2 species.

The redox chemistry of the ferrocenyl 1,2 and 1,7 species were investigated in Chapter 4. The electronic spectrum of the 1,2 species was compared to that given by Time Dependent DFT calculations and suggested a degree of charge transfer within the 1,2 species. Associated electrochemistry suggests this may be a sterically-induced charge transfer.

The steric deformation of the ferrocenyl 1,2 species leads to a relatively low-temperature isomerisation to the 1,7 species leading to renewed interest in the elucidation of the isomerisation mechanism of icosahedral carboranes. Chapter 5 details the synthesis and characterisation of labelled species with labels which can be reliably tracked upon isomerisation. A comparison of the experimental findings to the results of theoretical studies on the subject is examined.

1.8 References

1.1 J. Daintith, *Dictionary of Chemistry 3rd Ed.*, Oxford University Press, 1996.

1.2 M. F. Hawthorne, *Angew. Chem. Int. Ed*., 1993, **32**, 950.

1.3 L. F. Tietze, U. Griesbach, U. Bothe, H. Nakamura and Y. Yamamoto, *ChemBioChem*, 2002, **3**, 219.

1.4 S. H. Strauss, *Chem. Rev*., 1993, **93**, 927.

1.5 e.g. (a) K. Base, M. T. Tierney, A. Fort, J. Muller and M. W. Grinstaff, *Inorg. Chem*., 1999, **38**, 287; (b) J. Abe, N. Nemoto, Y. Nagase, Y. Shirai and T. Iyoda, *Inorg. Chem*., 1998, **37**, 172; (c) D. M. Murphy, D. P. M. Mingos and J. M. Forward, *J. Mater. Chem*., 1993, **3**, 67; (d) D. G. Allis and J. T. Spencer, *Inorg. Chem*., 2001, **40**, 3373.

1.6 M. Kozísek, P. Cígler, M. Lepsík, J. Fanfrlík, P. Rezácová, J. Brynda, J. Pokorná, J. Plesek, B. Grüner, K. Grantz Sasková, J. Václavíková, V. Král and J. Konvalinka, *J. Med. Chem*., 2008, **51**, 4839.

1.7 J. Rais, P. Selucky and M. Kyrs, *J. Inorg, Nucl. Chem*., 1976, **38**, 1376; C. Vinas, J. Bertran, S. Gomez, F. Teixidor, J. F. Dozol, H. Rouquette, R. Kivekas and R. Sillanpaa, *J. Chem Soc. Dalton Trans*., 1998, 2849.

1.8 A. Stock, *Hydrides of Boron and Silicon*, Cornell University Press, Ithaca, New York, 1933.

1.9 H. C. Longuet-Higgins, *J. Chim. Phys.*, 1949, **46**, 268; H. C. Longuet-Higgins and R. P. Bell, *J. Chem. Soc*., 1943, 250.

1.10 W. C. Price, *J. Chem Phys*., 1947, **15**, 614

1.11 H. W. Smith and W. N. Lipscomb, *J. Chem. Phys*., 1965, **43**, 1060.

1.12 (a) J. S. Casper, C. M. Lucht and D. Harker, *Acta. Crystallogr*., 1950, **3**, 436; (b) E. B. Moore Jnr., R. E. Dickson and W. N. Lipscomb, *J. Chem. Phys*., 1957, **27**, 209.

1.13 H. C. Longuet-Higgins and M. de V. Roberts, *Proc. Roy. Soc*., 1954, **A224**, 336; 1955, **A230**, 110.

1.14 A. R. Pitocelli and M. F. Hawthorne, *J. Am. Chem. Soc*., 1960, **82**, 3228.

1.15 M. H. Prosenc and B. R. Albert, *Chem. Commun*., 2007, 3097.

1.16 W. N. Lipscomb, *Boron Hydrides*, W. A. Benjamin, Inc., New York, 1963.

1.17 C. E. Housecroft, *Cluster Molecules of the p-Block Elements*, Oxford University Press, 1994.

1.18 K. Wade, *J. Chem. Soc. D*, 1971, 792.

1.19 R. E. Williams, *Inorg.Chem.*, 1971, **10**, 210; R. E. Williams, *Adv. Inorg. Chem., Radiochem*., 1976, **18**, 66.

1.20 T. L. Heying, J. W. Ager Jr., S. L. Clark, D. J. Mangold, H. L. Goldstein, M. L. Hillman, R. J. Polak, J. W. Szymanski, *Inorg. Chem*., 1963, **2**, 1089.

1.21 M. M. Fein, J. Bobinski, N. Meyers, N. Schwartz and M. S. Cohen, *Inorg. Chem*, 1963, **2**, 1111.

1.22 D. Grafstein, J. Bobinski, J. Dvorak, H. F. Smith, N. N. Schwartz, M. S. Cohen and M. M. Fein, *Inorg. Chem*., 1963, **2**, 1120.

1.23 T. L. Heying, J. W. Ager Jr., S. L. Clark, R. P. Alexander, S. Papetti, J. A. Reid and S. I. Trotz, *Inorg. Chem*., 1963, **2**, 1097.

1.24 R. A. Wiesboeck and M. F. Hawthorne, *J. Am. Chem. Soc*., 1964, **86**, 1642.

1.25 e.g. J. Buchanan, E. J. M. Hamilton, D. Reed and A. J. Welch, *J. Chem. Soc. Dalton Trans*., 1990, 667.

1.26 R. N. Grimes, *Comprehensive Organometallic Chemistry II*, edited by E. W. Abel, F. G. A. Stone, and G. Wilkinson, Volume 1, Chapter 9, Pergamon Press, Oxford, England, 1995, 373.

1.27 J. A. Potenza, W. N. Lipscomb, G. D. Vickers and H. Schroeder, *J. Am. Chem. Soc.*, 1996, **88**, 628; J. A. Potenza, W. N. Lipscomb, *Inorg. Chem*.,1966, **5**, 1471.

1.28 S. Kongpricha and H. Schroeder, *Inorg. Chem*., 1969, **8**, 2449.

1.29 Z. Zheng, W. Jiang, A. A. Zinn, C. B. Knobler and M. F. Hawthorne, *Inorg. Chem*., 1995, **34,** 2095.

1.30 A. Vaca, F. Teixidor, R. Kivekäs, R. Sillanpää and C. Vinas, *Dalton Trans*., 2006, 4884.

1.31 L. I. Zakharkin, V. A. Ol'shevskaya, E. V. Vorontsov and P. V. Petrovsky, *Russ. Chem. Bull*., 1996, **45**, 2614.

1.32 M. F. Hawthorne, D. C. Young and P. A. Wegner, *J. Am. Chem. Soc*., 1965, **87**, 1818.

1.33 M. F. Hawthorne, *Acc. Chem. Res*., 1968, **1**, 281.

1.34 G. B. Dunks, M. M. McKown and M. F. Hawthorne, *J. Am. Chem. Soc*., 1971, **93**, 2451.

1.35 W. J. Evans and M. F. Hawthorne, *J. Chem. Soc., Chem. Commun*., 1974, 38.

1.36 D. Ellis, M. E. Lopez, R. McIntosh, G. M. Rosair and A. J. Welch, *Chem. Commun*., 2005, 1917.

1.37 R. D. McIntosh, D. Ellis, G. M. Rosair and A. J. Welch, *Angew. Chem. Int. Ed.*, 2006, **45**, 4313.

1.38 L. Deng, J. Zhang, H. S. Chan and Z. Xie, *Angew. Chem. Int. Ed*., 2006, **45**, 4309.

1.39 W. N. Lipscomb and L. Massa. *Inorg. Chem*. 1992, **31**, 2299.

1.40 P. v. R. Schleyer, K. Najafian and A. M. Mebel, *Inorg. Chem*., 1998, **37**, 6765.

1.41 Z. X. Wang and P. R. Schleyer, *J. Am. Chem. Soc*., 2003, **125**, 10484.

1.42 A. Burke, D. Ellis, B. T. Giles, B. E. Hodson, S. A. Macgregor, G. M. Rosair and A. J. Welch, *Angew. Chem. Int. Ed*., 2003, **42**, 225.

1.43 e.g. R. D. McIntosh, D. Ellis, J. Gil-Lostes, K. J. Dalby, G. M. Rosair and A. J. Welch, *Dalton Trans*., 2005, 1842.

1.44 L. Deng, H. Chan and Z. Xie, *Angew. Chem. Int. Ed.*, 2005, **44**, 2128.

1.45 J. Zhang, L. Deng, H. S. Chan and Z. Xie, *J. Am. Chem. Soc*., 2007, **129**, 18.

1.46 D. Grafstein and J. Dvorak, *Inorg. Chem*., 1963, **2**, 1128.

1.47 S. Papetti and T. L. Heying, *J. Am. Chem. Soc*., 1964, **86**, 2295.

1.48 L. I. Zakharkin, V. N. Kalinin and L. S. Podvisotskaya, *Izv. Akad. Nauk SSSR, Ser. Khim*, 1967, 2310.

1.49 W. N. Lipscomb, *Science*, 1966, **153**, 3734.

1.50 W. N. Lipscomb and D. Britton, *J. Chem. Phys*., 1960, **33**, 275.

1.51 D. J. Wales, *J. Am. Chem. Soc*., 1993, **115**, 1557.

1.52 (a) L. I. Zakharkin, and V. N. Kalinin, *Dokl. Akad. Nauk. SSSR*, 1966, **169**, 590; (b) H. V. Hart and W. N. Lipscomb, *J. Am. Chem. Soc*. 1969, **91**, 771.

1.53 E. L. Muetterties and W. N. Knoth, *Polyhedral Boranes*, Marcel Dekker, New York, 1968, 70.

1.54 N. S. Hosmane, H. Zhang, J. A Maguire, Y. Wang, C. J. Thomas and T. G. Gray, *Angew. Cem. Int. Ed*., 1996, **35**, 1000.

1.55 Y. V. Roberts and B. F. G. Johnson, *J. Chem. Soc. Dalton. Trans*., 1994, 759.

1.56 D. J. Wales and A. J. Stone, *Inorg. Chem*., 1987, **26**, 3845.

1.57 B. F. G. Johnson, Y. V. Roberts and E. Parisini, *Inorg. Chim. Acta*., 1993, **211**, 17.

1.58 L. I. Zakharkin and V. N. Kalinin, *Izv. Akad. Nauk. SSSR. Ser. Khim.*, 1969, **3**, 607.

1.59 (a) S. H. Wu and M. Jones Jr., *J. Am. Chem. Soc*., 1989, **111**, 5373; (b) L. F. Warren Jr. and M. F. Hawthorne, *J. Am. Chem. Soc.*, 1979, **92**, 1157; (c) R. M.

Garrioch, P. Kuballa, K. S. Low, G. M. Rosair and A. J. Welch, *J. Organometal. Chem*., 1999, **575**, 57.

1.60 G. M. Edvenson and D. F. Gaines, *Inorg. Chem*, 1990, **29**, 1210.

1.61 H. S. Wong and W. N. Lipscomb, *Inorg. Chem*, 1975, **14**, 1350.

1.62 C. A. Brown and M. L. McKee, *J. Mol. Model*, 2006, **12**, 653.

1.63 J. J. Ott and B. M. Gimarc, *J. Am. Chem. Soc*., 1986, **108**, 4303.

1.64 S. Dunn, G. M. Rosair, Rh. Ll. Thomas, A. S. Weller and A. J. Welch, *Angew. Chem. Int. Ed. Engl.*, 1997, **36**, 645.

1.65 A. Burke, R. McIntosh, D. Ellis, G. M. Rosair and A. J. Welch, *Collect. Czech. Chem. Commun.*, 2002, **67**, 991.

1.66 e.g. (a) A. S. F. Boyd, A. Burke, D. Ellis, D. Ferrer, B. T. Giles, M. A. Laguna, R. McIntosh, S. A. Macgregor, D. L. Ormsby, G. M. Rosair, F. Schmidt, N. M. M. Wilson, and A. J. Welch, *Pure Appl. Chem.*, 2003, **75**, 9, 1325; (b) A. Burke, D. Ellis, D. Ferrer, D. L. Ormsby, G. M. Rosair and A. J. Welch, *Dalton Trans*, 2005, 1716.

1.67 D. R. Baghurst, R. C. B. Copley, H. Fleischer, D. M. P. Mingos, G. O. Kyd, L. J. Yellowlees, A. J. Welch, T. R. Spalding and D. O'Connell, *J. Organometal. Chem*., 1993, **447**, C14.

1.68 R. D. McIntosh, D. Ellis, B. T. Giles, S. A. Macgregor, G. M. Rosair and A. J. Welch, *Inorg. Chim. Acta*, 2006, **359**, 3745.

1.69 (a) S. Robertson, D. Ellis, T. D. McGrath, G. M. Rosair and A. J. Welch, *Polyhedron*, 2003, **22**, 1293; (b) S. Robertson, D. Ellis, G. M. Rosair and A. J. Welch, *J. Organometal. Chem*, 2003, **680**, 286; (c) S. Robertson, D. Ellis, G. M. Rosair and A. J. Welch, *Appl. Organometal. Chem*.,2003, **17**, 516; (d) S. Robertson, R. M. Garrioch, D. Ellis, T. D. McGrath, B. E. Hodson, G. M. Rosair and A. J. Welch, *Inorg. Chim. Acta*, 2005, **358**, 1485; (e) D. Ellis, R. M. Garrioch, G. M. Rosair and A. J. Welch, *Polyhedron*, 2006, **25**, 915.

1.70 S. Dunn, G. M. Rosair, A. S. Weller and A. J. Welch, *Chem. Commun*., 1998, 1065.

Chapter 2 The Use of Bulky Substituents for Polyhedral Expansion

2.1 Introduction

Generally, the synthesis of 4,1,6-*closo*-MC_2B_{10} thirteen-vertex metallacarboranes is achieved by reduction of either a 1,2- or 1,7-*closo*-C_2B_{10} carborane followed by metallation with a suitable $\{ML_x\}^{2+}$ fragment[1] (Figure 2.1) and this methodology has become widely established. Reduction affords a *nido* species where the carbon atoms are separated and subsequent metallation affords a metallacarborane of 4,1,6-*closo*-MC_2B_{10} topology adopting a docosahedral geometry.

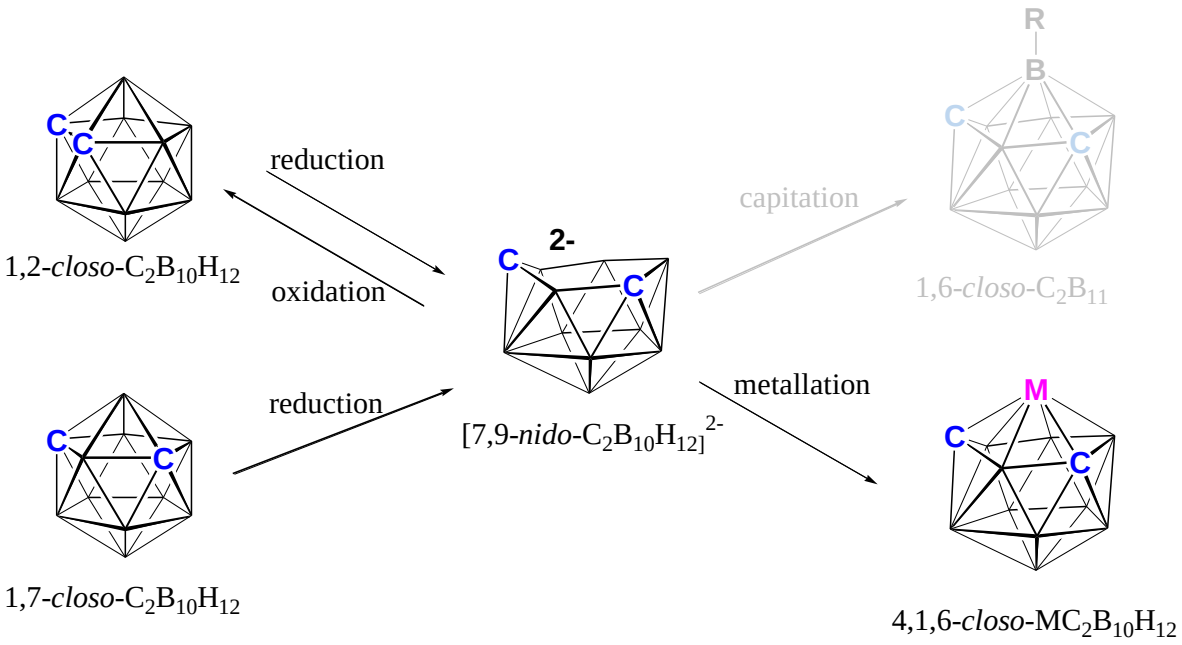

Figure 2.1 Possible chemistry of [7,9-*nido*-$C_2B_{10}H_{12}$]$^{2-}$ *nido* dianion

Attempts to capitate the *nido* species with a boron fragment to form a 1,6-*closo*-C_2B_{11} thirteen-vertex carborane are more challenging due to the relatively contracted orbitals of boron that do not overlap with the orbitals of the six-atom face of the *nido* cage as efficiently as those of a larger transition metal. Instead, the cage regularly oxidises and (re)forms a 1,2-*closo*-C_2B_{10} species.

Tantalisingly, reduction of 1,2-*closo*-$C_2B_{10}H_{12}$ followed by treatment with BI_3 produced 3-I-1,2-*closo*-$C_2B_{10}H_{11}$ (Figure 2.2) which suggests initial formation of a

thirteen-vertex carborane that spontaneously degraded by loss of a {BH} unit presumably from the unfavoured degree-6 site.[2]

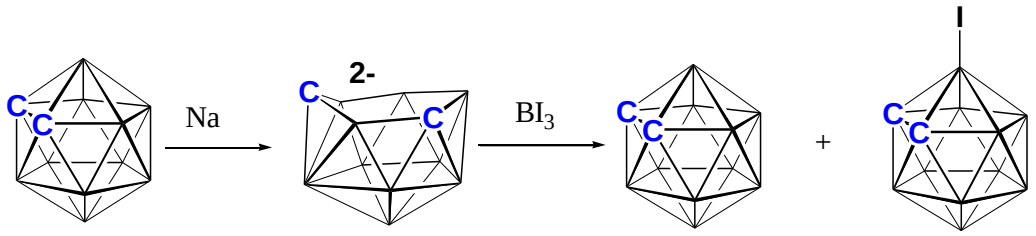

Figure 2.2 Capitation of [7,9-*nido*-C_2B_{10}]$^{2-}$ with a {BI}$^{2+}$ fragment resulting in minor amounts of 3-I-1,2-*closo*-$C_2B_{10}H_{11}$

Tethering together the carbon atoms in 1,2-*closo*-C_2B_{10} (discussed in Chapter 1) helped solve this problem by preventing the carbon atoms separating upon reduction. Another approach may be keeping the carbon atoms apart upon oxidation or capitation of the *nido* species. This can potentially be achieved by placing bulky substituents on the carbon atoms of 1,7-*closo*-$C_2B_{10}H_{12}$. Both 1,2 and 1,7 isomers generate the same [7,9-*nido*-C_2B_{10}]$^{2-}$ species upon reduction but this dianion exclusively forms the 1,2 isomer upon subsequent oxidation (Figure 2.1). Bulky groups may prevent the carbon atoms connecting (i.e. preventing oxidation) and allow easier capitation to form a 1,6-*closo*-C_2B_{11} supraicosahedral carborane (which, incidentally, is calculated to be thermodynamically more stable than the supraicosahedral 1,2 isomer).[3]

Certain criteria must be met in the selection of a bulky group: it must be unreactive towards sodium (the cage reducing agent) as well as any potential capping fragments; it should ideally be relatively easily synthesised and in good yield if further chemistry is likely to carried out and, most importantly, it needs to be sufficiently sterically demanding to keep the carbon atoms apart upon oxidation of the 7,9-*nido* species. One test for the latter is to attempt disubstitution directly onto 1,2-*closo*-$C_2B_{10}H_{12}$, a positive test producing only a monosubstituted carborane product. This chapter discusses some attempts to produce a 1,7-R_2-1,7-*closo*-$C_2B_{10}H_{10}$ species (R=bulky group) which, ultimately, were not entirely suitable for the synthesis of supraicosahedral carboranes but, nevertheless, generated some interesting molecules.

2.2 Nucleophilic Substitution with Acetone.

2.2.1 Synthesis of 1,7-$(CMe_2OH)_2$-1,7-*closo*-$C_2B_{10}H_{10}$ (1)

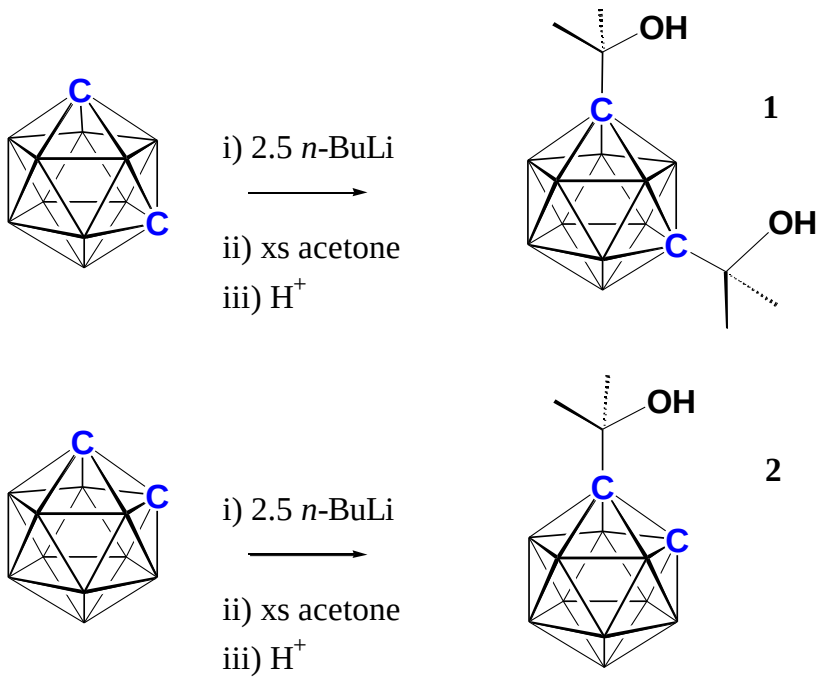

Scheme 2.1 Preparation of 1,7-$(CMe_2OH)_2$-1,7-*closo*-$C_2B_{10}H_{10}$ (top) and 1-(CMe_2OH)-1,2-*closo*-$C_2B_{10}H_{11}$ (bottom)

Reaction of dilithiocarboranes with ketones and aldehydes is known to give carboranes with alcohol substituents.[4] A ketone of type RR′CO produces a bulky alcohol substituent when reacted with a nucleophile (and subsequent protonation) and has the potential to be modified into a suitable substituent to enable cage reduction. Deprotonated 1,7-*closo*-$C_2B_{10}H_{12}$ was treated with excess acetone to yield disubstituted 1,7-$(CMe_2OH)_2$-1,7-*closo*-$C_2B_{10}H_{10}$ (**1**) (Scheme 2.1; top) in good yield. This compound has been reported previously by Papetti[5] detailing only the synthesis and elemental analysis. The yield has been improved from 30% to 80% by addition of a slightly larger excess of acetone and recrystallisation from hexane.

The ^{1}H NMR spectrum shows the hydroxyl protons as a broad singlet at δ 1.74 with an integral of two and a sharp singlet at δ 1.35 with an integral of twelve reveals the four methyl groups.

$^{11}B\{^1H\}$ NMR spectroscopy shows four resonances at δ -6.6, δ -11.7, δ -12.4 and δ 14.6 in a 2:2:4:2 ratio. This is typical for a 1,7 carborane that displays C_{2v} symmetry.

The mass spectrum shows a typical carborane isotopic envelope centred at *m/z* 260 with notable fragmentation occurring at 243 (M-OH), 226 (M- 2OH), 185 (M-{OH + CMe_2OH}) and 142 (M-2CMe_2OH). Elemental analysis was in good agreement with that expected for $C_8H_{24}B_{10}O_2$.

An X-ray diffraction study was carried out on **1** and some relevant structural data are shown in Table 2.1.

Table 2.1 Selected Interatomic distances (Å) and bond angles (°) for 1

C(1) -C(11)	1.574(2)	C(11)-C(1)-B(4)	117.50(11)
C(7) -C(71)	1.596(2)	C(11)-C(1)-B(5)	119.20(12)
C(1)-B(2)	1.711(2)	C(11)-C(1)-B(6)	120.28(12)
B(2)-B(3)	1.783(2)	C(71)-C(7)-B(12)	121.87(12)
B(3)-B(4)	1.768(2)	C(71)-C(7)-B(11)	119.79(11)
B(9)-B(10)	1.778(3)	C(71)-C(7)-B(2)	116.55(11)
C(11)-O(1)	1.4293(17)	C(71)-C(7)-B(3)	116.86(12)
C(71)-O(7)	1.4344(18)	C(71)-C(7)-B(8)	120.51(12)
C(11)-C(1)-B(2)	119.66(11)	C(1)-C(11)-0(1)	109.81(11)
C(11)-C(1)-B(3)	118.21(12)	C(7)-C(71)-0(71)	108.34(11)

The molecular structure of **1** (Figure 2.3) reveals the CMe_2OH substituents are orientated in opposite directions i.e. the C(1)-C(11) and C(7)-C(71) bonds are rotated so that both CMe_2OH substituents adopt an approximate 'head to tail' arrangement with the hydroxyl groups protruding in roughly opposite directions. There is a slight inclination of the C(1)-C(11) bond towards B(4) at angle of 117.50(11)°. This effect is slightly more pronounced on the C(7) substituent where the C(71)-C(7)-B(2) and C(71)-C(7)-B(3) angles are 116.55(11)° and 116.86(12)° respectively. The C(1)···C(7) distance is slightly elongated at 2.684(2) Å compared to that in unsubstituted 1,7-*closo*-$C_2B_{10}H_{12}$, 2.609(6) Å.[6]

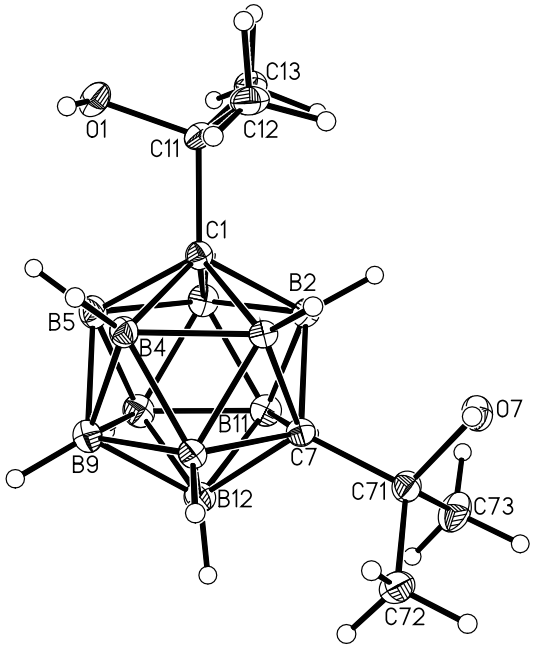

Figure 2.3 Molecular structure of 1

2.2.2 Synthesis of 1-(CMe_2OH)-1,2-*closo*-$C_2B_{10}H_{11}$ (2)

1,2-*closo*-$C_2B_{10}H_{12}$ was doubly deprotonated with *n*-BuLi and excess acetone was added to test whether the disubstituted species, 1,2-$(CMe_2OH)_2$-1,2-*closo*-$C_2B_{10}H_{10}$ could be formed. Only one carbon atom was successfully substituted yielding 1-(CMe_2OH)-1,2-*closo*-$C_2B_{10}H_{11}$ (**2**) (Scheme 2.1; bottom) indicating that two CMe_2OH groups may, indeed, be sufficiently bulky to not fit onto adjacent cage carbon atoms.

Despite the extensive derivative chemistry of icosahedral carboranes in the literature, compound **2** has yet to be reported. The ^1H NMR spectrum shows a broad singlet at δ 4.10 that corresponds to the cage CH proton. Another broad singlet is observed at δ 2.32 relating to the hydroxyl proton and a sharp resonance at δ 1.51 (6H) shows the two methyl groups.

The $^{11}B\{^1H\}$ NMR spectrum shows six resonances at δ -3.7, δ -4.4, δ -9.2, δ -11.7, δ -11.9 and δ -13.8 in ratio of 1:1:2:2:2:2, typical for a monosubstituted 1,2-*closo*-C_2B_{10} species.

Mass spectrometry shows a typical carborane isotopic envelope centred at *m/z* 202 with fragmentation occurring at 185 (M-OH) and 142 (M-CMe_2OH). Elemental analysis was in excellent agreement with that expected for $C_5H_{18}B_{10}O$.

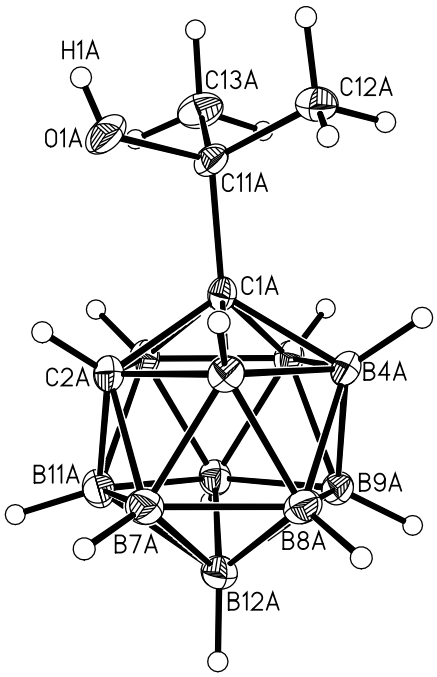

Figure 2.4 Molecular structure of 2 (molecule A)

The crystallographic study of **2** reveals two crystallographically independent molecules (A and B) in the asymmetric fraction of the unit cell. There is a degree of ambiguity over the unsubstituted carbon atom position in molecule B due to rotational disorder and C(2) is partially occupied over two sites, (2) and (4). Table 2.2 shows selected structural information.

Table 2.2 Selected Interatomic distances (Å) and bond angles (°) for 2 in molecules A, B

C(1) -C(11)	1.5677(17), 1.5674(16)	C(11)-O(1)	1.4327(15), 1.4319(15)
C(1) -*C*(2)	1.6586(17), *1.6884(18)*	C(11)-C(1)-*C*(2)	117.60(9), *120.89(10)*
C(2)-B(3)	1.7113(18), 1.734(2)	C(11)-C(1)-B(3)	115.95(12), 118.61(10)
B(3)-*B*(4)	1.769(2), *1.749(2)*	C(11)-C(1)-*B*(4)	123.15(10), *121.51(10)*
B(4)-B(5)	1.7782(19), *1.735(2)*	C(11)-C(1)-B(5)	123.81(10), 119.45(10)
B(5)-B(6)	1.7799(19), 1.769(2)	C(11)-C(1)-B(6)	117.66(9), 118.21(9)
B(9)-B(12)	1.774(2), 1.774(2)	C(1)-C(11)-O(1)	106.40(10), 107.31(10)

The molecular structure of **2** (Figure 2.4) shows a potential hydrogen bond between the electronegative oxygen atom of the hydroxyl group and the relatively acidic cage proton on C(2) at a distance of 2.358 Å, symptomatic of a relatively strong hydrogen bond[7] (Figure 2.5 - (a), molecule A). This causes an inclination of the entire CMe_2OH substituent (i.e. the C(1)-C(11) bond) towards C(2) and B(3), the oxygen atom partially eclipsing C(2) when viewed along the C(1)-C(11) bond (Figure 2.5 - (b), molecule A). The hydrogen bond in **2** is further exemplified by a change the chemical shift of the hydroxyl proton to a significantly higher frequency (δ 2.32) than that of **1** (δ 1.74) where is there is no propensity for hydrogen bonding due to disubstitution of both carbon atoms.

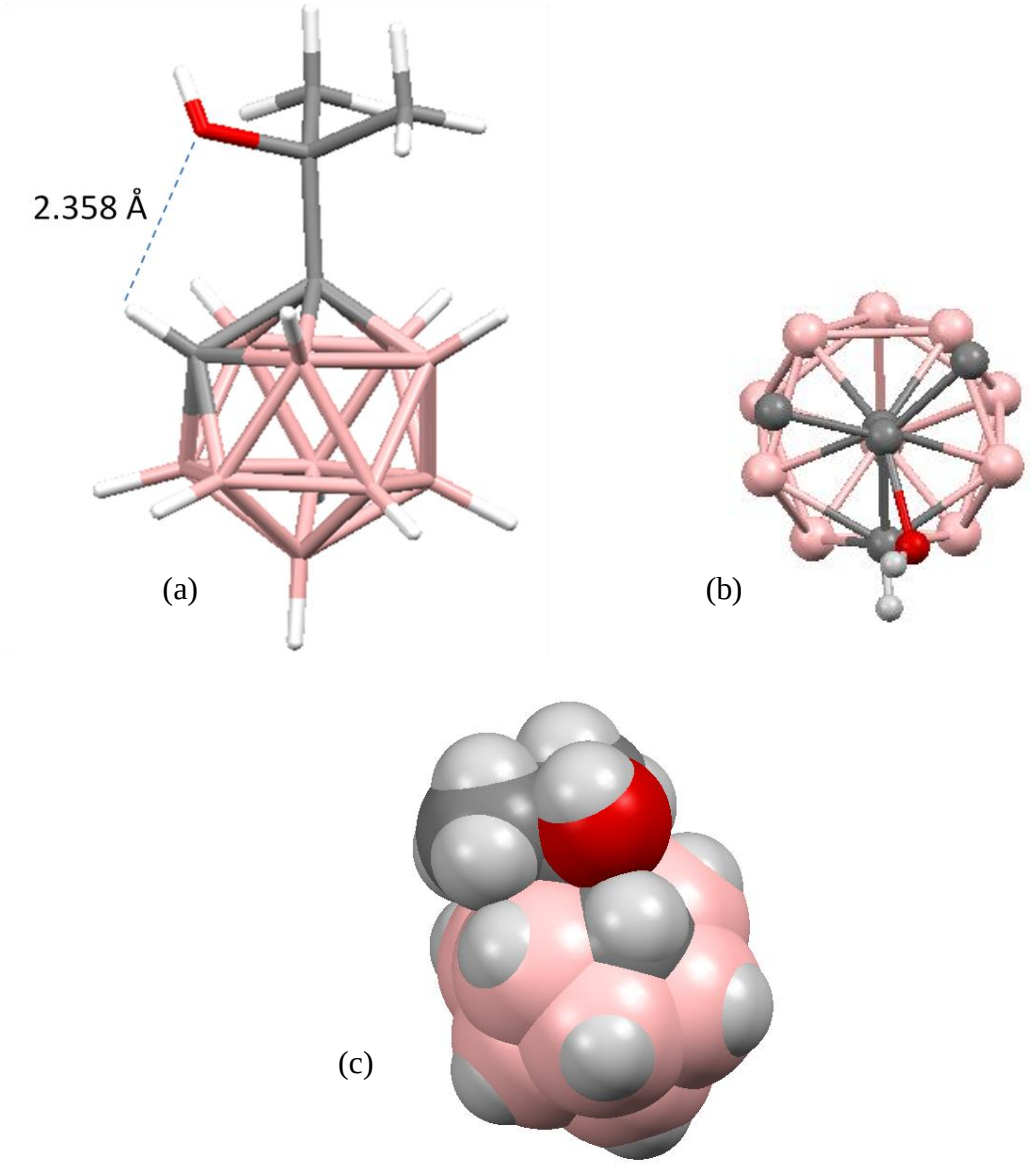

Figure 2.5 Mercury representations of 2 – (a) side view, (b) top view and (c) space filling diagram

A space filling diagram of **2** (Figure 2.5 - (c), molecule A) shows only a small degree of overlap from the CMe_2OH substituent over the unsubstituted carbon atom. It may still be that this substituent does offer enough steric bulk to prevent the adjacent carbon atom becoming substituted. However, the strong interaction between the OH group and the relatively acidic cage C*H* may also account for the inability to form a disubstituted species. The reaction could potentially proceed via an intermediate depicted in Figure 2.6. 1,2-*closo*-$C_2B_{10}H_{12}$ is deprotonated in both positions, with the charge of each cage carbanion being balanced by a lithium cation (from *n*-BuLi) which may also form a complex with the generated alkoxy anion. Such a species may be stable enough to prevent reaction with another acetone molecule. Attempts to isolate such an intermediate species were unsuccessful. Disubstitution readily occurs in 1,7-*closo*-$C_2B_{10}H_{12}$ as the carbon atoms are sufficiently apart to prevent such a species being formed.

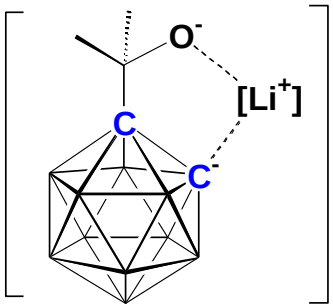

Figure 2.6 Speculated intermediate in formation of 2

2.2.3 Synthesis of 1,7-$(CMe_2OCH_2OCH_3)_2$-1,7-*closo*-$C_2B_{10}H_{10}$ (3)

The presence of a hydroxyl group is undesirable for sodium reduction. One common protecting group often utilised by organic chemists for the protection of alcohols is a methoxymethyl (MOM) group.[8] Compound **1** was treated with a large excess of dimethoxymethane in the presence of phosphorous pentoxide in DCM to yield 1,7-$(CMe_2OCH_2OCH_3)_2$-1,7-*closo*-$C_2B_{10}H_{10}$ (**3**) in excellent yield (Scheme 2.2) as a yellowish oil.

The ^{1}H NMR spectrum shows the CH_2 protons of the MOM chain as a singlet at δ 4.64 (4H). The terminal O-Me protons appear as a singlet at δ 3.30 (6H) and the CMe_2 methyl protons are observed at a singlet at δ 1.35 (12H).

$^{11}B\{^{1}H\}$ NMR spectroscopy shows three resonances at δ -6.4 (2B), δ -12.4 (6B) and δ -14.8 (2B). The 6B peak is presumably a coincident (2 + 4) resonance.

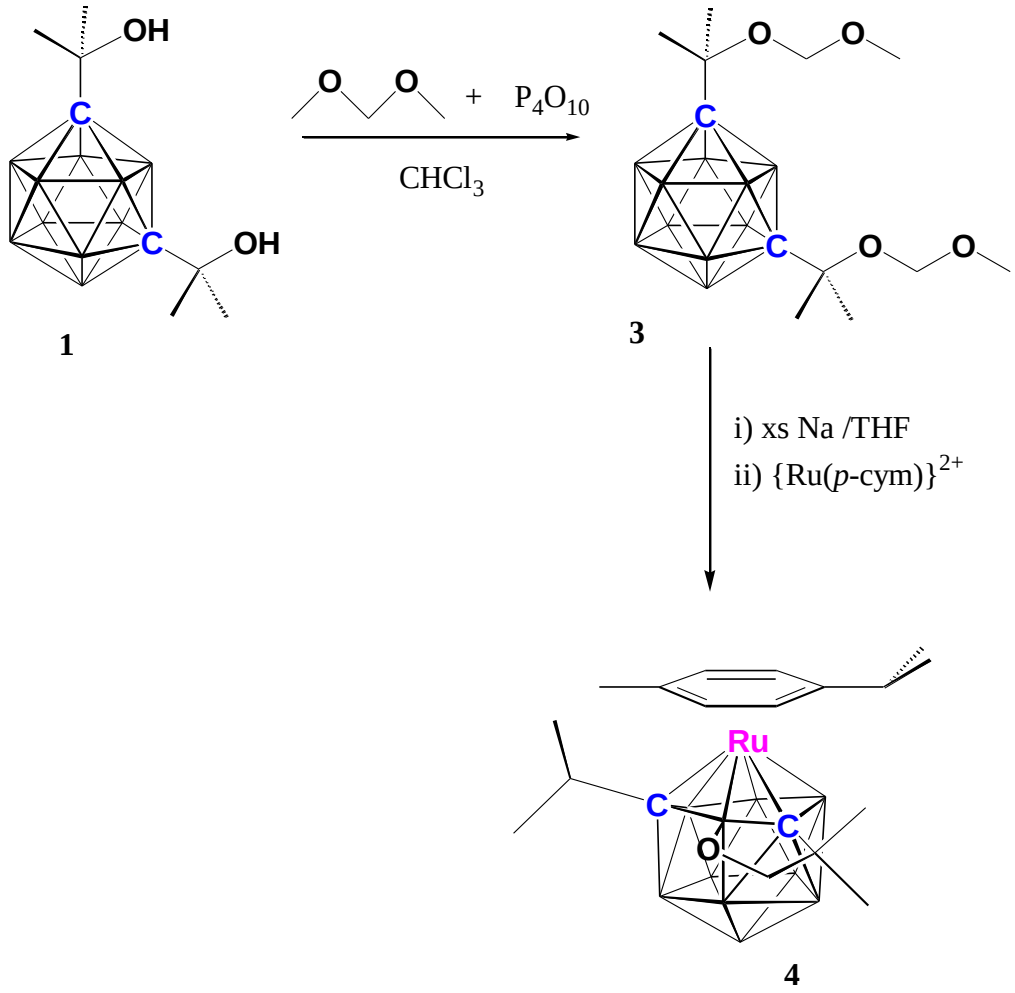

Scheme 2.2 MOM-protection of alcohols and subsequent polyhedral expansion

Mass spectrometry of **3** shows a typical carborane isotopic envelope centred at *m/z* 287 corresponding to **3** - OCH_2OCH_3. The expected molecular ion of *m/z* 348 is not observed. Fragmentation also occurs at 226 indicating the loss of two -OCH_2OCH_3 fragments. Elemental analysis was in good agreement with that expected for $C_{12}H_{32}B_{10}O_4$.

2.2.4 Synthesis of 4-(*p*-cymene)-2,6-μ-(OCH_2CMe_2)-4,1,6-$RuC_2B_{10}H_9$ (4)

Before any attempt to synthesise a supraicosahedral carborane, the MOM-protected carborane **3** was subjected to reduction and metallation as a test to ensure reduction was possible. **3** was treated with ten molar equivalents of sodium in THF and metallated with $[RuCl_2(p\text{-cymene})]_2$. Preparative TLC afforded a yellow band, the 13-vertex ruthenacarborane, 4-(*p*-cymene)-2,6-μ-(OCH_2CMe_2)-4,1,6-$RuC_2B_{10}H_9$ **(4)**, in low yield (Scheme 2.2).

The ^{1}H NMR spectrum of **4** shows four doublets in the range δ 5.91 to 6.43 which correspond to the four aromatic protons of the *p*-cymene ligand. Two apparent septets are visible at δ 2.95 (1H) and δ 3.27 (1H) showing both *i*-propyl CH protons, one of the *i*-propyl groups being directly bonded to a cage carbon atom and the other as part of the *p*-cymene ligand. The rigid CH_2 moiety contains two magnetically inequivalent protons which afford two overlapping doublets centred on δ 4.06. The *p*-cymene methyl group affords a singlet at δ 2.40. The six remaining methyl groups are bundled together in the range δ 1.00 to 1.40. Two singlet peaks at δ 1.07 and δ 1.32 arise from the two magnetically inequivalent methyl groups on the *exo*-polyhedral tether. Two doublets at δ 1.09 and δ 1.26 correspond to the *i*-propyl substituent on the cage and the apparent triplet (the product of two overlapping doublets) at δ 1.34 arises from both *i*-propyl methyl groups of the *p*-cymene ligand.

$^{11}B\{^1H\}$ NMR spectroscopy shows eight resonances at δ 7.5 (2B), δ 0.8 (1B), δ -1.7 (2B), δ -5.3 (1B), δ -7.1 (1B), δ -9.3 (1B), δ -10.9 (1B) and δ -22.0 (1B).

The ^{1}H-^{1}H NOE spectrum (Figure 2.7) differentiates the two *i*-propyl units. The *p*-cymene methyl group at δ 2.40 shows a through-space interaction to an *i*-propyl CH proton at δ 3.27 (Figure 2.7 - shaded yellow). This belongs to the cage *i*-propyl substituent: the *i*-propyl unit from *p*-cymene is in the *para* position to the *p*-cymene methyl group and would not induce such an interaction. The cage *i*-propyl proton at δ 3.27 shows NOE interactions to the two methyl groups (at δ 1.09 and δ 1.26 - shaded purple) with which it shares a carbon atom. The other two methyl groups (the apparent triplet at δ 1.34) therefore must belong to the *p*-cymene ligand. The ^{1}H-^{1}H COSY NMR spectrum (Figure 2.8) confirms this coupling between the *i*-propyl protons and their associated methyl groups and show two different *i*-propyl spin-coupling systems.

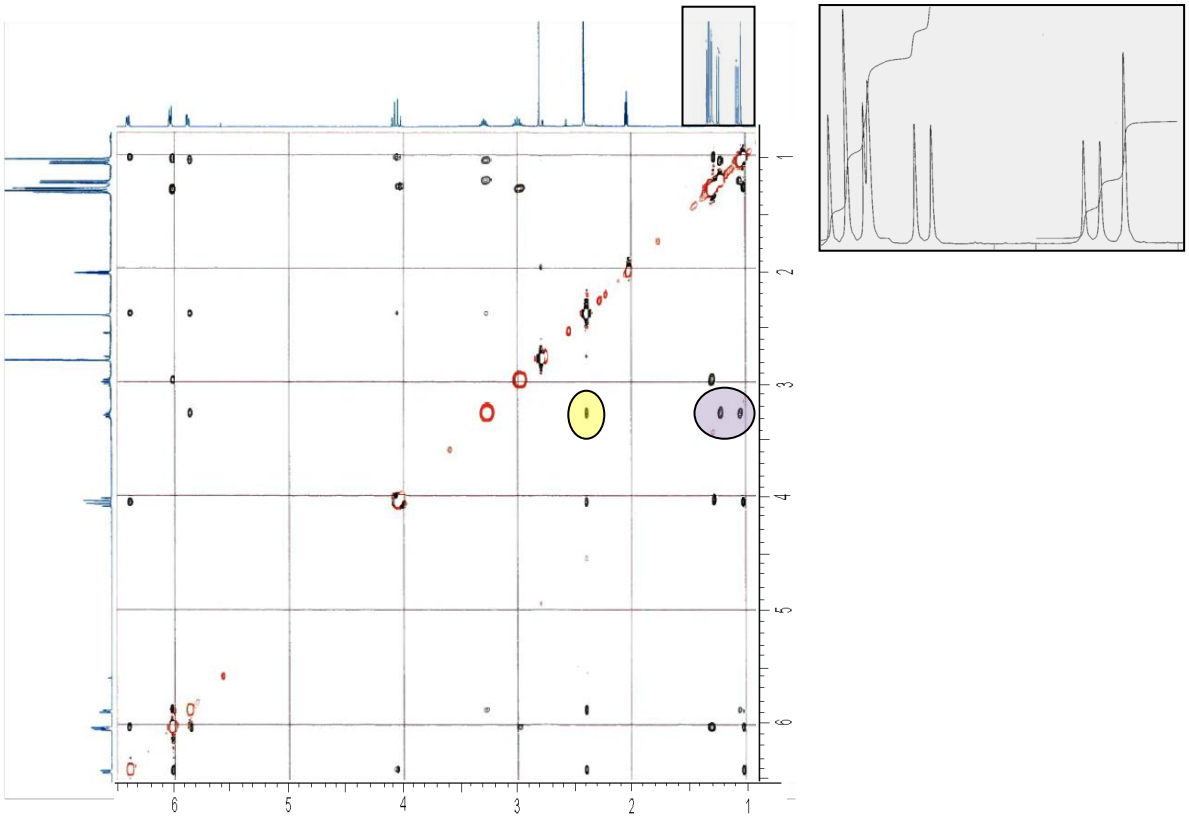

Figure 2.7 ^{1}H-^{1}H NOE spectrum of 4; shaded box - expansion of δ 1.0 - 1.4.

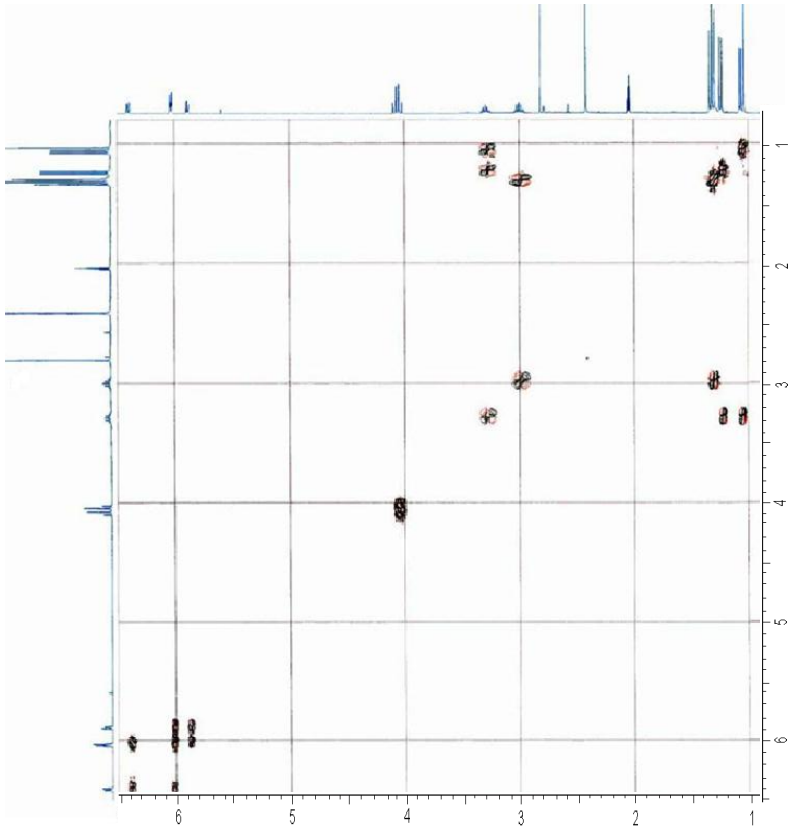

Figure 2.8 ^{1}H-^{1}H COSY NMR spectrum of 4

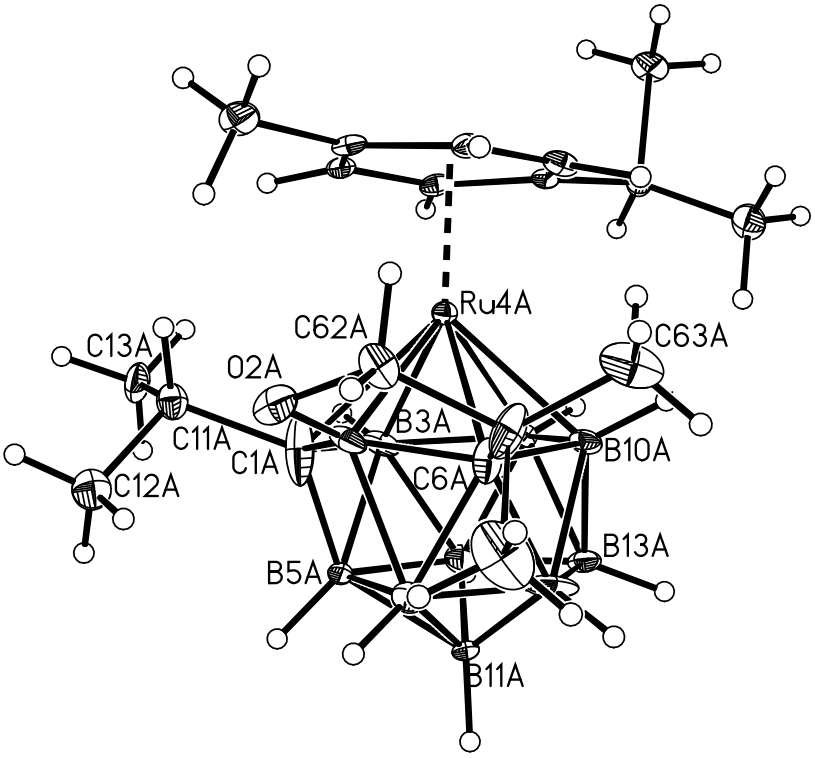

Figure 2.9 Molecular structure of 13-vertex ruthenacarborane 4

The vast majority of 4,1,6-*closo*-MC_2B_{10} type metallacarboranes exhibit a docosahedral structure. Conversley, thirteen-vertex carboranes, the majority of which contain a C-C tether adopt a henicosahedral geometry (Figure 2.10). Topologically this differs from the docosahedron only by the absence of the 2-5 connectivity. The thirteen-vertex ruthenacarborane **4** contains an *exo*-polyhedral μ-B(2)-C(6) tether and adopts a henicosahedral geometry as revealed by an X-ray crystallographic study. The molecular structure is shown in Figure 2.9 and Table 2.3 displays some relevant structural information.

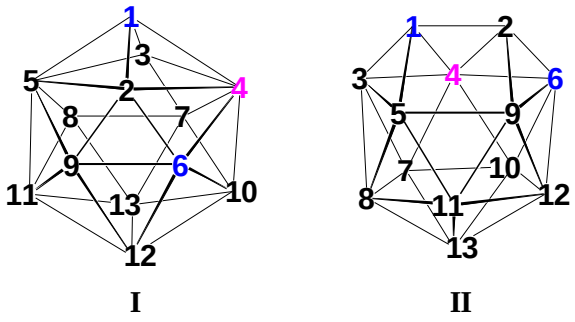

Figure 2.10 Docosahedral (I) and henicosahedral (II) geometries and numbering

Table 2.3 Interatomic distances (Å) of 4 in molecules A,B

C(1)-B(2)	1.538(18), 1.515(17)	Ru-C(6)	2.389(14), 2.559(12)
C(1)-B(3)	1.702(18), 1.680(17)	Ru-B(7)	2.204(13), 2.273(10)
C(1)-B(5)	1.749(17), 1.705(18)	Ru-B(10)	2.268(13), 2.273(10)
O-C(62)	1.575(12), 1.593(13)	Ru-C(40)	2.256(10), 2.257(11)
O-B(2)	1.368(16), 1.355(14)	Ru-C(41)	2.243(11). 2.220(11)
C(6)-C(61)	1.538(18), 1.576(15)	Ru-C(42)	2.283(9), 2.220(11)
C(6)-B(2)	1.625(19), 1.625(15)	Ru-C(43)	2.321(11), 2.322(11)
C(6)-B(12)	1.708(19), 1.647(17)	Ru-C(44)	2.251(11), 2.255(9)
C(6)-B(9)	1.837(16), 1.788(17)	Ru-C(45)	2.190(10), 2.223(10)
C(6)-B(10)	1.677(17), 1.629(18)	Ru-B(2)	2.285(14), 2.258(10)
Ru-C(1)	2.264(12), 2.269(12)	Ru-B(3)	2.291(11), 2.263(12)

The crystallographic asymmetric unit of **4** consists of two molecules (A and B) that are almost related by a centre of inversion (a *pseudo*-centre of symmetry of 89% fit). The Ru(*p*-cymene) sits atop a six-atom belt with carbon atoms in positions 1 and 6. B(2) is connected to the O atom of the *exo*-polyhedral tether. C(1) contains an *i*-propyl substituent. Figure 2.11 (left) shows the cage substituents of **4** more clearly.

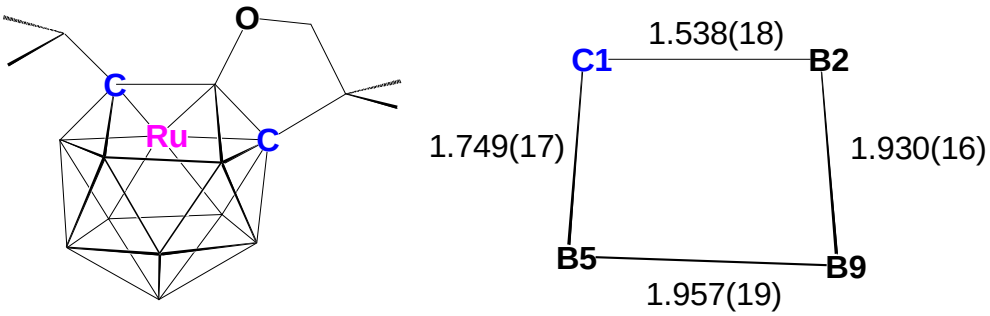

Figure 2.11 Left - view of cage substituents of 4; right - bond lengths (Å) of atoms in trapezoidal face (molecule A)

Compound **4** is a rare example of a 13-vertex species that contains atoms that occupy unfavourable positions and are often referred to as defective vertices.[9] Carbon atoms favour the low connected sites (e.g. there are two degree-4 vertices in a henicosahedron both favoured by carbon atoms in tethered 13-vertex carboranes) but compound **4** contains a degree-5 carbon atom and a degree-4 boron atom (Figure 2.11 left), a relatively unfavoured topology. Another interesting feature of **4** is the

location of the *exo*-polyhedral tether on the cage; all previous examples of henicosahedral heteroboranes incorporate the tether over two (carbon) atoms of the trapezoidal face whereas the tether in **4** sits over one connectivity of a deltahedral face. The trapezoidal C(1A)-B(2A)-B(5A)-B(9A) face contains relatively elongated B-B connectivities from B(9) to B(2) and B(5) at 1.930(16) Å and 1.957(19) Å respectively (Figure 2.12 right). The C-Ru distances are elongated when involving the unfavourable degree-5 carbon atoms at 2.389(14) Å and 2.559(12) Å for each molecule of the asymmetric unit compared to 2.264(12) Å and 2.269(12) Å respectively for the Ru-C(1) (degree-4) vertices.

The plane of the *p*-cymeme C_6 ring is tilted slightly from the bottom belt plane of five boron atoms [B(5)-B(9)-B(12)-B(13)-B(8]) by 9.50° and 12.09°, in both molecules of the asymmetric unit, away from the *i*-propyl and *exo*-polyhedral tether substituents which exert a slight steric influence on the *p*-cymene ligand.

The mechanism required to generate **4** from **3** is unclear and probably very complex. When ten molar equivalents of sodium are used it is entirely consumed in the reaction whereas usually any sodium metal not used in the reduction is required to be removed prior to any further treatment. The sodium may deprotonate a relatively positive methylene unit with the resulting carbanion driving the chemistry that forms **4**. There has been a bond formed between one O-*C*H_2-O carbon atom in **3** to a *C*Me_2 carbon atom and well as one of the oxygen atoms becoming attached to the cage. It is clear that a bulky substituent that will be subjected to reduction should be free of any potentially reactive heteroatoms to avoid unwanted chemistry.

2.3 Multiple Cage Compounds

One method of incorporating a quarternary carbon atom directly onto a lithiated cage carbon atom is that of treatment with (substituted) fulvenes.[10] This reaction produces 1,7-{$CR_2(C_5H_5)$}$_2$-1,7-*closo*-$C_2B_{10}H_{10}$ (**7**) from doubly deprotonated 1,7-*closo*-$C_2B_{10}H_{12}$ (Scheme 2.3) but only the singly substituted 1-{$CR_2(C_5H_5)$}-1,2-*closo*-$C_2B_{10}H_{11}$ from doubly deprotonated 1,2-*closo*-$C_2B_{10}H_{12}$. The synthesis and characterisation of compounds **7** (where R_2=Me_2 or pentamethylene) are described in detail in Chapter 3. The C_5H_5 rings can be deprotonated and reacted with a variety of metal fragments. This section describes the synthesis and characterisation of 1,7 carboranes with bulky cobaltacarborane-containing substituents (Scheme 2.3). This is an attractive approach as it is desirable to find methods of adding additional boron atoms to molecules that may enhance some potential heteroborane applications (e.g. BNCT).[11]

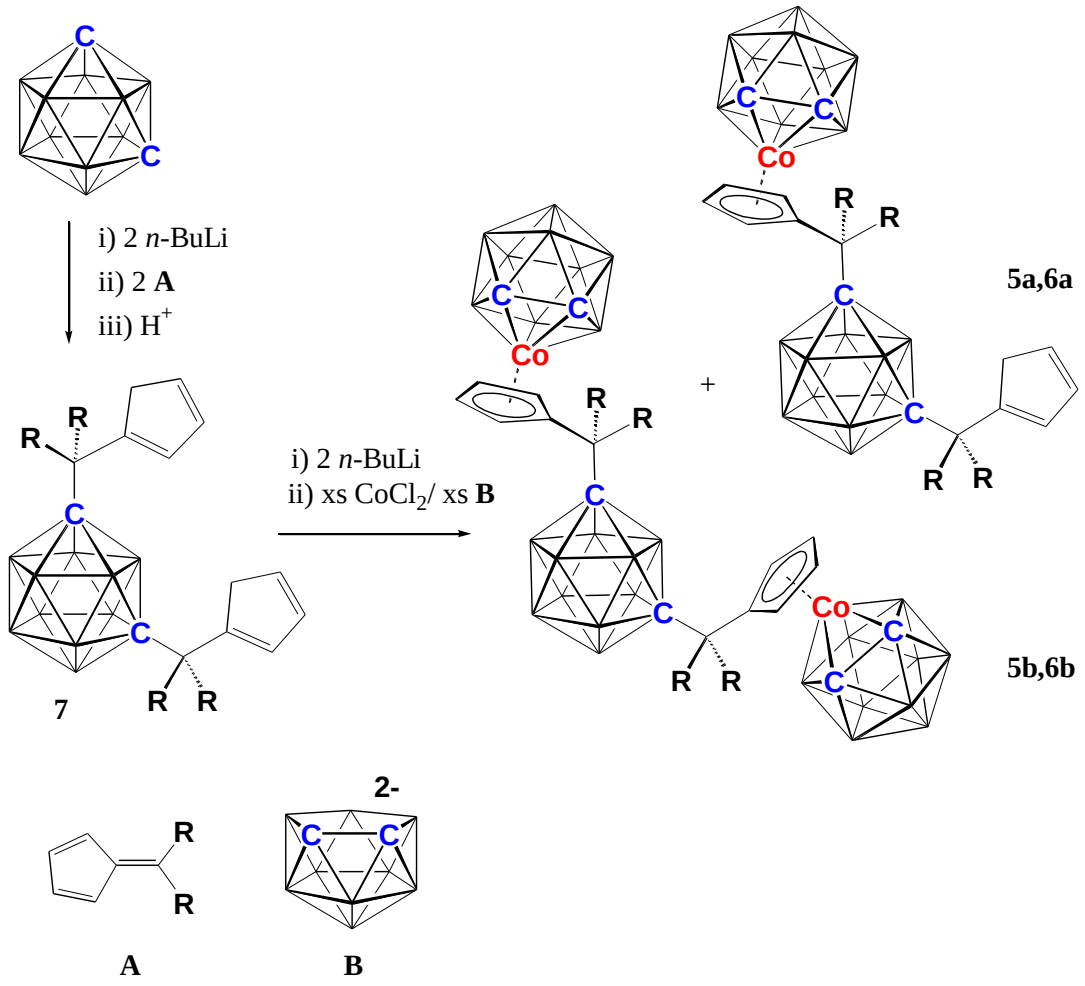

Scheme 2.3 Synthesis of Compounds 5-6 (5 - R=Me; 6 - R_2=Pm) Pm= pentamethylene

2.3.1 Multiple Cage Compounds Derived from 1,7-{$CMe_2(C_5H_5)$}$_2$-1,7-*closo*-$C_2B_{10}H_{10}$

Deprotonation of the C_5H_5 rings of **7a** followed by subsequent treatment with $CoCl_2$ and deprotonated $[HNMe_3][7,8\text{-}nido\text{-}C_2B_9H_{12}]$[12] (Scheme 2.3; R=Me) affords two compounds; the double-cage species 1-{$CMe_2(C_5H_5)$}-7-{CMe_2[3-(C_5H_4)-3,1,2-*closo*-$CoC_2B_9H_{11}$]}-1,7-*closo*-$C_2B_{10}H_{10}$ (**5a**) and the triple-cage species 1,7-{CMe_2[3-(C_5H_4)-3,1,2-*closo*-$CoC_2B_9H_{11}$]}$_2$-1,7-*closo*-$C_2B_{10}H_{10}$ (**5b**). Due to the extremely low yields, no further chemistry was carried out on **5a** or **5b**.

The ^{1}H NMR spectrum of **5a** shows two isomeric forms of the C_5H_5 moiety; the 1,3 diene (α) and the 1,4 diene (β). Multiplets at δ 6.48, δ 6.38 and δ 6.06 show telling similarites to those of the minor β isomer in compound **7a** (see chapter 3), therefore corresponding to the three olefinic protons in a 1,4 diene system. Likewise, the three resonances at δ 6.41, δ 6.32 and δ 6.22 show very similar chemical shifts to the olefinic protons of the major α isomer of **7a** and thus correspond to the 1,3 diene system of **5a**. The CH_2 units appear as multiplets at δ 2.95 and δ 2.87 for the β and α isomers respectively. All other resonances of **5a** are coincidences of both isomers. Multiplets at δ 5.71 and δ 5.35 are observed due to the four Co(C_5H_4) protons and the two cage CH protons are observed as a broad singlet at δ 3.92. Two pairs of methyl groups are observed as singlets at δ 1.48 and δ 1.32. The ratio of α:β, determined by the relative integrals, is 3:2.

Nineteen boron atoms are observed over eight resonances at δ 6.5 (1B), δ 3.5 (1B), δ -5.0 (3B), δ -6.5 (3B), δ -11.6 (6B), δ -14.6 (2B), δ -16.5 (2B) and δ -22.6 (1B) in the ^{11}B{^{1}H} NMR spectrum.

The mass spectrum of **5a** shows an isotopic envelope centred at *m/z* 546 with a complex pattern of boron isotopes and fragmentation occurring at *m/z* 411 indicative of the loss of the $C_2B_9H_{11}$ unit. Elemental analysis was in good agreement for that expected of $C_{20}H_{42}B_{19}Co$.

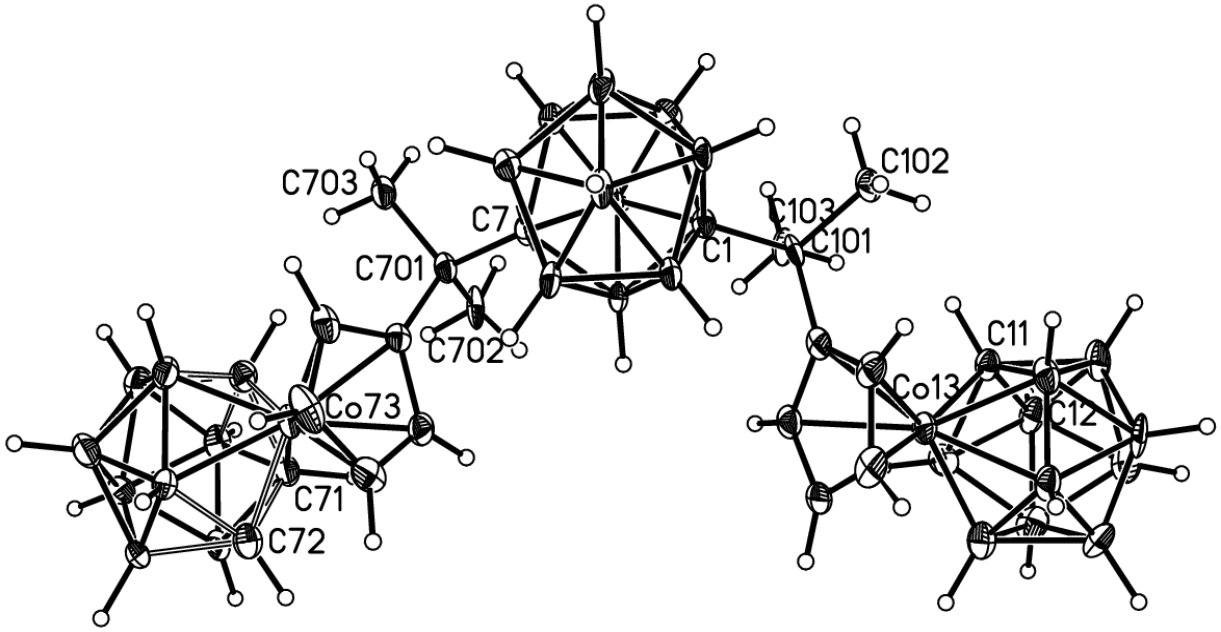

Figure 2.12 Molecular structure of triple-cage species 5b

Compound **5b** exhibits a simpler ^{1}H NMR spectrum showing two equivalent cobaltacarborane substituents on the central 1,7-*closo*-C_2B_{10} unit. The C_5H_4 units are signalled by multiplets centred on δ 6.15 and δ 5.96 each integrating as four protons. The methyl groups show as one singlet peak at δ 1.71 and a broad resonance at δ 4.47 corresponds to the four cage CH protons.

$^{11}B\{^{1}H\}$ NMR spectroscopy of **5b** reveals a total of twenty-eight boron atoms spread over eight relatively broad peaks at δ 5.5 (2B), δ 1.9 (2B), δ -6.0 (5B), δ -6.7 (5B), δ -11.8 (8B), δ -17.0 (4B), δ -21.6 (1B) and δ -22.9 (1B).

The mass spectrum of **5b** shows a complex isotopic envelope centred at *m/z* 736 with fragmentation occurring at *m/z* 728 and *m/z* 549. These are not straightforward fragmentations and are most likely the result of an intramolecular rearrangement of fragments during the ionisation process.

The molecular structure of **5b** was determined by X-ray crystallography (Figure 2.12). The substituents of the central 1,7 cage are orientated so that the C_5H_4 rings are facing onto the central cage and the cobaltacarborane clusters protrude outwards.

2.3.2 Multiple Cage Compounds Derived from 1,7-{CPm(C_5H_5)}$_2$-1,7-*closo*-$C_2B_{10}H_{10}$

Deprotonation of the C_5H_5 rings of **7b** followed by subsequent treatment with excess $CoCl_2$ and deprotonated $[HNMe_3][7,8\text{-}nido\text{-}C_2B_9H_{12}]$[12] (Scheme 2.3; R_2=Pm) affords two compounds; the double-cage species 1-{CPm(C_5H_5)}-7-{CPm[3-(C_5H_4)-3,1,2-*closo*-$CoC_2B_9H_{11}$]}-1,7-*closo*-$C_2B_{10}H_{10}$ (**6a**) and the triple-cage species 1,7-{CPm[3-(C_5H_4)-3,1,2-*closo*-$CoC_2B_9H_{11}$]}$_2$-1,7-*closo*-$C_2B_{10}H_{10}$ (**6b**). **6b** was only identified by mass spectrometry of the reaction mixture, after chromatographic removal of **6a**, and could not be isolated for any further characterisation. Due to the extremely low yield, no further chemistry was carried out on **6a**.

The ^{1}H NMR spectrum of **6a** also shows a mixture of α and β isomers of the C_5H_5 unit. Multiplets corresponding to the olefinic protons at δ 6.46, δ 6.41 and δ 6.07 show similarities to the major β isomer in compound **7b**. The olefinic protons of the α isomer appear at δ 6.53, δ 6.49 and δ 6.22 which are similar to those of **7b** (**7a** and **7b** are described in chapter 3). The CH_2 units are observed at δ 3.09 and δ 2.71 as broad doublets for the β and α isomers respectively. The ratio of α:β is 1:3. All other resonances of **6a** are coincidences of both isomers. The Co(C_5H_4) protons are observed over two multiplets at δ 5.52 and δ 5.29 each with an integral of two. The two cage CH protons are observed as a broad singlet at δ 3.90. The twenty protons of the two chemically inequivalent Pm units are observed over six broad multiplets over the range δ 2.40-0.90.

The ^{11}B{^{1}H} NMR spectrum of **6a** shows the same peak pattern as **5a** (1:1:3:3:6:2:2:1) with resonances at δ 6.2, δ 3.2, δ -5.1, δ -6.7, δ -11.8, δ -14.2, δ -16.5 and δ -22.7.

The mass spectrum of **6a** shows a complex carborane isotopic envelope centred at *m/z* 627 and no discernible fragmentation. Elemental analysis was in good agreement with that expected for $C_{26}H_{50}B_{19}Co$.

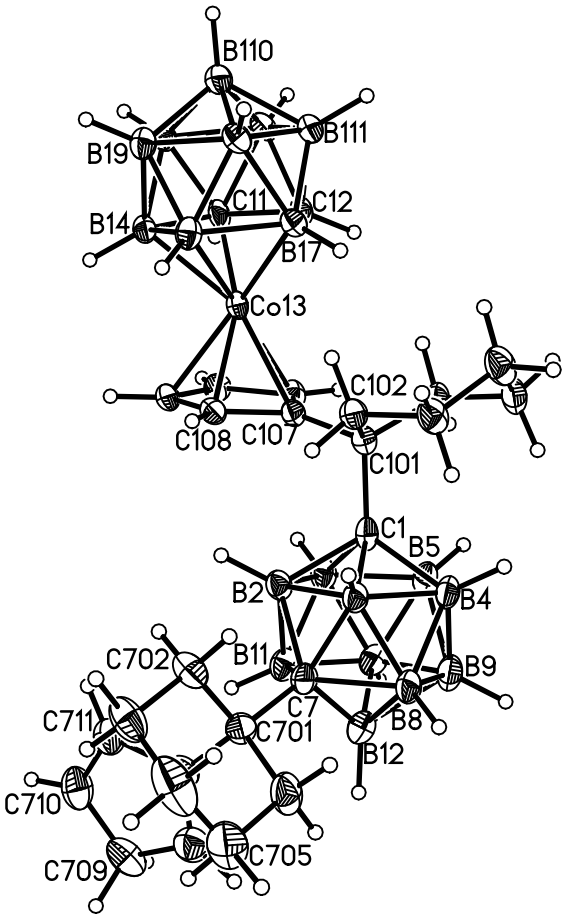

Figure 2.13 Molecular structure of double-cage species 6a, all rings are numbered cyclically

Table 2.4 Selected interatomic distances (Å) in 6a

C(1)-C(101)	1.597(5)	C(7)-B(12)	1.735(5)
C(7)-C(701)	1.591(5)	C(7)-B(11)	1.734(5)
Co-C(107)	2.136(3)	B(9)-B(10)	1.771(6)
Co-C(108)	2.049(3)	Co-C(12)	2.029(3)
Co-C(109)	2.030(3)	Co-B(17)	2.091(4)
Co-C(110)	2.049(3)	Co-B(18)	2.106(4)
Co-C(111)	2.081(3)	Co-B(14)	2.075(4)
C(11)-C(12)	1.633(4)	C(1)-B(2)	1.728(5)
C(707)-C(708)	1.376(5)	C(1)-B(3)	1.742(5)
C(708)-C(709)	1.473(5)	C(1)-B(4)	1.745(5)
C(709)-C(710)	1.445(5)	C(1)-B(5)	1.759(5)
C(710)-C(711)	1.372(5)	C(1)-B(6)	1.751(5)
C(707)-C(711)	1.458(5)	B(2)-B(3)	1.769(5)
Co-C(11)	2.029(3)	B(2)-B(11)	1.768(6)
C(7)-B(2)	1.713(5)	C(12)-B(17)	1.701(5)
C(7)-B(3)	1.721(5)	C(12)-B(111)	1.690(5)
C(7)-B(8)	1.755(5)	C(11)-B(14)	1.717(5)

The molecular structure of **6a** was determined crystallographically and is shown in Figure 2.13 and Table 2.4 presents some associated structural data. Both substituents of the 1,7 cage are similarly orientated with both C_5 rings pointing in approximately the same direction with the cobaltacarborane cage orientated away from the 1,7 cage. The dihedral angle between the C_5H_4 plane and the bottom belt of five boron atoms [B(19)-B(15)-B(16)-B(111)-B(112)] of the metallacarborane is 8.26° due to a slight steric interaction of the Pm unit on C(1) with the cobaltacarborane cluster, notably the short H···H distance of 1.966 Å between the protons on B(17) and C(102). The quaternary carbon atom C(101) is forced out of the plane of the adjacent C_5H_4 ring and is separated from this plane by 0.245 Å (Figure 2.14, *x*). This is significantly greater than the analogous distance involving the unmetallated C_5H_5, 0.069 Å. Despite this slight tilting of the C_5H_4 unit there is no slippage of the cobalt atom from the centre of the cluster.

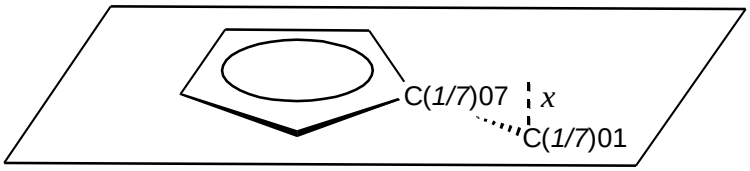

Figure 2.14 Distance, *x*, of quaternary carbon atom from plane of C_5H_4 unit

A comparison of the all the tetrahedral angles (six angles per tetrahedron) around both quaternary carbon atoms, C(101) and C(701), further shows the increased steric crowding between the Pm and the cobaltacarborane units. The angles at C(101) show larger deviations from the regular tetrahedral angle (~109.47°) than those at C(701). The C(1)-C(101)-C(107), C(1)-C(101)-C(106) and C(107)-C(101)-C(106) angles are 106.0(2)°, 113.5(3)° and 106.8(2)° respectively. In contrast, the largest tetrahedral angle deviation at C(701) is C(702)-C(701)-C(7), 111.4(3)°, the remaining angles only showing modest deviations.

The presence of the β CH_2 is confirmed by the contracted C-C bond distances of C(707)-C(708) and C(710)-C(711) at 1.367(5) Å and 1.372(5) Å respectively.

2.4 References

2.1 G. B. Dunks, M. M. McKeown and M. F. Hawthorne, *J. Am. Chem. Soc*., 1971, **93**, 2451.

2.2 A. S. F. Boyd, A. Burke, D. Ellis, D. Ferrer, B. T. Giles, M. A. Laguna, R. McIntosh, S. A. Macgregor, D. L. Ormsby, G. M. Rosair, F. Schmidt, N. M. M. Wilson and A. J. Welch, *Pure Appl. Chem.*, 2003, **75**, 9, 1325.

2.3 B. T. Giles, *PhD Thesis*, Heriot-Watt University, 2003.

2.4 H. Nakamura, K. Aoyagi and Y. Yamamoto, *J. Org. Chem*., 1997, **62**, 780.

2.5 C. O. Obenland and S. J. Papetti, *J. Org. Chem*, 1966, **31**, 3686.

2.6 M. G. Davidson, T. G. Hibbert, J. A. K. Howard, A. Mackinnon and K. Wade, *Chem. Commun*., 1996, 2285.

2.7 G. A. Jeffrey, *An Introduction to Hydrogen Bonding*, Oxford University Press, 1997, 12.

2.8 J. March, *March's Advanced Organic Chemistry: Reactions, Mechanisms and Structure*, Wiley-Interscience, 5th edition, 2001, 1065.

2.9 R. B. King, *J. Organomet. Chem.*, 2007, **692**, 1773.

2.10 E. Hong, Y. Kim and Y. Do, *Organometallics*, 1998, **17**, 2933.

2.11 (a) M. F. Hawthorne, *Angew. Chem. Int. Ed*., 1993, **32**, 950; (b) L. F. Tietze, U. Griesbach, U. Bothe, H. Nakamura and Y. Yamamoto, *ChemBioChem*, 2002, **3**, 219.

2.12 R. A. Wiesboeck and M. F. Hawthorne, *J. Am. Chem. Soc*., 1964, **86**, 1642.

Chapter 3 Synthesis of Crowded Ferrocenyl Compounds

3.1 Introduction

As seen in Chapter 2 there are several requirements essential for a suitable bulky group to facilitate polyhedral expansion via reduction and boron capitation.

The attached groups must be large enough so that it is impossible for two to fit on the adjacent carbon atoms of 1,2-*closo*-C_2B_{10}. One test would be to attempt to substitute these groups directly onto 1,2-*closo*-C_2B_{10} with formation of only the monosubstituted product being a positive result. The group must, ideally, also be easily attached to the carbon atoms of the cage using a small number of synthetic steps. The bulky groups should also be inert to sodium reduction (hence the unsuitability of compounds **1** and **3** from the previous chapter) and should be unreactive towards any capping $\{BR\}^{2+}$ fragments.

Deprotonated *meta*-carborane reacts readily with a variety of fulvene compounds to form bulky molecules containing a quaternary carbon atom attached directly to the cage carbon atom (Scheme 3.1).

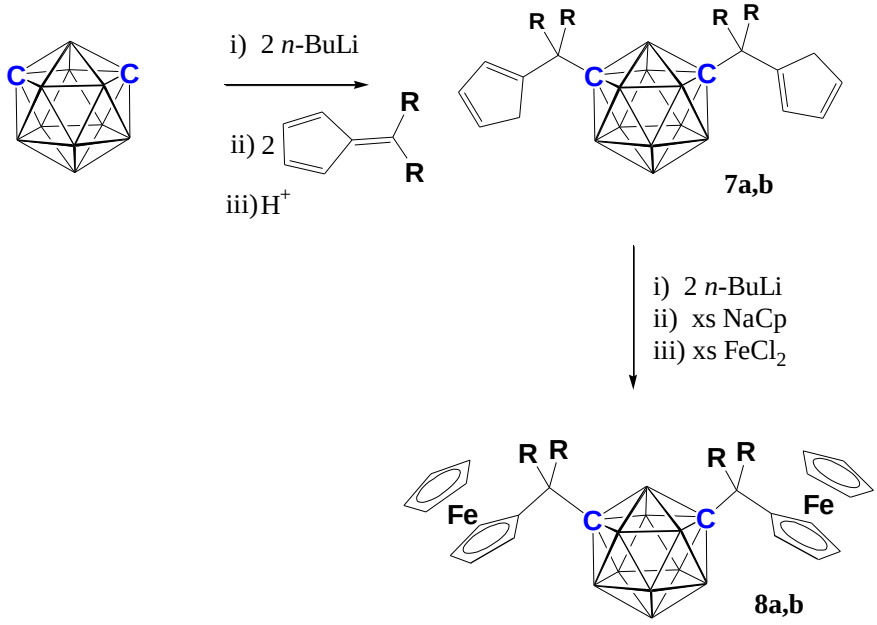

Scheme 3.1 Total route to bulky 1,7-$(CR_2Fc)_2$-1,7-*closo*-$C_2B_{10}H_{10}$ (a - R=Me, b - R_2=Pm)

Such groups can be modified into metallocene analogues to create a molecule with bulky groups that satisfy the requirements of unreactivity to sodium reduction and relative ease of preparation. Metallocenes offer the additional advantage of being coloured compounds resulting in simplified purification by the use of chromatography.

Are they, however, bulky enough to fulfil the ultimate aim of polyhedral expansion?

3.2 Bulky Groups Derived from 6,6-dimethylfulvene

3.2.1 Synthesis of 1,7-{$CMe_2(C_5H_5)$}$_2$-1,7-*closo*-$C_2B_{10}H_{10}$ (7a)

When 1,7-*closo*-$C_2B_{10}H_{12}$ is deprotonated with two equivalents of *n*-BuLi and treated with 6,6-dimethylfulvene in diethyl ether, the disubstituted 1,7-{$CMe_2(C_5H_5)$}$_2$-1,7-*closo*-$C_2B_{10}H_{10}$ (**7a**) is produced after aqueous work-up (Scheme 3.1; R = Me). When 1,2-*closo*-$C_2B_{10}H_{12}$ is subjected to the same conditions only the monosubstituted 1-{$CMe_2(C_5H_5)$}-1,2-*closo*-$C_2B_{10}H_{11}$ is produced suggesting the {$CMe_2(C_5H_5)$} unit has sufficient steric bulk for our purposes.

Mass spectrometric analysis of **7a** shows the parent ion to have a mass of 357 with a typical carborane envelope. Notable fragmentations are observed at *m/z* 341 (M - methyl group); *m/z* 327 (M - minus two methyl groups) and *m/z* 294 (M-{C_5H_5}). Elemental analysis was in good agreement with the expected values for $C_{18}H_{32}B_{10}$.

3.2.1.1 NMR Spectroscopy of 7a

Upon aqueous work-up, protonation of the {C_5H_4}$^-$ ring moiety can occur at either the α or the β position giving rise to a total of three molecular isomers (α-α, β-β and α-β protonated rings). ^{1}H NMR spectroscopy of **7a** (see one axis of Figure 3.1) shows what appears to be two C_5 ring isomers in *ca*. 2:1 ratio due to the presence of six olefinic protons in the region δ 6.05 - 6.62: the three multiplet peaks at δ 6.42, δ 6.30 and δ 6.23 have twice the integral of the three multiplet peaks at δ 6.62, δ 6.37 and δ 6.05.

Two sets of CH_2 signals (from $\{C_5H_5\}$) are also observed as multiplet peaks, one at δ 2.87 having double the integral of the other at δ 2.93. The four methyl groups for both isomers are observed as a coincident singlet at δ 1.31. As the two bulky side groups are amply far apart in the molecule an $\{\alpha\text{-}C_5H_5\}$ or $\{\beta\text{-}C_5H_5\}$ on the carbon atom on one side of the cluster has no bearing (at least in NMR terms) on the other bulky group on the other cage carbon atom hence why it appears only two isomers are observed when, in reality, there are likely to be three.

In the $^{11}B\{^1H\}$ spectrum of **7a** three resonances appear at δ 16.3 (2B), δ -12.0 (6B) and δ -14.2 (2B) which is not atypical of a high symmetry *closo* icosahedral carborane. The resonance at δ -12.0 containing six boron atoms constitutes the superposition of a 4B and a 2B signal.

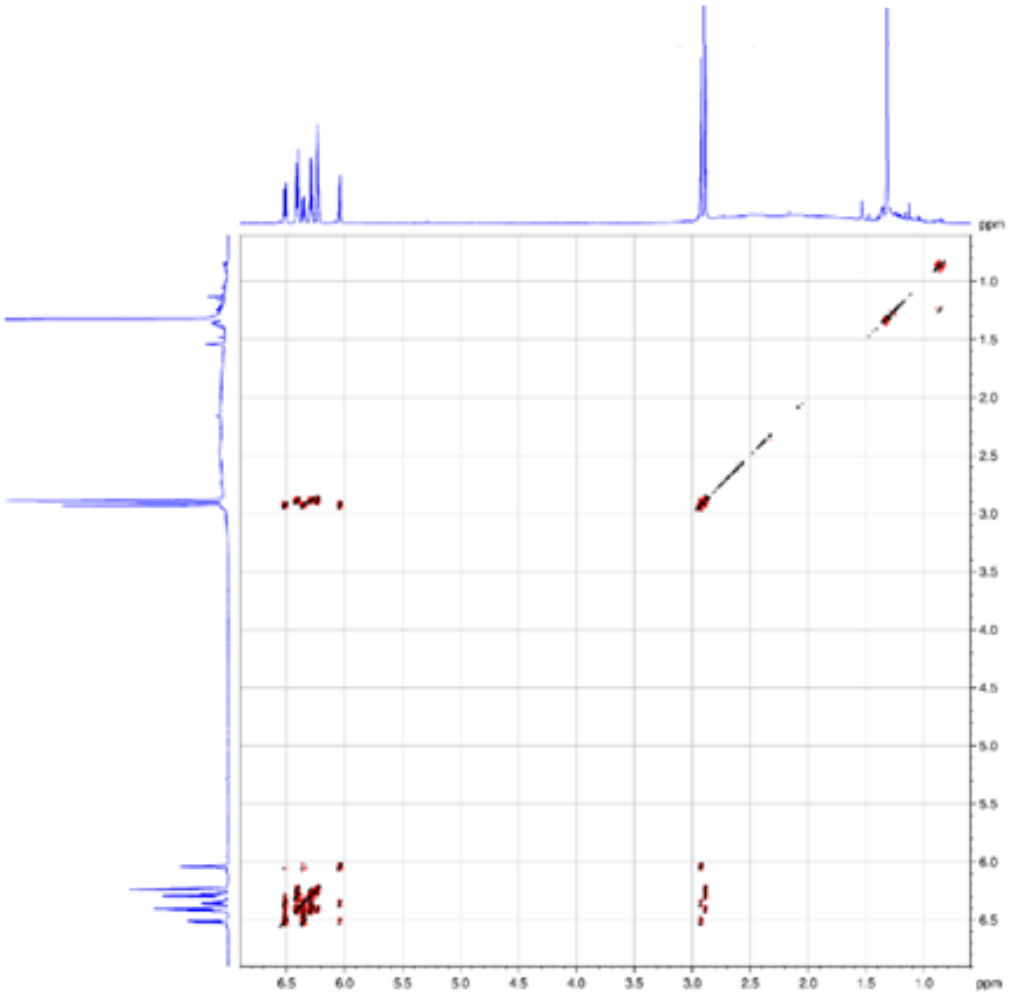

Figure 3.1 Full ^1H-^1H COSY NMR spectrum of 7a

To help identify which resonances belong to which C_5 ring isomer (α or β) the ^{1}H-^{1}H COSY NMR spectrum (Figure 3.1) was obtained. It is clearly seen by the correlation of CH and CH_2 peaks in the olefinic region (Figure 3.2) that there are two separate spin systems (α and β). The larger set of three multiplet peaks (δ 6.42, δ 6.30 and δ 6.23) correlate to the larger CH_2 multiplet at δ 2.87 and are representative of the major C_5 ring isomer. Similarly, the smaller set of three multiplet peaks (δ 6.52, δ 6.37 and δ 6.05) shows a correlation to the smaller of the CH_2 peaks indicative of the minor isomer at δ 2.93.

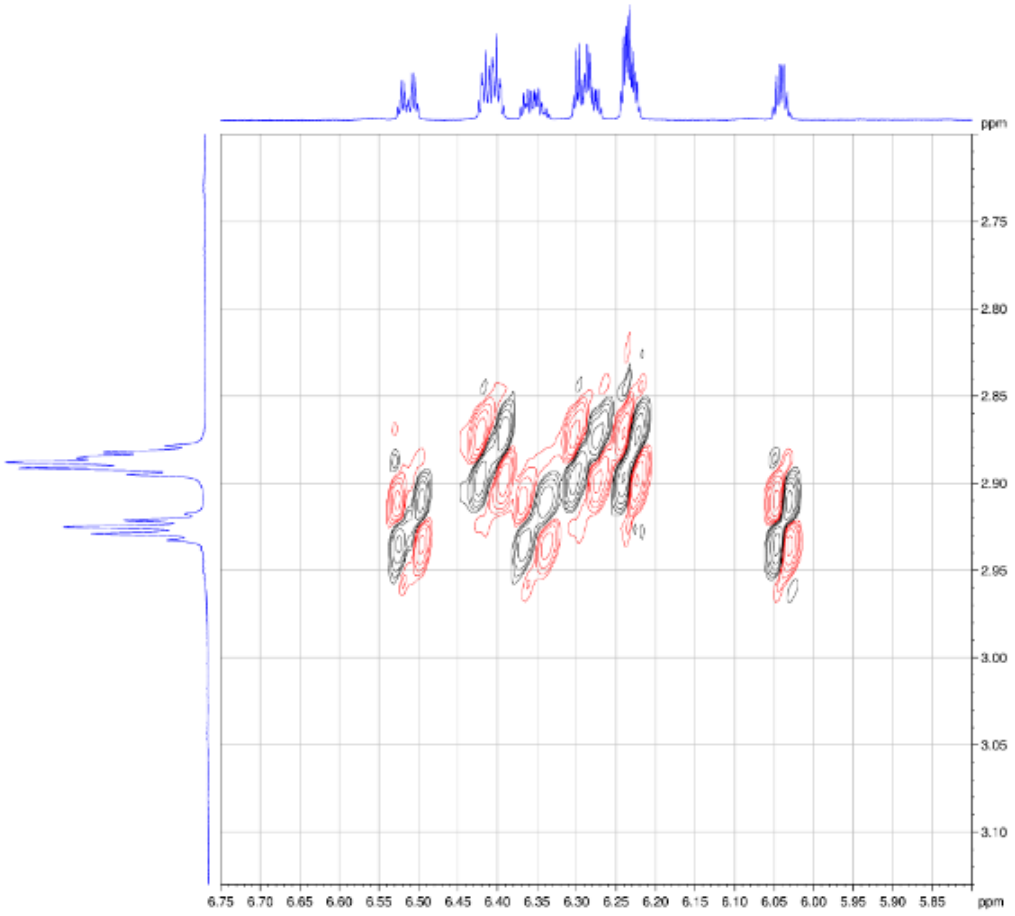

Figure 3.2 **Olefinic region of ^{1}H-^{1}H COSY NMR spectrum (horizontal axis – CH; vertical axis – CH_2)**

It was initially believed and reported[1] that the major isomer was the β ring due to the apparent absence of a π-conjugated ^5J coupling crosspeak (circled green where expected in Figure 3.3) corresponding to the two protons furthest apart in the β isomer. It was believed the α isomer would exhibit a π-conjugated ^4J coupling signal at δ 6.52 (circled blue) which, although weak, could potentially be observed in the spectrum. The

preference for β protonation was thought to be explained by steric effects that partially blocked off approach of H_3O^+ to the α positions. It is now apparent that the COSY spectrum alone cannot distinguish the identity of the two isomers.

Subsequent to publication[1], the ^1H-^1H NOE spectrum (Figure 3.4) was obtained revealing the major isomer to be, in fact, the α isomer.

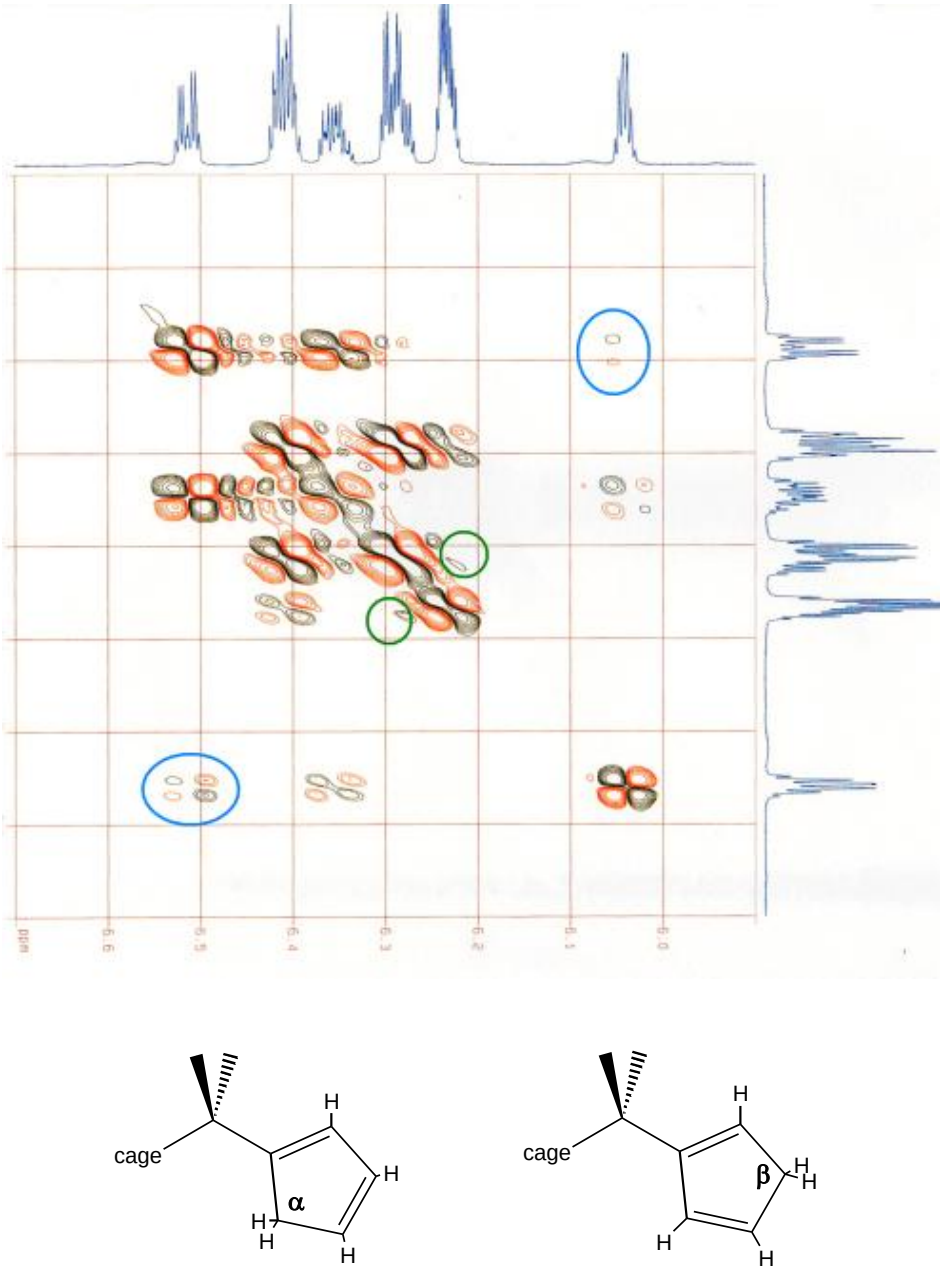

Figure 3.3 **top- olefinic CH region of ^1H-^1H COSY NMR of 7a; bottom- different isomeric forms of $CMe_2(C_5H_5)$ substituent**

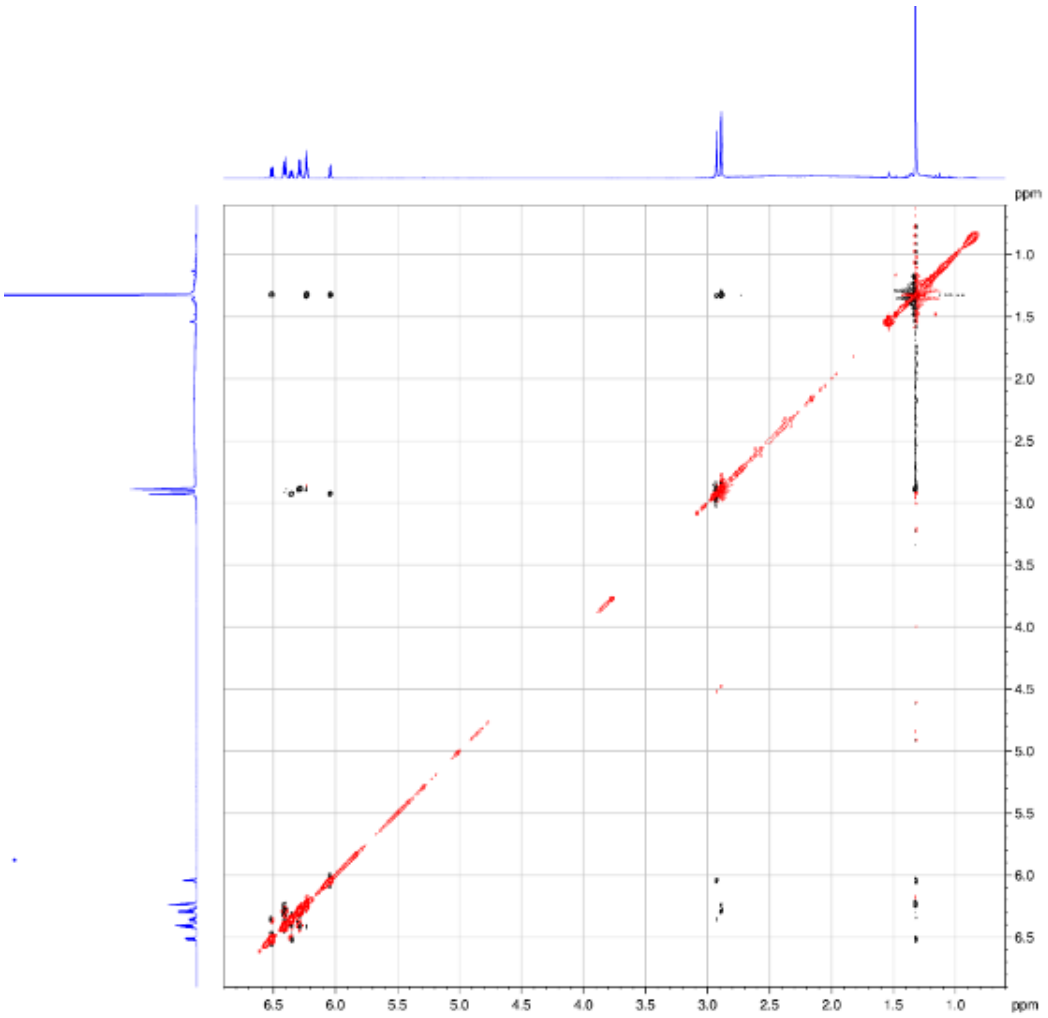

Figure 3.4 **^{1}H-^{1}H NOE spectrum of 7a**

The methyl groups in the unexpanded spectrum (i.e one axis of Figure 3.1) adjacent to both C_5 ring isomers appear as one coincident resonance at δ 1.32. Once expanded this peak resolves into two slightly overlapping singlets (methyl groups next to an α or β ring) separated by only a few thousandths of a ppm (vertical axis of Figure 3.5). As explained previously there are two C_5 ring isomers and hence a total of six olefinic protons are observed. The methyl groups show close proximity to three of these CHs: two from the minor isomer (δ 6.52 and δ 6.05) and only one from the major isomer (δ 6.23). Figure 3.6 shows that the minor isomer is the β as there are two olefinic protons nearby the methyl groups and only one proton nearby the methyl groups on the α isomer (Figure 3.6, black arrows).

Additionally, the NOE spectrum shows two strong through space interactions (red arrows - Figure 3.6 and Figure 3.7) between the β CH_2 at δ 2.93 and two olefinic protons whereas the α CH_2 at δ 2.87 only shows one strong correlation (and one

relatively weak interaction which is presumably due to one of the farther protons of the C_5H_5 unit).

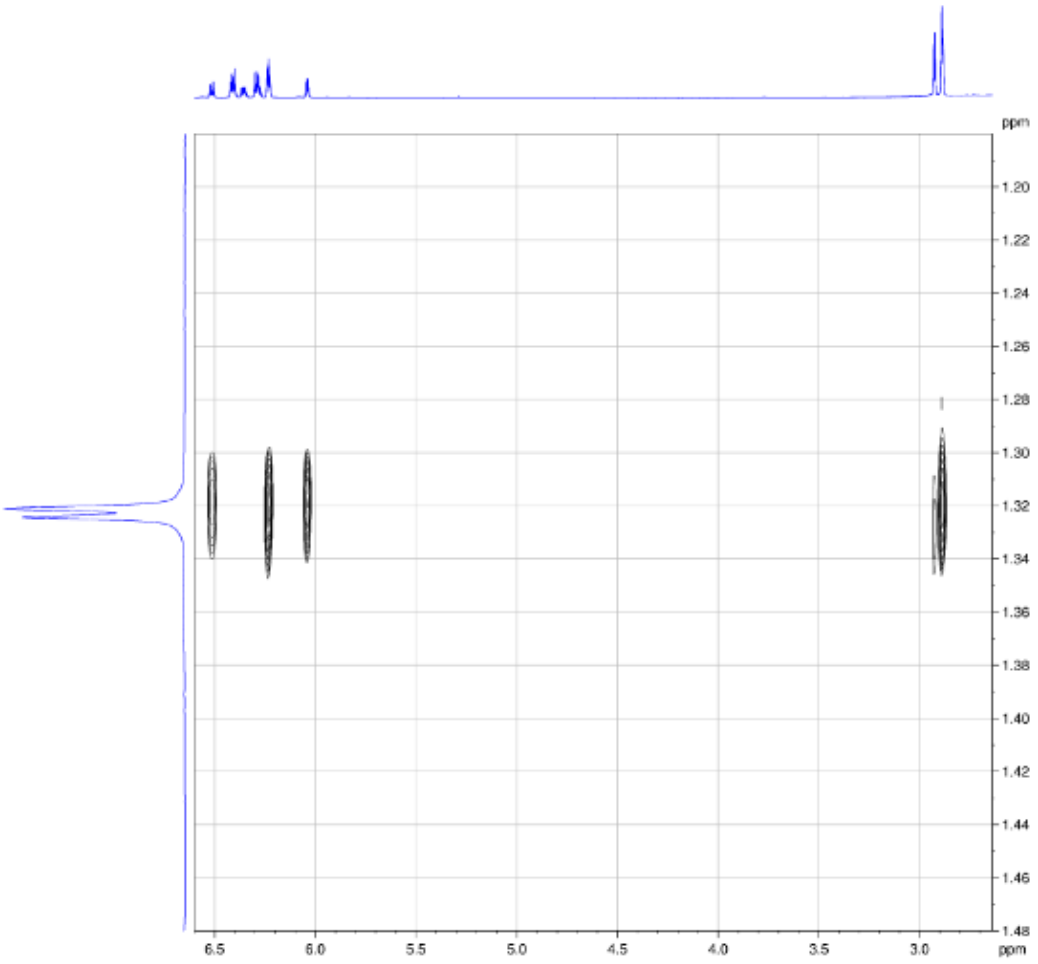

Figure 3.5 Olefinic region of NOE spectrum of 7a

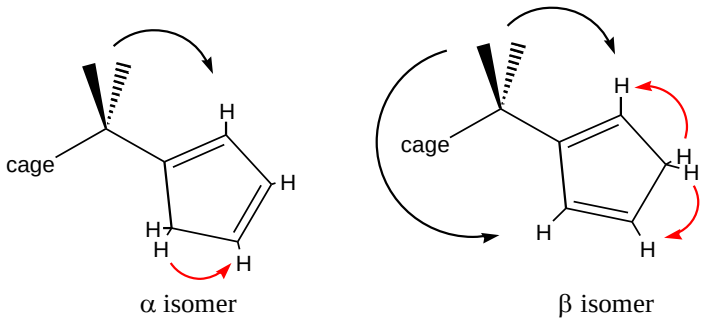

Figure 3.6 NOE interactions of *α* and *β* isomers of 7a

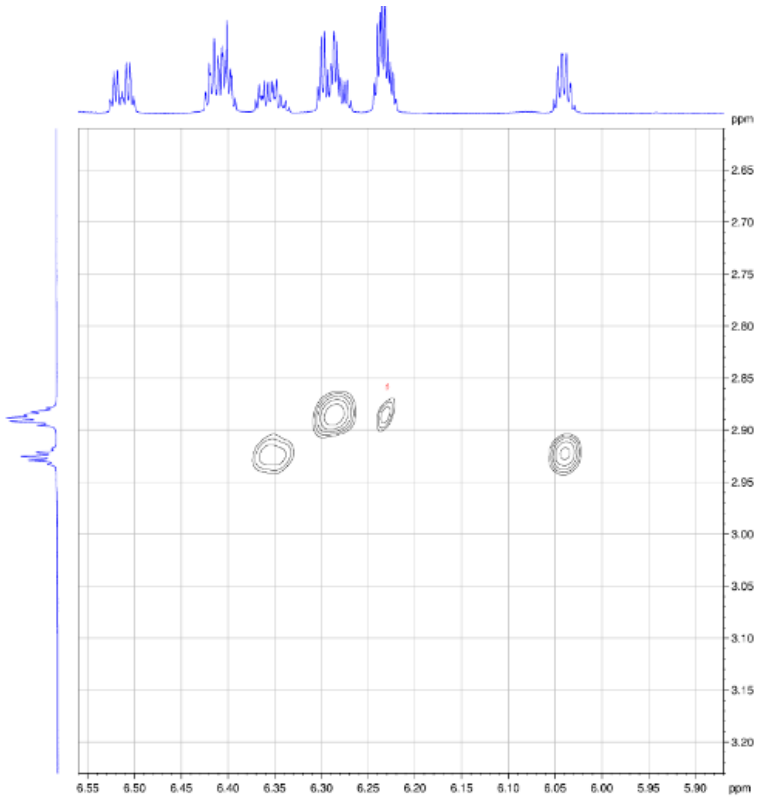

Figure 3.7 **NOE spectrum of 7a – olefinic region. Horizontal axis CH; Vertical axis CH_2**

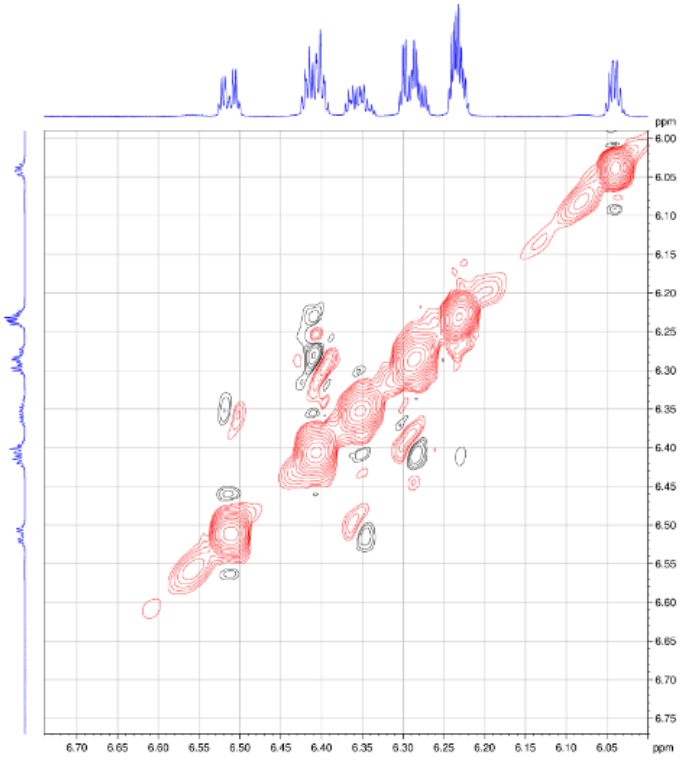

Figure 3.8 **NOE spectrum of 7a – olefinic region (CH's only)**

The NOE spectrum provides additional evidence for the β isomer being the minor one by examination of the olefinic region (Figure 3.8). The lowest frequency peak at δ 6.04 shows no correlation to either of the peaks at δ 6.52 and δ 6.37 (the smaller peaks). This would be expected as the β isomer has one isolated proton between the CH_2 and quaternary carbon atom and is too distant from the other olefinic protons to induce a NOE interaction. The α isomer, on the other hand, has all three olefinic protons (the larger peaks) on three adjacent carbon atoms, all of which show close proximity to at least one other proton.

3.2.1.2 Crystallography of 7a

A crystallographic study of **7a** (Figure 3.9) reveals a total of three complete and two half-molecules in the asymmetric fraction of the unit cell with the side groups consisting of a mixture of α and β isomers. The eight molecules in the cell are arranged as 4 × $\alpha\alpha$, 2 × $\beta\beta$ and 2 × $\alpha\beta$. This gives a 5:3 ratio in favour of the α isomer and is consistent with the aforementioned NMR studies (a 5:3 ratio over eight groups is close to the spectroscopically observed ratio of *ca*. 2:1).

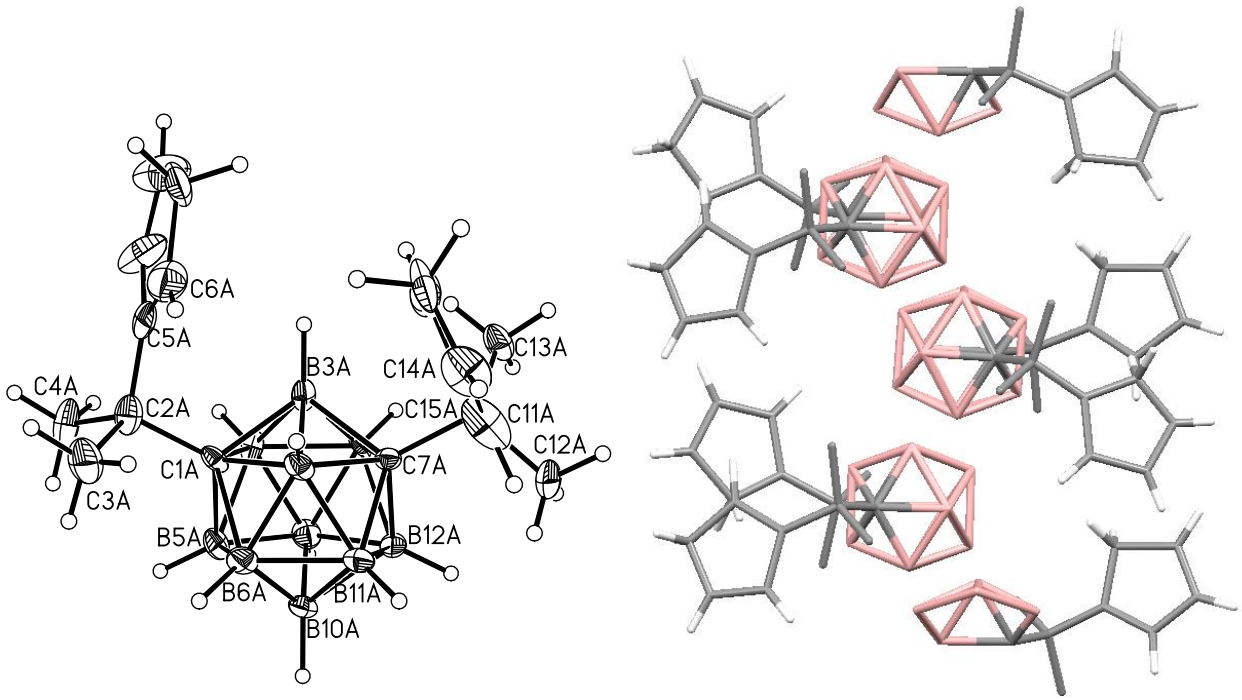

Figure 3.9 Molecular structure of the $\beta\beta$ form (left) and asymmetric unit (right, B*H* and CH_3 atoms omitted for clarity) of compound 7a

3.2.2 Synthesis of 1,7-{CMe_2Fc}$_2$-1,7-*closo*-$C_2B_{10}H_{10}$ (8a)

While the side groups of **7a** are potentially large enough to satisfy the requirement of steric bulk they actually require modification as the CH_2 group on the C_5 ring would be deprotonated by the sodium used in the reduction step. The [C_5H_5] rings were therefore converted into ferrocenyl groups by deprotonation with *n*-BuLi and addition of ten equivalents of both $FeCl_2$ and NaCp in THF to give 1,7-{CMe_2Fc}$_2$-1,7-*closo*-$C_2B_{10}H_{10}$ (**8a**) (Scheme 3.1; step 2) as a yellow solid in moderate yield. As would be expected, the $FeCl_2$ and the NaCp reagents do react together to form the thermodynamically stable ferrocene, hence the large excess of $FeCl_2$ and NaCp required. Although the addition of more of said reactants forms a larger quantity of ferrocene, the excess also gives the side groups on the carborane more chance to react to form a ferrocenyl group. Stoichiometric amounts of $FeCl_2$ and NaCp does, indeed, yield compound **8a** but the only evidence of its formation is from mass spectral analysis of the crude mixture subsequent to filtration through silica. The addition of more than ten equivalents of $FeCl_2$ and NaCp does not increase the overall yield of **8a**.

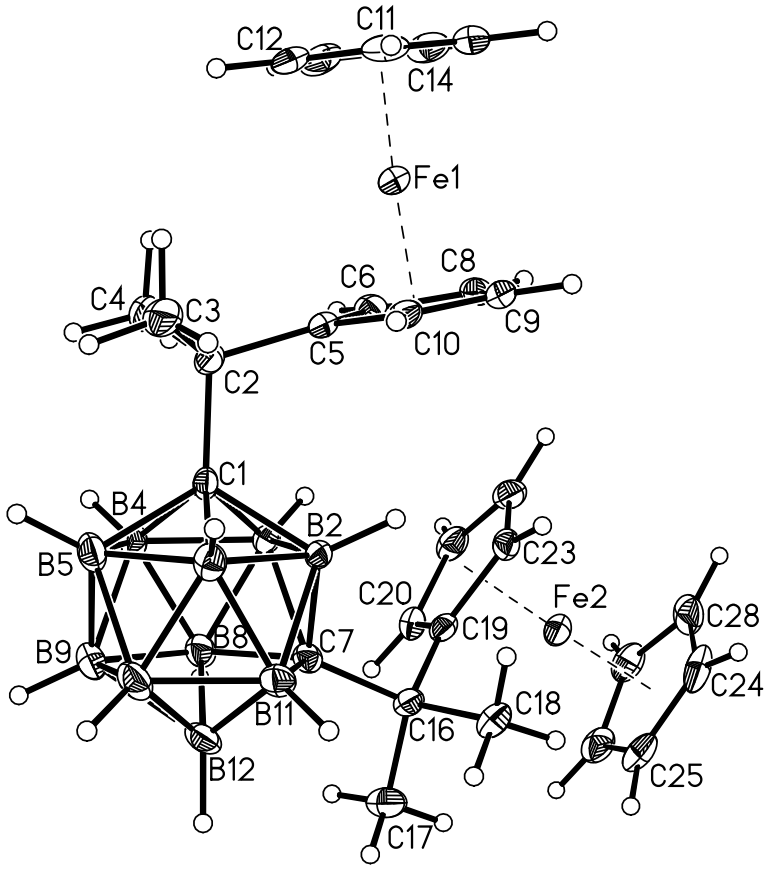

Figure 3.10 Molecular structure of icosahedral carborane 8a

The ^{1}H NMR spectrum of **8a** reveals a singlet at δ 4.10 that corresponds to the ten unsubstituted Cp protons. This peak is flanked by two multiplets at δ 4.15 and δ 4.01 which each integrate to four protons corresponding to the protons of the substituted ring. A further singlet is observed at δ 1.38 corresponding to the four methyl groups.

In the $^{11}B\{^{1}H\}$ spectrum of **8a** three resonances appear at δ -6.7 (2B), δ -12.2 (6B) and δ -14.1 (2B) which is representative of a high symmetry *closo* icosahedral carborane. The resonance at δ -12.2 containing six boron atoms constitutes the superposition of a 4B and a 2B signal.

Mass spectrometry shows typical carborane isotopic envelope centred at *m/z* 596 with very little fragmentation. Elemental analysis is in good agreement with that expected of $C_{26}H_{40}B_{10}Fe_2$.

The crystallographically determined structure shows the methyl groups pointing away from each other with the ferrocenyl groups near to a 'back to back' conformation (Figure 3.10). The ferrocenyl groups are slightly distorted to accommodate the methyl groups on the quaternary carbon atoms C(2) and C(16). The dihedral angles between the planes of the two C_5 rings of Fe(1) and Fe(2) are 3.72º and 3.68º respectively.

3.2.3 Reduction Reactions of 1,7-{CMe_2Fc}$_2$-1,7-*closo*-$C_2B_{10}H_{10}$

3.2.3.1 Reduction and Metallation of 1,7-{CMe_2Fc}$_2$-1,7-*closo*-$C_2B_{10}H_{10}$

Compound **8a** was reduced with sodium naphthalenide and capitated with a common transition metal fragment, $\{Ru(p\text{-cym})\}^{2+}$ to test the reducibility of the molecule. This yielded a 13-vertex metallacarborane as a yellow solid although in low yield (Scheme 3.2). Conventionally, the $2e^-$ reduction of a 1,7-*closo*-C_2B_{10} species would generate a 7,9-*nido* dianion and subsequent capitation with a transition metal fragment would afford the 4,1,6-MC_2B_{10} isomer.[2]

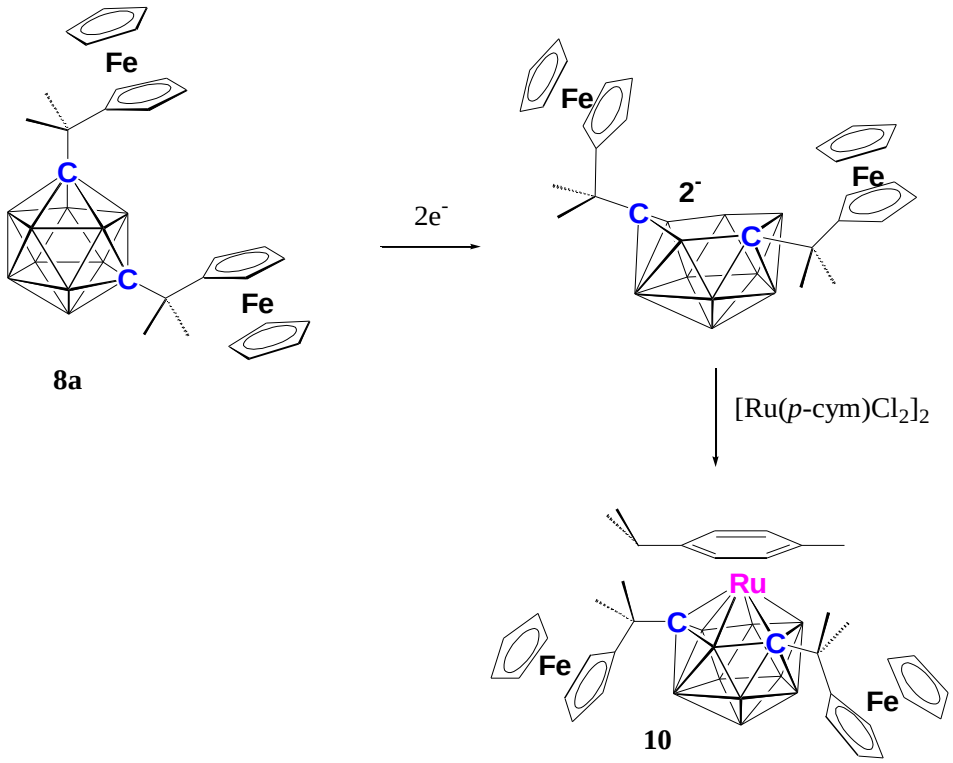

Scheme 3.2 Reduction and metallation of 8a to form a 13-vertex 4,1,6-ruthenacarborane

It is likely that the yellow compound formed is, in fact, 4-(*p*-cym)-1,6-$(CMe_2Fc)_2$-4,1,6-*closo*-$RuC_2B_{10}H_{10}$ (**10**) but without an X-ray crystallographic study the identity of the isomer cannot be accurately known. Some 4,1,6-metallacarboranes (specifically 4,1,6-MC_2B_{10} cobaltacarboranes) are known to isomerise to the 4,1,8- isomer and again to the 4,1,12 isomer at relatively low temperatures. However, 4,1,6-ruthenacarboranes are not known to rearrange easily in this way.[3]

The mass spectrum of **10** shows a broad B isotopic envelope centred on *m/z* 832. There is a peak at *m/z* 646 ascribed to the loss of a ferrocenyl unit.

The $^{11}B\{^1H\}$ NMR spectrum of **10** shows a range of resonances typical of a 13-vertex 4,1,6-ruthenacarborane.[4] Eight resonances appear at δ 15.0 (1B), δ 5.5 (1B), δ 1.8 (1B), δ -3.5 (1B), δ -5.6 (2B), δ -8.2 (1B), -12.5 (2B) and δ -20.4 (1B). This splitting pattern is consistent with the expected low symmetry of the cage assuming that both 2B peaks are coincidental overlaps of two single-intensity peaks.

The ^{1}H NMR spectrum of **10** shows the four aromatic H atoms as four doublets between δ 5.09 – 5.64. Four multiplets attributed to one proton each on the substituted Cp rings can be seen at δ 4.47, δ 4.30, δ 4.24 and δ 4.05. The remaining four proton resonances are observed as broad multiplets at δ 4.17 and δ 4.12. These resonances also incorporate five protons each belonging to the unsubstituted Cp ring therefore each resonance integrates to seven protons in total. The apparent non-equivalence of H atoms is due to restricted rotation of the entire CMe_2Fc substituents caused by their intrinsic steric bulkiness. The same non-symmetrical nature of the metallacarborane causes the splitting of the two *i*-propyl CH_3 groups into doublets (δ 1.14 and δ 1.12, 3H each). The isopropyl methine H appears at δ 2.62, not as the expected septet but as a broad multiplet. The singlet for the *p*-cymene CH_3 is at δ 2.11. The *p*-cymene peaks in the ^{1}H NMR spectrum show considerable broadening suggesting the bulky side groups restrict rotation of this ligand. The four methyl groups between the cage and the ferrocenyl groups give rise to four separate singlet resonances at δ 2.11, δ 1.77, δ 1.74 and δ 1.62.

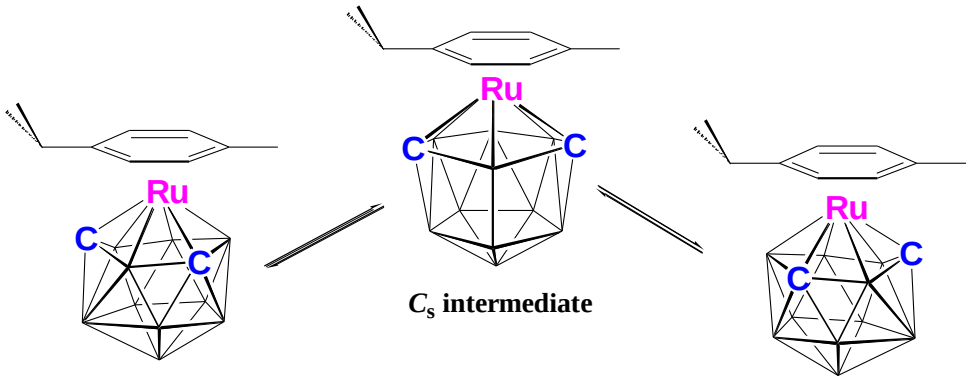

Figure 3.11 Fluxional process in 4,1,6- isomer of an uncrowded ruthenacarborane

The molecular rigidity of **10** is in contrast to that of uncrowded analogues (e.g. 4-(*p*-cymene)-4,1,6-*closo*-$RuC_2B_{10}H_{12}$[5]) where the ^{1}H and ^{11}B NMR spectra imply fluxionality in solution at room temperature (Figure 3.11). This involves a C_s-symmetric transition state, the symmetry of which affords 1:1:1:1:2:2:2 splitting in the ^{11}B spectrum. The splitting pattern of **10** is inconsistent with this (**10** affords a 1:1:1:1:2(1+1):1:2(1+1):1 pattern) rendering all boron atoms inequivalent. ^{1}H NMR spectroscopy of uncrowded species implies a mirror plane through the *p*-cymene as two pairs of aromatic protons are observed and the two *i*-propyl methyl groups are observed as one signal. Even though the fluxionality is, in all probability, still occurring in **10** the

restricted rotation of the *p*-cymene ligand and the CMe_2Fc substituents rarely allows for an overall C_s-symmetric species in solution.

The major product from this reaction, however, was found to be a dark red solid 1,2-$(CMe_2Fc)_2$-1,2-*closo*-$C_2B_{10}H_{10}$ **(9a)**. This was, surprisingly, the reoxidised 12-vertex 1,2-isomer in high yield (65%). Compound **9a** can also be prepared directly in 73% yield by reduction of the 1,7 isomer **8a** followed by re-oxidation in air (Scheme 3.3). This method also yields an uncharacterised light pink product in extremely low yield.

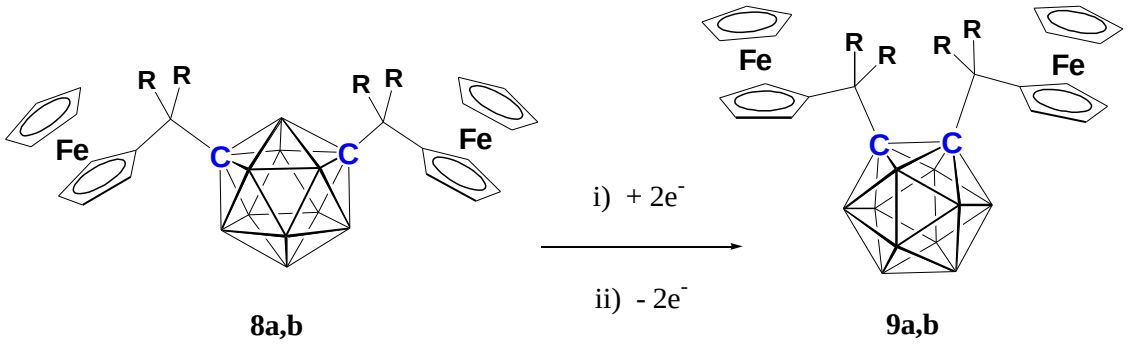

8a,b **9a,b**

Scheme 3.3 Reduction and oxidation of 1,7-(CR_2Fc)-1,7-*closo*-$C_2B_{10}H_{10}$, 8, generating the sterically-crowded 1,2 species, 9 (a - R=Me, b - R_2=Pm)

The mass spectrum of **9a** is identical to that of the 1,7-analogue **8a** but fragmentation is this time observed with peaks at *m/z* 370 (M-{CMe_2Fc}) and *m/z* 227 ({CMe_2Fc}) indicating the loss of an entire side group and showing that **9a** is more susceptible to fragmentation than **8a**. Elemental analysis is in good agreement with that expected for $C_{26}H_{40}B_{10}Fe_2$.

As to be expected the ^{1}H NMR spectrum of **9a** is similar to that of **8a**, the only major difference being that both sets of proton resonances from the substituted ring (δ 4.24 and δ 4.15, both 4H) are shifted to higher frequency than the Cp signals of the ten protons of the two unsubstituted rings at δ 4.12. The singlet peak corresponding to the four methyl groups is observed at δ 1.87.

The $^{11}B\{^1H\}$ NMR spectrum shows a splitting pattern of 2:4:2:2 as is expected of a high symmetry 1,2-*closo*-C_2B_{10} isomer. Resonances appear at δ -2.6 (2B), δ -6.6 (4B), δ -7.9

(2B), δ -12.6 (2B). The peaks in the ^{11}B NMR spectrum of the 1,2 isomer **9a** are slightly broader than those of the 1,7 analogue **8a.** This phenomenon is possibly the result of the increased steric crowding restricting free rotation of the bulky side groups.

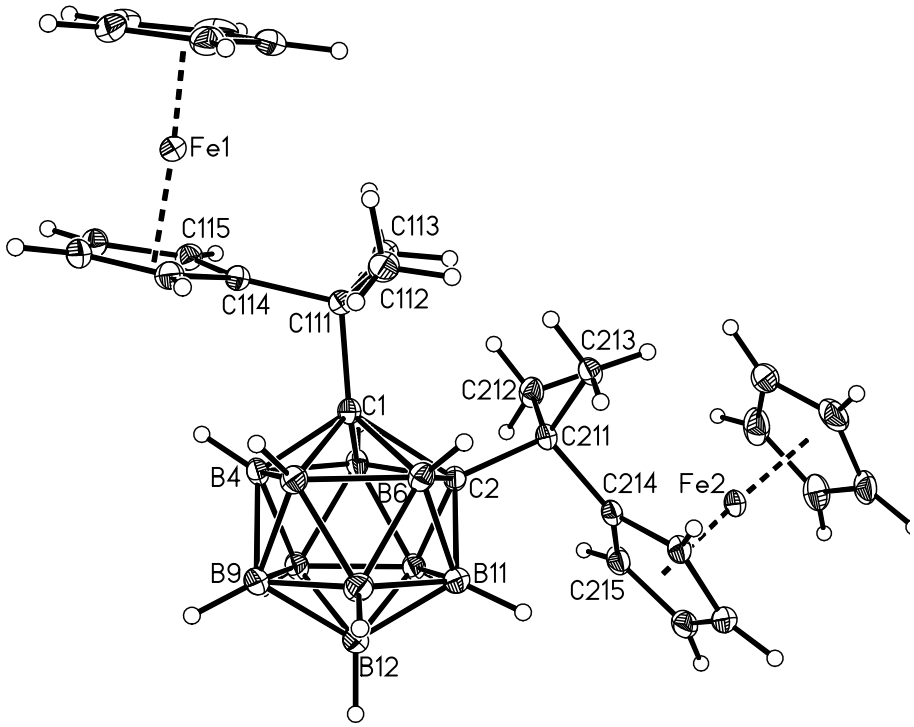

Figure 3.12 Molecular structure of compound 9a

In the crystallographically determined structure of **9a** (Figure 3.12) the two sets of methyl groups interdigitate with each other about an effective C_2 axis from the mid-point of C(1)-C(2) to the mid-point of B(9)-B(12) and the ferrocenyl groups are now as far apart as possible orientated away from each other. The carborane C-C distance is stretched to 1.9378(16) Å *cf*. 1,2-*closo*-$C_2B_{10}H_{12}$ where two independent C-C distances are 1.629(6) Å and 1.630(6) Å.[6] The ferrocenyl groups are slightly distorted to accommodate the methyl groups on the quaternary carbon atoms C(111) and C(211). The dihedral angles between the planes of the two C_5 rings of Fe(1) and Fe(2) are 3.99º and 5.04º respectively. A more detailed discussion of the molecular structure is presented later in this chapter.

3.2.3.2 Attempted Synthesis of a Supraicosahedral Carborane

Given that the reduction and metallation of **8a** to form a 13-vertex metallacarborane was successful (albeit in low yield), a capitation was attempted with a $\{BPh\}^{2+}$ fragment with the aim of creating a 13-vertex carborane.

The reduced species was taken up in toluene and $BPhCl_2$ was added at –78°C. Along with a large amount of **9a,** 1,2-$(CMe_2Fc)_2$-4-OH-1,2-*closo*-$C_2B_{10}H_9$ **(11)**, a deep purple solid, was isolated in low yield (17%) after work-up. The presence of a hydroxyl group attached to the cage was unanticipated but may have been caused by H_2O contamination during oxidation. Although rare, there is precedent for hydroxylation reactions in the literature: 2-OH-1,12-*closo*-$C_2B_{10}H_{11}$ has been identified as a minor product in palladium-catalysed nucleophilic substitutions on 2-I-1,12-*closo*-$C_2B_{10}H_{11}$ also thought to occur by H_2O contamination.[7]

The mass spectrum of **11** shows a broad B isotopic envelope centred at *m/z* 612 with fragmentation occurring through the loss of CMe_2Fc substituents (peaks at *m/z* 385 and *m/z* 227).

The ^{11}B NMR spectrum of **11** shows a narrow range of peaks from δ -1.3 to δ -19.0 (a total of 9B) typical of a *closo*-carborane. These peaks show coupling to ^1H and appear as doublets. The remaining B atom shows no coupling to ^1H and is at the relatively high frequency of δ 8.1. This is assigned to the B-OH vertex.

Due to the loss of the apparent C_2 axis that runs through the C-C bond in **9a**, ^1H NMR spectroscopy of **11** reveals that all the CH protons on the substituted Cp rings are inequivalent. These eight protons are observed over five different multiplets: peaks at δ 4.36 and δ 4.30 integrating as one proton each, a very broad and untidy multiplet at δ 4.20 integrates as four protons whilst the remaining two proton resonances are included in two different broad multiplets which each also incorporate the five Cp protons at δ 4.15 and δ 4.11. The presence of four different methyl group resonances is also indicative of the low symmetry of **11**. Four singlet methyl resonances are observed at δ 1.92, δ 1.91, δ 1.89 and δ 1.72. There is no resonance attributed to the B-OH proton but this is most likely due to the quadrupolar nature of the ^{11}B nucleus causing significant broadening of this peak.

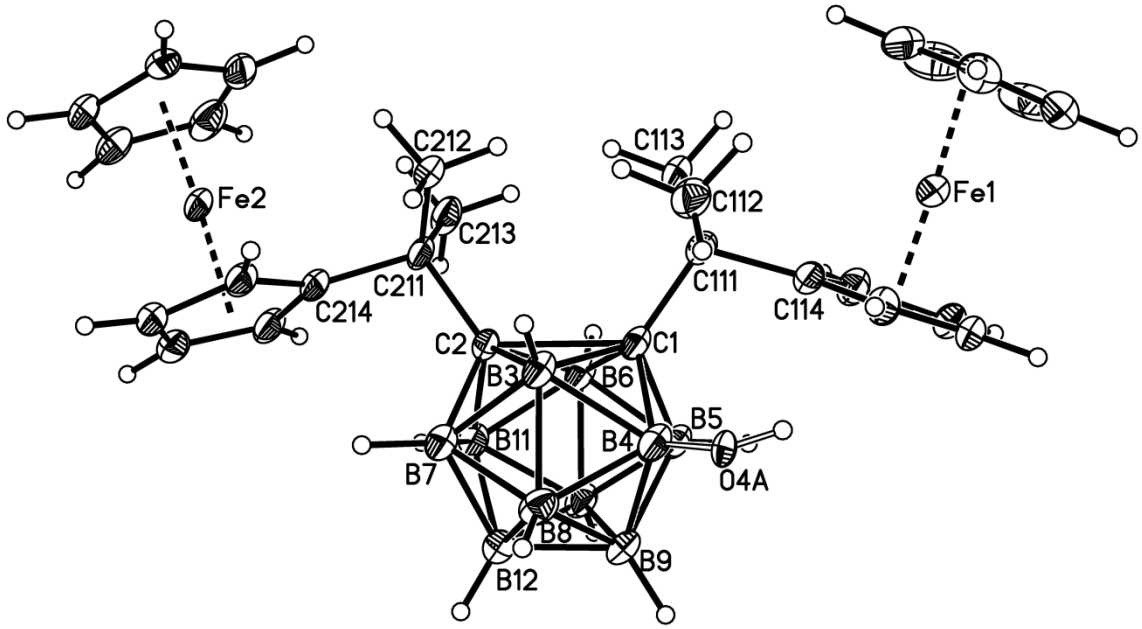

Figure 3.13 Molecular structure of compound 11

The crystallographically-determined structure (Figure 3.13) has the hydroxyl group on B(4) partially occupied (0.35) and disordered over four sites [B(5) (0.2), B(11) (0.2) and B(7) (0.25)] affording one hydroxyl group per cage. The arrangement of the CMe_2Fc substituents is analogous to the arrangement in **9a** with interlocking methyl groups. The C(1)-C(2) bond distance has increased to 2.102(3) Å with the presence of this B-substituted OH group possibly due to increased steric crowding from the hydroxyl group pushing the adjacent substituent on C(1) further up. The dihedral angles between the planes of the two C_5 rings of Fe(1)and Fe(2) are 5.02º and 3.62º respectively compared with 5.04º and 3.99º in **9a**.

3.3 Bulky Groups Derived from 6,6-pentamethylenefulvene

The method of substituting 1,7-*closo*-$C_2B_{10}H_{12}$ with bulky groups and electronically converting it to 1,2-*closo*-C_2B_{10} via a two electron reduction and subsequent oxidation is a new way to prepare sterically crowded 1,2-*closo*-C_2B_{10} derivatives with substituents that are too bulky to attach by direct methods.

3.3.1 Synthesis of 1,7-{CPm(C_5H_5)}$_2$-1,7-*closo*-$C_2B_{10}H_{10}$ (7b)

The molecular structure of **9a** shows there is barely enough space for the CMe_2Fc substituents to fit onto adjacent carbon atoms in 1,2-*closo*-C_2B_{10}. It was hoped that an even bulkier substituent may, in fact, prevent the movement of the carbon atoms of [7,9-*nido*-$C_2B_{10}]^{2-}$ altogether, preventing reoxidation back to 1,2-*closo*-C_2B_{10}. This could potentially be achieved by the reaction of deprotonated 1,7-*closo*-$C_2B_{10}H_{12}$ with a larger fulvene. 6,6-Pentamethylenefulvene was used as a starting material (Scheme 3.1, R_2=Pm) for synthesising 1,7-{CPm(C_5H_5)}$_2$-1,7-*closo*-$C_2B_{10}H_{10}$ **(7b)**. The synthesis is very similar to that of the methyl analogue, the only difference being the extended reaction time required to obtain suitable yields (twenty hours instead of just four) presumably due to the more bulky nature of 6,6-pentamethylenefulvene.

Mass spectrometric analysis of **7b** shows the parent ion to have a mass of 437 with a typical broad carborane isotopic envelope. One fragmentation is observed at *m/z* 370 (M – {C_5H_5}). Elemental analysis was in good agreement with the expected values for $C_{24}H_{40}B_{10}$.

3.3.1.1 NMR Spectroscopy of 7b

^{1}H NMR spectroscopy (see one axis of Figure 3.14) shows, as is the case in **7a**, a mixture of isomers is formed with protonation occurring at the α or β position of the C_5 ring giving rise to a total of three molecular isomers. The minor C_5 ring isomer shows three olefinic multiplet peaks at δ 6.47, δ 6.32 and δ 6.18. The major C_5 ring isomer reveals two peaks in this region: one multiplet for one proton at δ 6.03 and a larger multiplet at δ 6.38 that integrates for two protons, the superposition of two single proton resonances. The CH_2 moieties on the {C_5H_5} groups appear as two slightly overlapping

broad multiplets between δ 2.73 and δ 3.12. The CH_2 peak which corresponds to the major C_5 ring isomer appears at a higher frequency than that of the minor isomer. The CH_2 units of the pentamethylene ring appear in the normal aliphatic region of the spectrum. The major isomer shows two protons (presumably a methylene unit) as a narrow multiplet at δ 2.08 and the minor isomer an equivalent resonance at δ 1.90. The remainder of these CH_2 resonances all lie beneath the two very broad, lumpy peaks at δ 1.45 and δ 1.03 which integrate for six protons and two protons respectively. These are coincident resonances of both *α* and *β* ring isomers.

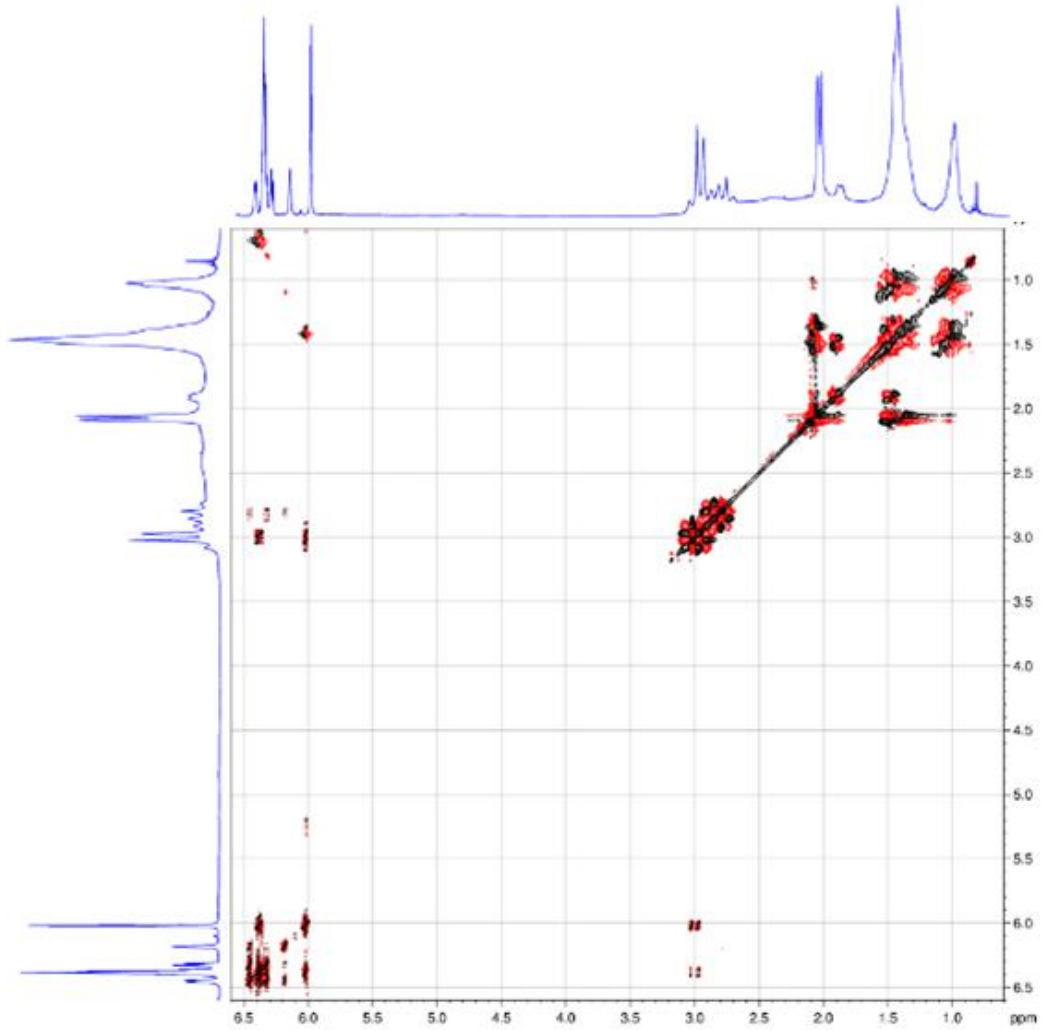

Figure 3.14 ^{1}H-^{1}H COSY NMR spectrum of 7b

In the $^{11}B\{^{1}H\}$ spectrum of **7b** three resonances appear at δ -6.6 (2B), δ -12.3 (6B) and δ -14.7 (2B) which is typical for a high symmetry *closo* icosahedral carborane. The resonance at δ -12.3 containing six boron atoms constitutes the superposition of a 4B and a 2B signal.

As with compound **7a** the nature of protonation can only be identified with a series of 2D correlation spectra. The ^{1}H-^{1}H COSY spectrum was obtained (Figure 3.14).

Inspection of the olefinic region of the COSY spectrum (Figure 3.15) reveals two spin systems, one for each isomeric form. The smaller (minor isomer) proton resonances at δ 6.47, δ 6.32 and δ 6.18 correlate to the smaller CH_2 resonance at δ 2.83. Consequently, the remaining three olefinic CH protons at δ 6.03 and δ 6.38 (a 1+1 coincidence) show much stronger crosspeaks to the larger of the CH_2 resonances indicative of the major isomer.

As was the case with the methyl analogue **7a** the identity of the major and minor isomer cannot be distinguished by COSY spectroscopy. The ^{1}H-^{1}H NOE spectrum (Figure 3.16), however, does clarify which peaks correspond to which isomer.

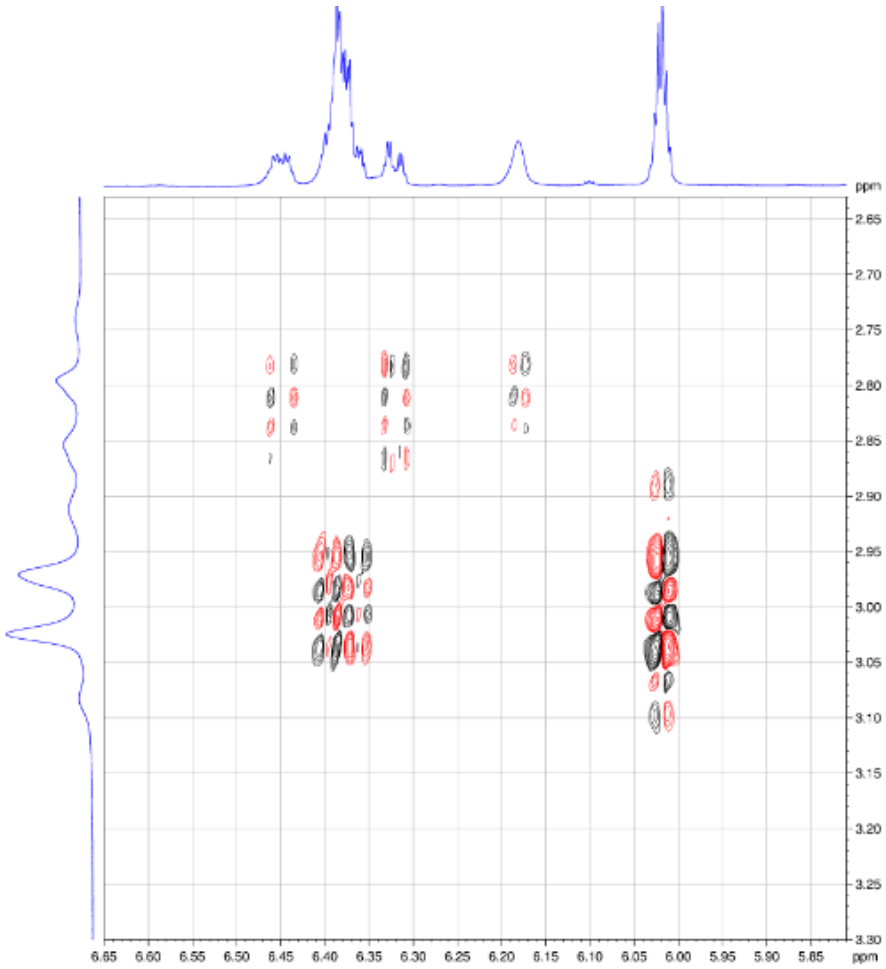

Figure 3.15 ^{1}H-^{1}H COSY NMR of compound 7b – olefinic region. Vertical axis CH_2, horizontal axis CH resonances

The $\{C_5H_5\}$ ring region of the NOE spectrum (Figure 3.18) shows the major C_5 ring isomer CH_2 bearing close proximity to two olefinic protons whereas the minor C_5 ring isomer CH_2 only shows a correlation to one olefinic proton. This is the expected pattern for the major isomer being the *β* one as deduced from Figure 3.17 (red arrows).

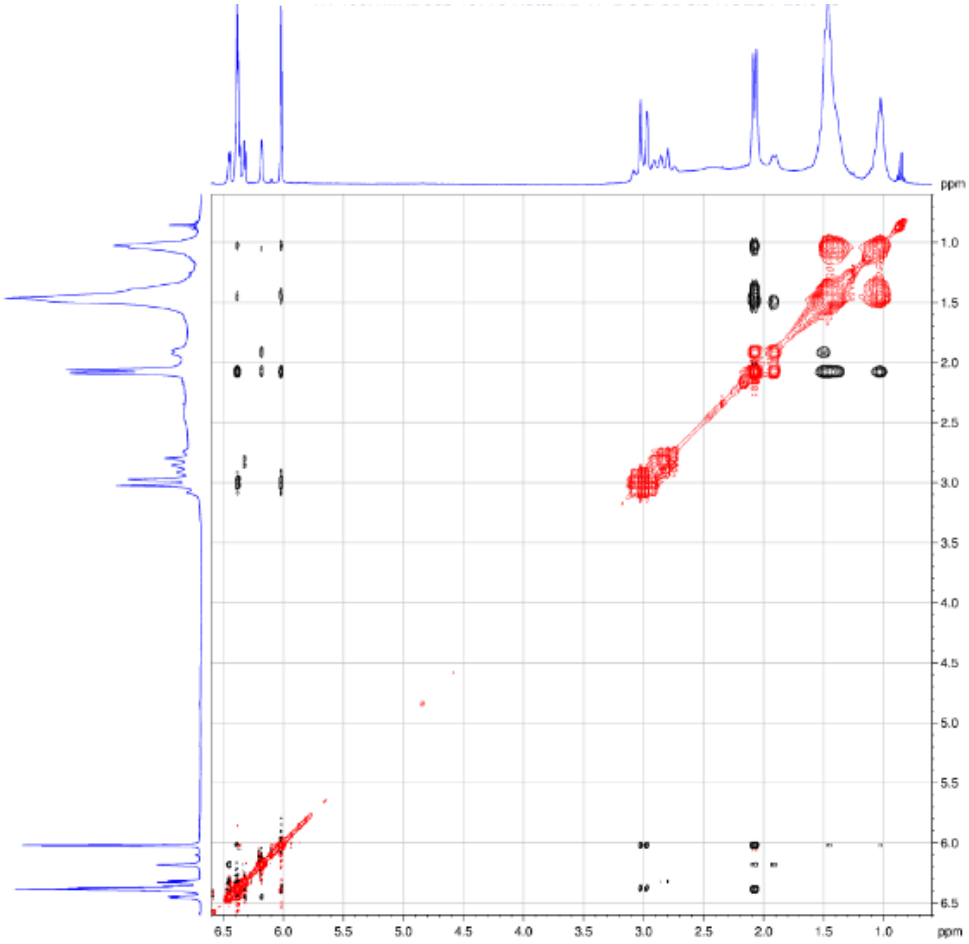

Figure 3.16 **Full ^{1}H-^{1}H NOE spectrum of 7b**

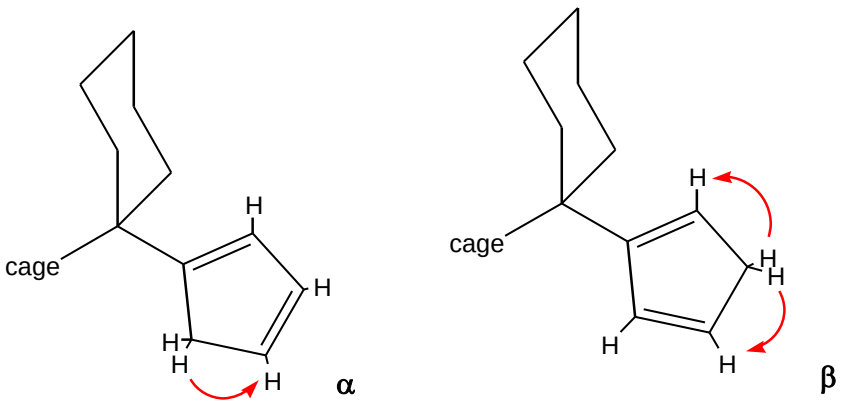

Figure 3.17 **NOE correlations of *α* and *β* side groups**

The ratio of α:β for **7b** is 2:9 compared to 2:1 for **7a**. The preference for β protonation can be explained by steric effects that partially block off approach of H_3O^+ to the α positions due to the bulkier nature of the pentamethylene unit.

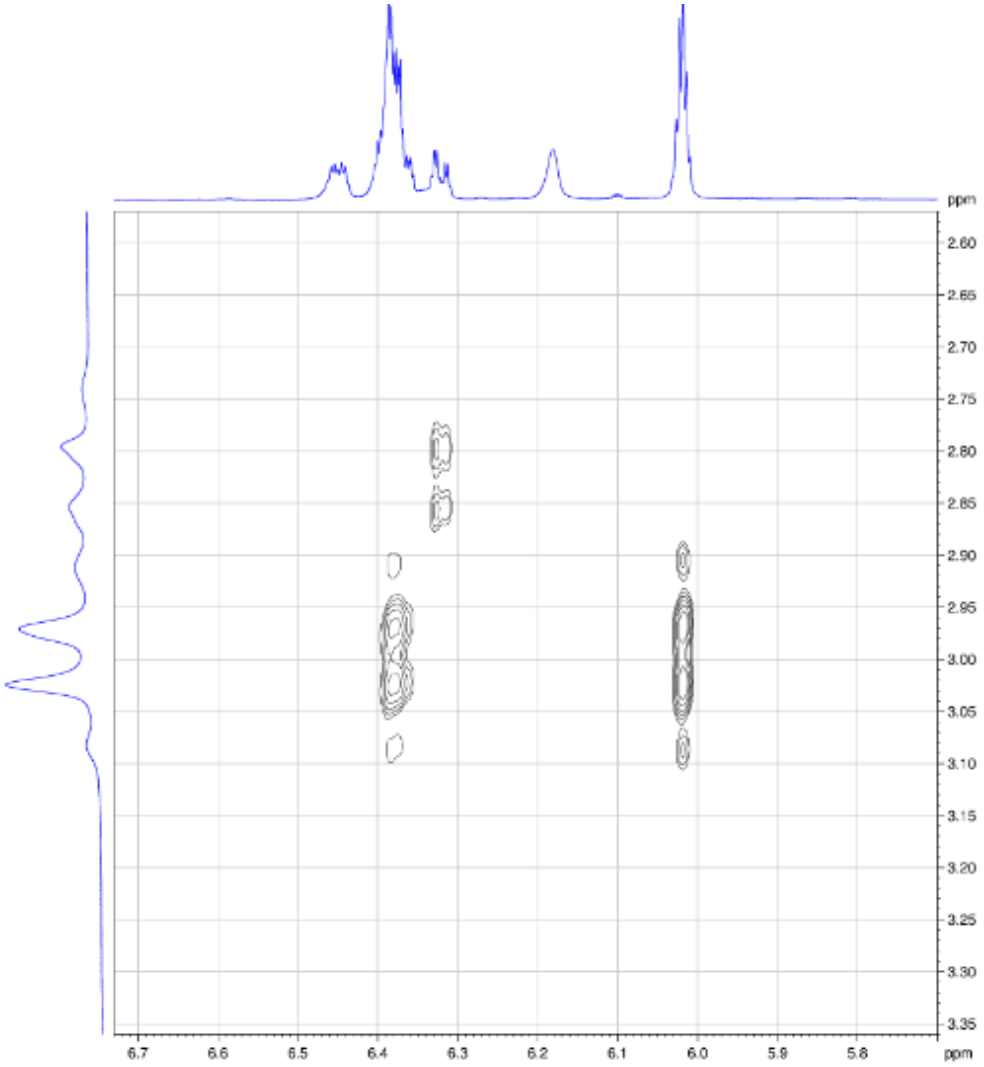

Figure 3.18 **^{1}H-^{1}H NOE spectrum of 7b – CH_2 against CH**

3.3.1.2 Crystallography of 7b

The crystallographically determined structure of **7b** (Figure 3.19) shows the pentamethylene groups in a chair conformation with the C_5H_5 group in an axial position in both cases. The isomer that crystallised was exclusively the $\beta\beta$ form.

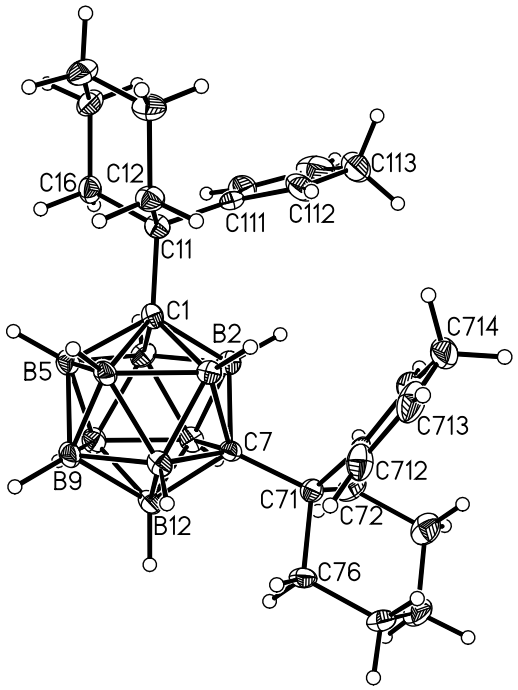

Figure 3.19 Molecular structure of compound 7b

3.3.2 Synthesis of 1,7-(CPmFc)$_2$-1,7-*closo*-$C_2B_{10}H_{10}$ (8b)

The C_5H_5 rings were converted to ferrocenyl units to yield the orange coloured bis-ferrocenyl analogue **(8b)** in an analogous way to **7a** being converted to **8a** using a large excess of $FeCl_2$ and NaCp.

The ^{1}H NMR spectrum of **8b** showed the same characteristic pattern in the ferrocenyl region as **8a** with a singlet resonance attributed to the ten protons of the two unsubstituted Cp rings at δ 4.07 being flanked by the substituted ring proton signals (δ 4.15 and δ 3.98, 4H each). A total of twenty protons attributed to the two Pm groups are observed over five large, lumpy, multiplet peaks at δ 2.17 (4H), δ 1.90 (8H), δ 1.59 (6H), δ 1.37 (2H).

In the ^{11}B{^{1}H} spectrum of **8b** two resonances appear at δ -5.9 (2B) and δ -12.4 (8B) which is representative of a high symmetry *closo* icosahedral carborane. The resonance at δ -12.4 containing eight boron atoms constitutes the superposition of one 4B and two 2B signals. Mass spectrometry shows typical carborane isotopic envelope centred at *m/z* 676 with very little fragmentation. Elemental analysis is in good agreement with that expected of $C_{34}H_{50}B_{10}Fe_2$.

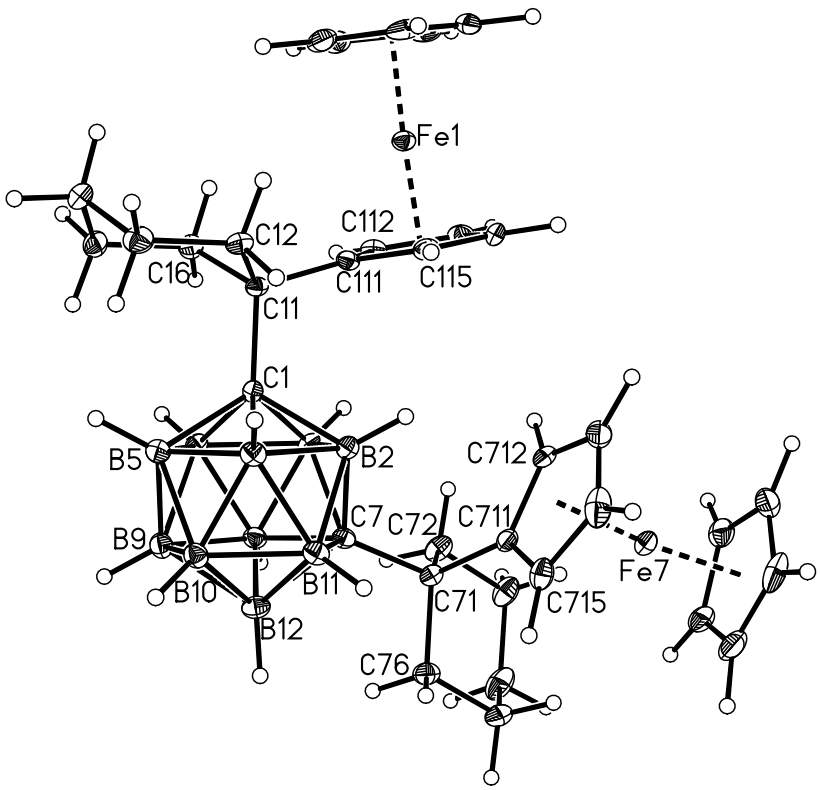

Figure 3.20 Molecular structure of compound 8b

The crystallographically determined structure of **8b** (Figure 3.20) shows the two substituents adopting different conformations. The pentamethylene group on C(11) has the ferrocenyl group in an equatorial position. The ferrocenyl group is slightly distorted, with a dihedral angle between C_5 rings of 3.09°, to accommodate the axial hydrogen atoms at the α positions on the pentamethylene group. The pentamethylene group on C(71) has the ferrocenyl group in an axial position. This ferrocenyl group is relatively more distorted, with a dihedral angle of 11.6°, with the β hydrogen atoms causing this steric crowding.

3.3.3 Reduction of 1,7-(CPmFc)$_2$-1,7-*closo*-$C_2B_{10}H_{10}$

In an attempt to synthesise a 13-vertex carborane, **8b** was reduced with sodium naphthalenide followed by the addition of $BPhCl_2$ to provide the capping fragment. The main product from this reaction was not a 13-vertex carborane but a deep purple solid, 1,2-(CPmFc)$_2$-1,2-*closo*-$C_2B_{10}H_{10}$ **(9b)**. Even with the increased bulk of the pentamethylene groups the [7,9-(CPmFc)$_2$-7,9-*nido*-C_2B_{10}]$^{2-}$ dianion still prefers to re-

oxidise to a *closo* 12-vertex carborane. Compound **9b** can also be prepared directly by reduction of the 1,7 isomer **8b** followed by re-oxidation in air.

The mass spectrum of **9b** is identical to that of the 1,7-analogue **8b** but fragmentation is this time observed with peaks at *m/z* 410 (M – {CMe_2Fc}) and *m/z* 266 ({CMe_2Fc}) indicating the loss of an CPmFc unit and showing that **9b** is more susceptible to fragmentation than **8b**. Elemental analysis is in good agreement with that expected for $C_{34}H_{50}B_{10}Fe_2$.

The ^{1}H NMR spectrum of **9b** shows that, like in the conversion from **8a** to **9a**, the CH resonances from the substituted ferrocenyl ring shift to higher frequency. Both sets of proton resonances from the substituted ring (δ 4.23 and δ 4.19, both 4H) are shifted to higher frequency than that of the ten protons of the two unsubstituted Cp signals at δ 4.11. A total of twenty protons attributed to the two Pm groups are observed over five large, lumpy, multiplet peaks at δ 2.63 (4H), δ 2.33 (4H), δ 2.24 (4H), δ 1.73 (6H) and δ 1.52 (2H).

In the ^{11}B{^{1}H} spectrum of **9b** three resonances appear at δ -0.7 (4B), δ -3.7 (4B) and δ -14.2 (2B) which is appropriate for a high symmetry *closo* icosahedral carborane. In an attempt to ascertain which of the two 4B peaks is the superposition of two 2B peaks a ^{1}H{^{11}B} NMR spectrum was obtained. In a regular ^{1}H spectrum (Figure 3.21 A) the B-*H* signals are often broadened (often so much they cannot be distinguished from the baseline) due to the directly connected quadrupolar ^{11}B atoms. When the ^{11}B nuclei are decoupled (Figure 3.21 B) the ^{1}H peaks sharpen up to some extent. When the initial ^{1}H spectrum is 'subtracted' from the ^{1}H{^{11}B} spectrum, (Figure 3.21 C) only the B-*H* resonances are observed. B-*H* resonances for **9b** appear at δ 2.57 (2B), δ 2.14 (2B), δ 2.03 (4B) and δ 1.88 (2B). An ^{11}B-^{1}H (B-*H* only) HMQC spectrum was obtained (Figure 3.22). The broad nature of the ^{11}B signals (due to the intramolecular steric crowding of **9b**) alongside the relatively broad ^{1}H (B-*H* only) signals results in an extremely poor signal to noise ratio and consequently incredibly weak crosspeaks. Analysis of this HMQC spectrum shows the ^{11}B resonance at δ -0.7 is correlated to two different B-*H* resonances at δ 2.14 and δ 2.57 thus giving strong evidence that this is the (2B + 2B) resonance from the original ^{11}B NMR spectrum assuming all other expected peaks are lost in the noisy baseline.

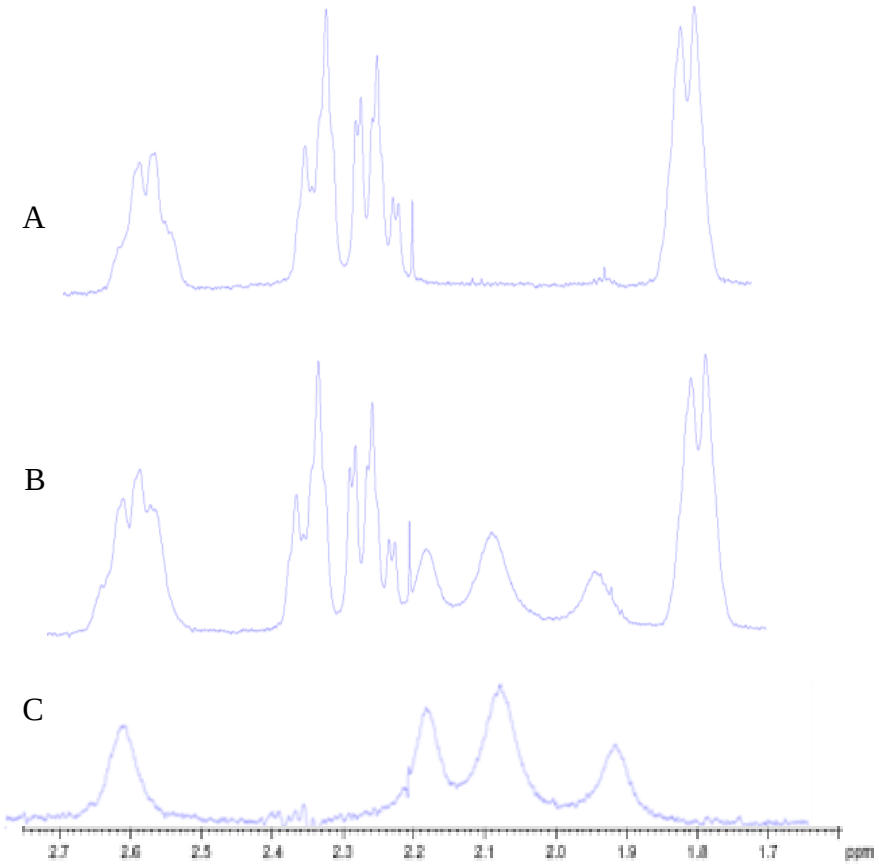

Figure 3.21 **^{1}H NMR spectrum (A); ^{1}H{^{11}B} NMR spectrum (B) and difference between A and B (C). Spectral range shows Pm and B-*H* resonances**

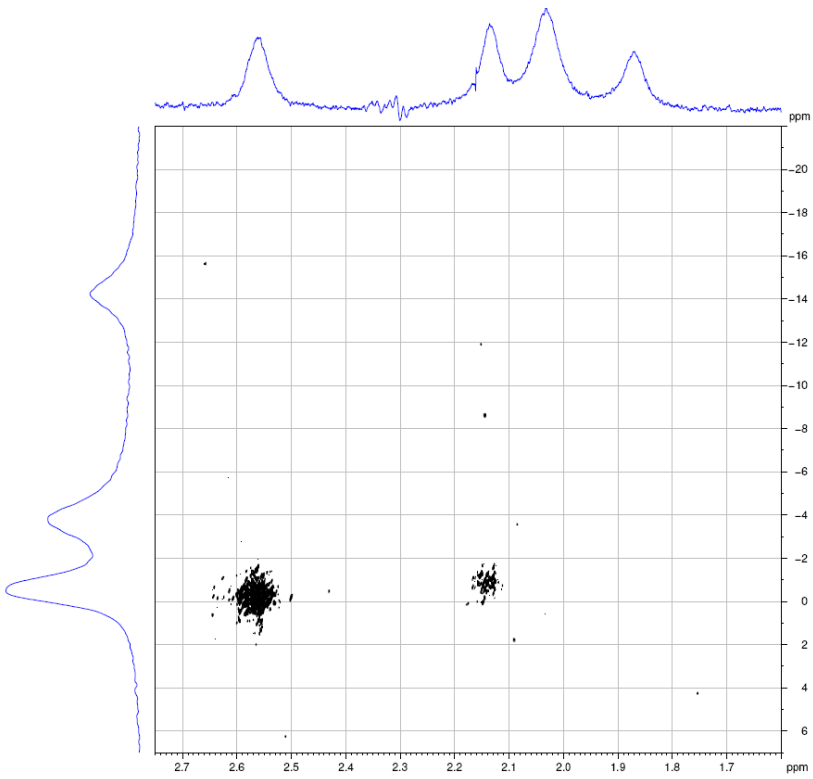

Figure 3.22 **^{11}B – ^{1}H (B-H only) HMQC NMR spectrum of 9b**

The crystallographically determined structure (Figure 3.23) of **9b** shows intensive steric crowding. The CPmFc substituent on C(1) has rotated so that its Pm group is side-on to the Pm group on C(21) and not face on (which presumably would be untenable) to minimise steric interaction. The severe intramolecular crowding is also shown by the presence of two H...H distances of *ca*. 2 Å (H12B…H26B 1.995 Å, H12…H22A 1.977 Å) and distortion of the ferrocenyl group on C(211) due to the forced orientation of the adjacent Pm group; the C(211)-C(215) ring is tilted at C(211) (the C(21)-C(211) bond meets the plane at 11.38° and the two Cp rings on Fe(2) subtend a dihedral angle of 11.65°. The C(1)-C(2) distance is thus elongated to 2.156(4) Å.

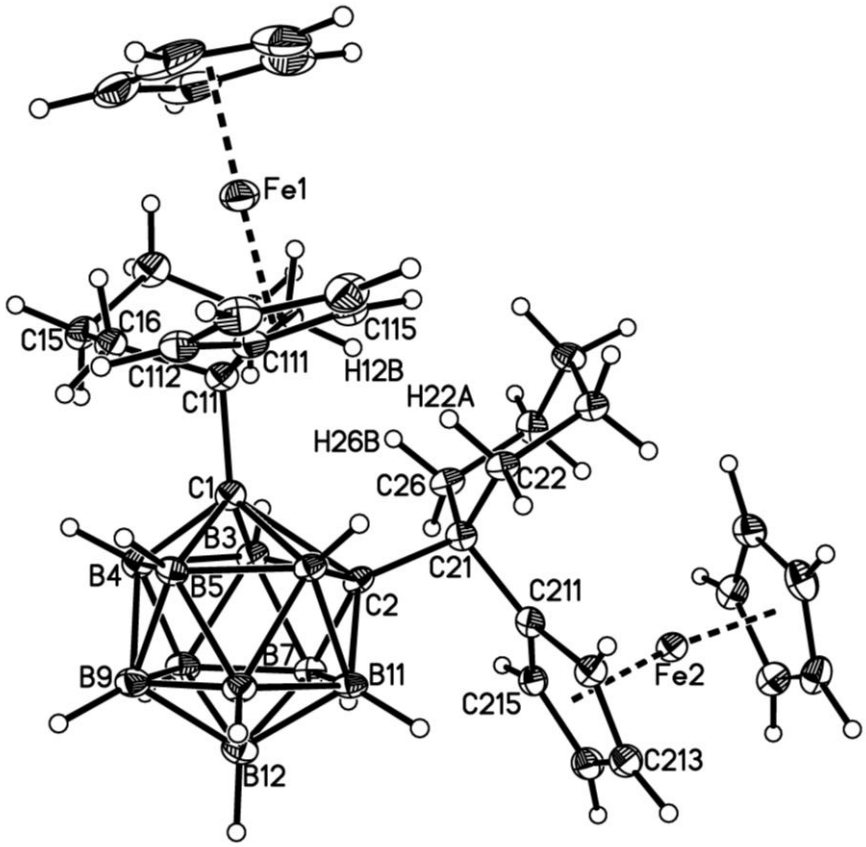

Figure 3.23 Molecular structure of compound 9b

3.4 Synthesis of 1,7-{CPm(Me$_4$)(C$_5$H$_5$)}$_2$-1,7-*closo*-C$_2$B$_{10}$H$_{10}$ (7c)

When 1,7-*closo*-$C_2B_{10}H_{12}$ is deprotonated with *n*-BuLi and treated with two equivalents of 6,6-dimethylfulvene and 6,6-pentamethylenefulvene the 1,7-R_2-1,7-*closo*-C_2B_{10} compounds **7a** and **7b** are produced respectively. When their C_5 rings are subjected to deprotonation and metallation (**8a** and **8b**) followed by subsequent reduction and re-oxidation the 1,2-R_2-1,2-*closo*-C_2B_{10} compounds **9a** and **9b** are formed and, whilst they certainly possess interesting structural features due to their intramolecular crowding, they still do not possess sufficient steric bulk to prevent the carbon atoms becoming adjacent upon reoxidation of the dianionic [7,9-R_2-7,9-*nido*-C_2B_{10}]$^{2-}$ intermediate.

The use of a larger fulvene (fulvene III) incorporating four methyl groups, was used to tackle this problem. When dilithated [1,7-*closo*-$C_2B_{10}H_{10}$]$^{2-}$ is treated with two equivalents of fulvene III (Figure 3.24) compound **7c** is formed in good yield. (Fulvene III was prepared by the reaction of cyclopentadiene and 3,3,5,5-tetramethylcyclohexanone following a general procedure.[8])

The mass spectrum of **7c** shows a typical carborane isotopic envelope of peaks centred on *m/z* 548 and elemental analysis is in excellent agreement with that expected for $C_{32}H_{56}B_{10}$.

In the $^{11}B\{^1H\}$ spectrum of **7c** three resonances appear at δ -6.4 (2B), δ -12.7 (4B) and δ -14.5 (4B) which is appropriate for a high symmetry *closo* icosahedral carborane.

The ^1H NMR spectrum reveals three aromatic multiplet resonances (2H each) at δ 6.49, δ 6.26 and δ 6.11. Both CH_2 units of the C_5 rings are observed as a multiplet at δ 2.92. All twelve protons (from both C_6 rings) are observed as individual singlets between δ 0.91 – 2.09. The eight methyl groups are observed over four singlet resonances at δ 0.89, δ 0.87, δ 0.84 and δ 0.68 each integrating for six protons. The presence of twelve single protons in the ^1H NMR spectrum indicates a degree of asymmetry within the molecule with respect to the positions of the bulky substituents. Should these side groups have free rotation, the ^1H spectrum would be expected to show a maximum of only six proton resonances as both groups are identical. Also only one isomer is observed (*ββ*) in the C_5 ring whereas less bulky analogues **7a** and **7b** exhibit a mixture of *α* and *β* isomers.

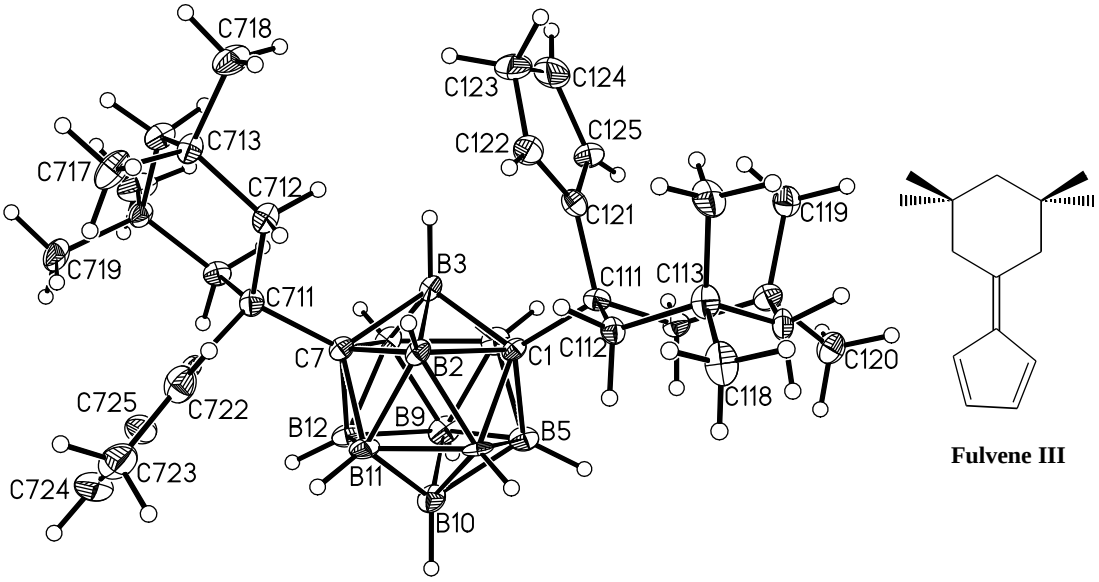

Figure 3.24 Molecular structure of compound 7c

Deprotonation of the C_5 rings of **7c** followed by treatment with excess $FeCl_2$ and NaCp was carried out in an attempt to create the bis-ferrocenyl compound analogous to **7a** and **7b**. The presence of the desired product (alongside the monosubstituted ferrocenyl product) was detectable from a mass spectrum of the crude mixture subsequent to filtration through silica. Spot TLC, in a variety of elution mixtures, of this orange layer revealed no visible products other than pure ferrocene. The desired bis-ferrocenyl compound was therefore produced but only in an impractically low yield.

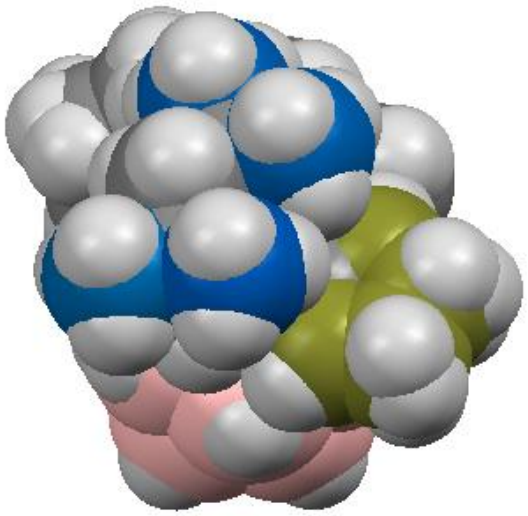

Figure 3.25 Space fill diagram of 7c showing C_5 ring partially blocked by methyl groups (methyl groups in blue, C_5 ring in green).

The crystallographically determined structure (Figure 3.24) shows both substituents in different conformations. The $CC_6Me_4H_6$ unit attached to C(1) has the C_5 ring pointing up and is almost face on to the C_6 ring positioned on C(7) i.e. the two C_5 rings are situated as far apart as possible. This is presumably the favoured orientation, even in solution, and such a conformation would give rise the asymmetric nature of the ^1H NMR spectrum described above assuming there is restricted rotation around bonds C(1)-C(111) and C(7)-C(711). Both C_6 rings adopt a chair conformation with the cluster situated in an equatorial position. Axial positions are taken up by the C_5 rings. The methyl groups can be seen to somewhat push against the face of the C_5 rings and incline them towards the cage (Figures 3.25 and 3.26) thus partially blocking the approach of any Fe^{2+} ions when trying to form the bis-ferrocenyl compound. The average angle C_{cage}-C-$C_{C_5H_5}$ in **7c** is 106.3(6)º, the smallest being 105.1(4)º from cage atom C(1). This is significantly smaller than the corresponding average angles in analogues **7a** and **7b** which are 109.5(6)º and 108.5(4)º respectively.

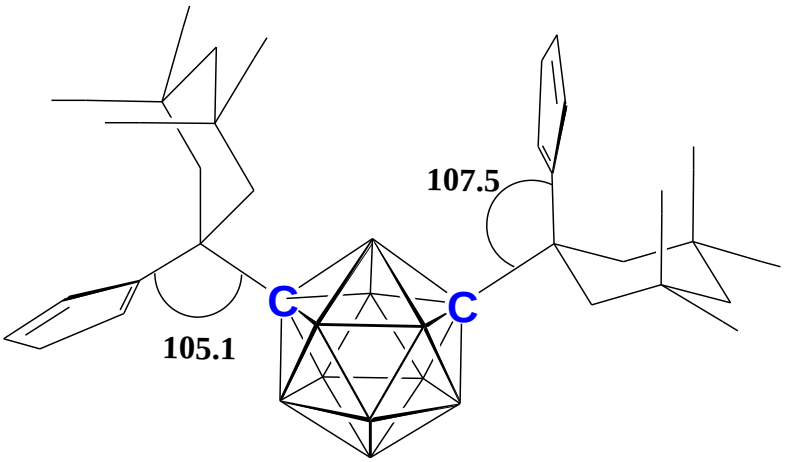

Figure 3.26 **Interbond angles of 7c showing significant steric strain from methyl groups**

3.5 Deformation of Sterically Crowded 1,2-*closo*-carboranes

It has been known for many years that 1,2-*closo*-$C_2B_{10}H_{12}$ possesses a slightly distorted icosahedral geometry[9] due to the presence of the two dissimilar carbon atoms within the molecule. Its precise molecular structure has historically proved difficult to obtain as the near spherical nature of the cage hindered any X-ray diffraction study through disorder. Nevertheless, in 1996 Davidson, Wade *et al.*[6] formed a supramolecular dimer with hexamethylphosphoramide utilising the acidic nature of the carborane CH units, locking them into CH···O hydrogen bonds allowing unambiguous location of the two carbon atoms within the C_2B_{10} clusters; the two independent C–C distances measured at 150 K were 1.629(6) and 1.630(6) Å. A subsequent electron diffraction study by Rankin and co-workers[10] determined the gas phase structure of 1,2-*closo*-$C_2B_{10}H_{12}$ revealing the C(1)-C(2) distance to be 1.624(8) Å. The C(1)-C(2) distance has been increased to *ca.* 1.8 Å by the introduction of bulky C-substituents[11] and incorporating the carbon atoms into exopolyhedral cycles[12] can increase the distance further to *ca.* 1.9 Å.

In order to accommodate large substituents, compounds **9a** and **9b** undergo a significant cage deformation. The C(1)-C(2) connectivity is considerably lengthened and the substituents interlock into a suitable conformation to minimise intramolecular steric strain. The C(1)-C(2) bond lengths are 1.9378(16) Å and 2.156(4) Å for **9a** and **9b** respectively compared with the C-C bond in naked 1,2-*closo*-$C_2B_{10}H_{12}$ of 1.630(8) Å[6] which is clearly much shorter. Compounds **9a** and **9b** are first examples of untethered icosahedral 1,2-*closo*-C_2B_{10} carboranes with quaternary carbon atoms attached to both cage carbon atoms. There are structurally characterised carboranes in the literature[13] with even longer C-C bonds than **9b** but such species can be argued to have formal polyhedral skeletal electron (PSE) counts in excess of the (2*n*+2) (*n*= no. of vertices) normally associated with *closo* species and so bear closer comparison with (2*n*+3) carborane radical anions or (2*n*+4) *nido*-dianions.

As the C-C bond lengthens the two B atoms on opposite sides of the trapezoidal face (B(3) and B(6)) are pulled together from a distance of 2.886 Å in 1,2-*closo*-$C_2B_{10}H_{12}$ to 2.756 Å and 2.663 Å in **9a** and **9b** respectively. This gives rise to a second order effect in the lengthening of connectivities B(3)-B(8) and B(6)-B(10) to 1.799(2) Å and 1.789(2) Å respectively for **9a**. These connectivities are even longer in **9b** at 1.815(5) Å and 1.820(5) Å compared to an average length of 1.766(8) Å in 1,2-*closo*-$C_2B_{10}H_{12}$.[6]

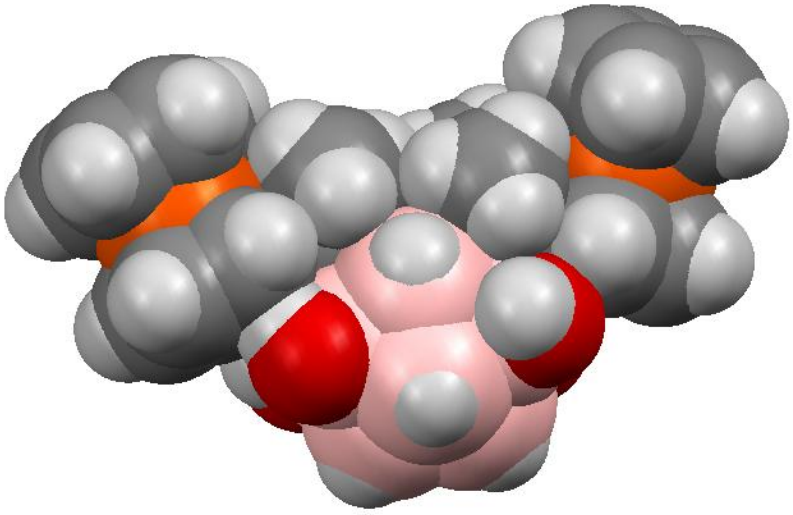

Figure 3.27 Space fill diagram of compound 11

Compound **11** also displays a significant cage deformation and has a C(1)-C(2) bond length of 2.102(3) Å. The presence of the hydroxyl group on vertex B(4) causes the deformation to be even more severe than its non-hydroxylated analogue **9a** presumably due to a slight steric interaction between the hydroxyl group and the ferrocenyl group pushing upon the underside of the latter (Figure 3.27). The B(3)-B(6) distance is thus reduced to 2.649 Å causing lengthening of the connectivities B(3)-B(8) and B(6)-B(10) to 1.783(4) Å and 1.805(4) Å respectively. The presence of cage substituents is seen to affect the severity of the deformation of the icosahedral cluster and further work on cage substituents is described in a later chapter.

The weighted average ^{11}B NMR chemical shift, $<\delta^{11}B>$, also provides information about this deformation. The ^{11}B NMR chemical shift is pushed to higher frequency with increased cage deformation. Table 3.1 shows the shift is predominantly due to the steric cage deformation and not any potential electronic effect of the substituents (compound **11** probably includes a slight electronic substituent effect due to the electronegative O atom attached to the B(4) vertex). This trend is also observed in *pseudocloso* MC_2B_9 metallacarboranes[14] (Figure 3.28) which also possess large C-C distances. *Pseudocloso* metallacarboranes show an even greater cage deformation than **9a**, **9b** or **11** causing the C-C distance to elongate officially breaking the connectivity. The weighted average ^{11}B NMR chemical shift movement to higher frequency is far more pronounced for *pseudocloso* species showing the cage deformation in compounds **9a** and **9b** is not as severe as in true *pseudocloso* metallacarboranes. The $<\delta^{11}B>$ values in *pseudocloso*

metallacarboranes are shifted *ca.* 15 ppm to high frequency relative to analogous non-deformed analogues, e.g. for 1,2-Ph_2-3-Cp*-3,1,2-*pseudocloso*-$RhC_2B_9H_9$[15] it is δ 6.0 whereas for 3-Cp*-3,1,2-*closo*-$RhC_2B_9H_{11}$[16] it is δ -8.6. Table 3.2 displays some structural and spectroscopic data of selected *pseudocloso* metallacarboranes as a comparison to **9a** and **9b**.

Table 3.1 Selected Weighted Average ^{11}B NMR chemical shifts

Cage Substituents	1,2-*closo* / ppm	1,7-*closo* / ppm
none	-10.8	-12.3
{CMe_2Fc}	-7.5 (**9a**)	-11.5 (**7a**)
{CPmFc}	-4.3 (**9b**)	-11.1 (**7b**)
B4-OH, {CMe_2Fc}	*-6.8 (**11**)*	*n/a*

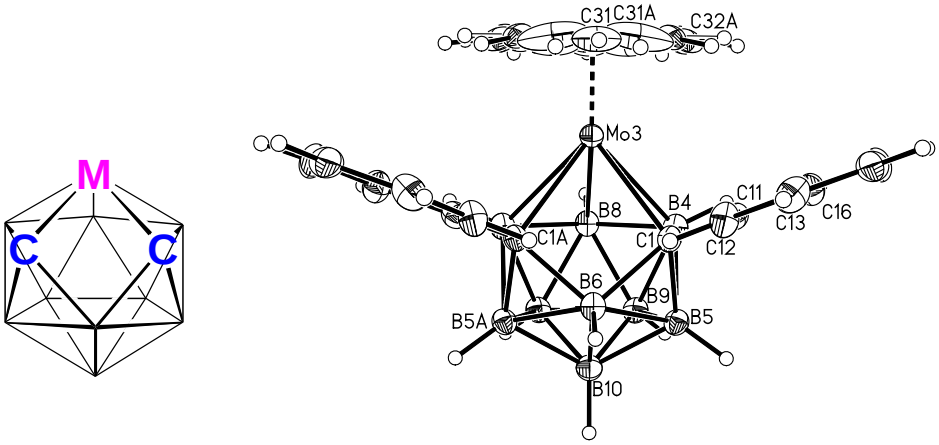

Figure 3.28 Framework topology and example of a *pseudocloso* metallacarborane[14]

Table 3.2 Structural Parameters (Å) and <δ^{11}B> (ppm) for selected literature *Pseudocloso* Metallacarboranes 1,2-Ph_2-3-(η-L)-3,1,2-$MC_2B_9H_9$.

{ML}	C(1)-C(2)	M(3)-B(6)	<δ^{11}B>	reference
RhCp*	2.51	2.92	6.0	15
Ru(η^6-C_6H_6)	2.49	2.95	5.4	17
Ru(*p*-cymene)	2.45	2.99	5.6	17
Rh(η^5-C_9Me_7)	2.49	2.96	6.0	18
Rh(η^5-C_8H_{13})	2.41	3.01	5.8	19

3.6 A Theoretical Study of the Oxidation Pathways of [7,9-*nido*-$C_2B_{10}H_{12}]^{2-}$

A DFT study (kindly performed by Dr D. McKay, Heriot-Watt University) of the $2e^-$ oxidation of [7,9-*nido*-$C_2B_{10}H_{12}]^{2-}$ was carried out[20] (Figure 3.29) to investigate the reasons behind the formation of a 1,2-*closo*-C_2B_{10} isomer (in the case of **9a** and **9b**) instead of the thermodynamically preferred 1,7-*closo*-C_2B_{10} species (**8a** and **8b**). A basket-shaped intermediate (**INT**) is formed 4.8 kcal mol^{-1} above the dianion which then rearranges to 1,2-*closo*-$C_2B_{10}H_{12}$ via a transition state (**TS1**) with an activation energy of +9.2 kcal mol^{-1}. An alternative pathway is for **INT** to rearrange into 1,7-*closo*-$C_2B_{10}H_{12}$ via a transition state (**TS2**) with a higher activation energy of +16.7 kcal mol^{-1}. It is clear, therefore, that the preferred oxidation pathway of [7,9-*nido*-$C_2B_{10}H_{12}]^{2-}$ is via **TS1** to form the carbons-adjacent *closo* isomer.

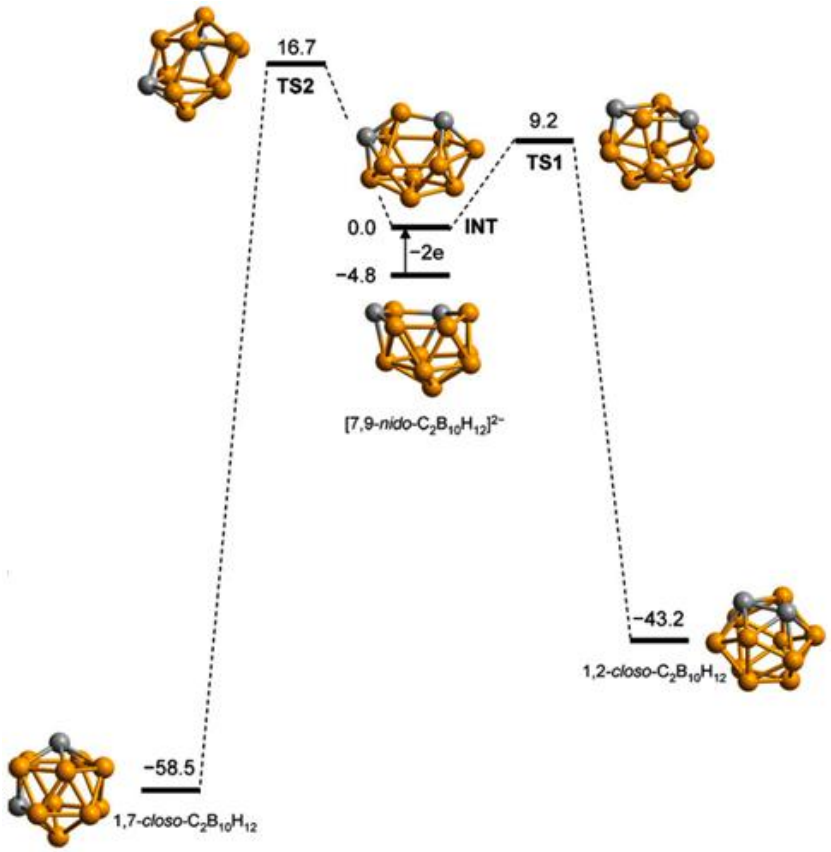

Figure 3.29 Computational study of the 2e oxidation of [7,9-*nido*-$C_2B_{10}H_{12}]^{2-}$. All energies in kcal mol^{-1}

An earlier computational study by Brown and McKee[21] has seen both **INT** and **TS2** already characterised whist investigating the isomerisation of 1,2- to 1,7-*closo*-$C_2B_{10}H_{12}$. This rearrangement occurs via a non-TFR pathway. **TS1**, however, has never previously been reported and has significantly lower energy than the transition state reported by McKee in the conversion from 1,2- to 1,7-*closo*-$C_2B_{10}H_{12}$ via a TFR pathway. The overall pathway from 1,2- to 1,7-*closo*-$C_2B_{10}H_{12}$ in Figure 3.29 has overall activation energy of +59.9 kcal mol^{-1} and is similar to McKee's TFR route and significantly more favourable than his non-TFR pathway.

3.7 References

3.1 B. W. Hutton, F. MacIntosh, D. Ellis, F. Herisse, S. A. Macgregor, D. McKay, V. Petrie-Armstrong, G. M. Rosair, D. S. Perekalin, H. Tricas and A. J. Welch, *Chem. Commun*., 2008, 5345.

3.2 e.g. G. B. Dunks, M. M. McKown and M. F. Hawthorne, *J. Am. Chem. Soc*., 1971, **93**, 2451.

3.3 A. Burke, R. McIntosh, D. Ellis, G. M. Rosair and A. J. Welch, *Collect. Czech. Chem. Commun.*, 2002, **67**, 991.

3.4 e.g. S. Zlatogorsky, *Ph.D Thesis*, Heriot-Watt University, 2007 (and references therein).

3.5 e.g. A. Burke, D. Ellis, D. Ferrer, D. L. Ormsby, G. M. Rosair and A. J. Welch, *Dalton Trans*., 2005, 1716.

3.6 M. G. Davidson, T. G. Hibbert, J. A. K. Howard, A. Mackinnon and K. Wade, *Chem. Commun*., 1996, 2285.

3.7 S. Eriksson, K. J. Winberg, R. T. Claro, S. J. Sjöberg, *J. Org. Chem*., 2003, 68, 3569.

3.8 K. J. Stone and R. D. Little, *J. Org. Chem*., 1984, **49**, 1849.

3.9 T. L. Heying, J. W. Ager Jr., S. L. Clark, D. J. Mangold, H. L. Goldstein, M. L. Hillman, R. J. Polak and J. W. Szymanski, *Inorg. Chem*., 1963, **2**, 1089.

3.10 A. R. Turner, H. E. Robertson, K. B. Borisenko, D. W. H. Rankin and M. A. Fox, *Dalton Trans*., 2005, 1310.

3.11 e.g. Y.-J. Lee, S.-J. Kim, C.-H. Kang, J. Ko, S. O. Kang and P. J. Carroll, *Organometallics*, 1998, **17**, 1109.

3.12 (a) e.g. F. Teixidor, C. Vinas, J. Rius, C. Miravitlles and J. Casabo, *Inorg. Chem.*, 1990, **29**, 149; (b) D.-H. Kim, J. Ko, K. Park, S. Cho and S. O. Kang, *Organometallics*, 1999, **18**, 2738.

3.13 (a) D. A. Brown, W. Clegg, H. M. Colquhoun, J. A. Daniels, I. R.Stephenson and K. Wade, *J. Chem. Soc., Chem. Commun.*, 1987, 889; (b) T. D. Getman, C. B. Knobler and M. F. Hawthorne, *Inorg.Chem*., 1992, **31**, 101; (c) K. Chui, H.-W. Li and Z. Xie, *Organometallics*, 2000, **19**, 5447; (d) L. A. Boyd, W. Clegg, R. C. B. Copley, M. G. Davidson, M. A. Fox, T. G. Hibbert, J. A. K. Howard, A. Mackinnon, R. J. Peace and K. Wade, *Dalton Trans.*, 2004, 2786.

3.14 R. D. McIntosh, D. Ellis, B. T. Giles, S. A. Macgregor, G. M. Rosair and A. J. Welch, *Inorg. Chim. Acta*, 2006, **359**, 3745.

3.15 Z. G. Lewis and A. J. Welch, *J. Organometal. Chem*., 1992, **430**, C45.

3.16 M. Bown, J. Plesek, K. Base, B. Stibr, X. L. R. Fontaine, N. N. Greenwood and J. D. Kennedy, *Magn. Reson. Chem*., 1989, **27**, 974.

3.17 P. T. Brain, M. Bühl, J. Cowie, Z. G. Lewis and A. J. Welch, *J. Chem. Soc. Dalton Trans.*, 1996, 231.

3.18 U. Grädler, A. S. Weller, A. J. Welch and D. Reed, *J. Chem. Soc. Dalton Trans*., 1996, 335.

3.19 D. J. Donohoe, *Ph.D Thesis*, University of Edinburgh, 1996.

3.20 D. McKay, *Ph.D Thesis*, Heriot-Watt University, 2010.

3.21 C. A. Brown and M. L. McKee, *J. Mol. Model*, 2006, **12**, 653.

Chapter 4 Physical Studies of bis-Ferrocenyl Compounds 8 & 9

4.1 UV-vis and Computational Studies of Compounds 8 and 9

The 1,2-$(CR_2Fc)_2$-1,2-*closo*-$C_2B_{10}H_{10}$ species (R=Me, R_2=Pm) described in chapter 3 are intriguingly coloured; **9a** is dark red and the slightly bulkier **9b** exhibits a very deep purple colour (the boron substituted hydroxy compound **11** is also a very deep purple). The 1,7 analogues **8a** and **8b** are coloured yellow and orange respectively, being more representative of ferrocenyl compounds. It generally appears that an increased degree of steric crowding and consequent cage deformation results in absorption bands with increased λ_{max} and intensity than typical ferrocenyl compounds (Figures 4.1 and 4.3).

The UV-vis spectra of the 1,7-$(CR_2Fc)_2$-1,7-*closo*-$C_2B_{10}H_{10}$ species (**8a** and **8b)** and the 1,2 analogous species (**9a** and **9b)** were recorded (Figures 4.1 and 4.3) and compared with time-dependent DFT (TD-DFT) calculated spectra (kindly performed by Prof. M. J. Paterson, Heriot-Watt University – Figures 4.2 and 4.4). For these calculations the crystal structures were used as a starting point and the molecules optimised with DFT (B3LYP/6-31G**). The resulting geometries were then used for TD-DFT. The calculated spectra show general similarities to the true spectra, namely the increased signal intensities and the relative shifts to a higher λ_{max} of the 1,2 species relative to the 1,7 species. Table 4.1 displays the pertinent spectral information. The λ_{max} difference between the 1,2 species and the 1,7 species were experimentally observed as 20 nm and 91 nm where R=Me and R_2=Pm respectively. The analogous calculated differences show comparable λ_{max} shifts at 13 nm and 68 nm. The relatively increased signal intensities of the 1,2 species **9a** and **9b** are qualitatively consistent with those from the calculated spectra.

Table 4.1 Experimental and TD DFT calculated UV-vis spectral data of compounds 8 and 9 in DCM

Compound	Concentration/ mol L^{-1}	λ_{max}/nm exp.	λ_{max}/nm calc.	Intensity exp.	Intensity calc.	Colour
8a	$1.68x10^{-3}$	449	487	Low	Low	Yellow
8b	$1.48x10^{-3}$	466	502	Low	Low	Orange
9a	$1.68x10^{-3}$	469	500	High	High	Red
9b	$1.48x10^{-3}$	557	570	High	High	Purple

A study of the molecular orbitals involved (Figures 4.2 and 4.4) reveals the main absorption bands leading to the intensified colours of **9a** and **9b** can be approximated as a partial charge transfer of electron density from the ferrocenyl group to the cage.

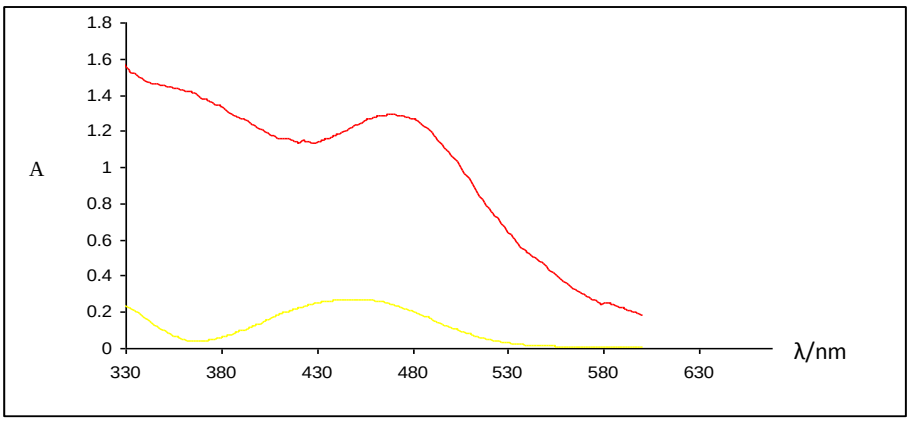

Figure 4.1 **Experimental UV-vis spectra of 8a (yellow) and 9a (red)**

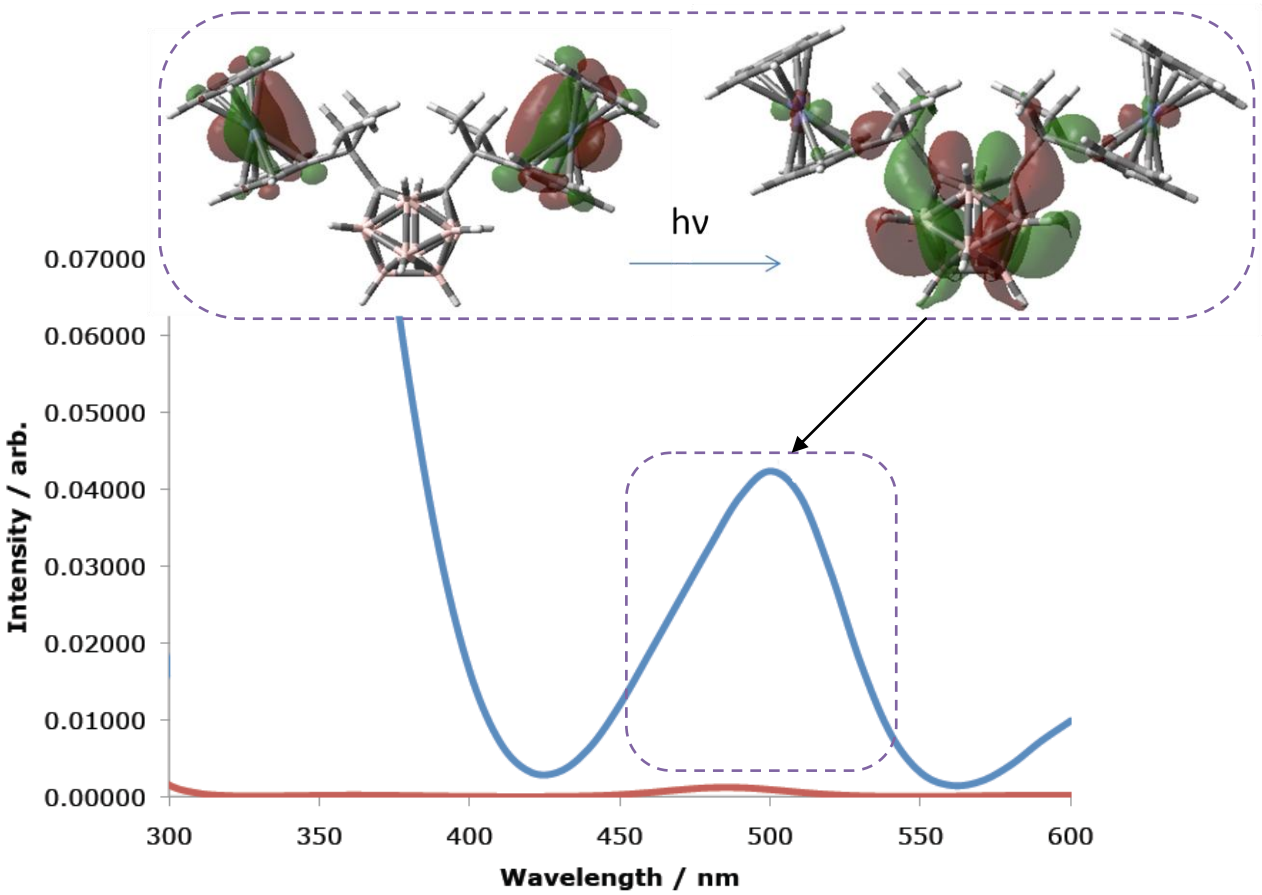

Figure 4.2 **TD-DFT calculated Uv-vis spectra of 8a (red) and 9a (blue) and associated molecular orbitals**

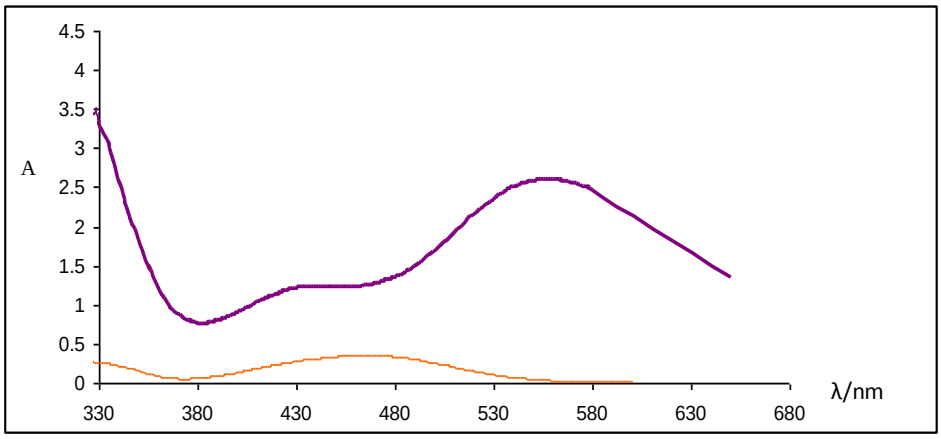

Figure 4.3 **Experimental UV-vis spectra of 8b (orange) and 9b (purple)**

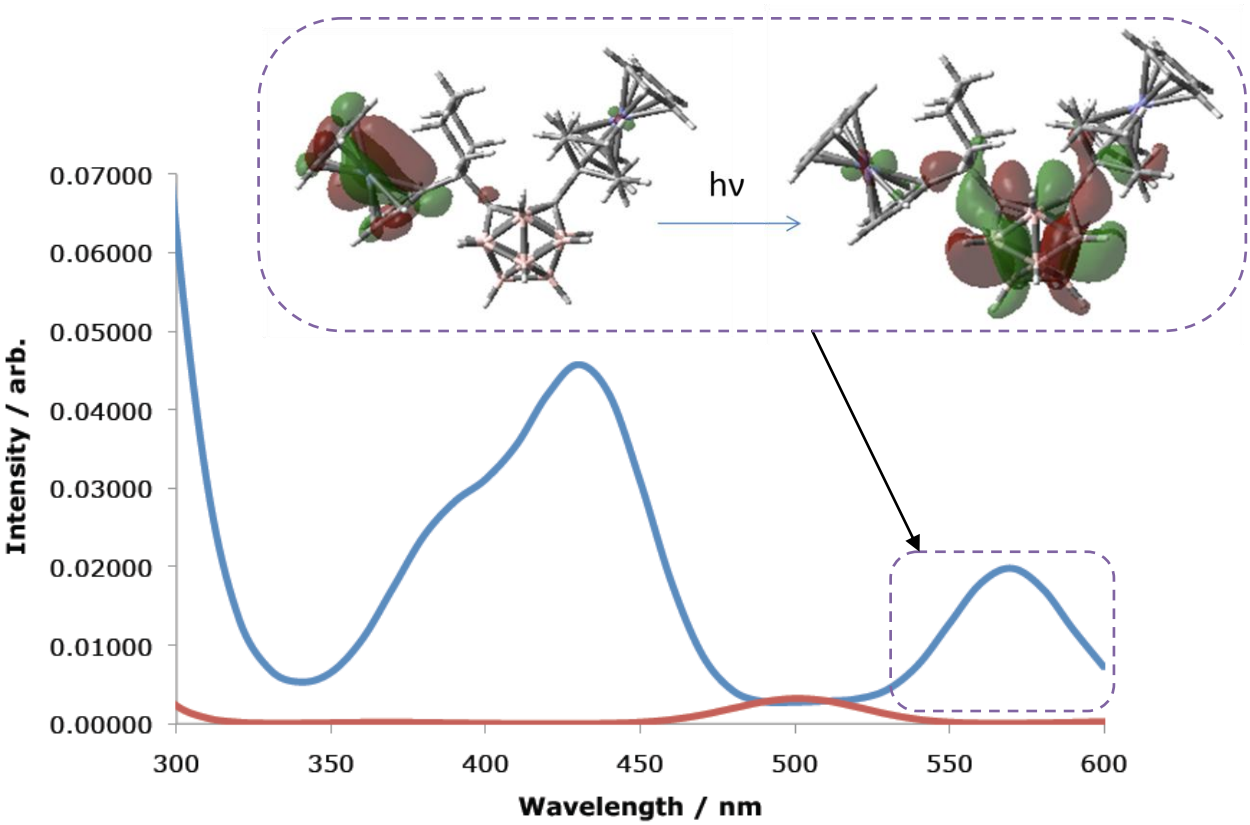

Figure 4.4 **TD-DFT calculated Uv-vis spectra of 8b (red) and 9b (blue) and associated molecular orbitals. (The computed signal, λ_{max} 435, is artificially large due to unoptimised peak broadening)**

4.2 Electrochemical Studies of Compounds 8 and 9

It may be expected, as the Fc unit of the 1,2 species **9a,b** possesses a slight $\delta+$ charge due to the partial ferrocenyl to carborane charge transfer, that the Fe centre would possess a larger oxidative electrode potential in a 1,2 species compared to that in the analogous 1,7 species. This is indeed the case as a study of the $Fe^{2+/3+}$ couple shows. **9a,b** exhibit increased electrode potentials relative to **8a,b** at the same temperature and in the same supporting electrolyte. Figure 4.5 compares the voltammetric profile of the 1,2 species **9a** and the analogous 1,7 species **8a**. Both isomers each display a slightly separated two-electron oxidation (in the presence of the poorly coordinating supporting electrolyte $[NBu_4][B(C_6F_5)_4]$) of the ferrocenyl units but the 1,2 species undergoes oxidation at potential values higher by about 0.6 V than those of the analogous 1,7 species. The pertinent formal electrode potentials are complied in Table 4.2. (Electrochemistry was kindly carried out by Prof. P. Zanello, University of Siena).

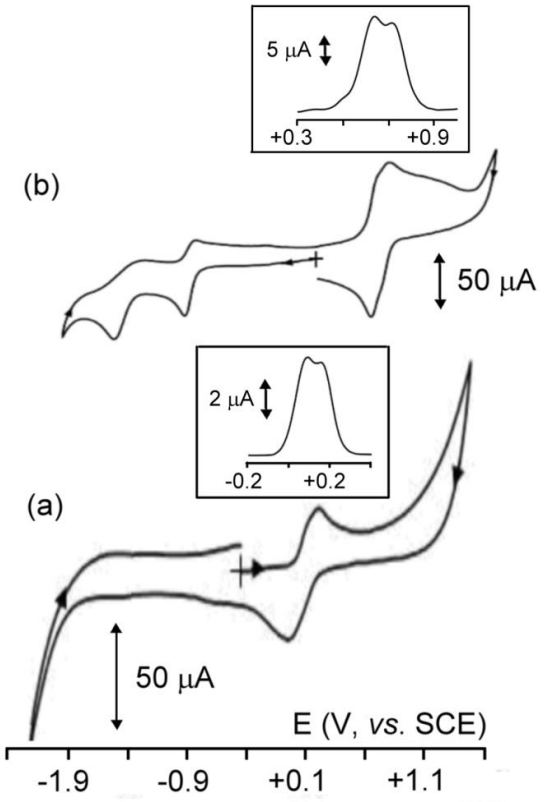

Figure 4.5 Cyclic and differential pulse voltammograms recorded at a gold electrode in THF solutions of (a) 8a ($1.0x10^{-3}$ M) and (b) 9a ($1.2x10^{-3}$ M) with $[NBu_4][B(C_6F_5)_4]$ supporting electrolyte (0.05 M)

Table 4.2 Formal electrode potentials (V, *vs.* SCE) for the redox changes exhibited by compounds 8a,b and 9a,b in THF containing different supporting electrolyte

Compound	$E^{\circ\prime}$ 1st oxidation	$E^{\circ\prime}$ 2nd oxidation	$E^{\circ\prime}$ 1st reduction	$E^{\circ\prime}$ 2nd reduction	Supporting electrolyte	Temperature /K
8a	+0.05	+0.15	-	-	$[NBu_4][B(C_6F_5)_4]$	293
	+0.04	+0.12	-	-		253
	+0.55	+0.55	-	-	$[NBu_4][PF_6]$	293
8b	+0.33	+0.40	-	-	$[NBu_4][B(C_6F_5)_4]$	293
	+0.27	+0.35	-	-		253
	+0.03	+0.03	-	-	$[NBu_4][PF_6]$	293
	+0.06	+0.06	-	-		253
9a	+0.64	+0.71	-0.94[a]	-1.56[a]	$[NBu_4][B(C_6F_5)_4]$	293
	+0.59	+0.66	-0.97[a]	-1.50[a]		253
	+0.60	+0.60	-0.93[a]	-1.52[a]	$[NBu_4][PF_6]$	293
9b	+0.62	+0.66	-0.79[a]	-1.34[a]	$[NBu_4][B(C_6F_5)_4]$	293
	+0.63	+0.67	-0.76[a]	-1.30[a]		253
	+0.58	+0.58	-0.78[a]	-1.43[a]	$[NBu_4][PF_6]$	293
$Fe(C_5H_5)_2$	+0.59	-	-	-	$[NBu_4][B(C_6F_5)_4]$	293
	+0.54	-	-	-	$[NBu_4][PF_6]$	293

[a] partial chemical reversibility

Figure 4.6 details the voltammetric response of **8b** in THF solutions in different supporting electrolytes. In the presence of a strong coordinating supporting electrolyte, $[NBu_4][PF_6]$, the 1,7-CPmFc disubstituted compound **8b** gives rise to a single, reversible oxidation (Figure 4.6 (a)), which in controlled potential coulometry consumes two electrons per molecule. The redox pattern of **8b** containing a poorly coordinating electrolyte, $[NBu_4][B(C_6F_5)_4]$, shows the splitting of the two electron oxidation into two slightly separated one-electron oxidations (Figure 4.6 (b) and (c)). The $[B(C_6F_5)_4]^-$ anion possesses a very low ion-pairing capacity so in the sequential oxidation processes of the Fc units in **8b** the electrostatic repulsion between the electrogenerated charged cations notably increases thus leading to separations in the relative anodic processes. The separation is only very slight ($\Delta E^{\circ\prime}$ = 0.07 V) indicating only a minimal interaction of the ferrocenyl units exists.

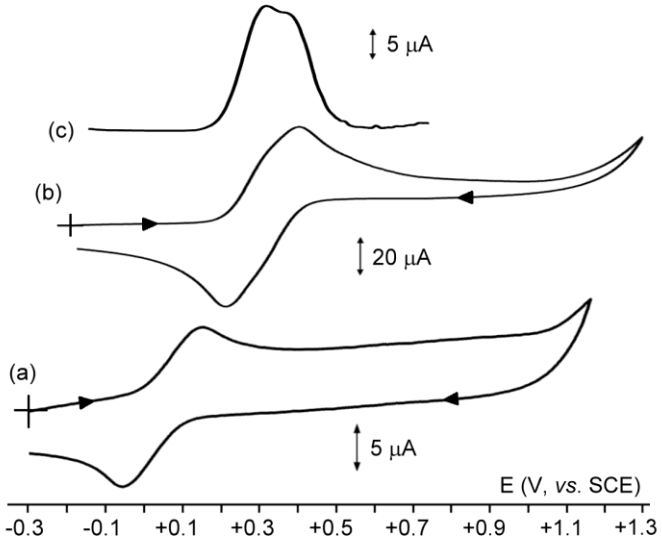

Figure 4.6 (a) Cyclic voltammogram of 8b ($0.2x10^{-3}$ M) in THF solution containing $[NBu_4][PF_6]$ (0.2 M) supporting electrolyte; (b) cyclic and (c) differential pulse voltammograms of 8b ($1.2x10^{-3}$ M) in THF solution containing $[NBu_4][B(C_6F_5)_4]$ (0.05 M) supporting electrolyte. Gold working electrode. Scan rates: (a,b) 0.1 V s^{-1}; (c) 0.01 V s^{-1}. T = 293 K

Cyclic voltammetric tests on the exhaustively oxidised solution afford profiles quite complimentary to those in Figure 4.6 thus indicating a relatively stable electrochemically generated dication $[\mathbf{8b}]^{2+}$. The solution progressively turns from yellow/orange to a typical green colour normally associated with ferrocenium derivatives. The UV-vis spectral changes, as **8b** is transformed into $[\mathbf{8b}]^{2+}$, recorded under the cumulative consumption of electrons are shown in Figure 4.7. The rising band at 640 nm is representative of a ferrocenium species. The isosbestic point at 690 nm supports the stability of the mono- and dications.

Exhaustive oxidation of **9a** affords a colour change from red to deep yellow after the addition of one electron per molecule and green after two electrons per molecule. The spectrochemical profiles of **9a** and **9b** are shown in Figure 4.8. The mono- and dications derived from **9a** are electrochemically quite stable as seen by the appearance of two isosbestic points at 431 and 560 nm. The rising band at 646 nm is typical of ferrocenium species. Exhaustive two-electron oxidation of **9b**, however, progressively turns the sample from purple to grey and finally pale yellow. The original broad bands at 529 and 600 nm in the THF solution disappear and an isosbestic point appears at 410 nm. The

occurrence of the final pale yellow is unexpected and suggests that the HOMO of **9b** may not be purely contributed to by the ferrocenyl ligands.

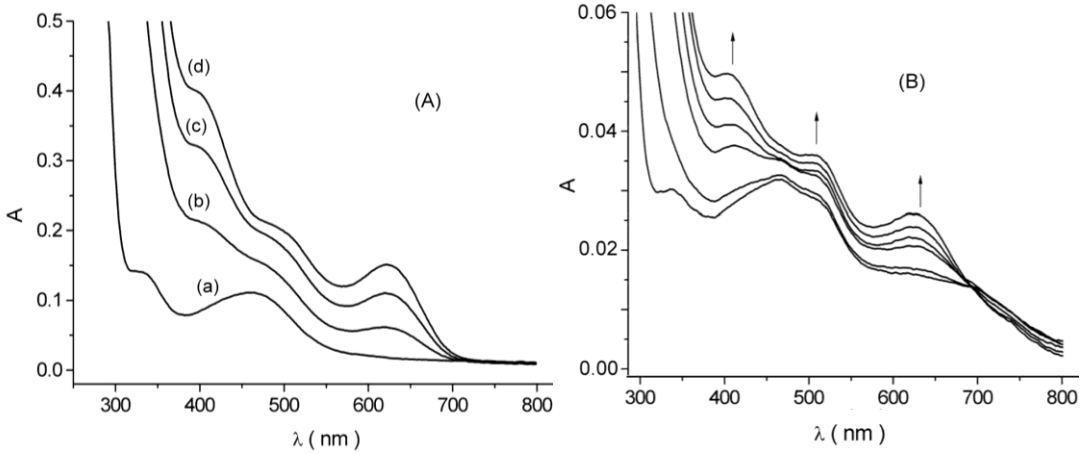

Figure 4.7 UV-vis spectral changes upon progressive oxidation of 8b. THF solution containing (A) [NBu$_4$][PF$_6$] ((a) original solution, (b,c,d) after overall consumption of *ca.* 0.5, 1, and 2 electrons/molecule respectively) and (B) [NBu$_4$][B(C$_6$F$_5$)$_4$] supporting electrolyte

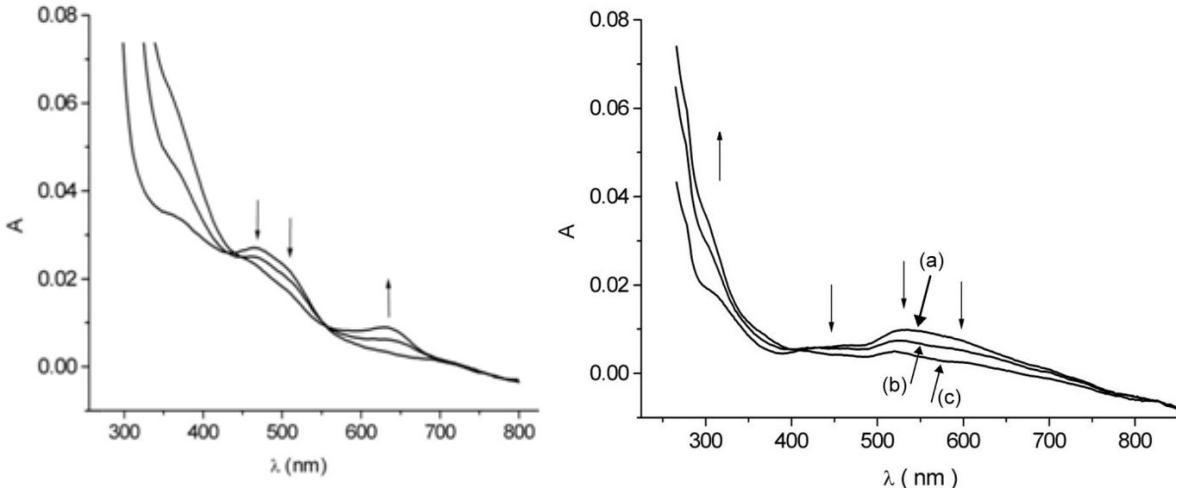

Figure 4.8 left - UV-vis spectral changes of 9a upon progressive oxidation in THF solution containing [NBu$_4$][[B(C$_6$F$_5$)$_4$] supporting electrolyte (0.05 M); right - UV-vis spectral changes upon progressive oxidation of 9b in THF solution containing [NBu$_4$][B(C$_6$F$_5$)$_4$] supporting electrolyte (0.03 M). (a) original solution; (b) after *ca.* 1-electron and (c) 2-electron oxidation

The voltammetric profiles of **9a** (Figure 4.5 (b)) and **9b** (Figure 4.9) are very similar. There is only a slight difference in the separation of the two almost overlapping anodic steps ($\Delta E^{\circ\prime}$= 0.04 V *vs.* 0.07 V) likely to be due to the bulkier Pm units of **9b** shielding the through-space interaction between the progressively charged ferrocenyl units with respect to the smaller methyl groups of **9a**.

The voltammetric profiles of both 1,2 species also displays two cathodic processes which are assigned to the one- and two-electron reductions of the central 1,2-*closo*-$C_2B_{10}H_{10}$ units. These reduction steps show signs of reversibility but are actually complicated by slow following chemical reactions and a relatively quick scan rate approaching 1.0 V s^{-1} is required to obtain their voltammeric profiles. The same experimental conditions show no reductive redox activity for the 1,7- analogues or the unsubstituted 1,2-, 1,7- and 1,12-*closo*-$C_2B_{10}H_{12}$ carboranes.

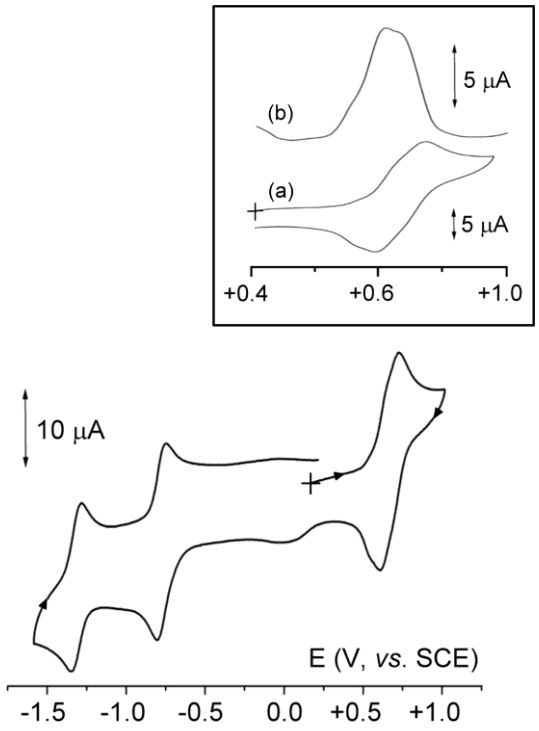

Figure 4.9 Cyclic voltammogram recorded at a gold electrode in THF solution of 9b ($0.3x10^{-3}$ M) (scan rate 0.2 V s^{-1}). The inset focuses on the anodic response: (a) cyclic voltammogram (scan rate 0.1 V s^{-1}); (b) differential pulse voltammogram (scan rate 0.02 V s^{-1}). $[NBu_4][B(C_6F_5)_4]$ supporting electrolyte (0.03 M). T=293 K

Table 4.3 Separation between formal electrode potentials (V *vs.* SCE) of the reduction processes exhibited by 9a and 9b compared to those exhibited by 1,2-Ph_2-1,2-*closo*-$C_2B_{10}H_{10}$ at room temperature

Compound	$E^{o\prime}$ 1st reduction	$E^{o\prime}$ 2nd reduction	$\Delta E^{o\prime}$	solvent
9a	-0.94	-1.56	0.62	THF
9b	-0.79	-1.34	0.55	THF
1,2-Ph_2-1,2-$C_2B_{10}H_{10}$ [1]	-1.18	-1.35	0.17	MeCN

[1] the presence of substituents in one of the phenyl rings does not substantially modify the electrode potentials

The TD-DFT calculations suggest a partial charge transfer from the ferrocenyl group to the central cage rendering the cage with a δ- charge. Table 4.3 reflects this as a relative ease of reduction of the 1,2 species **9a** and **9b** in comparison to 1,2-diphenyl carborane.

Table 4.3 also shows the carborane-centred reduction potentials are distinctly separate, more so than 1,2-diphenyl carborane which, interestingly, can undergo a one-electron reduction generating a stable radical anion[1] with ($2n$+3, n = no. of vertices) polyhedral skeletal electrons (PSE). **9a** and **9b** therefore present themselves as precursors for potentially attractive ($2n$+3) PSE synthetic targets. The 1,2-CPmFc substituted **9b**, perhaps unexpectedly, reduces more readily than the 1,2-CMe_2Fc analogue **9a** despite the Pm subunits being relatively more electron donating. It is therefore the actual cage deformation which presumably has a greater influence on cage reductions as the reductions actually become easier as the cage deformation becomes more severe.

Wade's rules[2] show the geometry of a cluster can be dramatically altered by changing the total number of electrons within. The addition of a single electron to a *closo* carborane derivative (such as 1,2-Ph_2-1,2-*closo*-$C_2B_{10}H_{10}$) has a serious impact on the geometry through the formation of a formal ($2n$+3) PSE radical anion[1] which has an elongated C-C distance, calculated to be 2.39 Å, compared with 1.76 Å for the neutral ($2n$+2) PSE analogous *closo* species. Addition of a second electron subsequently opens up the cluster generating a formal ($2n$+4) PSE *nido* species thus altering the geometry further where the cage carbon atoms are no longer connected. The addition of electron-donating substituents has been studied previously both experimentally[3] and computationally[4] and show a correlation between increased electron-donating ability of cage substituents and elongated C-C distance.

In the case of **9a** and **9b** it is the sterically induced cage deformation that primarily drives the electron transfer and not the electron-donating effect of the substituents. The sterically deformed cages of **9a** and **9b** may actually be stabilised by the presence of the extra electron density supplied by the charge transfer.

In conclusion, the stark colour differences and intensities of the 1,2 compared with the 1,7 species are consistent with those expected of charge transfer species. The relative increase in difficulty to oxidise the Fe^{2+} centres in the 1,2 species (due to the relatively low electron density at the metal centre) over the 1,7 species in conjunction with **9b** being slightly more susceptible to reduction than **9a** (due to the increased cage deformation) is consistent with this hypothesis.

4.3 References

4.1 M. A. Fox, C. Nervi, A. Crivello and P. J. Low, *Chem. Commun*., 2007, 2372.

4.2 K. Wade, *J. Chem. Soc. D*, 1971, 792.

4.3 M. A. Fox, C. Nervi, A. Crivello, A. S. Batsanov, J. A. K. Howard, K. Wade and P. J. Low, *J. Solid State Electrochem.*, 2009, **13**, 1483.

4.4 J. M. Oliva, N. L. Allan, P. v. R. Schleyer, C. Vinas and F. Teixidor, *J. Am. Chem. Soc*., 2005, **127**, 13538.

Chapter 5 Isomerisation Studies of Labelled Carboranes

5.1 Introduction

Since the early days of their discovery there has been much interest in the isomerisation mechanism of icosahedral carboranes. It was observed that 1,2-*closo*-$C_2B_{10}H_{12}$ undergoes thermal isomerisation at around 450°C to 1,7-*closo*-$C_2B_{10}H_{12}$ and as high as 700°C to 1,12-*closo*-$C_2B_{10}H_{12}$ (Figure 5.1).[1]

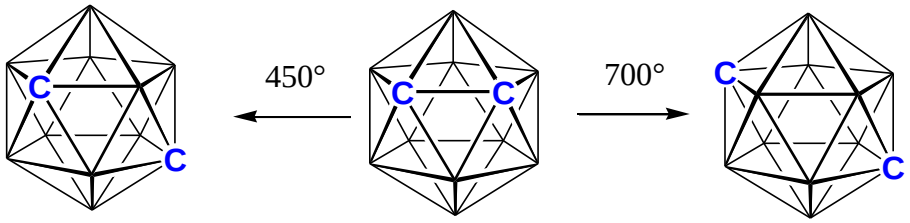

Figure 5.1 Isomerisation of 1,2-*closo*-$C_2B_{10}H_{12}$ to 1,7- and 1,12-*closo*-$C_2B_{10}H_{12}$

Many different theories have been suggested (e.g. hextuple diamond-square-diamond,[2] triangular face rotation[3] and pentagonal face rotation[4]) but an ultimate conclusion remains elusive, largely due to the high temperatures involved to facilitate such a rearrangement. Labelling experiments often fail or can be somewhat discredited as it has been shown that certain labelling groups often undergo intermolecular exchange at high temperature[5] rendering the results inconclusive in the context of isomerisation mechanisms.

Consequently experimentalists have resorted to sterically crowded metallacarboranes as a way of studying the isomerisation mechanisms of icosahedral carboranes.[6] The ability of such crowded metallacarboranes to isomerise at relatively low temperatures makes these potentially useful tools in the elucidation of the isomerisation mechanism of unmetallated carboranes. Early experiments saw deboronation and metallation of 1,2-Ph_2-1,2-*closo*-$C_2B_{10}H_{10}$ often yield an unexpected 2,1,8-MC_2B_9 metallacarborane species (where the carbon atoms are non-adjacent) and not the expected 3,1,2-MC_2B_9 species.[7] The 2,1,8-MC_2B_9 metallacarborane isomer had presumably formed via facile isomerisation of a transient 3,1,2-MC_2B_9 species which could not be isolated. Further experiments did isolate several metallated species possessing a highly distorted *pseudocloso* geometry which, when heated, affords a metallacarborane with the same

topology as a 1,7-*closo*-C_2B_{10} carborane i.e. the 2,1,8-MC_2B_9 isomer[8] (Figure 5.2). However, results of these studies using labelled metallacarboranes only show limited agreement between theoretical predictions (on carboranes) and experimental results (on metallacarboranes) possibly due to the increased electronic complexity of the incorporated metal vertex.

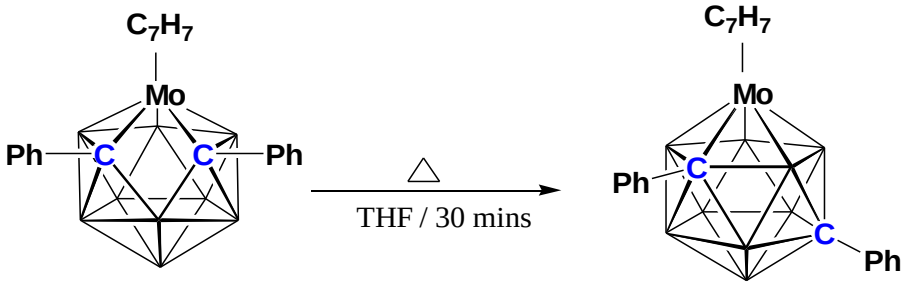

Figure 5.2 "1,2 → 1,7" isomerisation of a crowded molybdacarborane

Chapter 3 discussed the synthesis and study of 1,2-$(CR_2Fc)_2$-1,2-*closo*-$C_2B_{10}H_{10}$ (**9a,b**) that show some similarities to *pseudocloso* metallacarboranes, namely the highly distorted icosahedral structure incorporating a relatively increased C-C distance. If such a distortion results in a far easier thermal isomerisation for *pseudocloso* metallacarboranes would the same be true for distorted 1,2-*closo*-C_2B_{10} carboranes, 1,2-$(CMe_2Fc)_2$-1,2-*closo*-$C_2B_{10}H_{10}$ (**9a)** and 1,2-$(CPmFc)_2$-1,2-*closo*-$C_2B_{10}H_{10}$ (**9b)**? If so, it is theoretically possible to track labelled vertices throughout the isomerisation process at a relatively low temperature.

5.2 Thermolysis of 1,2-(CPmFc)$_2$-1,2-*closo*-$C_2B_{10}H_{10}$ (9b)

Compounds **9a** and **9b** were separately heated to reflux in toluene. **9a** showed no evidence of isomerisation (no colour change) and was recovered in almost 100% yield. The toluene solution of **9b,** however, changes from dark purple to light orange after sixteen hours of reflux. Three products were separated by chromatography: the orange species 1,7-(CPmFc)$_2$-1,7-*closo*-$C_2B_{10}H_{10}$ (**8b**) in 48% yield, a yellow solid 1-(CPmFc)-1,2-*closo*-$C_2B_{10}H_{11}$ (**12a**) in a 27% yield and an unidentified light orange species (**12b**), a product of decomposition, that could only be partially characterised (Scheme 5.1). **8b** was identified by ^{1}H and ^{11}B NMR spectroscopies.

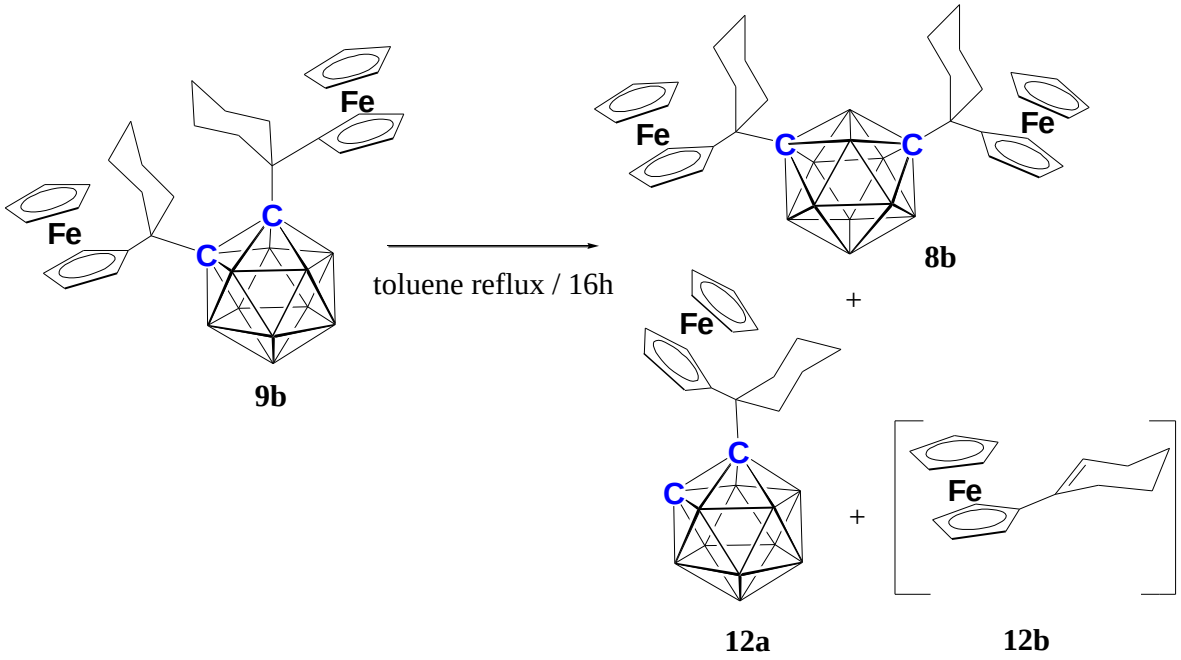

Scheme 5.1 Isomerisation of 9b to 8b and dissociation products

One of the lowest previous temperatures necessary for conversion of a 1,2- to a 1,7-species is 300^{o}C for the rearrangement of 1,2-(SiMe$_3$)$_2$-1,2-*closo*-$C_2B_{10}H_{10}$ as the addition of bulky silyl substituents very slightly elongate the C-C bond enough to help facilitate the isomerisation at this somewhat reduced temperature.[9] The temperature of refluxing toluene is now, by far, the lowest temperature required to thermally isomerise a 1,2-*closo*-C_2B_{10} species to a 1,7-*closo*-C_2B_{10} species and is less likely to succumb to the problems that have hindered previous labelling studies.

Mass spectrometric analysis of **12a** shows the parent ion to have a mass of 410 with a typical carborane envelope. Fragmentation is observed at *m/z* 266 (M - the C_2B_{10} cage). Elemental analysis was in good agreement with the expected values for $C_{18}H_{30}B_{10}Fe$.

The ^1H NMR spectrum of **12a** reveals a singlet at δ 4.14 that corresponds to the five unsubstituted Cp protons. Two multiplets at δ 4.23 and δ 4.07 sit either side of this and each integrates to two protons corresponding to the substituted C_5H_4 ring. A broad singlet observed at δ 2.49 is assigned to the cage C-*H*. The remaining ten protons from the Pm unit are observed over six multiplet peaks at δ 2.35 (2H), δ 2.20 (2H), δ 2.09 (2H), δ 1.77 (2H), δ 1.66 (1H) and δ 1.49 (1H).

In the $^{11}B\{^1H\}$ spectrum of **12a** four sharp resonances appear at δ -3.9 (2B), δ -9.4 (2B), δ -11.4 (2B) δ -14.2 (4B) which is representative of a high symmetry *closo* icosahedral carborane.

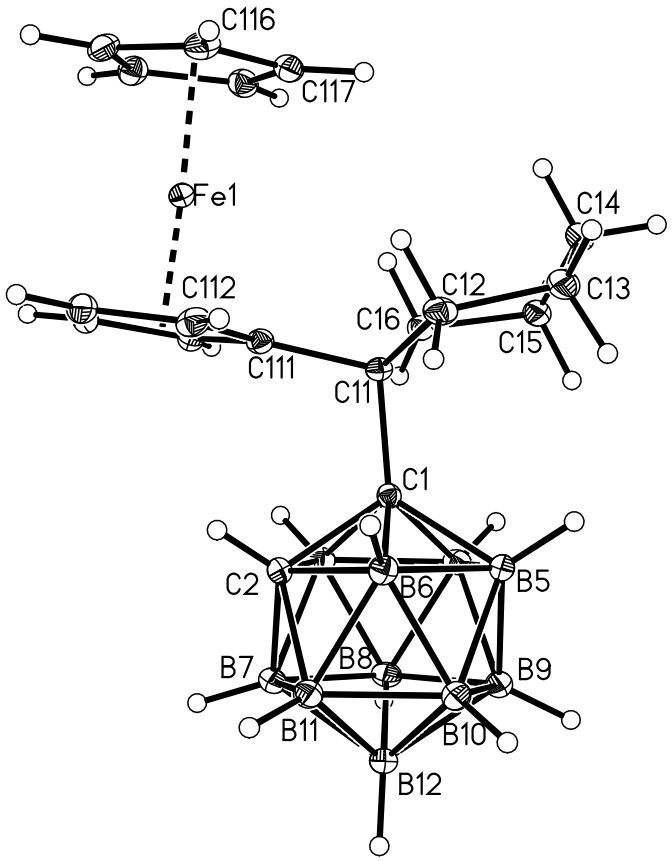

Figure 5.3 Molecular structure of 1-(CPmFc)-1,2-*closo*-$C_2B_{10}H_{11}$ (12a)

Figure 5.3 shows the molecular structure of **12a**. The C_6 ring adopts a chair conformation with the carborane occupying the axial position of C(11) and the ferrocenyl unit in the equatorial position. The CPmFc substituent on C(1) is slightly inclined away from positions B(4) and B(5) at angles of 123.31(7)° and 124.86(7)° respectively presumably due to a steric interaction between the H atoms on B(4) and B(5) and the axial H atoms on C(15) and C(13), the distances between these two pairs being 2.087 Å and 2.171 Å. The smallest angle between C(11)-C(1) and any of the five atoms on the top belt of the cage is to B(3) and measures 116.51(7)°. The dihedral angle between the two planes of the C_5 rings of the Fc unit measures 3.53° showing a slight distortion. Therefore even with only one bulky CPmFc substituent, a degree of intramolecular steric strain is evident within the molecule most notably around the C(11) position. Table 5.1 shows selected bond lengths and angles for compound **12a**.

Table 5.1 Selected interatomic distances (Å) and interbond angles (°) for 12a

C(1)-C(2)	1.6827(12)	C(11)-C(1)-C(2)	118.70(8)
C(1)-B(3)	1.7402(13)	C(11)-C(1)-B(3)	116.51(7)
C(1)-B(4)	1.7267(13)	C(11)-C(1)-B(4)	123.31(7)
C(1)-B(5)	1.7174(13)	C(11)-C(1)-B(5)	124.86(7)
C(1)-B(6)	1.7463(13)	C(11)-C(1)-B(6)	119.03(7)
C(1)-C(11)	1.5887(12)	C(1)-C(11)-C(12)	122.51(7)
C(1)-C(11)-C(111)	107.57(7)	C(1)-C(11)-C(16)	110.21(7)

A light orange species **12b** was also isolated in a similar yield to that of **12a**. Its mass spectrum shows a parent ion of *m/z* 266 and lacks a broad isotopic envelope that is often observed with heteroboranes. This non-cluster species consists of the second degradation product, derived from the CPmFc group. The isomerisation temperature of 110°C is sufficiently high to cleave this group from the cage which is also most likely aided by the severe intrinsic steric crowding that the precursor **9b** possesses.

The ^{1}H NMR spectrum of **12b** curiously shows a resonance in the olefinic region at δ 5.84 suggesting a C=C double bond is present in the C_6 unit. Supporting evidence for this is the presence of only eight other protons being observed over four multiplet peaks at δ 2.26, δ 2.10, δ 1.72 and δ 1.53 integrating to two protons each.

5.3 Labelling Studies of CPmFc Substituted Carboranes

By introducing labels onto the boron atoms of the crowded cage it may be possible to map their movement as it undergoes reduction and reoxidation followed by thermal isomerisation to provide evidence as to the nature of the isomerisation mechanism.

Substitution of iodine labels on the B(9) and B(10) positions of the 1,7-isomer using Grignard reagents was used to position R groups on the cage (R = Me, Ph).[10] Further reactions through to 9,10-R_2-1,7-$(CPmFc)_2$-1,7-*closo*-$C_2B_{10}H_8$ (**16**) yield a 1,7-*closo*-C_2B_{10} carborane with bulky substituents (Scheme 5.2) that is suitable for reduction and subsequent oxidation to a 1,2-*closo*-C_2B_{10} species.

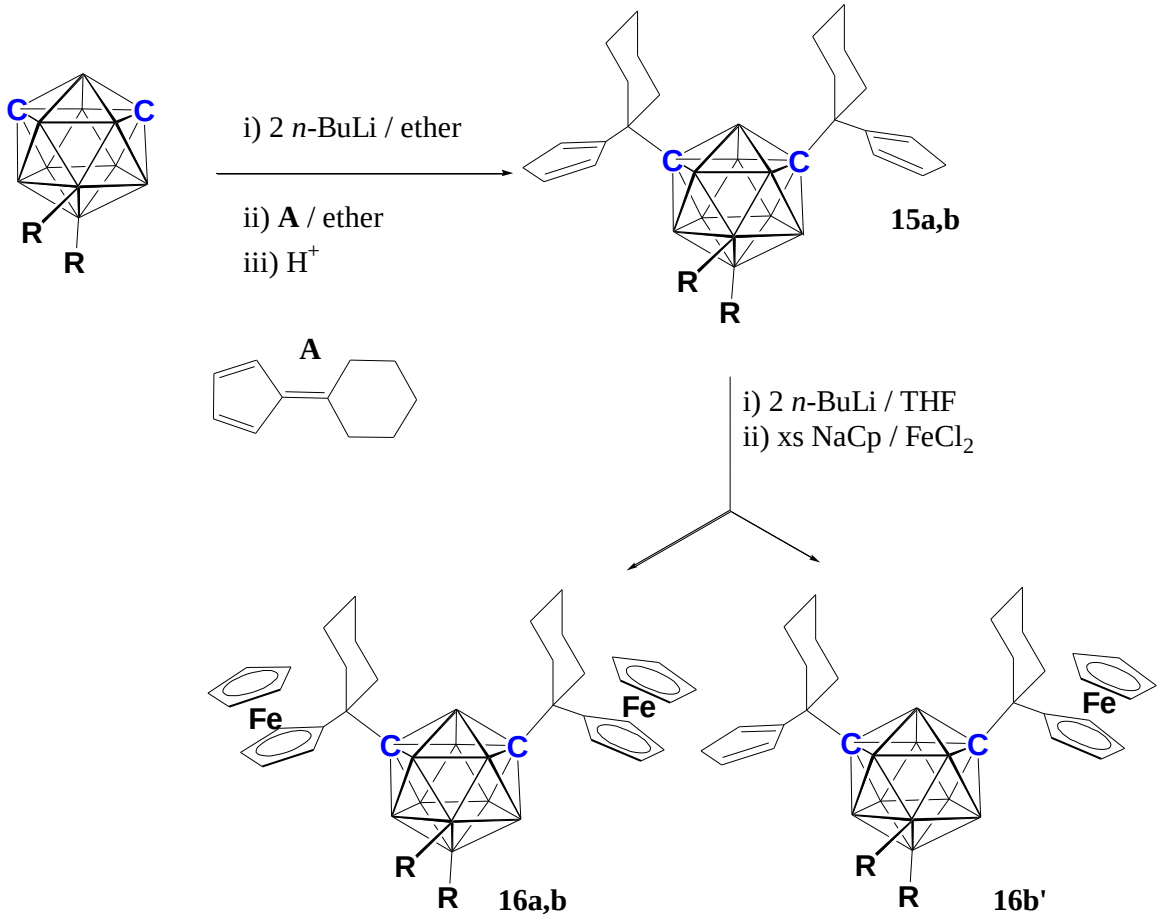

Scheme 5.2 Synthetic routes to compounds 15-16. (a, R=Me; b, R=Ph)

5.3.1 Reduction Reactions of 9,10-R_2-1,7-*closo*-$C_2B_{10}H_{10}$

5.3.1.1 1,7- to 1,2- 'Reverse Isomerisation' of 9,10-Me_2-1,7-*closo*-$C_2B_{10}H_{10}$

The B-disubstituted compound 9,10-Me_2-1,7-*closo*-$C_2B_{10}H_{10}$ was reduced with two equivalents of sodium dissolved in liquid ammonia followed by oxidation with $KMnO_4$[11] to afford a white solid 8,9-Me_2-1,2-*closo*-$C_2B_{10}H_{10}$ (**13a**) in moderate yield (Scheme 5.3). This reaction allows a comparison of the final B-labelled positions between C-unsubstituted carboranes with those of the C-disubstituted carboranes (which have been alluded to and are described in detail later in this chapter) when subjected to reduction and oxidation.

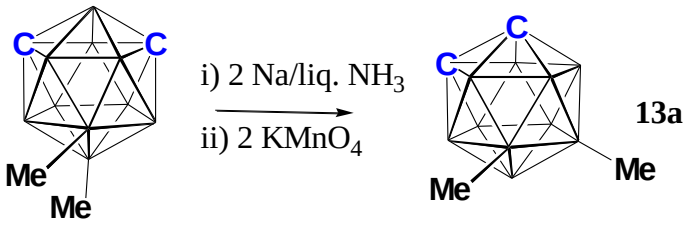

Scheme 5.3 Redox chemistry of 9,10-Me_2-1,7-*closo*-$C_2B_{10}H_{10}$

The ^{1}H NMR spectrum of **13a** shows the methyl resonances at δ 0.16 and δ 0.30 each of integral three and at δ 3.37 and δ 3.43 for each of the protons on the cage carbon atoms. The two sets of peaks indicate that there is no longer the same high symmetry as in 9,10-Me_2-1,7-*closo*-$C_2B_{10}H_{10}$ as the two cage protons and two methyl groups are no longer equivalent.

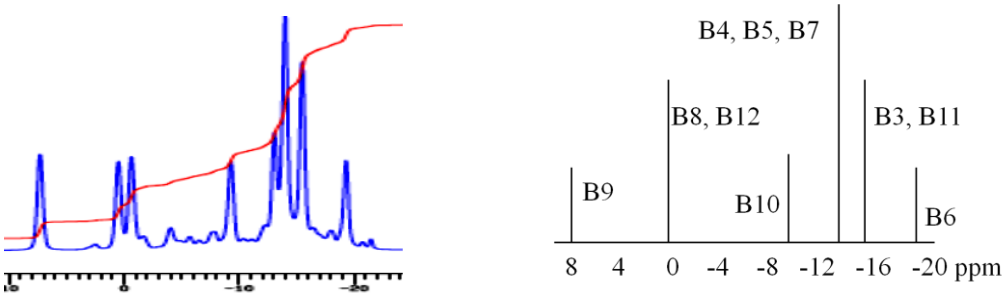

Figure 5.4 Experimental and DFT calculated $^{11}B\{^1H\}$ NMR spectra of 13a

This asymmetry is also observed in the $^{11}B\{^1H\}$ NMR spectrum. Eight signals can be seen from δ 7.3 to δ -19.3 of relative ratio 1:1:1:1:1:2:2:1 (Figure 5.4). The two highest frequency peaks belong to the labelled boron vertices and is evident by a lack of proton

coupling in the ^{11}B NMR spectrum. Attempts to identify the correct isomer of **13a** from the $^{11}B\{^{1}H\}$-$^{11}B\{^{1}H\}$ COSY NMR spectrum (Figure 5.5) **13a** were initially inconclusive as the cluster of peaks at δ -11 to -15 is very cluttered and difficult to decipher. An $^{11}B\{^{1}H\}$ NMR spectrum was calculated using DFT calculations[12] to predict the peak positions for **13a** (Figure 5.4). The spectrum obtained experimentally shows excellent agreement with that calculated, thus giving strong evidence that **13a** is 8,9-Me_2-1,2-*closo*-$C_2B_{10}H_{10}$.

With this information the $^{11}B\{^{1}H\}$-$^{11}B\{^{1}H\}$ COSY spectrum was retrospectively assigned and it can account for the structure with labels on positions B(8) and B(9). (N.B. due to C_{2v} symmetry of the parent 1,2-*closo*-C_2B_{10} species there are actually four equivalent forms of **13a** of which the 8,9-Me_2 isomer is only one).

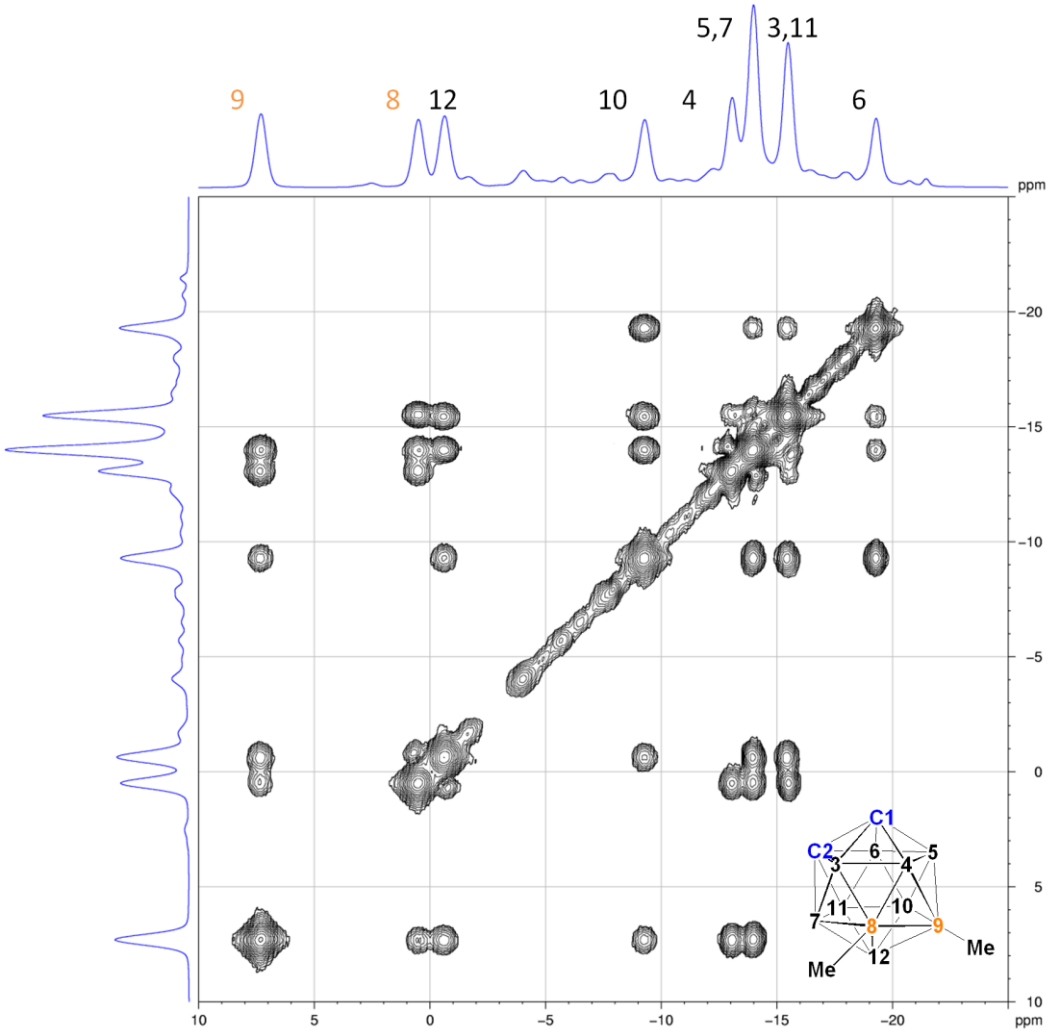

Figure 5.5 **$^{11}B\{^{1}H\}$-$^{11}B\{^{1}H\}$ COSY spectrum of 13a**

Computational studies[13] of the reduction and oxidation of unsubstituted 1,7-*closo*-$C_2B_{10}H_{12}$ also lend support to the 8,9-Me_2-1,2-*closo*-$C_2B_{10}H_{10}$ isomer being formed. The potential energy profile (Figure 5.6) shows the movement of boron atoms upon reduction of 1,7-*closo*-$C_2B_{10}H_{12}$ to the [7,9-*nido*-$C_2B_{10}H_{12}$]$^{2-}$ species. The labels are not highlighted but experimentally are positioned on B(9) and B(10).

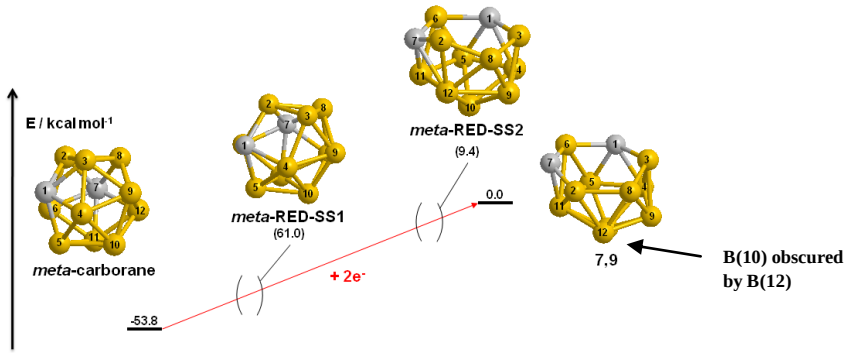

Figure 5.6 Potential energy diagram for the reduction of 1,7-*closo*-$C_2B_{10}H_{12}$ to [7,9-*nido*-$C_2B_{10}H_{12}$]$^{2-}$

Figure 5.7 details the oxidation pathway to 1,2-*closo*-$C_2B_{10}H_{12}$ from [7,9-*nido*-$C_2B_{10}H_{12}$]$^{2-}$. B(1) and B(4) in the [7,9-*nido*-$C_2B_{10}H_{12}$]$^{2-}$ species here correspond to the B(9) and B(10) positions in Figure 5.6. In the 1,2-*closo*-$C_2B_{10}H_{12}$ species which results from oxidation B(1) and B(4) correspond to B(8) and B(9) if numbered conventionally.

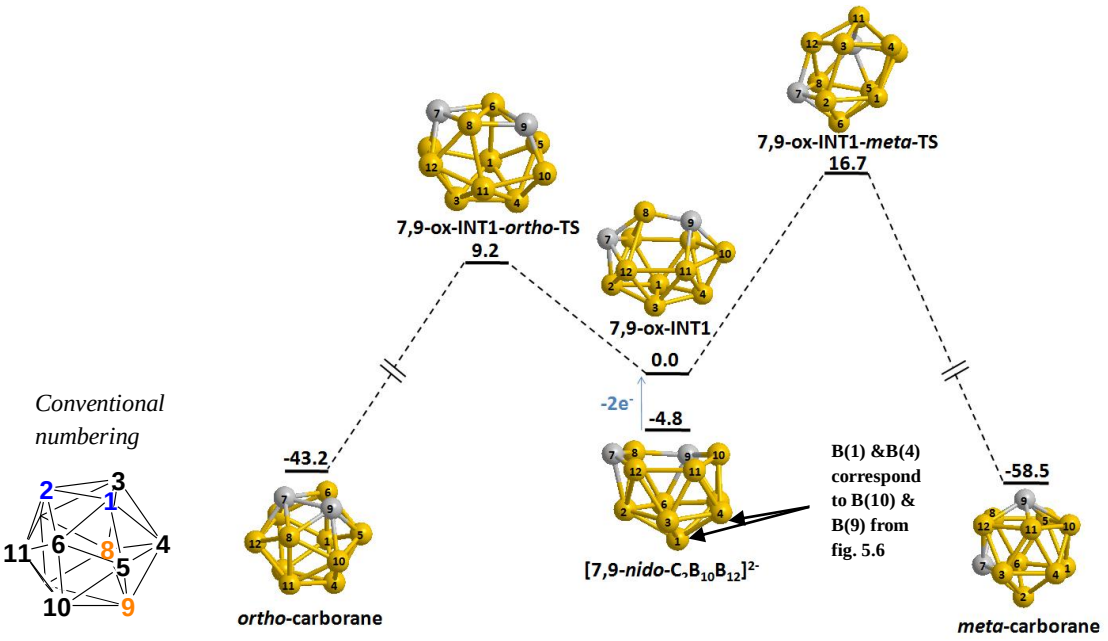

Figure 5.7 Potential energy diagram for the oxidation of [7,9-*nido*-$C_2B_{10}H_{12}$]$^{2-}$ to 1,7-*closo*-$C_2B_{10}H_{12}$ and 1,2-*closo*-$C_2B_{10}H_{12}$

5.3.1.2 Reduction and Metallation of 9,10-Me_2-1,7-*closo*-$C_2B_{10}H_{10}$

The two electron reduction followed by subsequent oxidation of 9,10-Me_2-1,7-*closo*-$C_2B_{10}H_{10}$ to produce 8,9-Me_2-1,2-*closo*-$C_2B_{10}H_{10}$ has been verified experimentally and theoretically. It was attempted to confirm the positions of the methyl labels in the calculated reduced species of 9,10-Me_2-1,7-*closo*-$C_2B_{10}H_{10}$ by 'trapping out' the intermediate methylated $[C_2B_{10}]^{2-}$ species with metallation of the six-atom open face. The resulting 13-vertex metallacarborane gives a representation of the *nido* species involved (Figure 5.8).

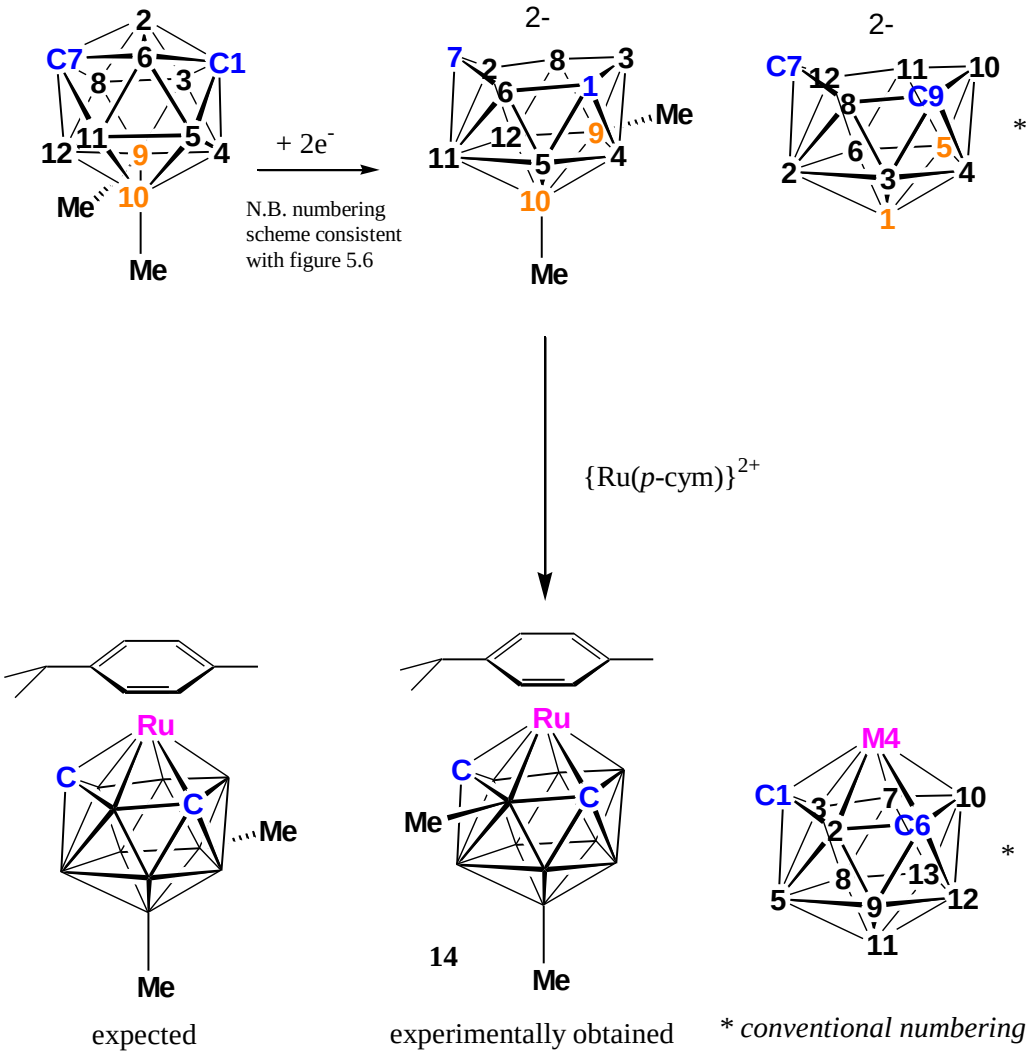

Figure 5.8 Reduction and metallation of 9,10-Me_2-1,7-*closo*-$C_2B_{10}H_{10}$, experimental and theoretical isomers

When 9,10-Me_2-1,7-*closo*-$C_2B_{10}H_{10}$ was reduced with excess sodium in liquid ammonia followed by subsequent reaction with [Ru(*p*-cymene)Cl_2]$_2$ a yellow band was isolated after preparative TLC. It was identified as 4-(*p*-cymene)-2,11-Me_2-4,1,6-*closo*-$RuC_2B_{10}H_{10}$ (**14**) by an X-ray diffraction study and was the highest yielding product of the reaction. Another three products were visible on the TLC plate but their low yields meant that they could not be successfully isolated and characterised.

This is an interesting anomaly as the expected isomer is actually 4-(*p*-cymene)-11,13-Me_2-4,1,6-*closo*-$RuC_2B_{10}H_{10}$ according to the calculated *nido* structure. The 'experimental' *nido* species, [1,8-Me_2-7,9-*nido*-$C_2B_{10}H_{10}$]$^{2-}$, looks unlikely to reoxidise to give 8,9-Me_2-1,2-*closo*-$C_2B_{10}H_{10}$ as the relative positions of the labels between the clusters are quite different. It is, however, known that several *nido* species may undergo facile isomerisation which may be rationalised by a series of TFRs.[14] It could ensue, therefore, the expected [1,5-Me_2-7,9-*nido*-$C_2B_{10}H_{10}$]$^{2-}$ could also rearrange in some manner prior to metallation in order to obtain the experimental ruthenacarborane. The remaining uncharacterised bands from chromatography are likely to be different isomers (with regards to the methyl group positions) of **14**.

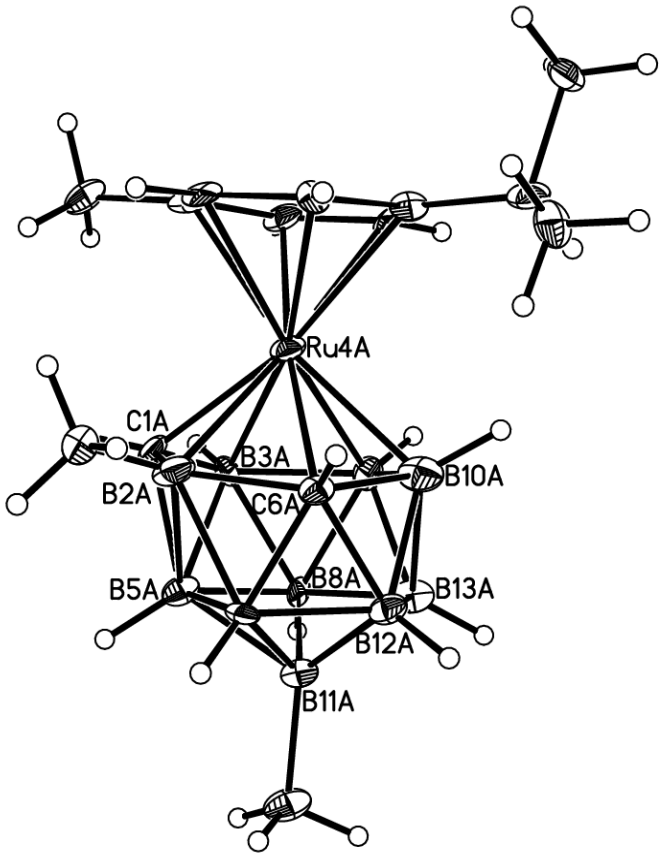

Figure 5.9 Molecular structure of ruthenacarborane 14

The ^{1}H NMR spectrum shows two doublets (centred on δ 5.65 and δ 5.78) assigned as the four aromatic protons of the *p*-cymene ligand and a single doublet for the six *i*-propyl methyl protons of the *p*-cymene ligand (δ 1.22). A septet at δ 2.74 corresponds to the *i*-propyl methine proton of the *p*-cymene ligand and a singlet at δ 2.13 reveals the three remaining methyl protons of the *p*-cymene ligand. The two cage C-*H* protons are visible as a broad singlet at δ 3.61.

The ^{11}B{^{1}H} NMR spectrum of **14** shows a 1:1:3:2:2:1 splitting pattern at δ 8.6, δ 5.4, δ -3.2, δ -8.4, δ -13.3 and δ -16.8. The proton-decoupled ^{11}B NMR spectrum shows the methyl labelled boron vertices occur at the highest frequency resonance, δ 8.6, and at δ -3.2, a co-incident signal.

The mass spectrum shows a parent ion within a typical carborane isotopic envelope centred at *m/z* 408 with no discernible fragmentation. Microanalytical data are in good agreement with the calculated values.

The molecular structure of **14** was determined by X-ray crystallography (Figure 5.9). There are two molecules in the asymmetric unit and appropriate structural data for both molecules are shown in Table 5.2.

Table 5.2 Selected interatomic distances (Å) and bond angles (°) for 14

C(1)-B(2)	1.525(15), 1538(15)	B(11)-B(13)	1.760(14), 1.779(14)
C(1)-B(3)	1.564(13), 1550(13)	B(11)-B(8)	1.749(14), 1.757(15)
C(1)-B(5)	1.766(10), 1.754(10)	B(11)-B(5)	1.800(14), 1.828(15)
C(6)-B(2)	1.734(15), 1.747(14)	B(11)-B(9)	1.734(13), 1.722(14)
B(2)-B(9)	1.856(12), 1.846(11)	B(11)-C(11Me)	1.615(10), 1.607(10)
B(3)-B(8)	1.794(11), 1.792(11)	B(2)-C(21Me)	1.565(13), 1.579(13)
B(3)-B(7)	1.819(15), 1.843(15)	C(Me)-B(2)-Ru	128.5(5), 127.9(5)
B(3)-B(5)	1.966(14), 1.965(14)	C(Me)-B(2)-C(1)	124.1(9), 123.0(9)
Ru-C(1)	2.110(10), 2.122(9)	C(Me)-B(2)-C(6)	119.4(9), 118.5(9)
Ru-B(2)	2.306(11), 2.286(10)	C(Me)-B(2)-B(9)	112.5(8), 112.4(8)
Ru-C(6)	2.272(8),2.285(8)	C(Me)-B(11)-B(12)	122.0(8), 123.5(8)
Ru-B(10)	2.242(10),2.225(10)	C(Me)-B(11)-B(13)	125.0(7), 125.8(7)
Ru-B(7)	2.290(9), 2.294(8)	C(Me)-B(11)-B(8)	119.8(8), 119.0(8)
Ru-B(3)	2.328(11), 2.317(11)	C(Me)-B(11)-B(5)	117.9(8), 116.3(8)
B(11)-B(12)	1.805(16), 1.774(16)	C(Me)-B(11)-B(9)	116.7(7), 116.8(8)

The B-Me bond is slightly shorter when positioned in the B(2) position at 1.565(13) Å and 1.579(13) Å compared to the B(11)-Me position where the bond lengths are 1.615(10) Å and 1.607(10) Å for each molecule in the asymmetric unit. C(6) is in a relatively unfavourable degree-5 site compared to C(1) which has a more favourable four connectivities. This added stability of C(1) perhaps allows for a stronger bond to the Ru atom. The Ru-C(1) bonds are relatively short at 2.110(10) Å and 2.122(10) Å compared to the Ru-C(6) bonds which are 2.272(8) Å and 2.285(8) Å. The methyl group at B(11) is inclined slightly towards the midpoint of B(5) and B(9). The methyl group on B(2) is inclined down towards B(9) at angles of 112.5(8)° and 112.4(8)° perhaps due to a slight steric interaction from the *p*-cymene ligand above.

5.3.1.3 Reduction and Oxidation of 9,10-Ph_2-1,7-*closo*-$C_2B_{10}H_{10}$

The need for a strong reducing agent is usually necessary for the reduction of 1,7-*closo* carboranes (and 1,12-*closo* carboranes) but the addition of certain substituents have been shown to aid the reduction process. The 1,7 carborane containing CPmFc substituents, **8b,** is readily reduced with relatively mild conditions of sodium metal in THF.

The literature also describes 1,12-Ph_2-1,12-*closo*-$C_2B_{10}H_{10}$ being readily reduced to [7,10-Ph_2-7,10-*nido*-$C_2B_{10}H_{10}$]$^{2-}$ with sodium in THF[15] whereas unsubstituted 1,12-*closo*-$C_2B_{10}H_{12}$ requires the more forcing conditions of sodium in liquid ammonia to be reduced.[15] The reduced form of 1,12-Ph_2-1,12-*closo*-$C_2B_{10}H_{10}$ in THF gives a deep red colour and is indicative of a successful reduction.

With this in mind 9,10-Ph_2-1,7-*closo*-$C_2B_{10}H_{10}$ was treated with two equivalents of sodium in THF (Scheme 5.4). A deep red colour was obtained after a few minutes suggesting the addition of electrons was successful. However, upon aerial oxidation, the product was identified by ^{1}H and $^{11}B\{^{1}H\}$ NMR spectroscopies as merely starting material, 9,10-Ph_2-1,7-*closo*-$C_2B_{10}H_{10}$, not the expected 8,9-Ph_2-1,2-*closo*-$C_2B_{10}H_{10}$ species (**13b**). A slightly different method of reduction is to treat excess sodium with a stoichiometric amount of naphthalene to give a dark green solution of sodium naphthalenide and use this solution as the reducing agent. This also produced the dark red colour associated with a reduced species but again yielded only starting material upon oxidation. A variety of reaction conditions were attempted by increasing the

amounts of sodium naphthalenide but there was no evidence of any 1,2-*closo* species being produced.

However, when 9,10-Ph_2-1,7-*closo*-$C_2B_{10}H_{10}$ was treated with sodium metal in liquid ammonia followed by oxidation with $KMnO_4$ two products were isolated: starting material and compound **13b**, tentatively assigned as 8,9-Ph_2-1,2-*closo*-$C_2B_{10}H_{10}$, in approximately equal amounts.

The mass spectrum of **13b** consists of a broad boron isotopic envelope centred on *m/z* 296 with no notable fragmentation. Elemental analysis is in good agreement with that expected for $C_{14}B_{10}H_{20}$.

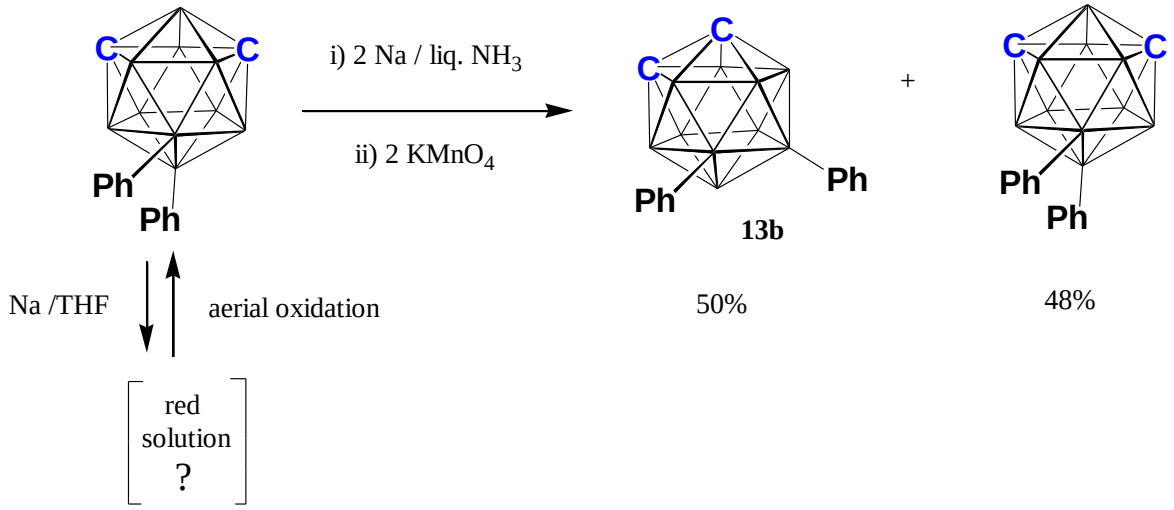

Scheme 5.4 Reduction and oxidation of 9,10-Ph_2-1,7-*closo*-$C_2B_{10}H_{10}$ in THF and liquid ammonia

The ^1H NMR spectrum shows a complex multiplet spanning a wide range from δ 7.06-7.38 integrating as ten protons in total which corresponds to the two phenyl substituents. A broad singlet signifying the cluster C-*H* protons is observed at δ 3.61. As **13b** is asymmetric it would be expected to show two C-*H* resonances therefore this peak is a (1 +1) coincidence for both protons.

$^{11}B\{^1H\}$ spectroscopy shows the asymmetry of **13b** more clearly. Seven peaks are observed at δ 8.0, δ 1.7, δ -2.5, δ -8.8, δ -13.9, δ -15.4 and δ -17.7 in a ratio of

1:1:1:1:3:2:1. The two highest frequency peaks show no coupling to ^{1}H in the ^{11}B NMR spectrum indicating these are the phenyl-substituted boron vertices.

It is unclear why THF as a solvent would inhibit the formation of a 1,2-*closo* species upon reduction and oxidation but it appears, by the visual colour change, that reduction of 9,10-Ph_2-1,7-*closo*-$C_2B_{10}H_{10}$, in some form, may occur. It is speculated that the two added electrons from sodium become delocalised within the phenyl substituents and do not possess a large enough reduction potential to reduce the cage whereas the stronger reducing conditions of sodium in liquid ammonia does offer at least some cluster reduction. The recovery of almost half of the starting material may support this hypothesis; a stoichiometric amount of sodium for the reduction of 9,10-Me_2-1,7-*closo*-$C_2B_{10}H_{10}$ yields only the 1,2-*closo* species (**13a**) as it is presumably reduced quantitatively and oxidises to yield exclusively the 1,2 carborane. A quantitative reduction of the diphenylated analogue may yield some 1,7-*closo* starting material if some electrons remain exclusively localised on the phenyl rings.

5.4 Synthesis and Characterisation of 9,10-R_2-1,7-$(CPmFc)_2$-1,7-*closo*-$C_2B_{10}H_8$ Compounds.

5.4.1 Synthesis of 9,10-Me_2-1,7-$\{CPm(C_5H_5)\}_2$-1,7-*closo*-$C_2B_{10}H_8$ (15a)

Deprotonation of 9,10-Me_2-1,7-*closo*-$C_2B_{10}H_{10}$ with *n*-BuLi in diethyl ether followed by addition of 6,6-pentamethylenefulvene yielded a pale yellow solid 9,10-Me_2-1,7-$\{CPm(C_5H_5)\}_2$-1,7-*closo*-$C_2B_{10}H_8$ (**15a**) (Scheme 5.2). Only one isomer is observed in the C_5H_5 rings of **15a** from ^{1}H NMR studies. Both rings are protonated in the β position in contrast to the B-unsubstituted analogue **7b** which exists as a mixture of both α and β isomers.

The ^{1}H NMR spectrum shows two multiplet peaks at δ 6.36 (4H) and δ 5.98 (2H) due to the presence of the olefinic protons on the C_5H_5 rings. A broad doublet, of integral four, at δ 2.98 signals the CH_2 protons of these rings. The pentamethylene ring protons are observed over several peaks: a broad doublet spanning δ 2.00 - 2.08 integrating as four protons, a broad multiplet over the range δ 1.32 - 1.51 consisting of twelve protons and another broad multiplet from δ 0.94 - 1.07 containing four protons. The two equivalent B-*Me* groups are observed as one singlet at δ 0.18 which integrates as six protons.

The $^{11}B\{^{1}H\}$ NMR spectrum has four signals at δ -2.8, δ -5.2, δ -12.70 and δ -18.8 of relative ratio 2:2:4:2 showing there is still C_{2v} symmetry within the cluster. The highest frequency resonance at δ -2.8 corresponds to the methylated boron atoms, B(9) and B(10). The ^{11}B NMR spectrum shows hydrogen coupling in all the other peaks except this one.

Mass spectrometric analysis of **15a** shows the parent ion to have a mass of 464 with a typical carborane isotopic envelope. Elemental analysis was in good agreement with the expected values for $C_{26}H_{44}B_{10}$.

5.4.2 Synthesis of 9,10-Me_2-1,7-$(CPmFc)_2$-1,7-*closo*-$C_2B_{10}H_8$ (16a)

The CH_2 group in the C_5H_5 rings of **15a** were deprotonated using *n*-BuLi in THF and a large excess of $FeCl_2$ and NaCp were added. This afforded a low-yielding orange solid after work up, 9,10-Me_2-1,7-$(CPmFc)_2$-1,7-*closo*-$C_2B_{10}H_8$ (**16a**) (Scheme 5.2).

The mass spectrum of **16a** shows the parent ion to have a mass of 705 with a typical carborane isotopic envelope. Elemental analysis was in reasonable agreement with the expected values for $C_{36}H_{52}B_{10}Fe_2$.

^{1}H NMR spectroscopy shows a singlet at δ 4.05 which corresponds to the ten C_5H_5 ring protons of the ferrocenyl units. Two multiplets are observed at δ 4.12 and δ 3.96, each integrating to four protons, indicative of the olefinic protons of the C_5H_4 units. Three large lumpy multiplet peaks represent the ten methylene units at δ 2.10 (4H), δ 1.88 (8H), δ 1.57 (6H) and δ 1.42 (2H). The B-*Me* groups are observed at δ 0.10 as a singlet corresponding to six protons. The presence of only one resonance each for the Cp and methyl units indicates the C_{2v} symmetry of the cluster has been retained.

The expected C_{2v} symmetry within the cluster is also evident from the $^{11}B\{^{1}H\}$ NMR spectrum. Three signals are observed at δ -2.9, δ -12.5 and δ -18.0 of relative ratio 4:4:2. The highest frequency resonance at δ -2.9 corresponds to the methylated boron atoms, B(9) and B(10), superimposed onto the resonance for two other boron atoms. The ^{11}B NMR spectrum shows hydrogen coupling in the form of doublets for both the other peaks and into an apparent triplet for the peak at δ -2.9. This is due to the *B*-Me atoms showing no coupling to ^{1}H (thus remaining a singlet) and the other *B*-H resonance splitting into a doublet.

5.4.3 Synthesis of 9,10-Ph_2-1,7-{CPm(C_5H_5)}$_2$-1,7-*closo*-$C_2B_{10}H_8$ (15b)

Deprotonation of 9,10-Ph_2-1,7-*closo*-$C_2B_{10}H_{10}$ with two equivalents on *n*-BuLi followed by addition of 6,6-pentamethylenefulvene yielded an off-white solid, 9,10-Ph_2-1,7-{CPm(C_5H_5)}$_2$-1,7-*closo*-$C_2B_{10}H_8$ (**15b**) in good yield (Scheme 5.2).

The ^{1}H NMR spectrum reveals the presence of two isomeric forms of the C_5H_5 rings as is commonly observed in such species. The two phenyl ring resonances at δ 7.27 and δ 7.08 are coincident for both the major (*β*) and minor (*α*) isomers. The *β* isomer shows three multiplets at δ 6.45, δ 6.41 and δ 6.07 which correspond to the olefinic protons of the C_5H_5 rings. The CH_2 moiety is observed as a broad doublet at δ 3.02. The pentamethylene units are observed over three broad lumpy peaks at δ 2.18, δ 1.13 – 1.66 and δ 0.97 – 1.11 integrating to a total of twenty protons. The minor *α* isomer shows coincident resonances with the *β* isomer for the phenyl rings and the Pm units which may explain the relatively increased peak broadness of the latter. The C_5H_5 rings of the *α* isomer are observed as three peaks in the olefinic region at δ 6.48, δ 6.43 and δ 6.22. The CH_2 is observed as a broad doublet at δ 2.89. The ratio of *α* to *β* is 1:4.

^{11}B{^{1}H} NMR spectroscopy shows four resonances at δ -1.8, δ -6.9, δ -12.5 and δ -17.3 in a 2:2:4:2 ratio. The highest frequency peak at δ -1.8 corresponds to the two substituted boron atoms as is observed by the presence of a singlet peak in the ^{11}B proton coupled spectrum.

The mass spectrum of **15b** shows a parent ion with the familiar boron isotopic envelope centred on *m/z* 588. Fragmentation occurs at *m/z* 511 and *m/z* 434 indicating the loss of one and two phenyl groups respectively. Elemental analysis shows reasonable agreement with the expected values for $C_{36}H_{48}B_{10}$.

5.4.4 Synthesis of 9,10-Ph_2-1,7-(CPmFc)$_2$-1,7-*closo*-$C_2B_{10}H_8$ (16b)

15b was deprotonated with two equivalents of *n*-BuLi in THF and excess $FeCl_2$ and NaCp were added to form the bis-ferrocenyl compound 9,10-Ph_2-1,7-(CPmFc)$_2$-1,7-*closo*-$C_2B_{10}H_8$ (**16b)** in poor yield. TLC analysis of the product mixture, in fact, revealed at least ten different compounds, only two of which (the two most intense and highest yielding bands) could be successfully isolated and characterised, **16b** and the

singly-metallated species, 9,10-Ph_2-1-{CPm(C_5H_5)}-7-(CPmFc)-1,7-*closo*-$C_2B_{10}H_8$ (**16b′**) in only slightly better yield than the former (Scheme 5.2).

The ^{1}H NMR spectrum of **16b** shows the B-Ph substituents over two multiplets at δ 7.19 and δ 7.08 integrating as four and six protons respectively. The ten Cp protons are observed as a single resonance at δ 4.10 and the C_5H_4 protons appear as multiplets at δ 4.16 and δ 4.05 each possessing an integral of four. The Pm signals appear as three broad multiplets ranging from δ 1.95 to δ 1.41 integrating to twenty protons in total.

^{11}B{^{1}H} NMR spectroscopy shows four signals with relative ratio 2:2:4:2 indicative of C_{2v} symmetry in the cluster. These resonances are found at δ -1.6, δ -6.0, δ -6.3 and δ -16.0. The highest frequency peak at δ -1.6 is the only resonance to remain uncoupled when ^{1}H coupling is allowed revealing this resonance to correspond to the phenyl-substituted boron vertices.

The mass spectrum of **16b** shows the parent ion at *m/z* 829 with notable fragmentation at *m/z* 752 and *m/z* 675 resulting from loss of one and two phenyl groups respectively. Elemental analysis was in excellent agreement with that expected for $C_{46}H_{56}B_{10}Fe_2$.

The other major compound, **16b′**, was analysed by ^{1}H NMR spectroscopy and, again, there are two isomeric forms (*α* and *β*) of the C_5H_5 unit. The major *β* isomer shows the three olefinic protons at δ 6.40 (2H) and 6.04 (1H) as multiplets. A broad doublet at δ 3.03 signifies the CH_2 moiety. The *α* isomer has three separate olefinic multiplet peaks at δ 6.47, δ 6.35 and δ 6.20. Another broad doublet is observed for the CH_2 part of the C_5H_5 ring spanning a range of δ 2.70 - 2.91. The ratio of *α*:*β* is 1:3. All remaining peaks are coincident for both *α* and *β* isomers. Resonances at δ 7.13 and δ 7.10 integrate to four and six protons respectively and correspond to the B-substituted phenyl rings. The ferrocenyl unit is signified by a singlet peak at δ 4.11 (5H) which corresponds to the unsubstituted C_5H_5 ring. The C_5H_4 protons are observed as two multiplets at δ 4.17 and δ 4.08 each integrating to two protons. The pentamethylene component of **16b′** is spread over five broad multiplets at δ 2.28, δ 1.95 – 2.12, δ 1.58 – 1.78, δ 1.34 – 1.53 and δ 1.00 – 1.10 with a total integral of twenty.

The ^{11}B{^{1}H} NMR spectrum shows four very broad resonances at δ -1.6, δ -6.4, δ -12.2 and δ -16.6 in a ratio of 2:2:4:2 suggesting some degree of symmetry remains even though each carbon vertex has a different substituent. The expected pattern for such a

species is 2:2:2:2:1:1. The broadness of the peaks may be explained by some of these resonances having very similar chemical shifts and significantly overlapping.

The mass spectrum of **16b′** shows a characteristic isotopic boron envelope centred on *m/z* 709. Elemental analysis is in good agreement with that expected for $C_{41}H_{52}B_{10}Fe$.

As small yields of both **16b** and **16b′** were obtained no further reactions were carried out. The remaining eight products, as observed by TLC analysis, were produced in much lower quantities and could not be isolated for any structural analysis. These competing reactions may explain the low yield of **16b**. It is unclear what the natures of these other species are but unknown chemistry may occur at the phenyl substituents. Such a plethora of products is not observed when metallating non-phenylated species (**7a**, **7b** and **15a**) and as each phenyl substituent possesses five unsubstituted carbon atoms these are potential sites for this unknown chemistry to occur.

5.5 Reduction and Oxidation of 9,10-Me_2-1,7-$(CPmFc)_2$-1,7-*closo*-$C_2B_{10}H_8$

Reduction of **16a** with four molar equivalents of sodium naphthalenide followed by aerial oxidation afforded two purple products in low yield, 8,9-Me_2-1,2-$(CPmFc)_2$-1,2-*closo*-$C_2B_{10}H_8$ (**17a)** and 9,12-Me_2-1,2-$(CPmFc)_2$-1,2-*closo*-$C_2B_{10}H_8$ (**17b)** in a ratio of approximately 3:2 (Scheme 5.5).

The ^{1}H NMR spectrum of **17a** shows multiplets at δ 4.20 and δ 4.18 each integrating to four protons which correspond to the protons on the C_5H_4 rings. A singlet at δ 4.09 signifies the Cp rings and integrates to ten protons and is the consequence of a (5+5) coincidence as the asymmetry of the cluster renders both CPmFc units chemically and hence magnetically inequivalent. The methylene units are observed over five multiplets at δ 2.57 (4H), δ 2.30 (4H), δ 2.20 (2H), δ 1.68 (6H) and δ 1.53 (4H). The B-*Me* substituents are observed as singlets at δ 0.29 and δ 0.01 each integrating to three protons. The presence of two inequivalent methyl groups corroborates the asymmetry of **17a** and a subsequent X-ray diffraction study reveals the methyl labels to be on the B(8) and B(9) positions.

This asymmetry is also apparent in the $^{11}B\{^1H\}$ NMR spectrum as six signals are observed at δ 10.9, δ 9.9, δ 0.2, δ -3.7, δ -14.0 and δ -17.3 in the ratio 1:1:4:2:1:1 (assuming that the integral four resonance is a (1+1+1+1) coincidence and the integral

two resonance is a (1+1) coincidence). The two highest frequency resonances correspond to the *B*-Me vertices as is observed by the lack of proton coupling in the ^{11}B NMR spectrum.

The mass spectrum of **17a** shows the parent ion at *m/z* 705 with a characteristic boron isotopic envelope. Fragmentation occurs at *m/z* 439 due to the loss of a CPmFc unit. The increased steric crowding presumably facilitates this fragmentation as it is not observed in the 1,7-*closo* analogue **16a.** Elemental analysis was in good agreement with that expected of $C_{36}H_{52}B_{10}Fe_2$.

The second product 9,12-Me_2-1,2-$(CPmFc)_2$-1,2-*closo*-$C_2B_{10}H_8$ (**17b**) shows spectroscopic evidence of C_{2v} symmetry within the cage. The ^1H NMR spectrum shows both methyl groups are magnetically equivalent due to a single resonance at δ 0.01 integrating to six protons. All eight protons from both C_5H_4 rings are observed as a multiplet at δ 4.21 and the ten protons from the Cp units are observed as a singlet at δ 4.10. The Pm unit produces three lumpy multiplets at δ 2.52, δ 2.18-2.34 and δ 1.58 integrating to twenty protons in total.

In the $^{11}B\{^1H\}$ NMR spectrum of **17b** four resonances are observed at δ 8.2, δ 2.6, δ -3.2 and δ -15.1 in a ratio of 2:2:4:2 giving clear indication of C_{2v} symmetry in the cage. The highest frequency resonance at δ 8.2 is due to the boron vertices containing the methyl substituents as is seen by the lack of proton coupling in the ^{11}B NMR spectrum.

The mass spectrum of **17b** shows the parent ion at *m/z* 705 with a characteristic boron isotopic envelope. Fragmentation occurs at *m/z* 439 due to the loss of a CPmFc unit. Once again, we assume that the increased steric crowding facilitates this fragmentation as such fragmentation is not seen in **16a.** Elemental analysis was in fairly good agreement for that expected of $C_{36}H_{52}B_{10}Fe_2$.

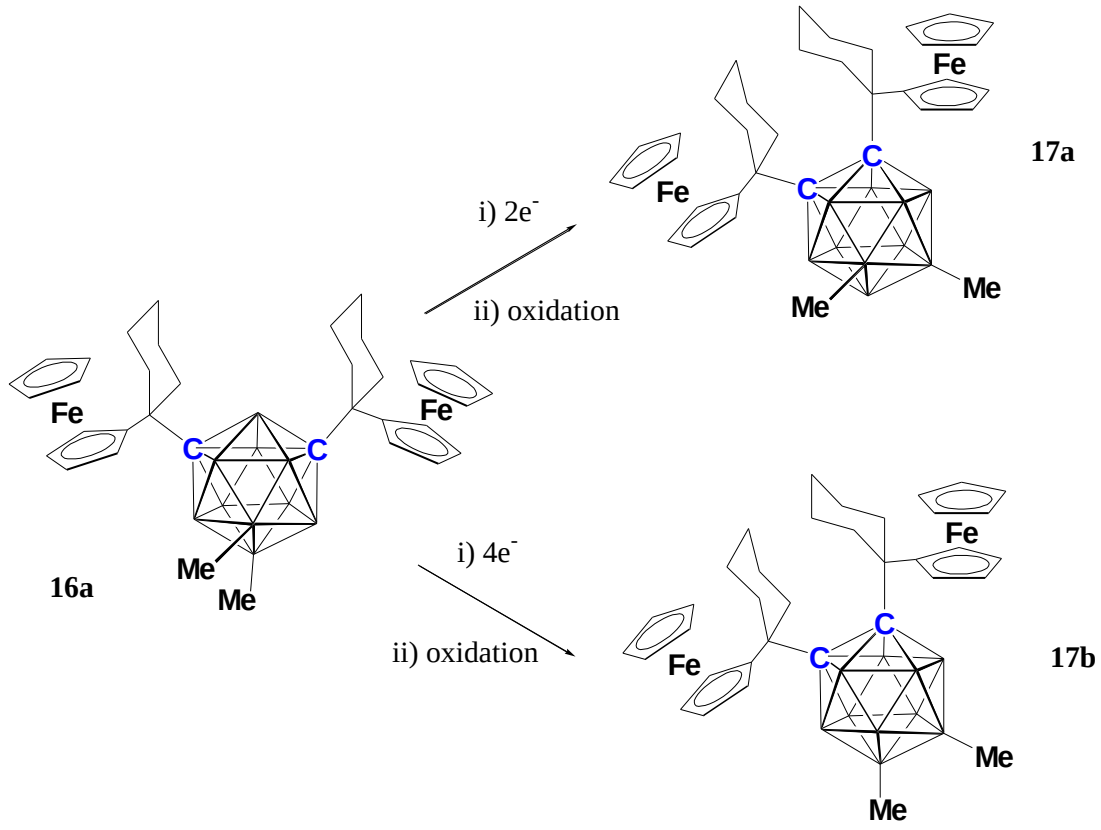

Scheme 5.5 Redox chemistry of 16a affording two 1,2 isomers, 17a and 17b

The unexpected occurrence of two 1,2 isomers raises questions as to the nature of the reduction process of **16a**. The reduction of **16a** was subsequently carried out using precisely two equivalents of sodium naphthalenide and the product oxidised by stirring in air to reveal only one isomer, the asymmetric isomer **17a**. To ascertain whether the second isomer, **17b**, was the result of a $4e^-$ reduction four equivalents of sodium naphthalenide were used. The dark green colour of the naphthalenide was rapidly decolourised after two equivalents and again (albeit very slightly slower) after a further two indicating reduction was occurring. Further equivalents (up to eight) did, in fact, decolourise but at a much slower rate to that observed previously after addition of four equivalents of sodium naphthalenide. A further experiment was carried out with pure ferrocene and two equivalents of sodium naphthalenide. This also showed slow decolourisation similar to that observed when excess naphthalenide was added to **16a**. Therefore it is a reasonable assumption that the first two equivalents of sodium naphthalenide carried out a $2e^-$ reduction with a further two carrying out a $4e^-$ reduction (which is not without precedent).[16] This reduction of **16b** is the first example of a $4e^-$ reduction of a non-C-C-tethered icosahedral carborane. Further decolourisation of naphthalenide may be attributed to reactions on the Fc units by the reactive nature of the

naphthalenide radical anion. $^{11}B\{^{1}H\}$ NMR spectroscopy of the product mixture shows the presence of both **17a** and **17b** in approximately 3:2 ratio after four equivalents of sodium naphthalenide were used.

5.6 Crystallographic Study of Compounds 15-17

The molecular structures of compounds **15-17** were determined by single-crystal X-ray diffraction studies. Some structural comparisons are made with naked 1,2-*closo*-$C_2B_{10}H_{12}$, 1,7-*closo*-$C_2B_{10}H_{12}$ and the B-unlabelled species 1,2-$(CPmFc)_2$-1,2-*closo*-$C_2B_{10}H_{10}$ (**9b**) and 1,7-$(CPmFc)_2$-1,7-*closo*-$C_2B_{10}H_{10}$ (**8b**).

Table 5.3 Selected interatomic distances (Å) for 15a and 15b

15a		15b	
C(1)-C(11)	1.5853(16)	C(1)-C(11)	1.589(3)
C(11)-C(12)	1.5244(17)	C(11)-C(12)	1.535(4)
C(12)-C(13)	1.4009(17)	C(12)-C(13)	1.374(4)
C(13)-C(14)	1.4406(19)	C(13)-C(14)	1.483(5)
C(14)-C(15)	1.479(2)	C(14)-C(15)	1.413(5)
C(15)-C(16)	1.4067(19)	C(15)-C(16)	1.393(5)
C(16)-C(12)	1.4261(17)	C(16)-C(12)	1.443(4)
B(9)-B(10)	1.801(3)	B(9)-B(10)	1.811(6)
B(9)-Me	1.5951(19)	B(9)-Ph	1.582(4)
C(1)...C(7)	2.714(2)	C(1)...C(7)	2.708(6)

Table 5.4 Selected Interatomic R-B-B-R distances (Å). Shaded entries allow B-B distance comparison with B-unlabelled species

1,7-$C_2B_{10}H_{12}$ [17]	B(9)-B(10)	1.768(9)
8b	B(9)-B(10)	1.782(5)
1,2-$C_2B_{10}H_{12}$ [17]	B(9)-B(12)	1.783(8), 1.768(9)
9b	B(9)-B(10)	1.776(5)
	B(9)-B(12)	1.756(5)
15a	B(9)-B(10)	1.801(3)
15b	B(9)-B(10)	1.811(6)
16a	B(9)-B(10)	1.802(3)
16b	B(9)-B(10)	1.804(5)
17a	B(8)-B(9)	1.800(9), 1.815(14)
17b	B(9)-B(12)	1.773(6)

The molecular structure of **15a** (Figure 5.10; left), determined crystallographically, confirms the methyl groups on the B(9) and B(10) positions. The position of the β-CH_2 on the C_5H_5 ring is also confirmed. Table 5.3 shows some important structural data for **15a**.

15a possesses C_{2v} symmetry and the asymmetric unit consists of only half the molecule split by a σ-plane dissecting through connectivities B(9)-B(10) and B(2)-B(3). The B(9)-B(10) connectivity is of interest due to the presence of the methyl groups (the crystallographically numbered vertex B(9A) is equivalent to B(10) when numbered conventionally). This has increased to 1.801(3) Å compared to 1.778(4) Å found in the previously synthesised 1,7-{CPm(C_5H_5)}$_2$-1,7-*closo*-$C_2B_{10}H_{10}$ (**9b**) and 1.768(9) Å in 1,7-*closo*-$C_2B_{10}H_{12}$.[17] This increase in bond length is expected due to the increased steric influence of the methyl groups. Table 5.4 contains selected RB-BR (R = Me, Ph) substituted bond lengths. In **15a** the planes of both C_5H_5 rings are orientated not quite face on subtending a dihedral angle of 23.99°. The shortened bond lengths between C(15)-C(16) and C(12)-C(13) confirm the presence of double bonds at these positions.

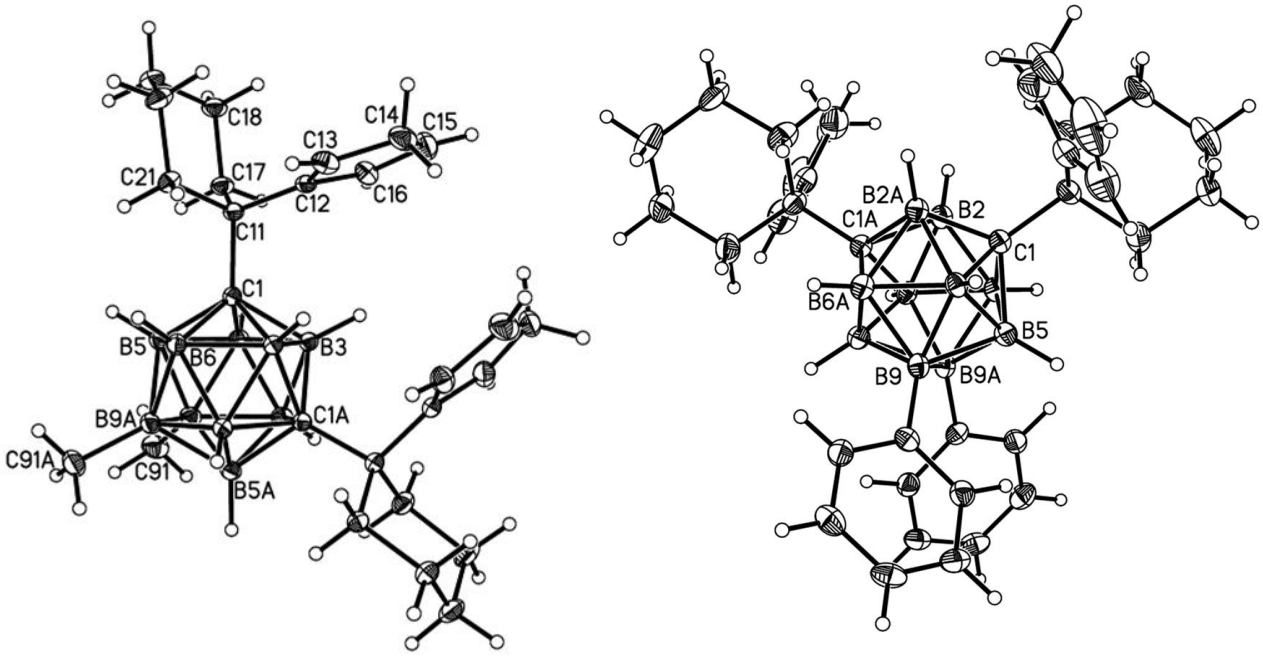

Figure 5.10 Molecular structures of 15a (left) and 15b (right). Both molecules share the same numbering scheme and all planes are numbered cyclically

The crystallographic study of **15b (**Figure 5.10; right**)** containing two B-Ph substituents, unsurprisingly shows a further increase in B(9)-B(10) bond length to 1.811(6) Å due to the slightly bulkier nature of the phenyl substituents which themselves subtend to a dihedral angle of 56.68°. The CPm(C_5H_5) substituents are orientated in opposite directions i.e. the Pm units and the C_5H_5 rings are on opposite sides of the cluster in relation to the other group as seen in Figure 5.11 (left). The position of the β-CH_2 in the C_5H_5 ring is supported by the shortened bond lengths of C(15)-C(16) and C(12)-C(13). Appropriate structural data for compound **15b** is given in Table 5.3.

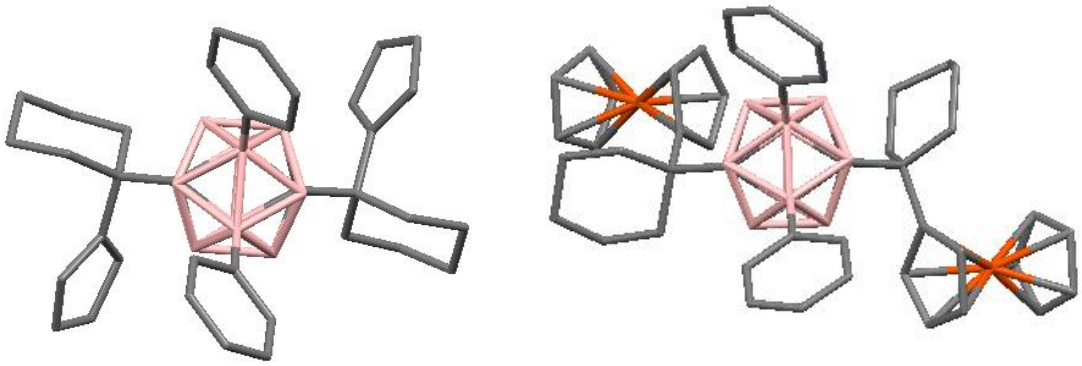

Figure 5.11 View perpendicular to B(9)-B(10) in 15b (left) and 16b (right) showing different Ph and CPmFc orientations. H atoms are omitted for clarity

Table 5.5 Selected interatomic distances (Å) and interbond angles (°) for 16a and 16b

16a		16b	
C(1)-C(11)	1.598(2)	C(1)-C(11)	1.598(4)
C(7)-C(71)	1.599(2)	C(7)-C(71)	1.616(4)
B(9)-C(9)	1.591(2)	B(9)-C(9)	1.581(5)
B(10)-C(10)	1.590(2)	B(10)-C(10)	1.576(5)
B(9)-B(10)	1.802(3)	B(9)-B(10)	1.804(5)
C(1)-C(11)-C(17)	105.40(12)	C(1)-C(11)-C(17)	106.9(2)
C(7)-C(71)-C(77)	107.54(12)	C(7)-C(71)-C(77)	107.0(3)
C(11)-C(1)-B(2)	118.69(12)	C(11)-C(1)-B(2)	118.7(2)
C(71)-C(7)-B(3)	116.72(12)	C(71)-C(7)-B(3)	119.8(2)
B(2)-B(3)	1.775(2)	B(2)-B(3)	1.773(5)
C(1)...C(7)	2.716(2)	C(1)...C(7)	2.724(5)

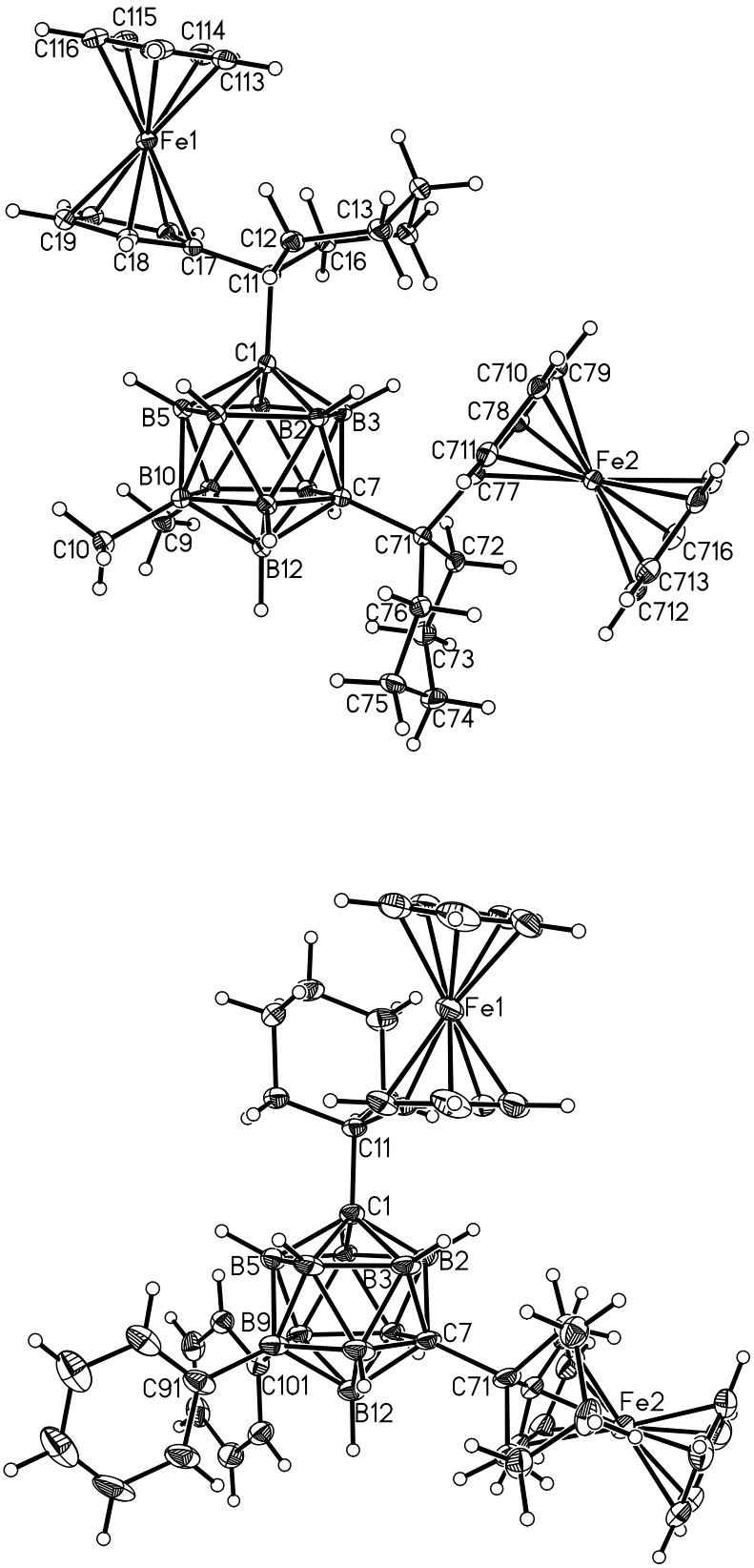

Figure 5.12 Molecular structures of 16a (top) and 16b (bottom)

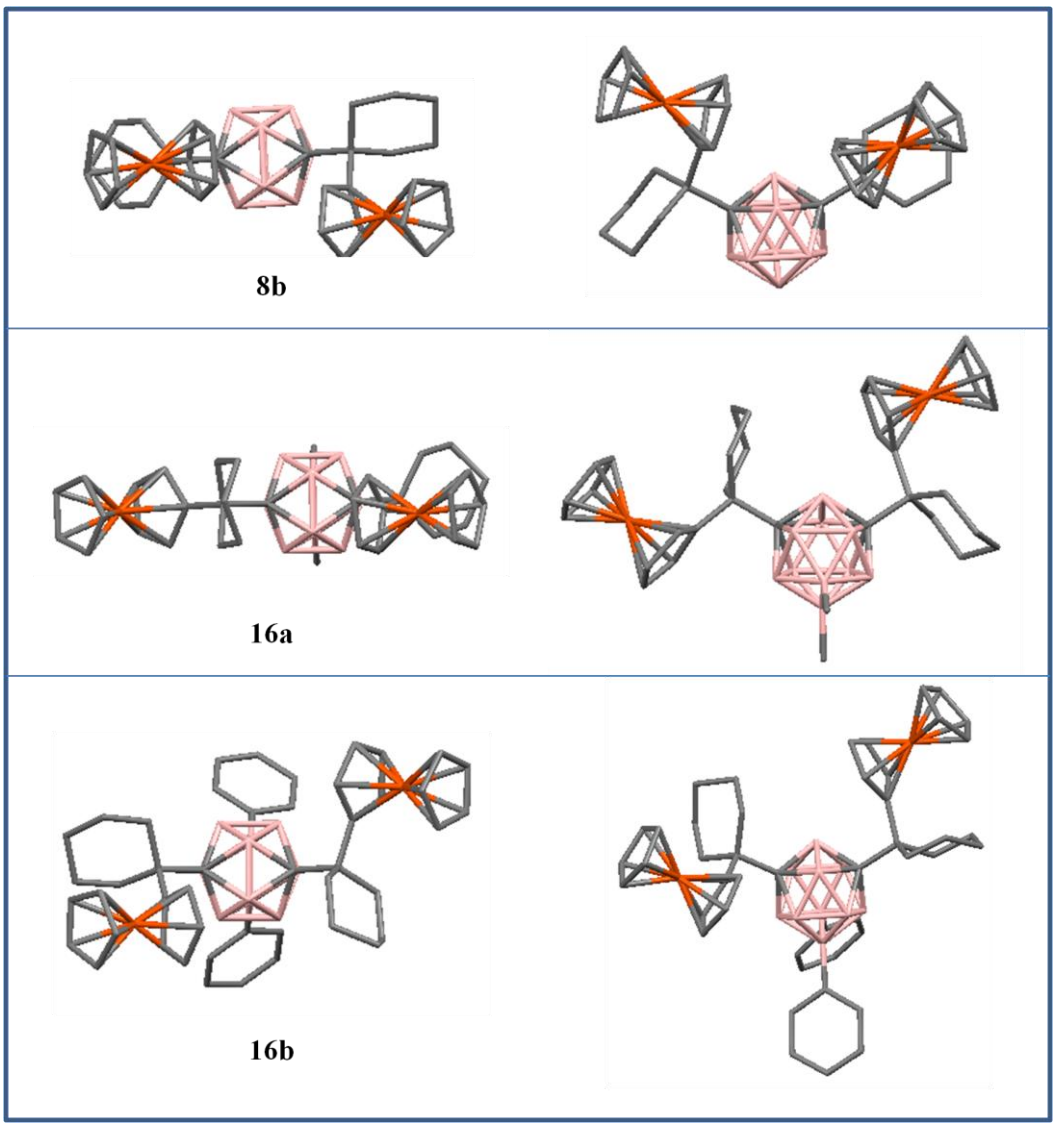

Figure 5.13 Orientations of CPmFc substituents on 1,7 species 8b, 16a and 16b. Left – top view; Right – side view. H atoms omitted for clarity

The molecular structure of **16a** (Figure 5.12; top) was also confirmed by an X-ray crystallographic study and appropriate data are given are Table 5.5. The addition of the FeCp unit has no effect on the B(9)-B(10) bond length compared to **15a**. In **16a** the length of this connectivity is 1.802(3) Å. The dihedral angles between the two C_5 rings on the Fe atoms are both small (4.01° and 2.99°) as both Fc units occupy the less sterically demanding equatorial positions of the C_6 ring. There is not much interference between the two CPmFc units; they are far enough apart in the molecule not to invoke any steric crowding. The orientations of the CPmFc units are different to that of the B-unlabelled analogue **8b**. In **8b** one Fc group is rotated almost orthogonally to the other while **16a** consists of a linear 'head to tail' arrangement i.e. the Pm unit on C(1) is in

close proximity to the Fc unit on C(7). A comparison of CPmFc orientation in **16a** with that in **8b** and **16b** is given in Figure 5.13.

The molecular structure of compound **16b** (Figure 5.12; bottom) was determined crystallographically and appropriate data are given in Table 5.5. The dihedral angle between C_5 units on Fe(1) and Fe(2) are 15.40° and 4.41° respectively. As seen in previous structures these dihedral angles are larger when the ferrocenyl substituent is situated on the more sterically-demanding axial position of the cyclohexyl ring. Both CPmFc substituents are orientated in almost opposite directions in **16b** (Figure 5.13) i.e. one Fc group is as far apart from the Ph substituents as possible and the other CPmFc group is almost orthogonally orientated to the other so that the Fc moiety is sited closer to one of the Ph groups.

X-ray crystallographic studies of **17a** (Figure 5.14; left) confirm the labels are positioned on B(8) and B(9) as expected; the labels were in the same positions predicted from the DFT calculations detailing the reduction and oxidation of 1,2-*closo*-$C_2B_{10}H_{12}$ and the product of experimental reduction-oxidation of 9,10-Me_2-1,7-*closo*-$C_2B_{10}H_{10}$. Important structural information is given in Table 5.6.

The crystallographic study (which revealed two crystallographically independent molecules in the aymmetric unit) shows that by sterically crowding the 1,2 carborane the C(1)-C(2) bond lengths increases to 2.181(9) Å and 2.195(10) Å. There is also a significant distortion in the Fc groups. The dihedral angles between the C_5 rings, all of which are on a more sterically demanding axial postion of the cyclohexyl ring, have increased to 10.87°, 11.10°, 11.52° and 12.86°. The two Pm units lie close to parallel with relatively small dihedral angles between the two mean planes of the C_6 rings of 28.67° and 18.34°.

It has been observed in Chapter 3 that increasing the C(1)-C(2) bond distance results in a decrease of the B(3)-B(6) distance, an effect also evident in **17a**. The B(3)-B(6) distance in 1,2-*closo*-$C_2B_{10}H_{12}$ is 2.886(12) Å[17] and has now decreased to 2.635(17) Å and 2.624(15) Å in in both molecules seen in the aymmetric unit. This in turn causes the B(6)-B(10) bonds to lenghthen to 1.814(17) Å and 1.838(13) Å and also the B(3)-B(8) bond lengths to increase to 1.807(16) Å and 1.852(13) Å, compared to 1.766(8) Å (averaged from four connectivities from two crytallographically independent molcules) in 1,2-*closo*-$C_2B_{10}H_{12}$.[17]

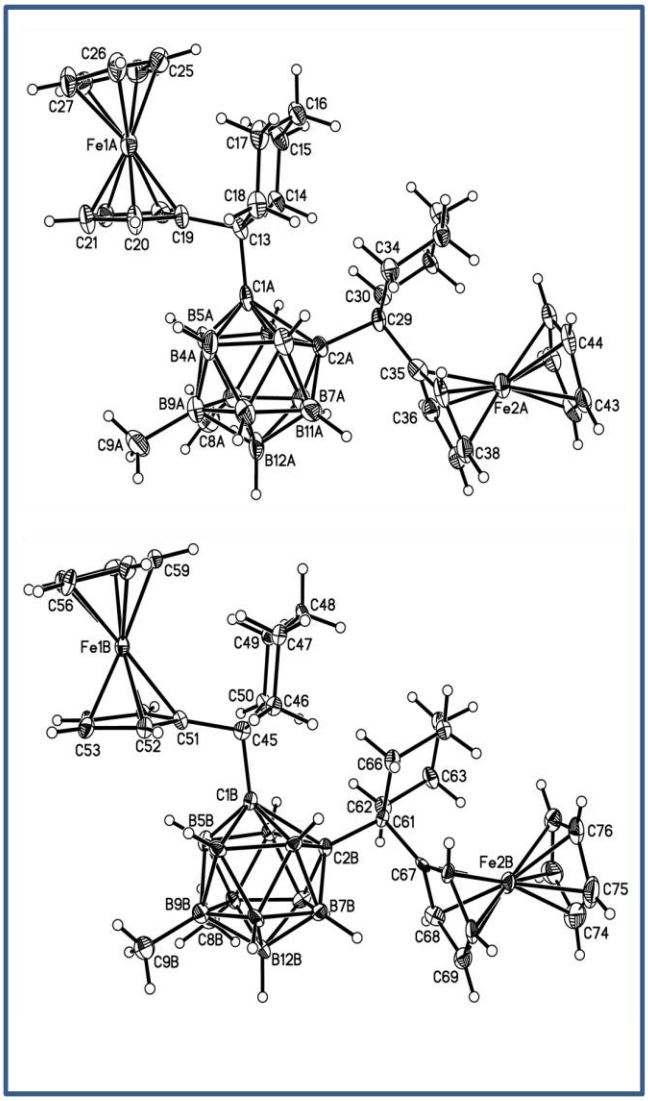

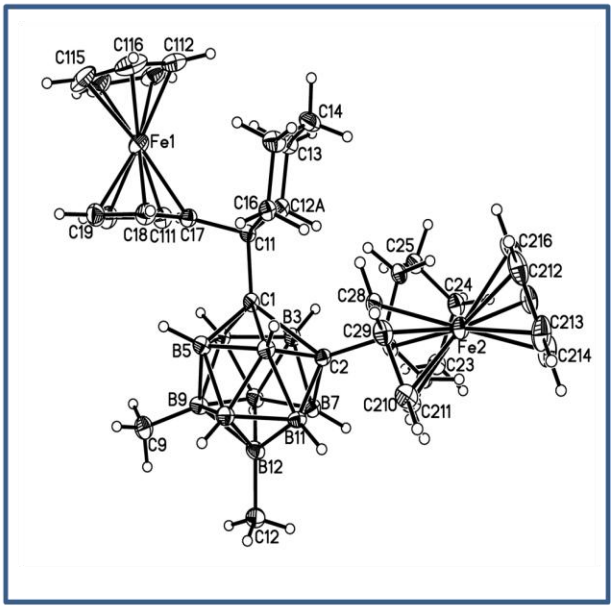

Figure 5.14 Molecular structures of crowded 1,2 B-labelled species, 17a (left) and 17b (right)

Table 5.6 Selected interatomic distances (Å) and interbond angles (°) for 17a and 17b

17a		17b	
C(1)-C(2)	2.181(12), 2.195(11)	C(1)-C(2)	2.204(4)
C(1)-B(4)	1.651(13), 1.644(12)	C(1)-B(4)	1.644(5)
C(1)-B(6)	1.776(14), 1.745(11)	C(1)-B(6)	1.756(5)
B(3)...B(6)	2.635(17), 2.642(15)	B(3)...B(6)	2.644(6)
B(3)-B(8)	1.807(16), 1.852(13)	B(3)-B(8)	1.820(5)
B(6)-B(10)	1.814(17). 1.838(13)	B(6)-B(10)	1.827(5)
C(8)-B(8)	1.560(15), 1.582(12)	B(12)-C(12)	1.592(5)
B(8)-B(9)	1.800(2), 1.815(14)	C(9)-B(9)	1.596(5)
C(13A)-C(1A)-B(3A)	124.0(7)	B(8)-B(9)	1.785(6)
C(19A)-C(13A)-C(14A)	110.2(7)	B(9)-B(12)	1.778(6)
C(45B)-C(1B)-B(3B)	123.0(6)	C(11)-C(1)-B(3)	122.8(3)
C(51B)-C(45B)-C(50B)	111.5(6)	C(12)-C(11)-C(16)	110.6(3)

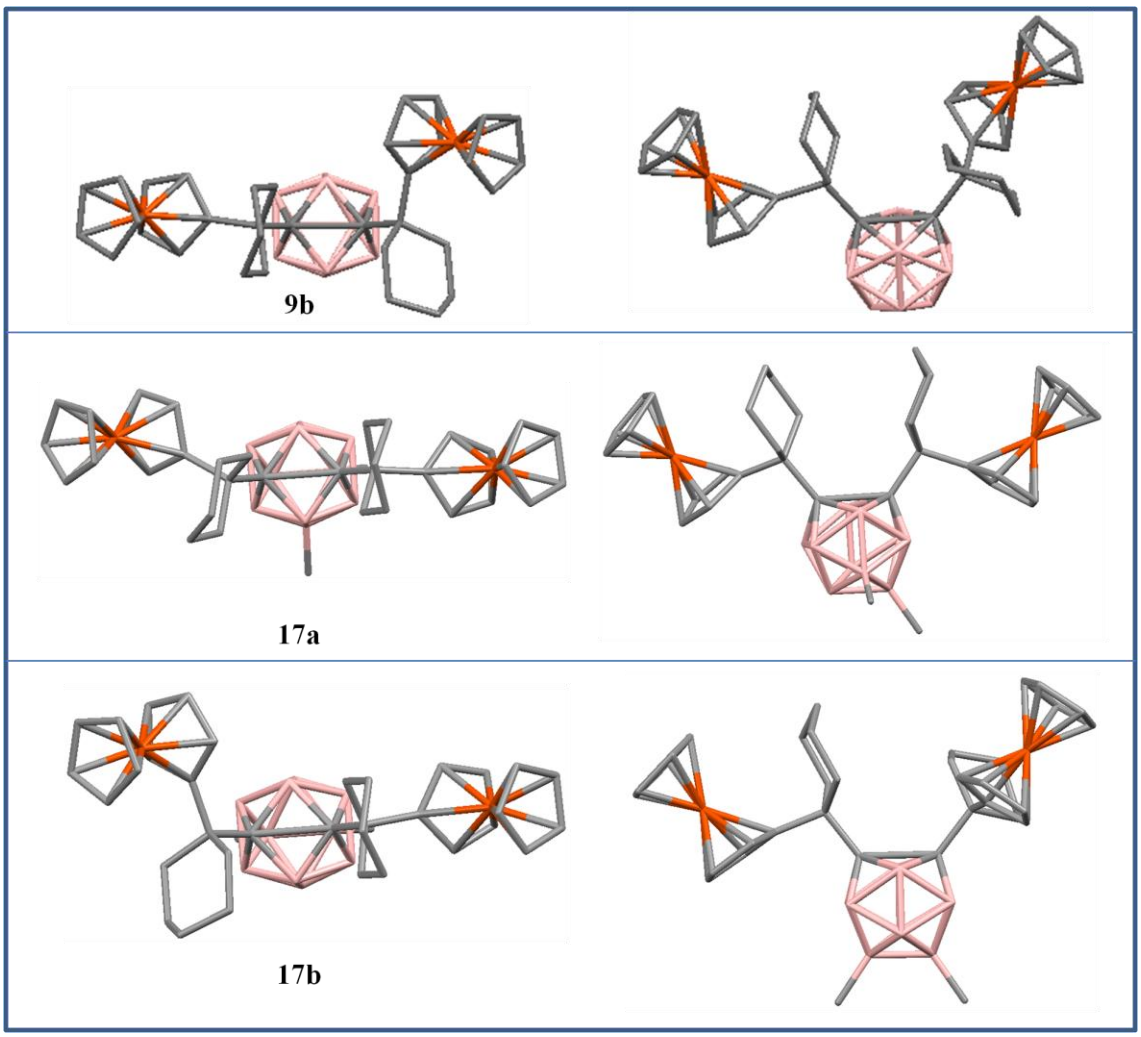

Figure 5.15 **Orientations of CPmFc substituents on 1,2 species 9b, 17a and 17b. Left – top view; Right – side view**

Table 5.7 **Ferrocenyl dihedral angles (°) inc. comparible data from chapter 3 (shaded). *a* = axial, *e* = equitoral indicates stereochemical position on C_6 ring**

8a	3.72, 3.68
8b	3.09 ***e*** , 11.60 ***a***
9a	3.99, 5.04
9b	11.65 ***a***, 4.97 ***e***
11	5.04, 3.62
16a	4.01 ***e***, 2.99 ***e***
16b	15.40 ***a***, 4.41 ***e***
17a	10.87 ***a***, 11.10 ***a***, 11.52 ***a***, 12.86 ***a***
17b	11.68 ***a***, 4.04 ***e***

The symmetric 1,2 species **17b** has methyl labels on positions B(9) and B(12) in agreement with the C_{2v} symmetry suggested by the ^{11}B NMR spectrum. Important structural information for **17b** is given in Table 5.6. The dihedral angle of the two C_5 rings on Fe(1) is relatively large at 11.68° but the dihedral angle of the C_5 rings on Fe(2) is relatively small, 4.04°. There is less distortion in the latter due to the different orientation of the CPmFc substituent minimising the steric crowding by the Fc unit occupying an equitorial cyclohexyl position. The C(1)-C(2) connectivity of **17b** is 2.204(4) Å which is longest now known in a (2*n*+2) PSE 1,2-*closo* carborane. This causes a shortening of the B(3)-B(6) distance to 2.644(6) Å. As expected, both B(3)-B(8) and B(6)-B(10) are elongated to 1.820(5) Å and 1.827(5) Å respectively. The distance between the two labelled boron atoms is 1.778(6) Å, identical to that of the unlabelled 1,7 isomer (**9b**) and, in fact, smaller than both Me-B–B-Me distances in **17a**. Figure 5.15 shows the PmFc substituents are practically orthogonally orientated (similar to the oreintation of CPmFc substituents in **9b**) which minimises steric crowding between CPmFc substituents. This results in the mean planes of the C_6 units subtending a dihedral angle of 43.84° and not being orientated face-on as is the case for **17a** (where the equivalent angles are 28.67° and 18.34° for each molecule in the asymmetric unit). Table 5.7 gives an overview of the ferrocenyl distortions.

5.7 Isomerisations of 17a and 17b

Both isomers, **17a** and **17b**, were independently dissolved in toluene and heated to reflux to thermally isomerise the 1,2-species to 1,7-species (Figure 5.16). A toluene reflux (110^{o}C) is sufficiently high in temperature to effect these isomerisations due to the steric bulk of the CPmFc groups and is currently the lowest temperature documented for such a rearrangement.

The isomerisation of **17a** afforded four species. The major product was an orange compound that was revealed to be 4,9-Me_2-1,7-$(CPmFc)_2$-1,7-*closo*-$C_2B_{10}H_8$ (**18**). A small amount of unisomerised **17a** was isolated as well as two other products that could not be fully characterised due to miniscule yields. The latter two compounds' R_f values and colours were consistent with the decomposition products **12a** and **12b** from the toluene reflux of the unlabelled species **9b** (the monosubstituted CPmFc species presumably is the B-Me disubstituted derivative of **9b** with methyl substituents on vertices B(8) and B(9)).

Upon isomerisation of **17b** the 1,7-compound obtained was revealed to be identical to **16a** by ^{1}H and ^{11}B{^{1}H} spectroscopies showing that **17a** returns to the original 1,7-species **16a** prior to initial reduction and oxidation. A small amount of unisomerised **16b** was recovered and the associated decomposition products were also evident but the latter two compounds could not be isolated and characterised.

The ^{1}H NMR spectrum of **18** indicates the asymmetry of **17a** has been retained throughout the isomerisation process as two separate methyl groups are observed at δ 0.10 and δ 0.44. The latter high frequency resonance is presumably due to the methyl group on vertex B(4) as it lies between a carbon atom and the remaining methyl substituted boron vertex, B(9). This asymmetry is also evident from studying the ferrocenyl units. There are three multiplets at δ 4.18 (4H), δ 4.15 (2H) and δ 3.98 (2H) all due to the C_5H_4 moieties of the molecule. Should both CPmFc groups be chemically and magnetically equivalent only two resonances of this type would be expected. A singlet at δ 4.10 (10H) is a (5+5) coincidence due to the two C_5H_5 rings. The Pm unit is observed over four large lumpy peaks spanning the range δ 2.18 – 1.28.

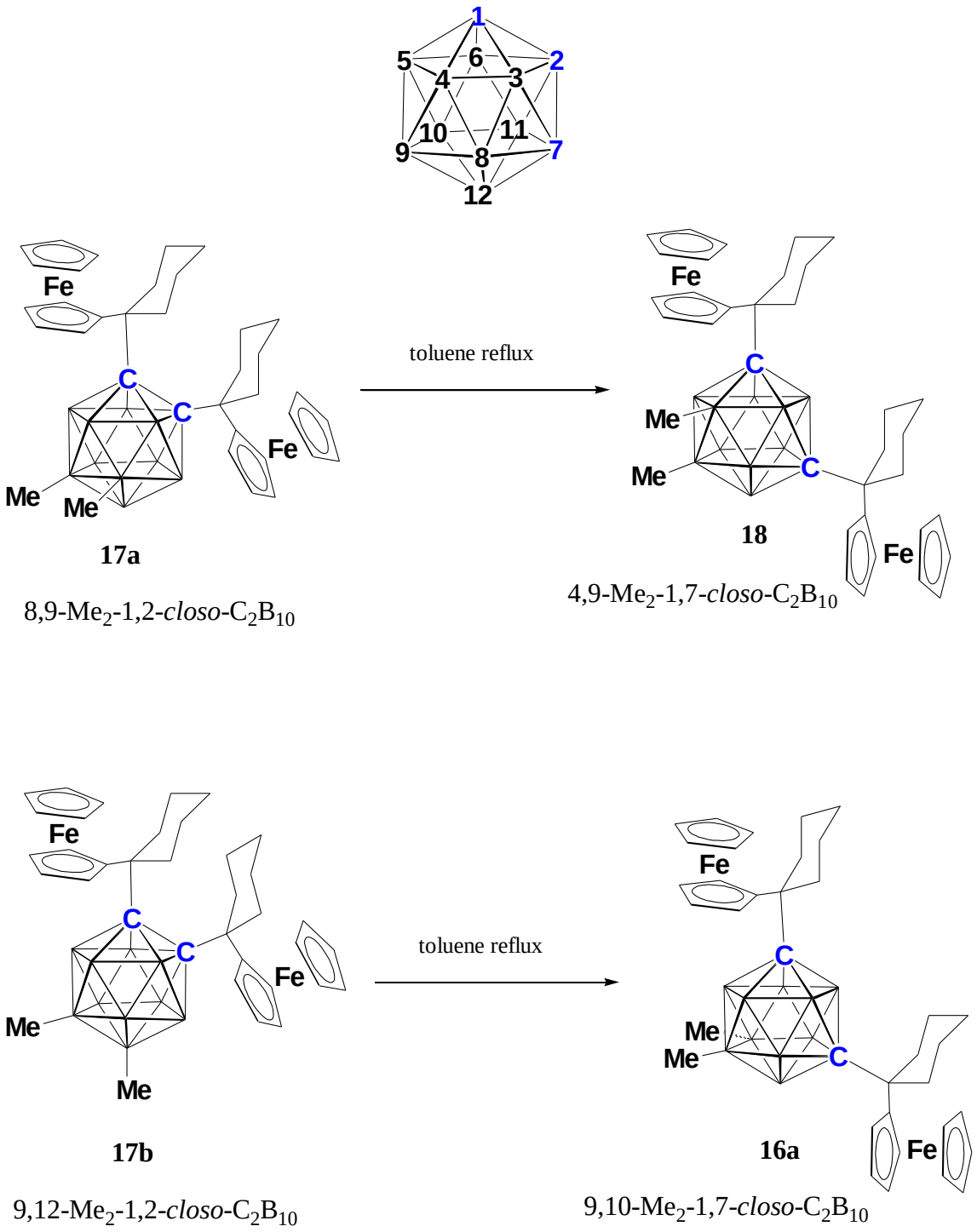

Figure 5.16 Thermal isomerisations of 17a and 17b in toluene

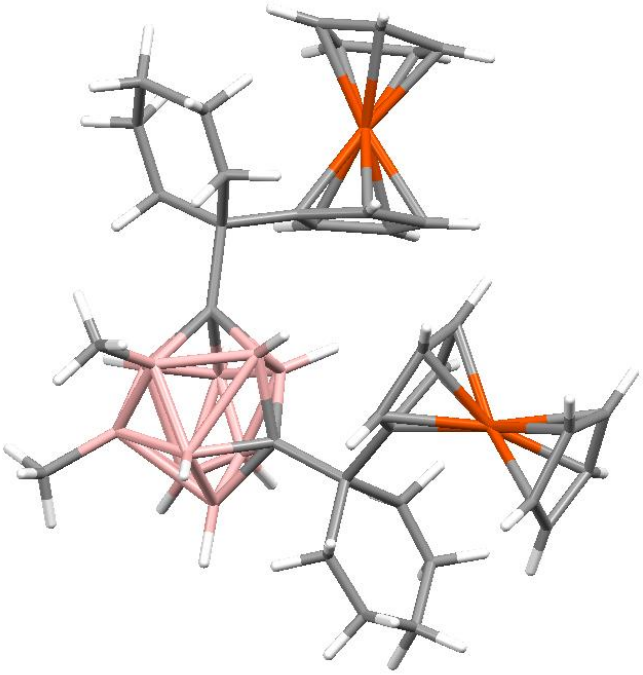

Figure 5.17 Approximate molecular structure of 18

The $^{11}B\{^{1}H\}$ NMR spectrum of **18** consists of a range of broad overlapping signals in the region δ -1.9 to δ -15.8 again emphasising the asymmetry of the cluster however it is not possible to determine the label positions from spectroscopy. X-ray crystallographic study of **18** (Figure 5.17) confirms that the labels are positioned on the B(4) and B(9) positions. Although the structure is only approximate (and not publishable) the positions of the methyl labels are unambiguous.

The mass spectrum of **18** shows a parent ion at *m/z* 705 with no discernible fragmentation.

5.7.1 Isomerisation Mechanisms

To elucidate a potential isomerisation mechanism it is necessary to track the labels as they move from the 1,2 isomer through to the 1,7 isomer. However, it is a complex process especially for the asymmetric species **17a** as the C_{2v} symmetry of 1,2-*closo*-$C_2B_{10}H_{12}$ means there are four possible orientations as a starting point i.e. 8,9-Me_2 and 10,12-Me_2 and their respective enantiomers 9,10-Me_2 and 8,12-Me_2. As the asymmetry is retained as **17** is formed it follows that the final 4,9-Me_2-1,7-*closo*-C_2B_{10} species could also assume up to four possible orientations. There are therefore as many as

sixteen permutations that could account for the label movements in the isomerisation of **17a** to compound **18** (Figure 5.18).

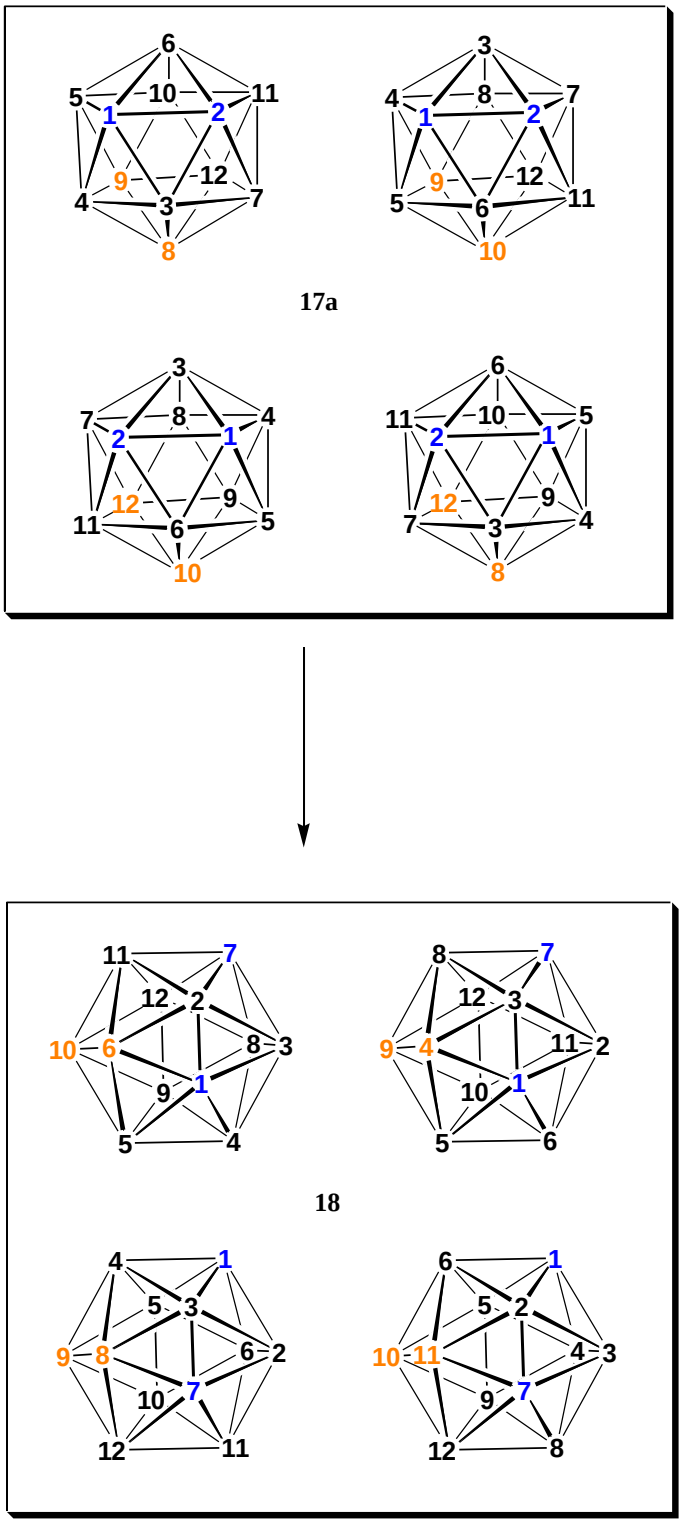

Figure 5.18 Summary of all possible orientations and permutations of 17a to 18 isomerisation. (Blue – carbon atom; orange – labelled boron atom)

The symmetric species **17b** has fewer options for label movement as the C_{2v} symmetry of the cluster is retained. The labels begin on positions B(9) and B(12) and finish on B(9) and B(10). Either B(9) remains stationary and B(12) moves to position B(10) or B(9) moves to B(10) whilst B(12) moves to B(9).

5.7.1.1 Comparison with Wales' Computational Studies

Computational methods have been widely used to try and rationalise the isomerisation mechanism. Wales[18] calculated potential energy surfaces for the isomerisation and in doing so was able to identify different pathways by which isomerisation can be achieved via different transition states and intermediates. He showed that isomerisation between the three carborane isomers may proceed through a number of high energy, low symmetry intermediates linked by transition states of higher energy and low symmetry (Figure 5.19 – only the routes to 1,7-*closo*-$C_2B_{10}H_{12}$ are shown). Pathways are found to consist of stepwise DSD processes and any higher symmetry or 'open' cage geometries were discounted as they were deemed to be too high in energy.

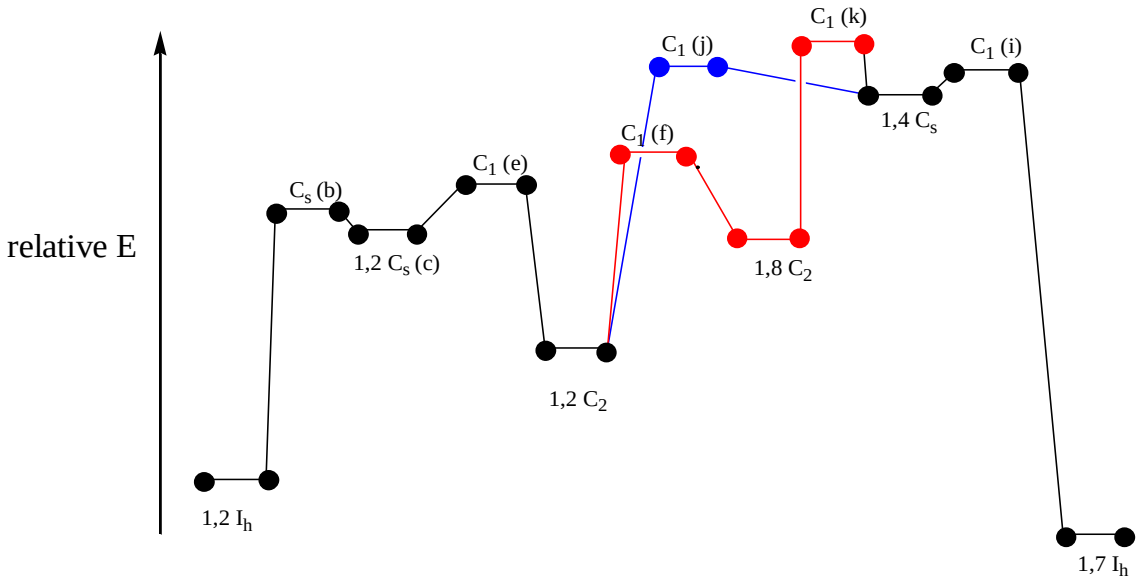

Figure 5.19 Wales' potential energy surface for the rearrangement of 1,2-*closo*-$C_2B_{10}H_{12}$ to 1,7-*closo*-$C_2B_{10}H_{12}$

This theory looked promising as the result of experimental findings by Dunn et al[6b] showed that the key 1,2 C_2 intermediate was isolatable but with one boron atom replaced by a molybdenum metal fragment. The 1,2 C_2 intermediate has the carbon atoms close to antipodal and only 4-connected. Dunn's molybdacarborane may be partially stabilised by the presence of the molybdenum atom in a 6-connected site which would be less favourable for a {BH} fragment. Gentle heating of this compound formed a 1,7 type metallacarborane confirming it as an intermediate in the isomerisation. Figure 5.20 shows a structural representation of the formation of the 1,2 C_2 intermediate that allows all vertices to be tracked.

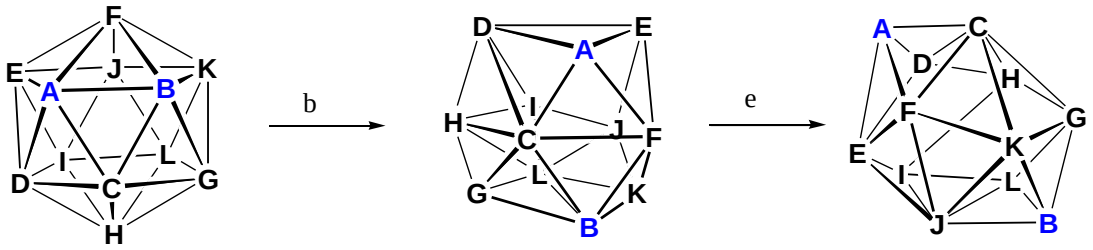

1,2 I_h 1,2 C_s (C) 1,2 C_2

Figure 5.20 Pictorial representation of pathways (b) and (e). A and B are the carbon atoms

Figure 5.19 shows a single pathway which converts the icosahedral 1,2-*closo*-$C_2B_{10}H_{12}$ into the lowest energy 1,2 C_2 intermediate via pathway (b + e). Subsequently, there are two possible routes to convert this intermediate into 1,7-*closo*-$C_2B_{10}H_{12}$: (j + i) or the slightly longer (f + k + i). The shorter route of (j + i) has previously been disregarded from studies of metallacarboranes as the mechanism does not produce the desired isomer, moving the metal atom to a position which is incorrect relative to the positions of the two carbon atoms. However, as **17a** and **17b** have no metal atom within the cage it cannot be immediately eliminated as a potential rearrangement mechanism. As previously stated, metallacarborane studies only show partial agreement with Wales' predictions. This study focuses on the rearrangement of carboranes and should provide a better comparison with the calculations.

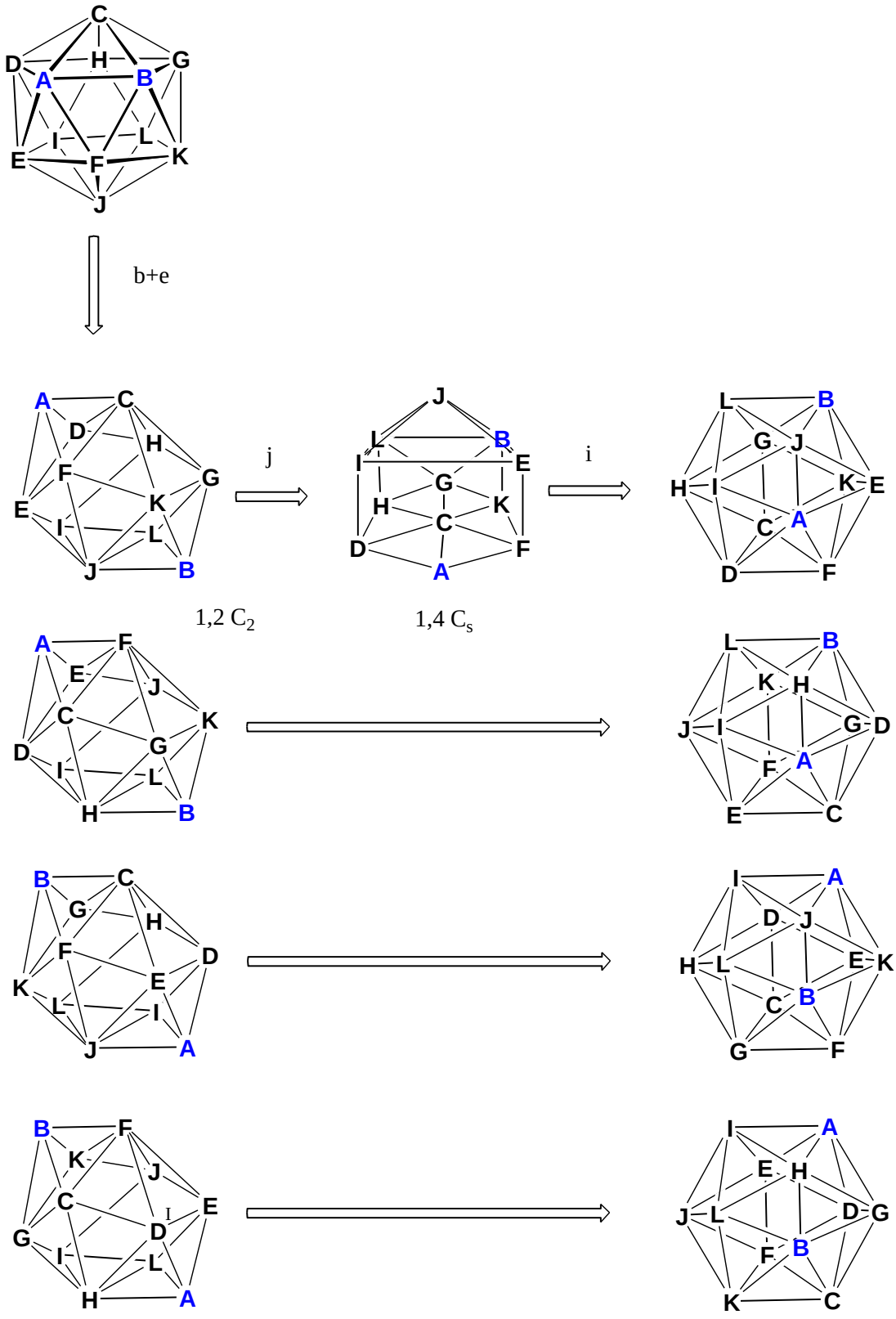

Figure 5.21 Overall pictorial representation of pathways (b + e + j + i) ultimately showing four possible 1,7 frameworks

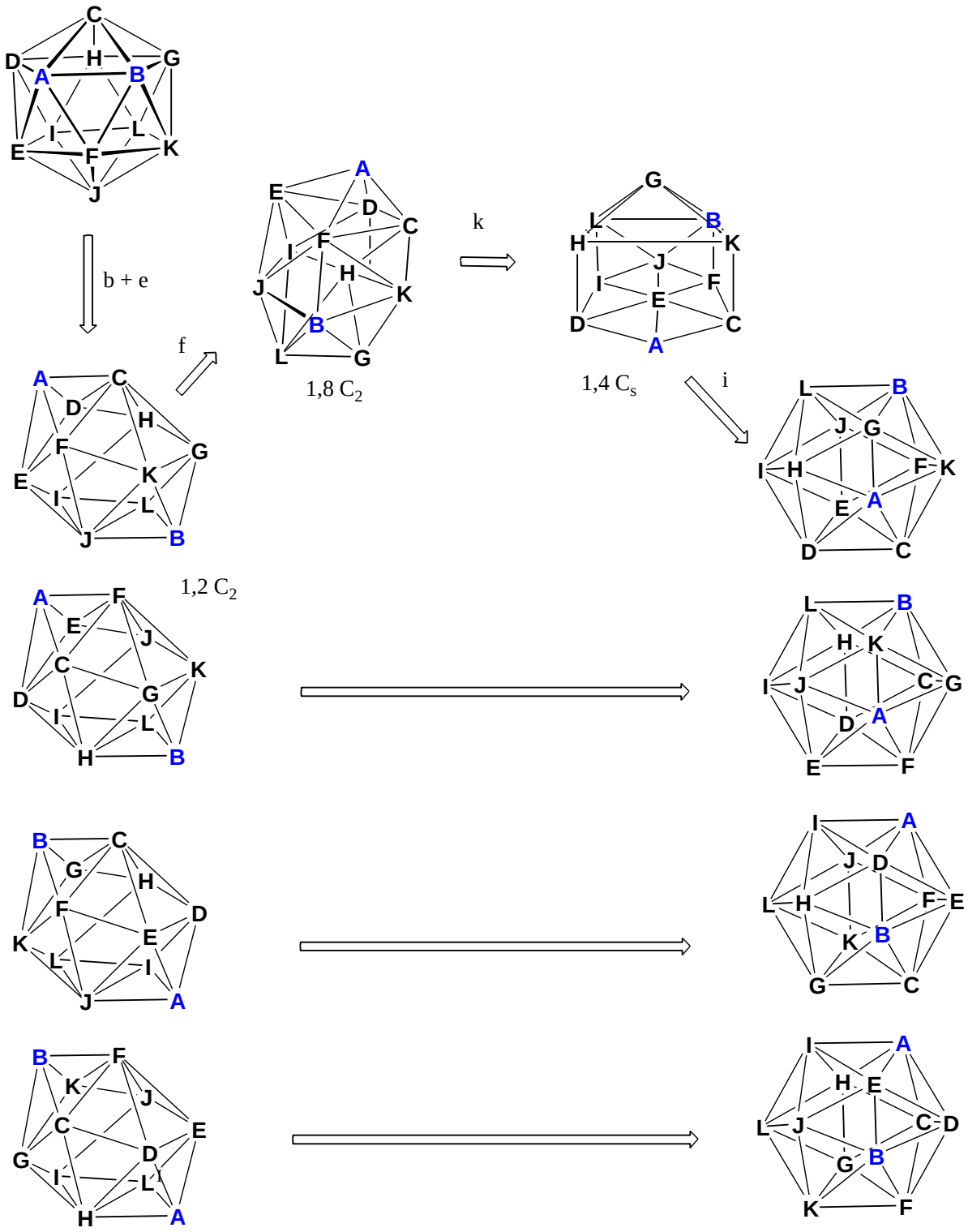

Figure 5.22 Overall pictorial representation of pathways (b + e + f + k +i) ultimately showing four possible 1,7 frameworks

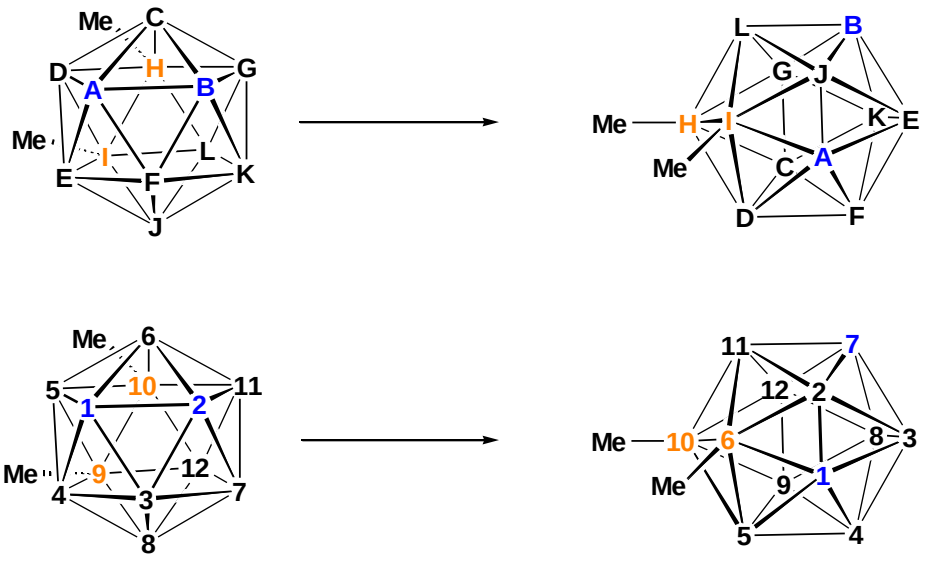

Figure 5.23 **Overall representation of pathways (b + e) followed by (j + i) that agrees with experiment. Top - general scheme that allows tracking of every vertex; bottom - conventional numbering**

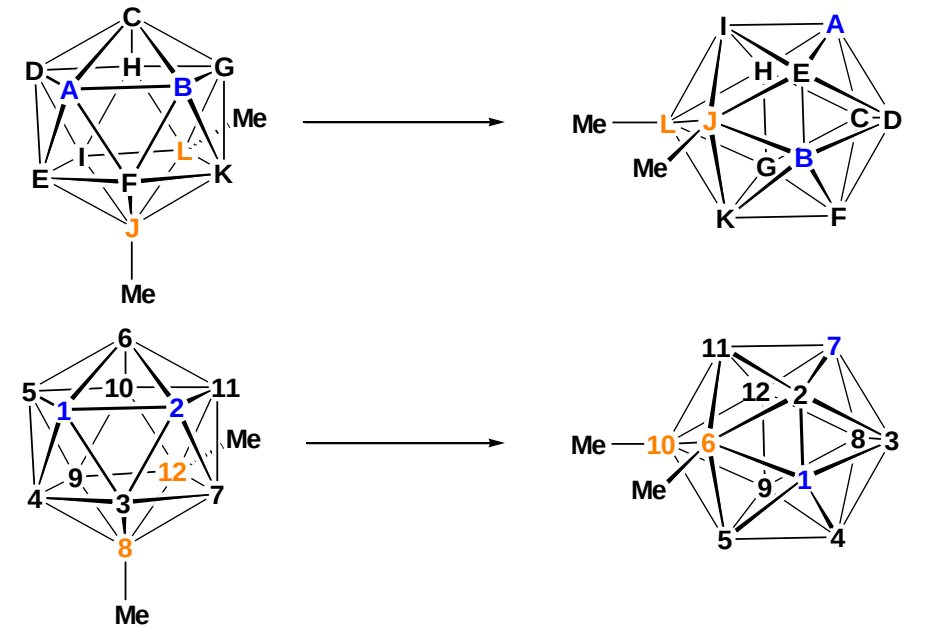

Figure 5.24 **Overall representation of pathways (b + e) followed by (f + k + i) that agrees with experiment. Top - general scheme that allows tracking of every vertex; bottom - conventional numbering**

Figure 5.21 shows a general representation of Wales' (b + e + j + i) mechanism. **17a** can be viewed in four equivalent orientations (due to two mirror planes in the C_{2v} point group) with the labels positioned at **HI**, **HL**, **JI** and **JL** which subsequently gives four possible 1,2 C_2 intermediates. This rearranges to a 1,4 C_s intermediate through two DSD steps ultimately forming the 1,7 isomer. Tracking the labels as the mechanism proceeds through (j + i) can give four possible (equivalent) orientations of **18.**

This mechanism can account for the rearrangement from **17a** to **18** and one potential route is shown in Figure 5.23 where 9,10-Me_2-1,2-$(CPmFc)_2$-1,2-*closo*-$C_2B_{10}H_8$ can isomerise to 6,10-Me_2-1,7-$(CPmFc)_2$-1,7-*closo*-$C_2B_{10}H_8$. However, the isomerisation from **17b** to **16a** cannot be described by this mechanism. The experimental label positions in **16a** are adjacent to each other but not connected to any carbon atom. All four of the calculated 1,7 species possess both labelled boron atoms (**I** and **L**) adjacent to a carbon atom.

Wales' (b + e + f + k + i) mechanism shows similar results. Again, the four possible 1,2 C_2 intermediates can form four potential 1,7 species via a 1,8 C_2 intermediate followed by a 1,4 C_s intermediate (Figure 5.22) through a stepwise series of concerted DSD steps. When tracking the labels from a 1,2 to a 1,7 species it can be seen that the isomerisation from **17a** to **18** may be explained by this route (Figure 5.24) but the isomerisation from **17b** to **16a** cannot. **16a** requires both labelled boron atoms (**I** and **L**) not to be adjacent to any carbon atom but this is not the case for any calculated product by the (f + k + i) route.

5.7.1.2 Comparison with McKee's Computational Studies

McKee[19] has also suggested that isomerisation may occur by two, shorter, distinct pathways: TFR and non-TFR (Figure 5.25). The TFR pathway was shown to be the lower energy pathway from 1,2-*closo*-$C_2B_{10}H_{12}$ to 1,7-*closo*-$C_2B_{10}H_{12}$ (but, interestingly, higher in energy than a two step non-TFR pathway connecting 1,7-*closo*-$C_2B_{10}H_{12}$ and 1,12-c*l*oso-$C_2B_{10}H_{12}$). The non-TFR pathways reported involved *pseudonido* geometries, earlier discounted by Wales.

This non-TFR pathway from 1,2-*closo*-$C_2B_{10}H_{12}$ to 1,7-*closo*-$C_2B_{10}H_{12}$ proceeds to form a basket-shaped intermediate **(o-m-INT**) that has also been independently calculated in the oxidation of [7,9-*nido*-$C_2B_{10}H_{12}]^{2-}$ to 1,2-*closo*-$C_2B_{10}H_{12}$[20] adding

credibility to **o-m-INT** being a true intermediate and perhaps, even, a potential synthetic target.

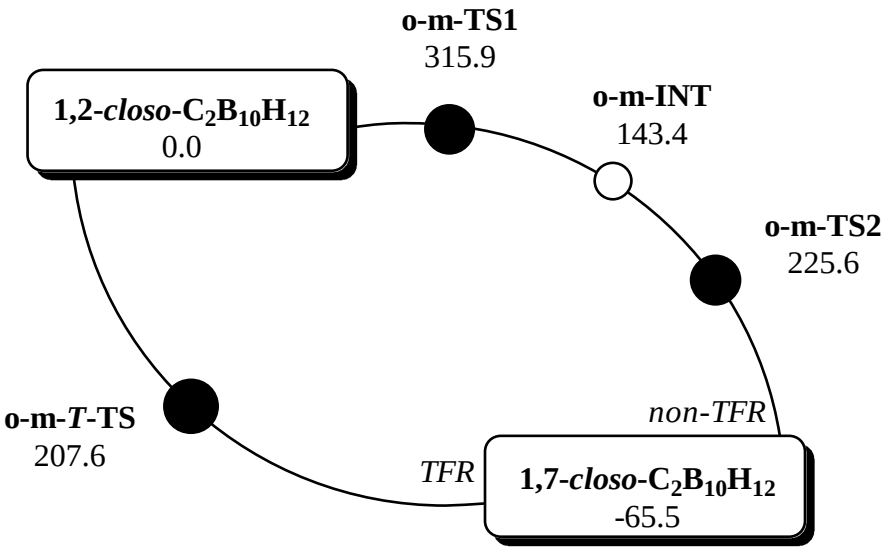

Figure 5.25 Energy level diagram showing McKee's TFR and non-TFR routes in the isomerisation of 1,2-*closo*-$C_2B_{10}H_{12}$ to 1,7-*closo*-$C_2B_{10}H_{12}$, energies in kcal mol^{-1}

The TFR route (Figure 5.26 and 5.27) simply consists of taking an equilateral triangle of three atoms, lifting them up slightly; rotating them by 120° and lowering them back down. The C_{2v} symmetry of 1,2-*closo*-$C_2B_{10}H_{12}$ again provides four separate (but equivalent) triangle rotations that could yield four possible 1,7-*closo*-C_2B_{10} species.

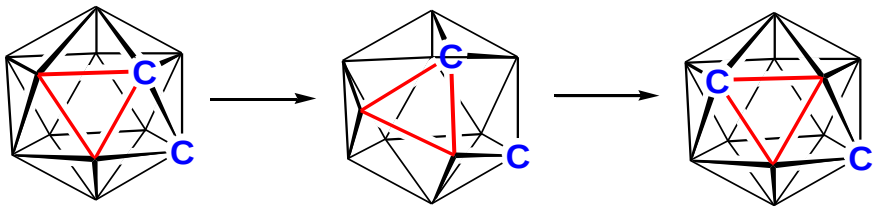

o-m-*T*-TS

Figure 5.26 TFR pathway showing the transition state o-m-*T*-TS displaying three quadrilateral faces

Figure 5.26 shows that one TFR is essentially the same as three concerted DSD processes with the transition state showing the three simultaneous square faces. If this type of mechanism is possible it is conceivable that almost any isomer can be produced via one or more clockwise or anticlockwise TFRs around any equilateral B-B-B triangle.

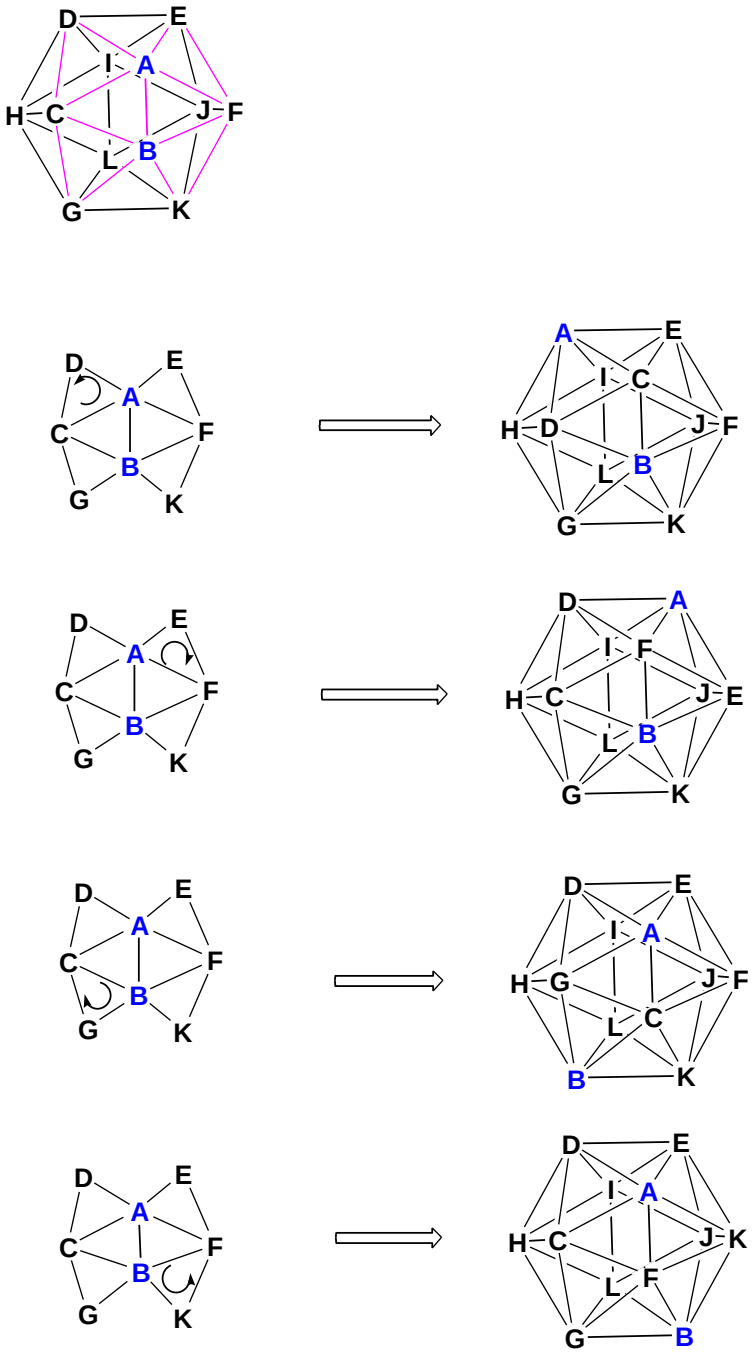

Figure 5.27 Four different TFR processes from 1,2-*closo*-$C_2B_{10}H_{12}$ leading to four possible 1,7 isomers

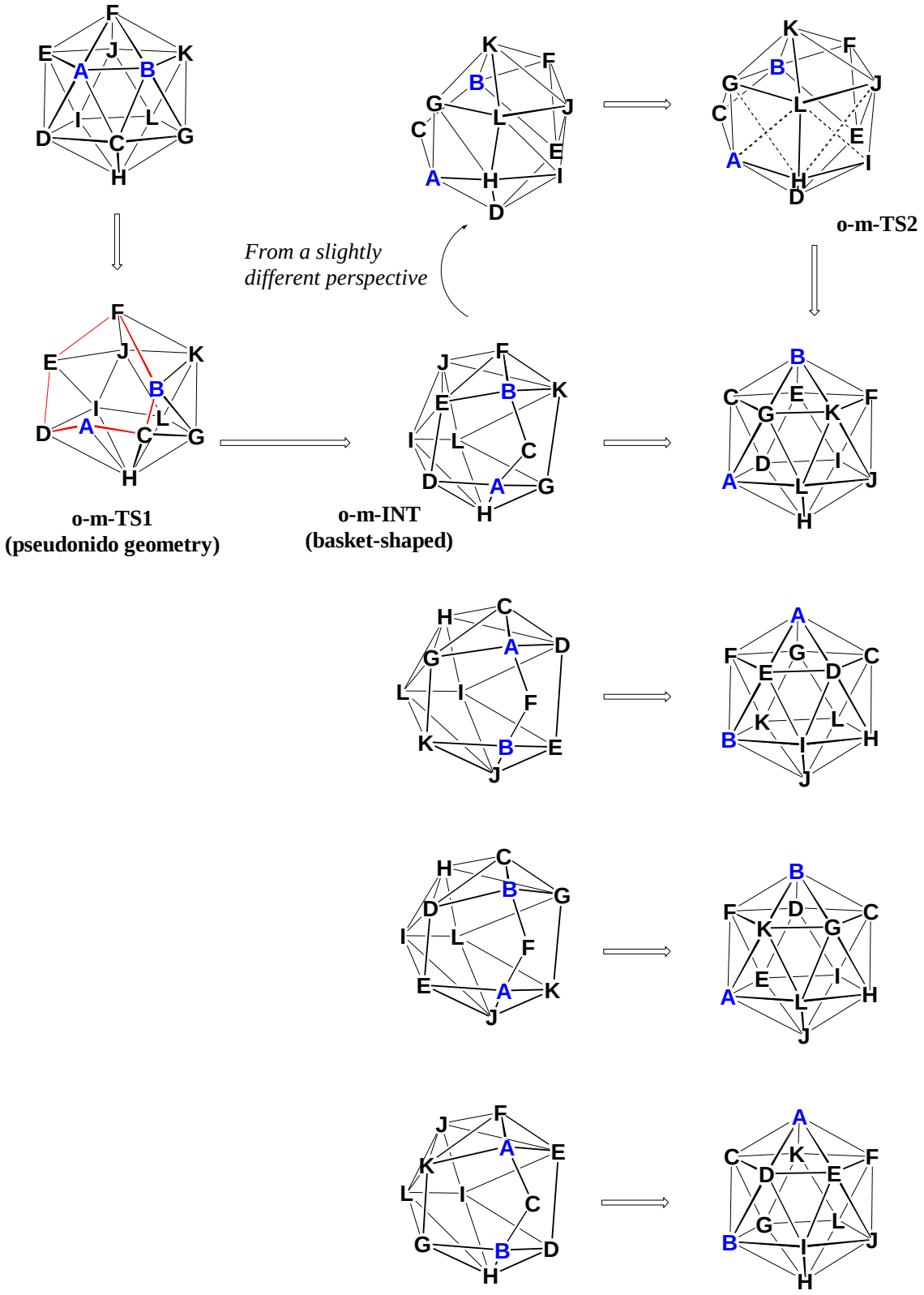

Figure 5.28 General representation of McKee's non-TFR mechanism giving four possible 1,7-*closo*-$C_2B_{10}H_{12}$ isomers

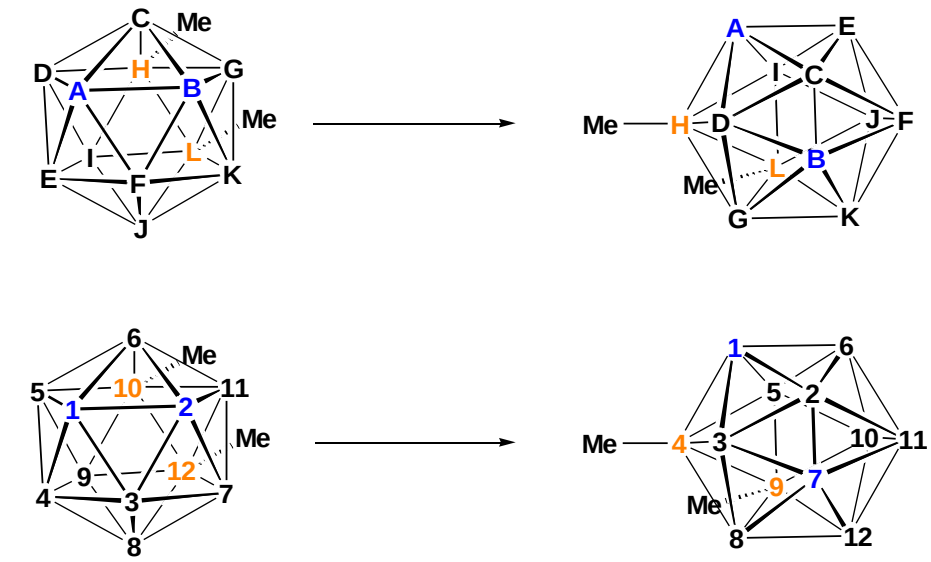

Figure 5.29 **Overall representation of TFR pathway that agrees with experiment. Top - general scheme that allows tracking of every vertex; bottom - conventional numbering**

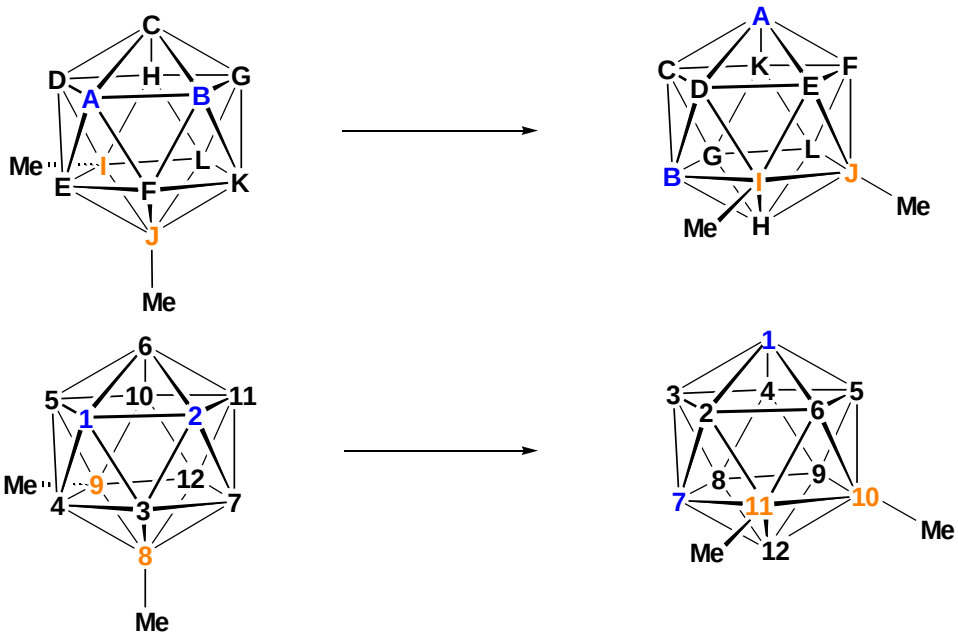

Figure 5.30 **Overall representation of non-TFR pathway that agrees with experiment. Top - general scheme that allows tracking of every vertex; bottom - conventional numbering**

It can be seen that the isomerisation from **17a** to **18** is possible by this TFR route: the 10,12-Me_2 to 4,9-Me_2 route is shown in Figure 5.29. The **17b** to **16a** isomerisation, however, is impossible by this TFR method as the 1,7 species produced experimentally has both labelled boron atoms in sites where neither is adjacent to a carbon atom. All 1,7 species predicted by the TFR route (Figure 5.27) possess this arrangement.

McKee's non-TFR mechanism (Figure 5.28) proceeds by one carbon atom at the apex of a pentagonal cap breaking three bonds while performing a DSD transition with a boron vertex on the lower pentagonal belt to form **o-m-TS1**. This forms an unstable *pseudonido* geometry which subsequently develops into the aforementioned basket-shaped intermediate (**o-m-INT**). 1,7-*closo*-$C_2B_{10}H_{12}$ is then formed via a transition state (**o-m-TS2**) due to two adjacent DSD transitions on opposing sides of the cage. This mechanism can also account for the formation of **18** from **17a** and one possible route is shown in Figure 5.30. It cannot account, however, for the isomerisation from **17b** to **16a** as label **I** or **L** is always adjacent to a carbon atom in all four of the calculated 1,7 isomers.

It has been seen that thermal isomerisation can occur at relatively low temperatures, thus preventing loss of the labels from the cage. Calculations by both Wales and McKee offer potential pathways from 1,2-C_2B_{10} to 1,7-C_2B_{10} derivatives. However, none of these mechanisms provide a full match for both **17a** and **17b** rearrangements. **17b** to **16a** cannot, in fact, be rationalised by any of the suggested routes. It seems unlikely that **17a** and **17b** should isomerise by different mechanisms unless the relative positions of the methyl substituents influence the mechanism in some way.

In theory product **18** (the asymmetric 1,7 species) can undergo another redox reaction followed by another thermal isomerisation to give a new labelled 1,7 carborane compound. This sequence of reactions can, in theory, be repeated until each individual boron movement has been labelled and tracked allowing the boron atom movements to be catalogued. Using distinguishable labels also would provide an advantage as it would give a clearer indication of individual boron atom movement.

5.8 References

5.1 D. Grafstein and J. Dvorak, *Inorg. Chem*., 1963, **2**, 1128.

5.2 W. N. Lipscomb and D. Britton, *J. Chem. Phys*., 1960, **33**, 275

5.3 E. L. Mutterties and W. N. Knoth, *Polyhedral Boranes*, Marcel Dekker, New York, 1968, 70.

5.4 H. V. Hart and W. N. Lipscomb, *J. Am. Chem. Soc*., 1969, **91**, 771.

5.5 L. I. Zakharkin and V. N. Kalinin, *Izv. Akad. Nauk. SSSR*, 1969, **3**, 607.

5.6 (a) S. Dunn, G. M. Rosair, A. S. Weller and A. J. Welch, *Chem. Commun*., 1998, 1065; (b) S. Dunn, G. M. Rosair, Rh. Ll. Thomas, A. S. Weller and A. J. Welch, *Angew. Chem. Int. Ed*., 1997, **36**, 645; (c) e.g. S. Robertson, D. Ellis, G. M. Rosair and A. J. Welch, *Appl. Organomet. Chem*., 2003, **17**, 518; (d) S. Robertson, D. Ellis, G. M. Rosair and A. J. Welch, *J. Organomet. Chem*., 2003, **680**, 286; (e) S. Robertson, R. M. Garrioch, D. Ellis, T. D. McGrath, B. E. Hodson, G. M. Rosair and A. J. Welch, *Inorg. Chim. Acta*, 2005, **358**, 1485.

5.7 e.g. D. R. Baghurst, R. C. B. Copley, H. Fleischer, D. M. P. Mingos, G. O. Kyd, L. J. Yellowlees, A. J. Welch, T. R. Spalding and D. O'Connell, *J. Organometal. Chem*., 1993, **447**, C14.

5.8 e.g. R. D. McIntosh, D. Ellis, B. T. Giles, S. A. Macgregor, G. M. Rosair and A. J. Welch, *Inorg. Chim. Acta*, 2006, **359**, 3745.

5.9 R. M. Salinger and C L. Frye, *Inorg. Chem*., 1965, **4**, 1815.

5.10 Z. Zheng, W. Jiang, A. A. Zinn, C. B. Knobler and M. F. Hawthorne, *Inorg. Chem*., 1995, **34**, 2095.

5.11 L. I. Zakharkin, V. N. Kalinin and L. S. Podvisotskaya, *Izv. Akad. Nauk. SSSR, Ser. Khim*., 1967, 2310.

5.12 D. McKay, unpublished results.

5.13 D. McKay, *PhD Thesis*, Heriot-Watt University, 2010.

5.14 S. Zlatogorsky, D. Ellis, G. M. Rosair and A. J. Welch, *Chem. Commun*., 2007, 2178.

5.15 S. Zlatogorsky, M. J. Edie, D. Ellis, S. Erhardt, M. E. Lopez, S. A. Macgregor, G. M. Rosair and A. J. Welch, *Angew. Chem. Int. Ed*., 2007, **46,** 6706.

5.16 e.g. G. Zi, H-W. Li and Z. Xie, *Organometallics*, 2002, **21**, 5415.

5.17 M. G. Davidson, T. G. Hibbert, J. A. K. Howard, A. Mackinnon and K. Wade, *Chem. Commun*., 1996, 2285.

5.18 D. J. Wales, *J. Am. Chem. Soc*., 1993, **115**, 1557.

5.19 C. A. Brown and M. L. McKee, *J. Mol. Model*., 2006, **12**, 653.

5.20 B. W. Hutton, F. MacIntosh, D. Ellis, F. Herisse, S. A. Macgregor, D. McKay, V. Petrie-Armstrong, G. M. Rosair, D. S. Perekalin, H. Tricas and A. J. Welch, *Chem. Commun*., 2008, 5345.

Chapter 6 Experimental Section

6.1 General Experimental

Syntheses

All experiments were carried out under a dry, oxygen-free, nitrogen atmosphere, using Schlenk-line techniques, with some subsequent manipulation being completed in the open laboratory. Most of the ultimate compounds reported are stable both as solids and as solutions. All solvents were dried with the appropriate drying agents under nitrogen immediately before use [DCM and CH_3CN with CaH_2; THF and diethyl ether with sodium wire and benzophenone; toluene and light petroleum (b.p. 40-60ºC) with sodium wire].

Analyses

NMR spectra were recorded on a Bruker AC200 spectrometer (^1H spectra at 200.1 MHz, ^{11}B spectra at 64.2 MHz) or a DPX400 spectrometer (^1H spectra at 400.1 MHz, ^{11}B spectra at 128.4 MHz). Unless stated otherwise, NMR spectra were obtained from CD_2Cl_2 solutions at 298K; proton and carbon chemical shifts are reported relative to external $Si(CH_3)_4$ and boron chemical shifts relative to external $BF_3.OEt_2$. Electron Ionisation mass spectrometry was carried out using a Kratos Concept mass spectrometer. Mass spectra of compounds **1-18** are reported as the most abundant peak of the stated isotopic envelope range where there are significant mixtures of isotopes and any fragmentations are subsequently reported without the range. Elemental analyses were carried out by the Heriot-Watt University departmental service.

Hazards

Standard principles of safe handling and good general laboratory practice were followed, including the wearing of protective clothing and safety glasses. Extra care and attention was employed when handling flammable solvents, sodium metal and other toxic chemicals.

Crystallographic Data Collection

Single crystals suitable for *X*-ray diffraction were mounted in inert oil on a glass fibre and cooled to 100 K by an Oxford Cryosystems Cryostream. Data was collected on a Bruker X8 APEX2 diffractometer,[1] employing graphite-monochromated Mo-*K*α *X*-radiation (λ = 0.71069 Å) and were corrected for absorption semi-empirically from symmetry-equivalent and repeated reflections. Structures were solved by direct and difference Fourier methods and refined by full-matrix least-squares against F^2 using the SHELXTL program suite.[2] Refinement was completed with all non-hydrogen atoms assigned anisotropic displacement parameters. Geometry measurements were made using Mercury[3] or OLEX2.[4]

Standard Preparations

The compounds 6,6-pentamethylenefulvene,[5] 6,6-dimethylfulvene,[5] 9,10-I_2-1,7-*closo*-$C_2B_{10}H_{10,}$[6] 9,10-$(CH_3)_2$-1,7-*closo*-$C_2B_{10}H_{10,}$[6] 9,10-Ph_2-1,7-*closo*-$C_2B_{10}H_{10}$[6] and $[Ru(p\text{-cymene})Cl_2]_2$[7] were prepared by literature methods or slight variants thereof. All other reagents and solvents were supplied commercially and were used as received.

6.2 Improved Synthesis of 1,7-$(CMe_2OH)_2$-1,7-*closo*-$C_2B_{10}H_{10}$ (1)

A solution of 1,7-*closo*-$C_2B_{10}H_{12}$ (2.00 g, 13.86 mmol) in dry diethyl ether (30 ml) was cooled to 0°C and a solution of *n*-BuLi in *n*-hexane (2.5M, 12.2 ml, 30.49 mmol) was slowly added. The mixture was stirred overnight. This solution was cooled to 0°C and acetone (reagent grade dried over 3Å molecular sieves, 2.5 ml, 34.65 mmol) was added dropwise and stirred for two hours whilst warming to room temperature. Hydrolysis was completed with the addition of very dilute hydrochloric acid. The organic layer was separated and dried over anhydrous magnesium sulphate. The white solid, recovered by solvent evaporation, was recrystallised from hexane to yield 1,7-$(CMe_2OH)_2$-1,7-*closo*-$C_2B_{10}H_{10}$ (**1**).

Yield 2.98 g (80%)

$^{11}B\{^1H\}$ NMR δ -6.6 (2B), -11.7 (2B), -12.4 (4B), -14.6 (2B)

^1H NMR δ 1.74 (br. s, 2H, -O*H*), 1.35 (s, 12H, methyl groups)

CHN $C_8H_{24}B_{10}O_2$: calc. C 36.9%, H 9.29%; found C 37.3%, H 9.54%

MS *m/z* 260 (M^+) (with an isotopic envelope spanning *m/z* 255-264), 243 (M – OH), 226 (M – 2 OH), 185 (M – [OH + $CCMe_2OH$]), 142 (M – 2 $CCMe_2OH$)

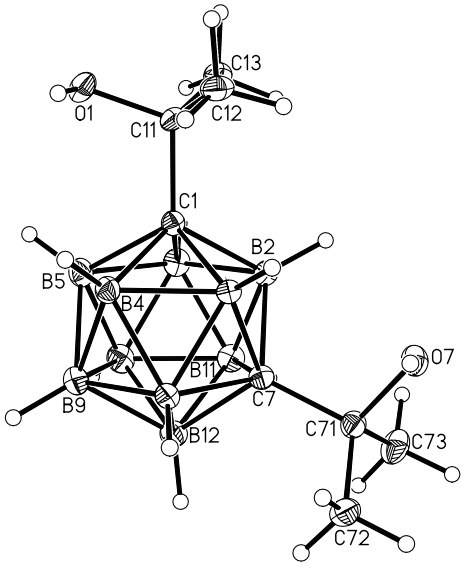

6.3 Synthesis of 1-(CMe_2OH)-1,2-*closo*-$C_2B_{10}H_{11}$ (2)

A solution of 1,2-*closo*-$C_2B_{10}H_{12}$ (0.250 g, 1.73 mmol) in dry diethyl ether (20 ml) was cooled to 0°C and a solution of *n*-BuLi in *n*-hexane (2.5 M, 1.4 ml, 3.50 mmol) was added. This solution was stirred for three hours at room temperature and then acetone (0.3 ml, 4.09 mmol) was added at 0°C. The solution was stirred for 1.5 hours at room temperature and subsequently washed several times with water. The colourless organic layer was dried over magnesium sulphate. The solvent was removed and the white solid was purified using silica gel chromatography (petrol ether : ethyl acetate 2:1) to yield 1-(CMe_2OH)-1,2-*closo*-$C_2B_{10}H_{11}$ (**2**).

Yield 0.287 g (84%)

$^{11}B\{^1H\}$ NMR δ -3.7 (1B), -4.6 (1B), -9.2 (2B), -11.7 (2B), -11.9 (2B), -13.8 (2B)

^1H NMR δ 4.10 (br. s, 1H, carborane C*H*), 2.32 (br. s, 1H, -O*H*), 1.51 (s, 6H, methyl groups)

CHN $C_5H_{18}B_{10}O$: calc. C 29.7%, H 8.97%; found C 29.9%, H 9.12%

MS *m/z* 202 (M^+) (with an isotopic envelope spanning *m/z* 197-206), 185 (M-OH), 142 (M-$CCMe_2OH$)

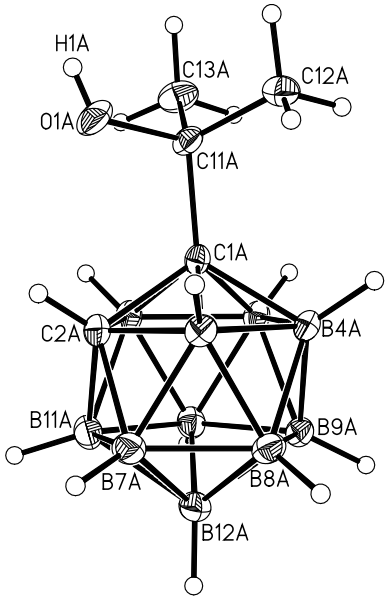

6.4 Synthesis of 1,7-$(CMe_2OCH_2OCH_3)_2$-1,7-*closo*-$C_2B_{10}H_{10}$ (3)

To a solution of 1,7-$(CMe_2OH)_2$-1,7-*closo*-$C_2B_{10}H_{10}$ (1.40 g, 5.38 mmol) in chloroform (40 ml) phosphorous pentoxide (20.00 g) then dimethoxymethane (28.0 ml, 316 mmol) were added. The reagents were stirred at room temperature for 0.5 hours and the solid phosphorous pentoxide changed from colourless to orange to black over this time. Stirring was stopped, as the black solid was very sticky and viscous. The solution was decanted into a new flask and stirring continued overnight. The mixture was filtered and the filtrate was poured into ice-cold sodium bicarbonate solution (150 ml). The mixture was extracted with chloroform; the combined organic layers were washed with brine and dried over magnesium sulphate. Removal of the solvent and purification using silica gel chromatography (solvent gradient: petrol ether: DCM 5:1 followed by pure DCM followed by pure THF) resulted in methoxymethyl protected 1,7-$(CMe_2OCH_2OCH_3)_2$-1,7-*closo*-$C_2B_{10}H_{10}$ **(3)** as a slightly yellow oil.

Yield	1.76 g (94%)
$^{11}B\{^{1}H\}$ NMR	δ -6.4 (2B), -12.4 (6B), -14.8 (2B)
^{1}H NMR	δ 4.64 (s, 4H, OC*H*$_2$O), 3.30 (s, 6H, OC*H*$_3$), 1.35 (s, 12H, methyl groups)
CHN	$C_{12}H_{32}B_{10}O_4$: calc. C 41.4%, H 9.26%; found C 42.0%, H 9.17%
MS	*m/z* 348 (not observed M^+), 287 ($M–OCH_2OCH_3$ (with an isotopic envelope spanning *m/z* 282-291), 226 ($M–2OCH_2OCH_3$)

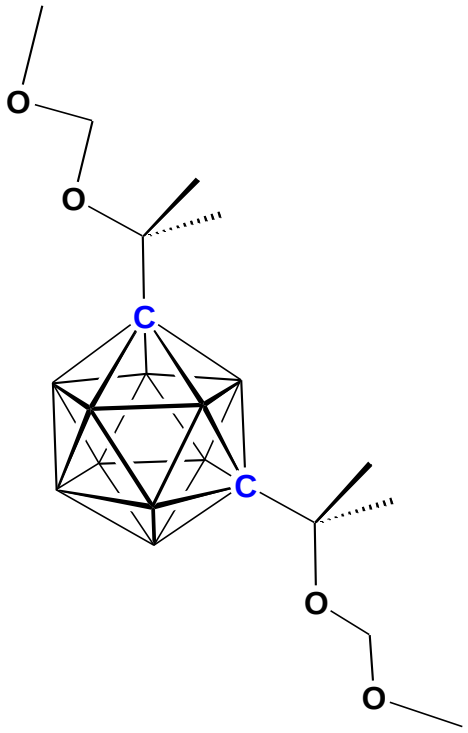

6.5 Reduction and Metallation of 1,7-($CMe_2OCH_2OCH_3$)$_2$-1,7-*closo*-$C_2B_{10}H_{10}$ Forming Compound 4

The MOM-protected carborane **3** (0.350 g, 1.00 mmol) was dissolved in a small amount of dry THF and quickly transferred into a Schlenk tube containing 30 ml dry THF. This gave a yellow solution that was degassed via three freeze-pump-thaw cycles. Sodium metal (0.230 g, 10 mmol) was added along with a catalytic amount of naphthalene. The reagents were stirred for 48 hours to produce a dark red solution. This was transferred via cannula to a frozen suspension of [$RuCl_2$(*p*-cymene)]$_2$ (310 mg, 0.5 mmol) in degassed THF. This was placed in an ice bath and stirred overnight. The THF was removed *in vacuo* and the dark residue redissolved in DCM and filtered. Spot TLC showed a yellow band with R_f 0.75 in a 4:1 DCM:petrol ether mixture. This was isolated on a silica column and purified further on a TLC plate to yield the yellow 13-vertex ruthenacarborane (**4**).

Yield 0.071 g (14%)

$^{11}B\{^{1}H\}$ NMR d_6-acetone: δ 7.5 (2B), 0.8 (1B), -1.7 (2B), -5.3 (1B), -7.1 (1B), -9.3 (1B), -10.9 (1B), -22.0 (1B)

^{1}H NMR δ 5.91 (d, 1H, $CH_3C_6H_4CH(CH_3)_2$), 6.05 (2×d, 2H, $CH_3C_6H_4CH(CH_3)_2$), 6.43 (d, 1H, $CH_3C_6H_4CH(CH_3)_2$), 4.05 (d, 1H, CH_2), 4.07 (d, 1H, CH_2), 3.27 (app. sep, 1H, C*H*), 2.95 (app. sep, 1H, C*H*), 2.40 (s, 3H, CH_3), 1.34 (app. t, 6H, $2CH_3$), 1.32 (s, 3H, CH_3), 1.26 (d, 3H, CH_3), 1.09 (d, 3H, CH_3), 1.07 (s, 3H, CH_3)

^{13}C NMR δ 17.93, 21.49, 23.30, 23.42, 25.25, 30.53, 31.63 (all CH_3), 31.95 (CH), 36.91 (CH), 46.66 (quaternary C), 84.09 (CH_2), 84.29, 89.31, 92.39, 96.10 (all CH), 110.97, 116.90 (both quaternary C)

CHN $C_{19}H_{38}B_{10}ORu$: calc. C 46.4%, H 7.97%; found C 44.4%, H 7.67%

MS *m/z* 491 (M^+) (with an isotopic envelope spanning *m/z* 483-499)

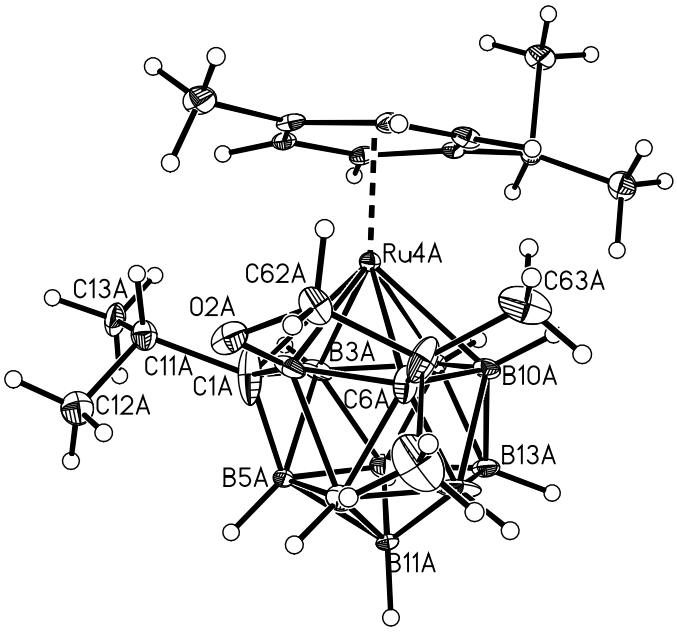

6.6 Synthesis of 1-{$CMe_2(C_5H_5)$}-7-{CMe_2[3-(C_5H_4)-3,1,2-*closo*-$CoC_2B_9H_{11}$]}-1,7-*closo*-$C_2B_{10}H_{10}$ (5a) and 1,7-{CMe_2[3-(C_5H_4)-3,1,2-*closo*-$CoC_2B_9H_{11}$]}$_2$-1,7-*closo*-$C_2B_{10}H_{10}$ (5b)

1,2-*closo*-$C_2B_{10}H_{12}$ (2.00 g, 13.9 mmol) was dissolved in ethanol (30 ml). Added to this were KOH pellets (2.6 g, 46.3 mmol) and the reagents heated to reflux for 72 hours. Dry CO_2 was bubbled through the solution and the solid K_2CO_3 formed from the excess KOH was filtered off. The ethanol was removed *in vacuo* and water (30 ml) was added forming a milky suspension. This was filtered to leave a clear aqueous solution. $Me_3N.HCl$ (3.30 g, 34.4 mmol) was slowly added as a solution in 12 ml of water. A fine white precipitate formed which was collected and recrystallized from hot ethanol yielding [$HNMe_3$][$C_2B_9H_{12}$] (2.09 g, 11.65 mmol, 84%). A portion of this (2.015 g, 11.2 mmol) was dissolved in 20 ml dry THF. This solution was cooled in ice and *n*-BuLi (2.1 ml, 5.25 mmol) was added. Once at room temperature the solution was heated to reflux for 1h then left to cool to room temperature as a Li^+ solution of the dianionic $[C_2B_9H_{11}]^{2-}$.

In a separate Schlenk tube 1,7-{$CMe_2(C_5H_5)$}$_2$-1,7-*closo*-$C_2B_{10}H_{10}$ (400 mg, 1.12 mmol) was dissolved in 20 ml THF and cooled in ice. *n*-BuLi (2.5 M in hexanes, 9.4 ml, 23.6 mmol) was added. The contents were added to the first Schlenk tube forming one THF solution which was subsequently frozen in liquid nitrogen. $CoCl_2$ (1.45 g, 11.2 mmol) was added as a solid on top of the frozen solution which was then allowed to thaw and then stirred at room temperature overnight. Air was bubbled through the solution for 30 mins. The solvent was removed *in vacuo* and the residue was extracted into DCM and filtered through silica to leave a dark yellow solution. Removal of the solvent left a yellow residue that was subjected to prep. TLC using 2:1 petrol: DCM as the eluent. A yellow band with R_f 0.45 was isolated as the double cage species **5a** (42 mg, 6.8%). Further chomatography of the residual baseline in 12:1 DCM:petrol revealed an additional yellow band (R_f 0.30) identified as the triple cage species **5b** (12 mg, 1.5%).

1-{$CMe_2(C_5H_5)$}-7-{CMe_2[3-(C_5H_4)-3,1,2-*closo*-$CoC_2B_9H_{11}$]}-1,7-*closo*-$C_2B_{10}H_{10}$ (5a)

Yield	42 mg (6.8%)
$^{11}B\{^1H\}$ NMR	δ 6.5 (1B), 3.5 (1B), -5.0 (3B), -6.5 (3B), -11.6 (6B), -14.6 (2B), -16.5 (2B), -22.6 (1B)
^1H NMR	Minor (*β*) isomer; δ 6.48 (m, 1H, C*H*), 6.38 (m, 1H, C*H*), 6.06 (m, 1H, C*H*), 5.71* (m, 2H, C_5H_4), 5.35* (m, 2H, C_5H_4), 3.92* (br. s, 2H, cage C*H*'s), 2.95 (m, 2H, CH_2), 1.48* (s, 6H, CH_3), 1.32* (s, 6H, CH_3). Major (*α*) isomer; δ 6.41 (m, 1H, C*H*), 6.32 (m, 1H, C*H*), 6.22 (m, 1H, C*H*), 5.71* (m, 2H, C_5H_4), 5.35* (m, 2H, C_5H_4) 3.92* (br. s, 2H, cage C*H*'s), 2.87 (m, 2H, CH_2), 1.48* (s, 6H, CH_3), 1.32* (s, 6H, CH_3). Relative integrals are given and the ratio of *α:β* is 3:2. * = coincident resonance
CHN	$C_{20}H_{42}B_{19}Co$: calc. C 43.9%, H 7.74% found C 44.7%, H 7.81%
MS	*m/z* 546 (M^+) (with an isotopic envelope spanning *m/z* 539-552), 411 (M-$C_2B_9H_{11}$)

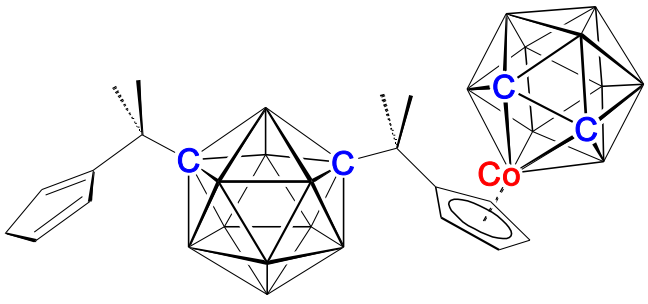

1,7-{CMe_2[3-(C_5H_4)-3,1,2-*closo*-$CoC_2B_9H_{11}$]}$_2$-1,7-*closo*-$C_2B_{10}H_{10}$ (5b)

Yield	12 mg (1.5%)
$^{11}B\{^1H\}$ NMR d_6-acetone	δ 5.5 (2B), 1.9 (2B), -6.0 (5B), -6.7 (5B), -11.8 (8B), -17.0 (4B), -21.6 (1B), -22.9 (1B).
^1H NMR	δ 6.15 (m, 4H, C_5H_4), 5.96 (m, 4H, C_5H_4), 4.47 (br. s, 4H, cage C*H*'s), 1.71 (s, 12H, methyl groups)
MS	*m/z* 736 (M^+) (with an isotopic envelope spanning *m/z* 727-742), 728, 549

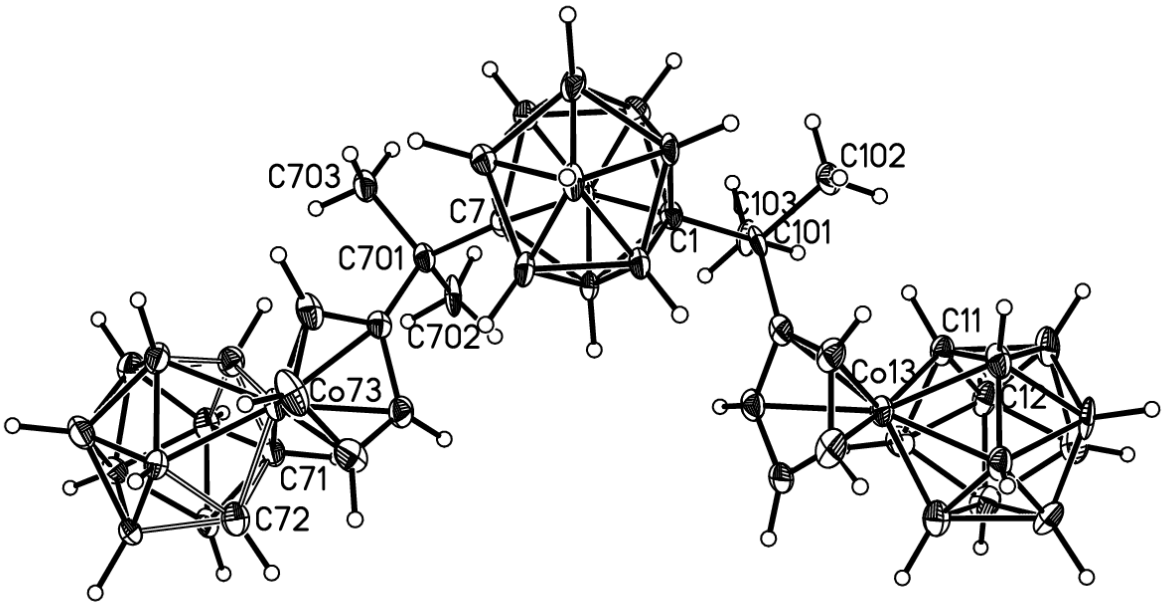

6.7 Synthesis of 1-{CPm(C_5H_5)}-7-{CPm[3-CoCp-1,2-*closo*-$C_2B_9H_{11}$]}-1,7-*closo*-$C_2B_{10}H_{10}$ (6a)

1,7-{CPm(C_5H_5)}$_2$-1,7-*closo*-$C_2B_{10}H_{10}$ (425 mg, 0.98 mmol) was dissolved in 20 ml THF and cooled in ice. *n*-BuLi (2.5 M in hexanes, 0.81 ml, 2.05 mmol) was added. The contents were added to a Schlenk tube containing a THF solution of $Li_2[C_2B_9H_{11}]$ (9.5 mmol) frozen in liquid nitrogen. $CoCl_2$ (1.125 g, 8.66 mmol) was added as a solid on top of the frozen solution which was allowed to thaw and then stirred at room temperature overnight. Air was bubbled through the solution for 30 mins. The solvent was removed *in vacuo* and the residue was extracted into DCM and filtered through silica to leave a dark yellow solution. Removal of the solvent left a yellow residue that was subjected to prep. TLC using 2:1 petrol: DCM as the eluent. A yellow band with R_f 0.37 was isolated and shown to be the double cage species **6a** (39 mg, 6.5%). Further chomatography of the residual baseline in solvents of increasing polarity did not yield any triple cage species (**6b**) although a mass spectrum of the crude mixture prior to any chromatography indicated its presence.

Yield (6a) 0.039 g (6.5%)

$^{11}B\{^1H\}$ NMR δ 6.2 (1B), 3.2 (1B), -5.1 (3B), -6.7 (3B), -11.8 (6B), -14.2 (2B), -16.5 (2B), -22.7 (1B)

^1H NMR major (*β*) isomer: δ 6.46 (m, 1H, CH [C_5H_5]), 6.41 (m, 1H, CH [C_5H_5]), 6.07 (m, 1H, CH [C_5H_5]), 5.52* (m, 2H, Co(C_5H_4)), 5.29* (m, 2H, Co(C_5H_4)), 3.90* (br. s, 2H, cage C*H*s), 3.09 (br. d, 2H, [C_5H_5]), 2.30-2.40* (br. m, 2H, CH_2 [Pm]), 2.05 – 2.15* (br. m, 2H, CH_2 [Pm]), 1.60 – 1.81* (br. m, 6H, CH_2's [Pm]), 1.25-1.58* (br. m, 8H, CH_2's [Pm]), 0.90- 1.08* (br. m, 2H, CH_2's [Pm]). Minor (*α*) isomer: δ 6.53 (m, 1H, CH, [C_5H_5]), 6.49 (m, 1H, CH [C_5H_5]), 6.22 (m, 1H, CH [C_5H_5]), 5.52* (m, 2H, Co(C_5H_4)), 5.29* (m, 2H, Co(C_5H_4)), 3.90* (br. s, 2H, cage C*H*s), 2.71 (br. d, 2H, [C_5H_5]), 2.30-2.40* (br. m, 2H, CH_2 [Pm]), 2.05 -2.15* (br. m, 2H, CH_2 [Pm]), 1.60 – 1.81* (br. m, 6H, CH_2s [Pm]), 1.25-1.58* (br. m, 8H, CH_2's [Pm]), 0.90- 1.08* (br. m,

2H, CH_2's [Pm]). Relative integrals are given and the ratio of α:β is 1:3. * = coincident resonance

CHN $C_{26}H_{50}B_{19}Co$: calc. C 49.8%, H 8.04%; found C 50.2%, H 9.12%

MS *m/z* 627 (M^+) (with an isotopic envelope spanning *m/z* 620-633)

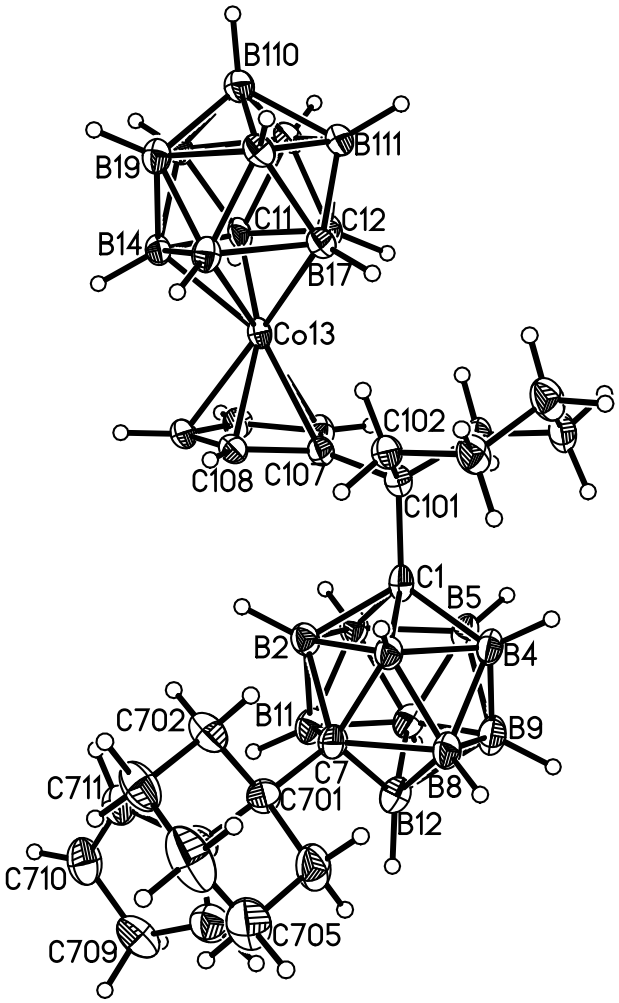

6.8 Attempted Synthesis of 1,2-{$CMe_2(C_5H_5)$}$_2$-1,2-*closo*-$C_2B_{10}H_{10}$

1,2-*closo*-$C_2B_{10}H_{12}$ (0.20 g, 1.4 mmol) was dissolved in 20 ml dry diethyl ether and cooled to 0°C. Added to this was *n*-BuLi (2.5M in hexane, 1.8 ml, 4.5 mmol). Stirring whilst warming to room temperature overnight afforded a white precipitate. Freshly distilled 6,6-dimethylfulvene (0.55 ml, 4.5 mmol) was added dropwise as an ether solution and the reagents heated to reflux for 4 hours. The solution was cooled to 0^{o}C and an excess of dilute HCl was added and the product was extracted into diethyl ether three times. The combined organic layers were evaporated to leave a yellow residue. Mass spectrometric analysis of this showed a large peak centred on *m/z* 250 and no evidence of the disubstituted product. The residue was dissolved in ethanol (4-5 ml) and placed in the freezer for 24 hours to induce crystallisation. The isolated product, 1-{$CMe_2(C_5H_5)$}-1,2-*closo*-$C_2B_{10}H_{10}$, was identified by ^{1}H and ^{11}B{^{1}H} NMR spectroscopies as reported by Hong et al[8] in 68% yield (0.27 g).

6.9 Synthesis of 1,7-{$CMe_2(C_5H_5)$}$_2$-1,7-*closo*-$C_2B_{10}H_{10}$ (7a)

1,7-*closo*-$C_2B_{10}H_{12}$ (2.00 g, 13.9 mmol) was dissolved in 40 ml dry diethyl ether and cooled to 0°C. Added to this was *n*-BuLi (2.5M in hexane, 11.7 ml, 29.1 mmol). Stirring whilst warming to room temperature overnight afforded a white precipitate. Freshly distilled 6,6-dimethylfulvene (4.2 ml, 34.7 mmol) was added dropwise as an ether solution and the reagents heated to reflux for 4 hours. The solution was cooled to 0^oC and an excess of dilute HCl was added and the product was extracted into diethyl ether three times. The combined organic layers were evaporated to leave a yellow oil. This was dissolved in ethanol (10 ml) and placed in the freezer for 24 hours to induce crystallisation. The crystals were filtered off and used in the next step as a mixture of isomers.

Yield	2.80 g (56%)
$^{11}B\{^{1}H\}$ NMR	δ -6.4 (2B), -12.0 (6B), -14.2 (2B), <δ(^{11}B)> -11.34
^{1}H NMR	Major (*β*) isomer; δ 6.42 (m, 1H, C*H*), 6.30 (m, 1H, C*H*), 6.23 (m, 1H, C*H*), 2.87 (m, 2H, CH_2), 1.31* (s, 6H, CH_3). Minor (*α*) isomer; δ 6.62, (m, 1H, C*H*), 6.37 (m, 1H, C*H*), 6.05 (m, 1H, C*H*), 2.93 (m, 2H, CH_2), 1.31* (s, 6H, CH_3). Relative integrals are given and the ratio of *α:β* is 2:1. * = coincident resonance
CHN	$C_{18}H_{32}B_{10}$: calc. C 60.6%, H 9.05%; found C 60.1%, H 9.11%
MS	*m/z* 357 (M^+) (with an isotopic envelope spanning *m/z* 352-361), 341 (M – Me), 327 (M – 2Me), 294 (M – C_5H_5)

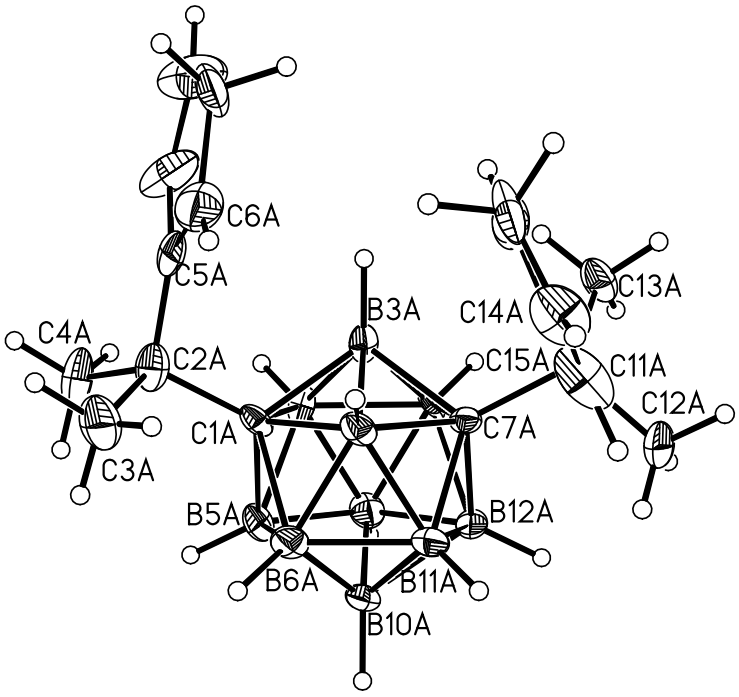

6.10 Synthesis of 1,7-$(CMe_2Fc)_2$-1,7-*closo*-$C_2B_{10}H_{10}$ (8a)

1,7-$\{CMe_2(C_5H_5)\}_2$-1,7-*closo*-$C_2B_{10}H_{10}$ (0.5 g, 1.40 mmol) was dissolved in dry THF (20 ml) and cooled to 0°C. Added to this was *n*-BuLi (2.5M in hexane, 1.2 ml, 3.00 mmol) and the solution was left to stir at room temperature for 2 hours. It was then frozen in liquid N_2 and $FeCl_2$ (1.8 g, 14.2 mmol) and NaCp (2.0 M in THF, 7.5 ml, 15.0 mmol) were added, followed by warming to room temperature whilst stirring overnight. The mixture was heated to reflux for 2 hours. After removal of solvent the residue was taken up in DCM and filtered through silica to give a dark orange solution. This was evaporated and the solid was washed with cold petroleum ether to remove both ferrocene and monosubstituted product. The product was isolated as a yellow solid. Single crystals were grown by slow evaporation of a 40-60 petrol/dichloromethane mixture.

Yield	0.290 g (25%)
$^{11}B\{^{1}H\}$ NMR	δ -6.7 (2B), -12.2 (6B), -14.1 (2B), <δ(^{11}B)> -11.50
^{1}H NMR	δ 4.15 (m, 4H, C_5H_4), 4.10 (s, 10H, Cp), 4.01 (m, 4H, C_4H_5), 1.38 (s, 12H, CH_3)
CHN	$C_{26}H_{40}B_{10}Fe_2$: calc. C 56.4%, H 6.76%; found C 56.0%, H 6.73%
MS	*m/z* 596 (M^+) (with an isotopic envelope spanning *m/z* 590-601)

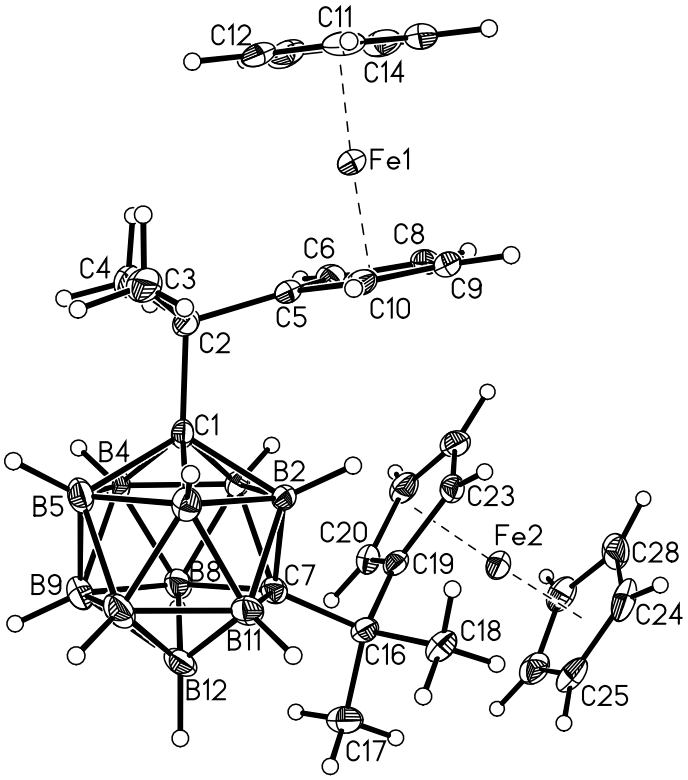

6.11 Synthesis of 1,2-$(CMe_2Fc)_2$-1,2-*closo*-$C_2B_{10}H_{10}$ (9a)

1,7-$\{CMe_2Fc\}_2$-1,7-*closo*-$C_2B_{10}H_{10}$ (100 mg, 0.167 mmol) was dissolved in dry degassed THF. Added to this were Na metal (40 mg, 1.74 mmol) and a catalytic amount of napthalene and the mixture stirred at room temperature for 36 hours. The Na metal was removed from the solution which was then left open to air for 20 mins. The solvent was removed and the products were extracted into dichloromethane and separated by chromatography on silica with an elution mixture of dichloromethane and petroleum ether (50:50). This revealed two mobile bands, one deep red R_f 0.7, and an uncharacterised light pink band R_f 0.5. The red product was isolated as a dark red solid.

Yield 0.073 g (73%)

$^{11}B\{^1H\}$ NMR δ -2.6 (2B), -6.6 (4B), -7.9 (2B), -12.6 (2B), $<\delta(^{11}B)>$ -7.25

^1H NMR δ 4.24 (m, 4H, C_5H_4), 4.15 (m, 4H, C_5H_4), 4.12 (m, 10H, Cp), 1.87 (s, 12*H*, CH_3)

CHN $C_{26}H_{40}B_{10}Fe_2$: calc. C 56.4%, H 6.76%; found C 56.1%, H 6.79%

MS *m/z* 597 (M^+) (with an isotopic envelope spanning *m/z* 590-601), 370 (M – $\{CMe_2Fc\}$), 227 ($\{CMe_2Fc\}$)

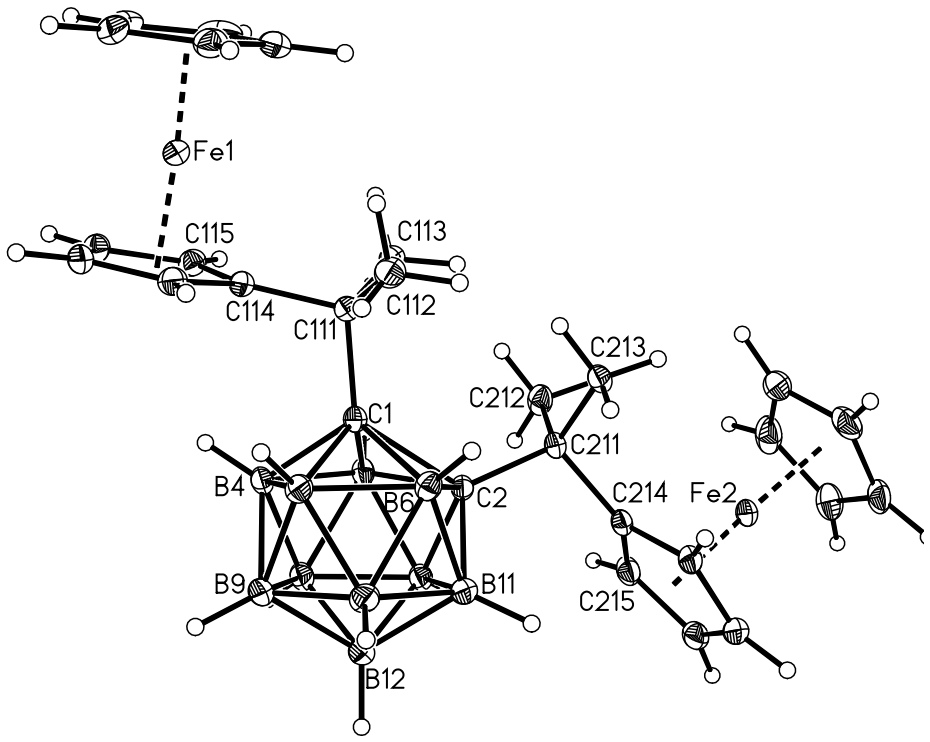

6.12 Reduction and Metallation of 1,7-$(CMe_2Fc)_2$-1,7-*closo*-$C_2B_{10}H_{10}$ forming 10

1,7-$(CMe_2Fc)_2$-1,7-*closo*-$C_2B_{10}H_{10}$ (**8a**) (100 mg, 0.16 mmol) was dissolved in 40 ml of degassed THF. To this was added sodium metal (50 mg, 2.1 mmol) together with a catalytic amount of naphthalene and the mixture stirred for 24 hours. The reaction was frozen with liquid N_2 before $[RuCl_2(p\text{-cym})]_2$ (55 mg, 0.08 mmol) was added and the mixture left to stir at ambient temperature overnight. The solvent was removed *in vacuo* and the products were extracted into dichloromethane and separated by chromatography on silica with an elution mixture of dichloromethane and petroleum ether (50:50). This revealed a mobile yellow band with R_f 0.2. The product was isolated as a yellow solid **10**. Another 65% of **8a** was converted to **9a** as identified by ^1H and ^{11}B NMR spectroscopies.

Yield 13 mg (10%)

$^{11}B\{^1H\}$ NMR δ 15.0 (1B), 5.5 (1B), 1.8 (1B), -3.5 (1B), -5.6 (2B), -8.2, (1B), -12.5 (2B), -20.4 (1B)

^1H NMR δ 5.64 - 5.09 (4 d, 4H, $CH_3C_6H_4CHMe_2$), 4.47 (m, 1H, C*H*), 4.30 (m, 1H, C*H*), 4.24 (m, 1H, C*H*), 4.17 (br. m, 7H, Cp + 2C*H*), 4.12 (br. m, 7H, Cp + 2C*H*), 4.05 (m, 1H, C*H*), 2.62 (br. m, 1H, $CH_3C_6H_4CHMe_2$), 2.11 (s, 3H, $CH_3C_6H_4CHMe_2$), 1.77 (s, 3H, Me), 1.74 (s, 3H, Me), 1.62 (s, 3H, Me), 1.41 (s, 3H, Me), 1.14 (d, 3H, $CH_3C_6H_4CHMe_2$), 1.12 (d, 3H, $CH_3C_6H_4CHMe_2$)

MS *m/z* 832 (M^+) (with an isotopic envelope spanning *m/z* 821-839), 646 (M- Fc)

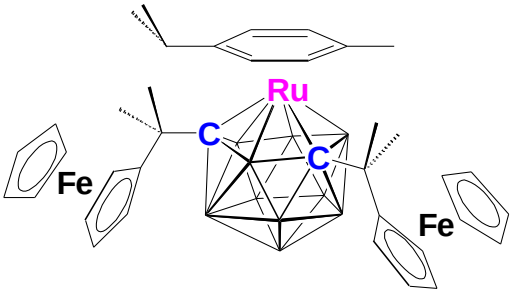

6.13 Attempted Synthesis of 4-Ph-1,6-$(CMe_2Fc)_2$-1,6-*closo*-$C_2B_{11}H_{10}$

1,7-$(CMe_2Fc)_2$-1,7-*closo*-$C_2B_{10}H_{10}$ (100 mg, 0.16 mmol) was dissolved in 40 ml of degassed THF. To this sodium metal (50 mg, 2.1 mmol) was added along with a catalytic amount of naphthalene and the mixture stirred for 24 hours. The excess sodium was removed and the solvent replaced with degassed toluene. $BPhCl_2$ (0.06 ml, 0.44 mmol) was added at –78°C and the reagents were left stirring at ambient temperature overnight. The solvent was removed *in vacuo* and the products were extracted into dichloromethane and were separated by chromatography on silica with an elution mixture of dichloromethane and petroleum ether (50:50). This revealed a deep purple band, isolated as 1,2-$(CMe_2Fc)_2$-4-OH-1,2-*closo*-$C_2B_{10}H_9$ (**11)**

Yield 0.018 g (17%)

$^{11}B\{^1H\}$ NMR δ 8.1 (1B {*B*-OH}), -1.3 (1B), -3.4 (2B), -4.8 (1B), -7.8 (1B), -10.2 (1B), -13.1 (2B), -19.0 (1B) <δ(^{11}B)> -6.8

^1H NMR δ 4.36 (m, 1H, C*H*), 4.30 (m, 1H, C*H*), 4.20 (br. m, 4H, 4C*H*), 4.15 (br. m, 6H, Cp + C*H*), 4.11 (br. m, 6H, Cp + C*H*), 1.92 (s, 3H, Me), 1.91 (s, 3H, Me), 1.89 (s, 3H, Me), 1.72 (s, 3H, Me)

CHN $C_{26}H_{40}B_{10}Fe_2O$: calc C 54.9%, H 6.58% found C 57.3, H 7.02%

MS *m/z* 612 (M^+) (with an isotopic envelope spanning *m/z* 606-617), 385 (M – {CMe_2Fc}), 227 ({CMe_2Fc})

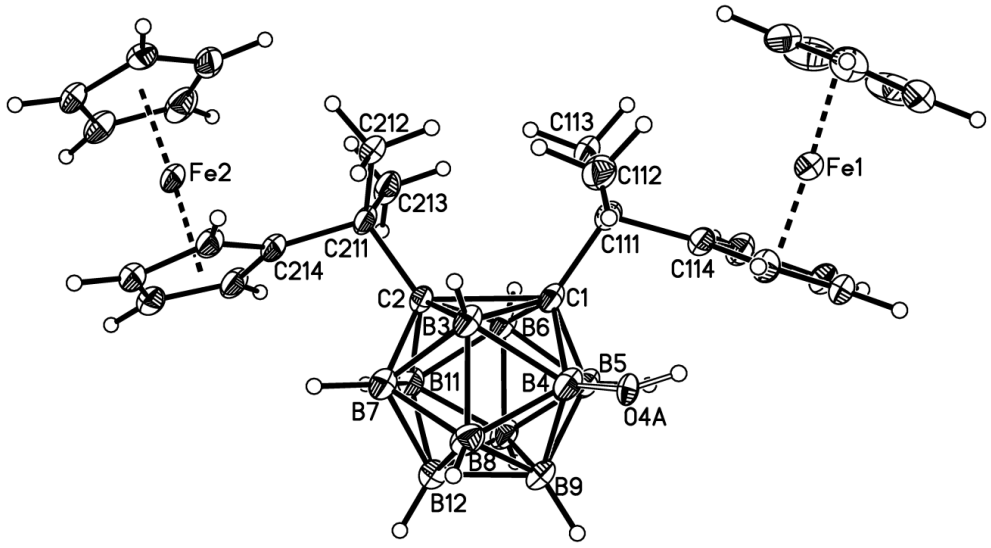

6.14 Synthesis of 1,7-{CPm(C_5H_5)}$_2$-1,7-*closo*-$C_2B_{10}H_{10}$ (7b)

1,7-*closo*-$C_2B_{10}H_{12}$ (2.00 g, 13.9 mmol) was dissolved in 40 ml dry diethyl ether and cooled to 0°C. Added to this was *n*-BuLi (2.5M in hexane, 11.7 ml, 29.1 mmol) and the solution left to stir whilst warming to room temperature overnight to afford a white precipitate. Freshly distilled 6,6-pentamethylenefulvene (4.7 g, 35.1 mmol) was added dropwise as an ether solution and the reagents heated to reflux for 20 hours. An excess of dilute HCl was added at 0°C to the cooled solution and the product was extracted into diethyl ether three times. The combined organic layers were evaporated to leave a yellow oil. This was dissolved in ethanol (10 ml) and placed in the freezer for 24 hours to induce crystallisation. The crystals were filtered off and used in the next step as a mixture of isomers.

Yield	3.20 g (53%)
^{11}B{^{1}H} NMR	δ -6.6 (2B), -12.3 (6B), -14.7 (2B), <δ(^{11}B)> -11.65
^{1}H NMR	Major (*β*) isomer; δ 6.38 (m, 2H, C*H*), 6.03 (m, 1H, C*H*), 2.9 (br. m, 2H, C*H*$_2$ {C_5H_5}), 2.08 (br. d, 4H, C*H*$_2$ {Pm}), 1.45 (br. m, 12H, C*H*$_2$ {Pm}) 1.03 (br. m, 4H, C*H*$_2$ {Pm}). Minor (*α*) isomer; δ 6.47, (m, 1H, C*H*), 6.32 (m, 1H, C*H*), 6.18 (m, 1H, C*H*), 2.83 (br. m, 2H, C*H*$_2$, {C_5H_5}), 1.90 (br. d, 2H, C*H*$_2$ {Pm}), 1.03 (br. m, 4H, C*H*$_2$ {Pm}). Relative integrals are given and the ratio of *α:β* is 2:9
CHN	$C_{24}H_{40}B_{10}$: calc. C 66.0%, H 9.23%; found C 66.2%, H 9.48%
MS	*m/z* 437 (M^+) (with an isotopic envelope spanning *m/z* 431-441), 370 ($M - C_5H_5$)

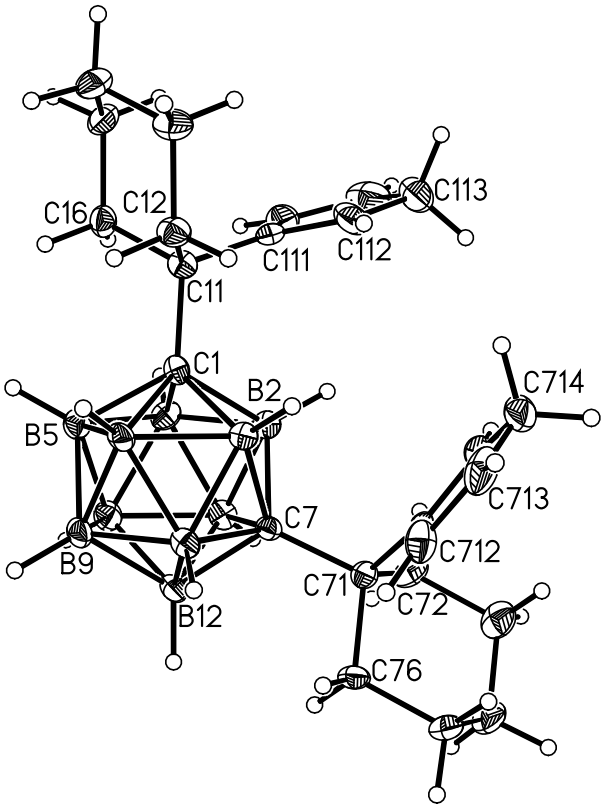

6.15 Synthesis of 1,7-{CPmFc}$_2$-1,7-*closo*-$C_2B_{10}H_{10}$ (8b)

1,7-{CPm(C_5H_5)}$_2$-1,7-*closo*-$C_2B_{10}H_{10}$ (0.5 g, 1.15 mmol) was dissolved in 20 ml dry THF and cooled to 0^{o}C. Added to this was *n*-BuLi (2.5M in hexane, 0.96 ml, 2.40 mmol) and the mixture stirred at room temperature for 2 hours. This solution was frozen in liquid N_2 and added to it were $FeCl_2$ (1.46 g, 11.5 mmol) and NaCp (2.0M in THF, 6.5 ml, 13.0 mmol). The reaction was allowed to warm to room temperature whilst stirring overnight and then heated to reflux for 2 hours. After removal of solvent the residue was taken up in DCM and filtered through silica to give a dark orange solution. This was evaporated and the solid washed with cold petroleum ether to leave an orange solid (310 mg). This was purified by chromatography on silica with an elution mixture of dichloromethane and petroleum ether (50:50) to reveal an orange band R_f 0.52. The product was isolated as an orange solid.

Yield	230 mg (29%)
$^{11}B\{^{1}H\}$ NMR	δ -5.9 (2B), -12.4 (8B), <δ(^{11}B)> -11.12
^{1}H NMR	δ 4.15 (m, 4H, C_5H_4), 4.07 (s, 10H, Cp), 3.98 (m, 4H, C_4H_5), 2.17 (m, 14H, CH_2), 1.90 (m, 8H, CH_2), 1.59 (m, 6H, CH_2), 1.37 (m, 2H, CH_2)
CHN	$C_{34}H_{50}B_{10}Fe_2$: calc. C 60.4%, H 7.15%; found C 61.1%, H 6.91%
MS	*m/z* 676 (M^+) (with an isotopic envelope spanning *m/z* 670-681)

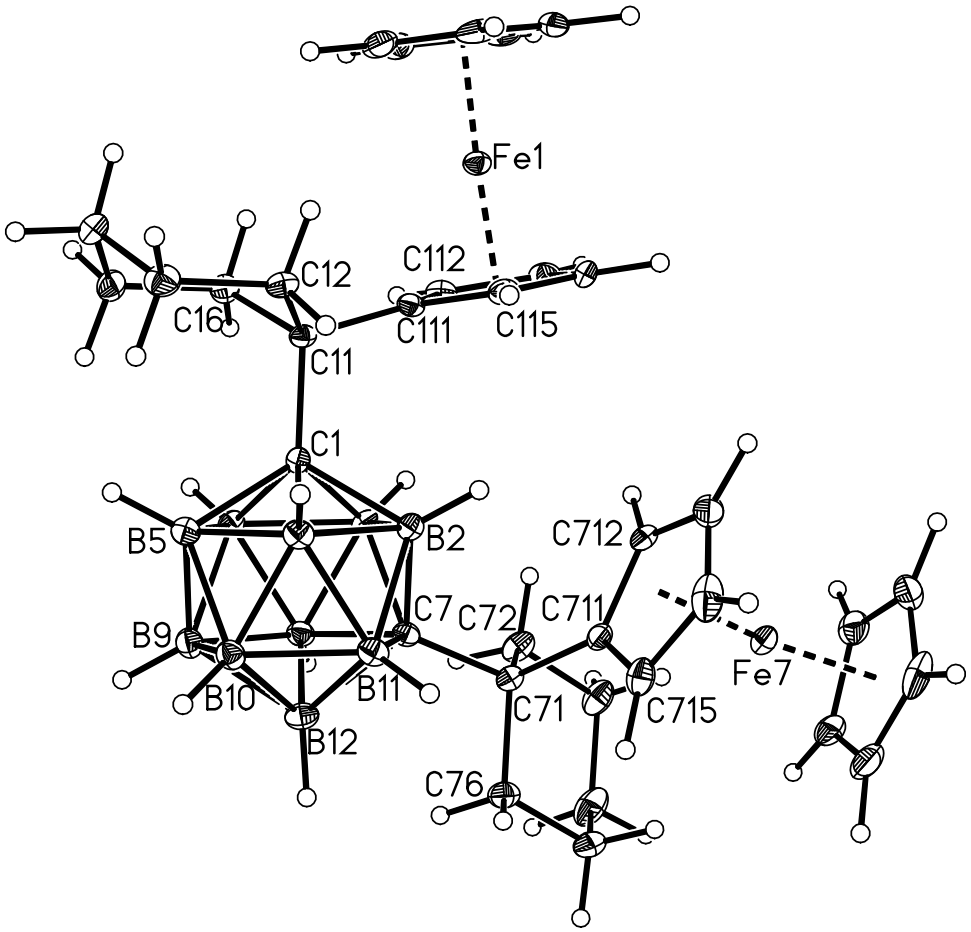

6.16 Synthesis of 1,2-{CPmFc}$_2$-1,2-*closo*-$C_2B_{10}H_{10}$ (9b)

1,7-(CPmFc)$_2$-1,7-*closo*-$C_2B_{10}H_{10}$ (100 mg, 0.147 mmol) was dissolved in 20 ml dry degassed THF and sodium metal (50 mg, 2.2 mmol) was added along with a few crystals of naphthalene. The solution darkened whilst stirring over 24 hours. In an attempt to synthesise a 13-vertex carborane $BPhCl_2$ (0.60 mmol, 0.8 ml) was added at -78^{o}C after a solvent change to dry degassed toluene. The mixture was stirred for 18 hours. The now purple solution was evaporated and preparative TLC with 2:1 petrol: DCM afforded a deep purple band as the main product.

Yield 0.043 g (43%)

$^{11}B\{^1H\}$ NMR δ -0.7 (4B), -3.7 (4B), -14.2 (2B). <δ(^{11}B)> -4.61

^{1}H NMR δ 4.23 (m, 4H, C_5H_4), 4.19 (m, 4H, C_4H_5), 4.11 (s, 10H, Cp), 2.63 (m, 4H, CH_2), 2.33 (m, 4H, CH_2), 2.24 (m, 4H, CH_2), 1.73 (m, 6H, CH_2), 1.52 (m, 2H, CH_2)

CHN $C_{34}H_{50}B_{10}Fe_2$: calc. C 60.4%, H 7.15%; found C 59.5%, H 7.07%

MS *m/z* 676 (M^+) (with an isotopic envelope spanning *m/z* 670-681), 410 (M – {CPmFc}), 266 ({CMe_2Fc})

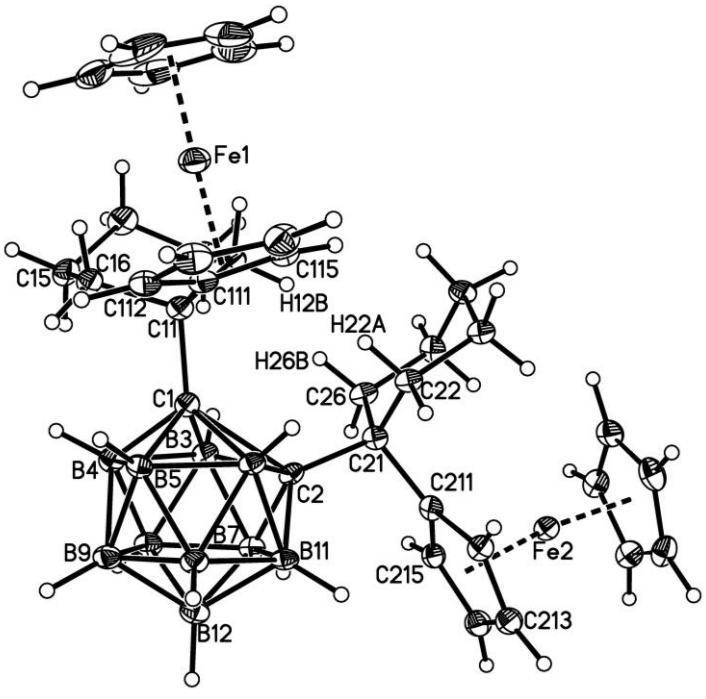

6.17 Synthesis of 1,7-{CPm(Me$_4$)(C$_5$H$_5$)}$_2$-1,7-*closo*-C$_2$B$_{10}$H$_{10}$ (7c)

1,7-*closo*-$C_2B_{10}H_{12}$ (0.50 g, 3.48 mmol) was dissolved in 20 ml dry diethyl ether and cooled to 0°C. Added to this was *n*-BuLi (2.5M in hexane, 3.0 ml, 7.3 mmol) and the solution left to stir whilst warming to room temperature overnight to afford a white precipitate. Fulvene III* (1.62 g, 8.0 mmol) was added slowly and the mixture heated to reflux for 24 hours. An excess of dilute HCl was added at 0°C to the cooled solution and the product was extracted into diethyl ether three times. The combined organic layers were evaporated to leave a pale yellow solid. This was recrystallised from hot ethanol (10 ml) and cooled in ice to induce crystallisation. The product was collected as white crystals.

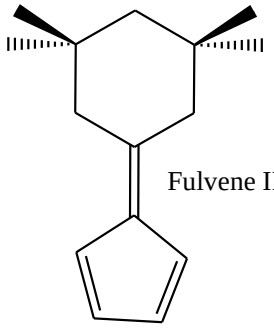

Fulvene III

*Fulvene III made by the reaction of cyclopentadiene and 3,3,5,5-tetramethylcyclohexanone following the general procedure of Stone and Little.[4] ^{1}H NMR δ 6.48 (app. s, 4H, arom CH's), 2.32 (s, 4H, 2 x CH_2), 1.35 (s, 2H, CH_2), 0.89 (s, 12H, 4 x CH_3). MS: *m/z* 202.

Yield 1.44 g (76%)

$^{11}B\{^{1}H\}$ NMR δ -6.4 (2B), -12.7 (4B), -14.5 (4B)

^{1}H NMR δ 6.49 (m, 2H, C*H*), 6.26 (m, 2H, C*H*), 6.11 (m, 2H, C*H*), 2.92 (m, 4H, CH_2), 2.09 (s, 1H, C*H*), 2.04 (s, 1H, C*H*), 1.99 (s, 1H, C*H*), 1.92 (s, 1H, C*H*), 1.32 (s, 1H, C*H*), 1.29 (s, 1H, C*H*), 1.27 (s, 1H, C*H*), 1.22 (s, 1H, C*H*), 1.13 (s, 1H, C*H*), 1.11 (s, 1H, C*H*), 0.94 (s, 1H, C*H*), 0.91 (s, 1H, C*H*), 0.89 (s, 6H, CH_3), 0.87 (s, 6H, CH_3), 0.84 (s, 6H, CH_3), 0.68 (s, 6H, CH_3)

CHN $C_{32}H_{56}B_{10}$: calc. C 70.0%, H 10.3%; found C 70.5%, H 10.3%

MS *m/z* 548 (M^+) (with an isotopic envelope spanning *m/z* 543-552)

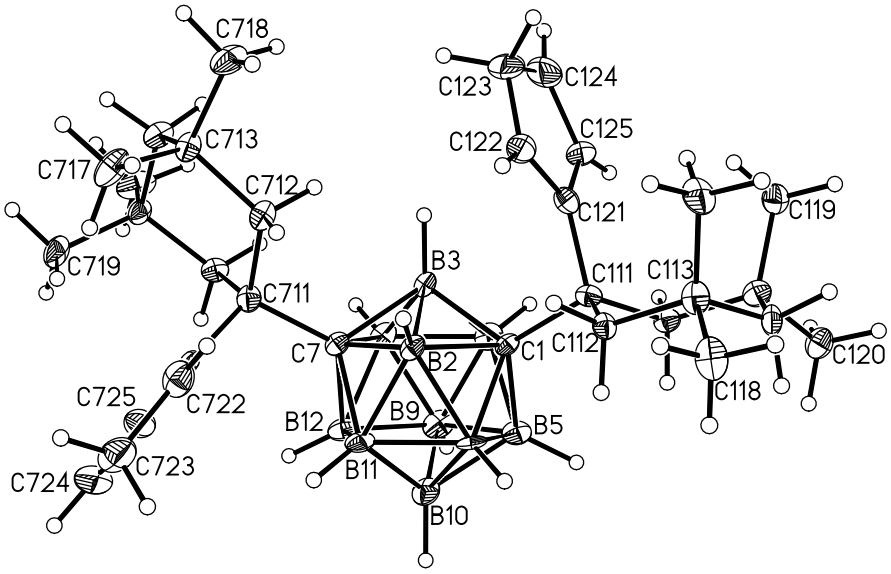

6.18 Thermolysis of 1,2-{CPmFc}$_2$-1,2-*closo*-$C_2B_{10}H_{10}$

1,2-{CPmFc}$_2$-1,2-*closo*-$C_2B_{10}H_{10}$ (30 mg, 0.067 mmol) was dissolved in 20 ml toluene and the solution was heated to reflux for 16 hours. The dark purple colour changed to light orange during this time. The solvent was removed and the products were separated by chromatography on silica using a 3:1 petrol:DCM eluent to give three products: 1,7-{CPmFc}$_2$-1,7-*closo*-$C_2B_{10}H_{10}$ **8b** (14 mg, 48%), a yellow solid 1-(CPmFc)-1,2-*closo*-$C_2B_{10}H_{11}$ **12a** (6 mg, 27%, R_f 0.68) and an unidentified light orange species **12b** (3 mg, R_f 0.82). The latter two compounds are products of decomposition.

1-(CPmFc)-1,2-*closo*-$C_2B_{10}H_{11}$ (12a)

Yield 6 mg (27%)

$^{11}B\{^1H\}$ NMR δ -3.9 (2B), -9.4 (2B), -11.4 (2B), -14.2 (4B)

^1H NMR δ 4.23 (m, 2H, C*H*), 4.14 (s, 5H, Cp), 4.07 (m, 2H, C*H*), 2.49 (br. s, 1H, cage C*H*), 2.35 (m, 2H, CH_2) 2.20 (m, 2H, CH_2), 2.09 (m, 2H, CH_2), 1.77 (m, 2H, CH_2), 1.66 (m, 1H, CH_2), 1.49 (m, 1H, CH_2)

CHN $C_{18}H_{30}B_{10}Fe$: calc. C 52.7%, H 7.37%; found C 52.8%, H 7.32%

MS *m/z* 410 (M^+) (with an isotopic envelope spanning *m/z* 404-414), 266 (M-cage)

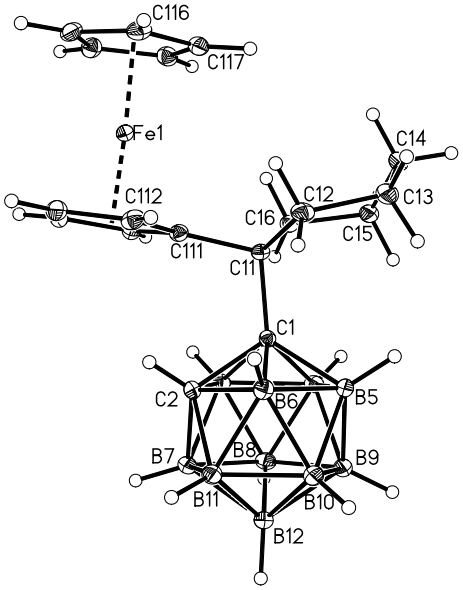

Product (12b) - unknown structure

Yield	3 mg (25%)
^{1}H NMR	δ 5.84 (m, 1H, tentatively assigned as an olefinic C*H*), 4.38 (m, 2H, C*H*), 4.21 (m, 2H, C*H*), 4.10 (s, 5H, Cp), 2.26 (m, 2H, CH_2), 2.10 (m, 2H, CH_2), 1.72 (m, 2H, CH_2), 1.53 (m, 2H, CH_2)
MS	*m/z* 266 (M^+), 238 (M-{2 x CH_2})

6.19 Synthesis of 8,9-Me_2-1,2-*closo*-$C_2B_{10}H_{10}$ (13a)

9,10-Me_2-1,7-*closo*-$C_2B_{10}H_{10}$ (0.150 g, 0.86 mmol) was stirred in a solution of liquid ammonia and sodium metal (0.040 g, 1.72 mmol) at -78°C for 1 hour. Potassium permanganate (0.272 g, 1.72 mmol) was added to the colourless solution and the mixture was allowed to warm to room temperature whilst stirring. The ammonia was evaporated and the green residue was treated with ether (50 ml). The ether solution was washed with water followed by 5% NaOH solution. After removal of solvent, the residue was dissolved in petrol and filtered through silica. The petrol was removed under vacuum to leave a white solid 8,9-Me_2-1,2-*closo*-$C_2B_{10}H_{10}$ (**13a**).

Yield 0.050 g (33%)

$^{11}B\{^1H\}$ NMR δ 7.3 (1B-Me), 0.5 (1B-Me), -0.6 (1B), -9.3 (1B), -13.1 (1B), -14.0 (2B), -15.5 (2B), -19.3 (1B)

^1H NMR δ 3.43 (br. s, 1H, C*H*), 3.37 (br. s, 1H, C*H*), 0.30 (br. s, 3H, B-CH_3), 0.16 (br. s, 3H, B-CH_3)

MS *m/z* 173 (M^+) (with an isotopic envelope spanning *m/z* 169-177)

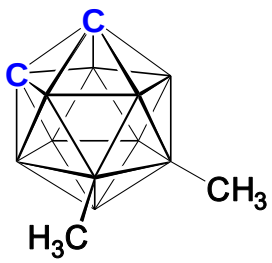

6.20 Reduction and Reoxidation of 9,10-Ph_2-1,7-*closo*-$C_2B_{10}H_{10}$ (formation of 13b)

In liquid NH_3: 9,10-Ph_2-1,7-*closo*-$C_2B_{10}H_{10}$ (300 mg, 1.0 mmol) was stirred in a solution of liquid ammonia and Na metal (4.6 mg, 2.0 mmol) at -78^oC for 1.5 hours. Potassium permanganate (316 mg, 2.0 mmol) was added and the mixture was warmed to room temperature with stirring allowing evaporation of NH_3. The residue was extracted into diethyl ether (25 ml) and the solvent was removed leaving a white powder. This was subjected to preparative TLC (petroleum ether: DCM 4:1) to reveal two bands visible under UV light: starting material 9,10-Ph_2-1,7-*closo*-$C_2B_{10}H_{10}$ (144 mg, 48%, R_f 0.69) and the 1,2 isomer, presumably 8,9-Ph_2-1,2-*closo*-$C_2B_{10}H_{10}$ (**13b**) (150 mg, 50%, R_f 0.42).

Compound 13b

^{11}B NMR δ 8.0 (1B-Ph), 1.7 (1B-Ph), -2.5 (1B), -8.8 (1B), -13.9 (3B), -15.4 (2B), -17.8 (1B)

^{1}H NMR δ 7.06-7.38 (m, 10H, B-Ph), 3.61 (br s, 2H, cage C-H's)

MS *m/z* 296 (M^+) (with an isotopic envelope spanning *m/z* 291-300)

CHN $C_{14}B_{10}H_{20}$: calc. C 56.7%, H 6.80%; found 56.4%, H 6.85%

In THF: 9,10-Ph_2-1,7-*closo*-$C_2B_{10}H_{10}$ (300 mg, 1.0 mmol) was dissolved in degassed THF (20 ml). Added to this were small pieces of Na metal (4.6 mg, 2.0 mmol) and a catalytic amount of naphthalene. The solution turned dark red after approximately 10 minutes (usually indicating a successful reduction) and was left stirring for 4 hours. The reaction vessel was disconnected from the N_2 supply and the contents were stirred for 0.5 hours in air. Excess Na metal was filtered off and the solution evaporated giving an off-white solid. This was analysed by ^{1}H and ^{11}B NMR spectroscopies and identified as mainly 9,10-Ph_2-1,7-*closo*-$C_2B_{10}H_{10}$.
(An alternative method is to add excess Na metal to a stoichiometric amount of naphthalene, filtering off the excess Na metal leaving a dark green solution of a stoichiometric amount of sodium naphthalenide solution).

The reaction was repeated using:

a) 4 equivalents of Na naphthalenide stirred overnight
b) 8 equivalents of Na naphthalenide stirred overnight
c) 20 equivalents of Na naphthalenide stirred for 3 days.

Each reaction gave only starting material 9,10-Ph_2-1,7-*closo*-$C_2B_{10}H_{10}$ as observed by ^{1}H and ^{11}B NMR spectroscopies.

6.21 Reduction and Metallation of 9,10-Me_2-1,7-*closo*-$C_2B_{10}H_{10}$ (formation of 14)

9,10-Me_2-1,7-*closo*-$C_2B_{10}H_{10}$ (400 mg, 2.33 mmol) was treated with Na metal (112 mg, 4.90 mmol) in liquid ammonia at -78^oC for 2 hours. After the mixture was warmed to room temperature the flask was briefly evacuated to ensure removal of all ammonia. Degassed THF (30 ml) was added and the solution was filtered under nitrogen (to remove excess Na) into another Schlenk tube containing [Ru(*p*-cymene)Cl_2]$_2$ (716 mg, 1.17 mmol) and degassed THF (20ml) frozen in liquid nitrogen. After refreezing, the contents were warmed to room temperature overnight with stirring. THF was removed under reduced pressure and the dry residue dissolved in DCM. The mixture was subjected to preparative TLC (DCM: petroleum ether 3:2) which allowed the isolation of a yellow band (R_f 0.63) identified as a 13-vertex ruthenacarborane 4-(*p*-cymene)-2,11-Me_2-4,1,6-*closo*-$RuC_2B_{10}H_{10}$ (**14**). Another three yellow bands were visible on the TLC plate with R_f values of 0.58, 0.52 and 0.48 but they were very weak and could not be isolated and characterised.

Yield	0.152 g (16%)
$^{11}B\{^{1}H\}$ NMR	δ 8.6 (1B-Me), 5.4 (1B), -3.2 (3B including 1B-Me), -8.4 (2B), -13.3 (2B), -16.8 (1B)
^{1}H NMR	δ 5.65, 5.78 (2 d, 2×2H, *p*-cym), 3.61 (br. s, 2×cage C-*H*), 2.74 (sept, 1H, C*H*Me$_2$), 2.13 (s, 3H, Me), 1.22 (d, 6H, CH*Me$_2$*), 0.71 (s, 1H, B-Me), 0.02 (s, 1H, B-Me)
CHN	$C_{14}H_{30}B_{10}Ru$: calc. C 41.3%, H 7.42%; found C 42.1%, H 8.20%
MS	*m/z* 408 (M^+) (with an isotopic envelope spanning *m/z* 398-414)

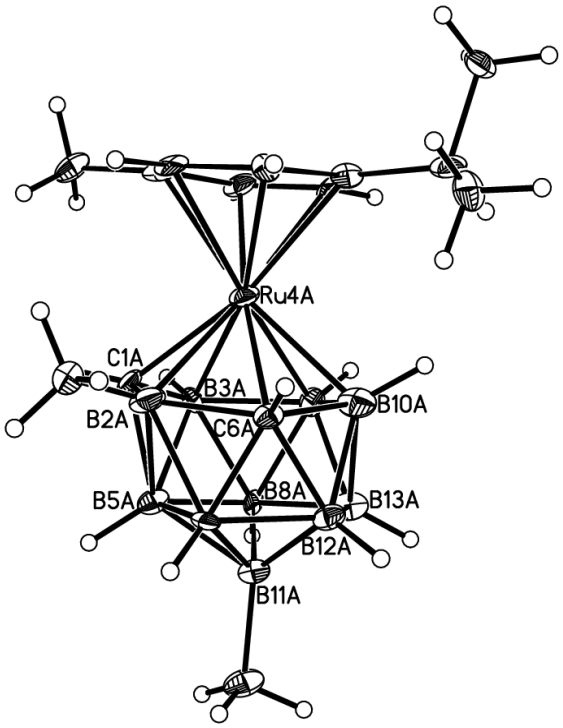

6.22 Synthesis of 9,10-Me_2-1,7-{$CPm(C_5H_5)$}$_2$-1,7-*closo*-$C_2B_{10}H_8$ (15a)

A 2.5 M solution of *n*-BuLi in hexanes (4.8 ml, 12 mmol) was added to a stirred diethyl ether solution (20 ml) of 9,10-Me_2-1,7-*closo*-$C_2B_{10}H_{10}$ (1.00g, 5.7 mmol) at 0°C. The mixture was heated to reflux for 2-3 hours yielding a precipitate. Freshly distilled 6,6-pentamethylenefulvene (2.01 g, 14 mmol) in dry diethyl ether (10 ml) was added dropwise to the mixture which was then heated to reflux for 20 hours. The mixture was cooled to 0°C and water (30 ml) was added. The product was extracted using diethyl ether (3 x 20 ml). The solvent was removed and recrystallisation from diethyl ether and ethanol afforded an pale yellow solid 9,10-Me_2-1,7-{$CPm(C_5H_5)$}$_2$-1,7-*closo*-$C_2B_{10}H_8$ (**15a**).

Yield 1.415 g (52%)

$^{11}B\{^1H\}$ NMR δ -2.8 (2B-Me), -5.2 (2B), -12.7 (4B), -18.8 (2B)

^1H NMR (*ββ*) isomer; δ 6.36 (m, 4H, C*H* [C_5H_5]), 5.98 (m, 2H, C*H* [C_5H_5]), 2.98 (br. d, 4H, CH_2 [C_5H_5]), 2.00 – 2.08 (br. d, 4H, CH_2 [Pm]), 1.32 – 1.51 (br m, 12H, CH_2 [Pm]), 0.94 – 1.07 (br. m, 4H, CH_2 [Pm]), 0.18 (s, 6H, B-Me)

MS *m/z* 464 (M^+) (with an isotopic envelope spanning *m/z* 459-469)

CHN $C_{26}H_{44}B_{10}$: calc. C 67.5%, H 9.15%; found C 66.7%, H 9.86%

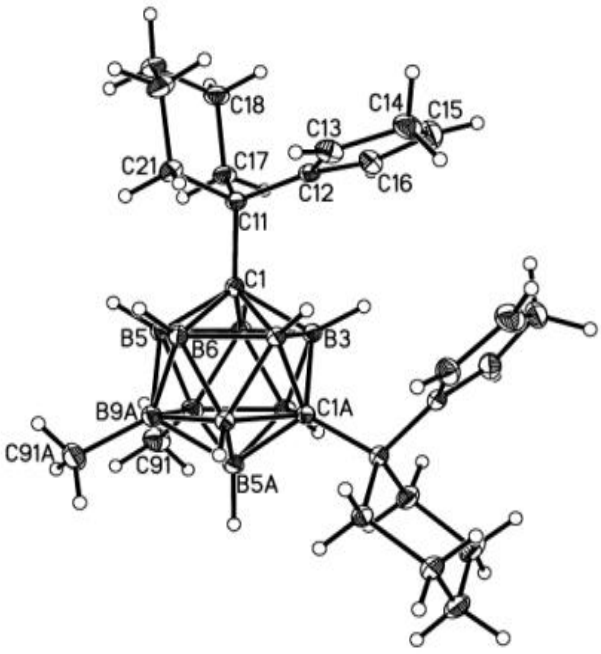

6.23 Synthesis of 9,10-Ph_2-1,7-{$CPm(C_5H_5)$}$_2$-1,7-*closo*-$C_2B_{10}H_8$ (15b)

A 2.5 M solution of *n*-BuLi in hexanes (5.4 ml, 13.5 mmol) was added to a stirred diethyl ether solution (25 ml) of 9,10-Ph_2-1,7-*closo*-$C_2B_{10}H_{10}$ (2.00g, 6.75 mmol) at 0°C. The mixture was heated to reflux for 2-3 hours giving a yellow solution. Freshly distilled 6,6-pentamethylenefulvene (2.34 g, 16.0 mmol) in dry diethyl ether (10 ml) was added dropwise to the mixture which was then heated to reflux for 20 hours. The mixture was cooled to 0°C and water (30 ml) was added. The product was extracted using diethyl ether (3 x 20 ml). The solvent was removed and the residue was subjected to silica gel chromatography, firstly with pure 40-60 petroleum ether followed by a 40-60 petroleum ether:DCM mixture (3:1) yielding an off-white solid, 9,10-Ph_2-1,7-{$CPm(C_5H_5)$}$_2$-1,7-*closo*-$C_2B_{10}H_8$ (**15b**).

Yield 2.74 g (69%)

CHN $C_{36}H_{48}B_{10}$: calc. C 73.2%, H 8.53%; found C 71.4%, H 8.22%

$^{11}B\{^1H\}$ NMR δ -1.8 (2B-Me), -6.9 (2B), -12.5 (4B), -17.3 (2B)

^1H NMR major (*β*) isomer: δ 7.27* (m, 4H, C_6H_5), 7.08* (m, 6H, C_6H_5), 6.45 (m, 2H, C*H* [C_5H_5]), 6.41 (m, 2H, C*H* [C_5H_5]), 6.07 (m, 2H, C*H* [C_5H_5]), 3.02 (br. d, 4H, CH_2 [C_5H_5]), 2.18* (br. d, 4H, CH_2 [Pm]), 1.13 – 1.66* (br. m, 12H, CH_2 [Pm]), 0.97 – 1.11* (m, 4H, CH_2 [Pm]). Minor (*α*) isomer: δ 7.27* (m, 5H, C_6H_5), 7.08* (m, 5H, C_6H_5), 6.48 (m, 2H, C*H*, [C_5H_5]), 6.34 (m, 2H, C*H* [C_5H_5]), 6.22 (m, 2H, C*H* [C_5H_5]), 2.89 (br. d, 4H, CH_2 [C_5H_5]), 2.18* (br. d, 4H, CH_2 [Pm]), 1.13 – 1.66* (br. m, 12H, CH_2 [Pm]), 0.97 – 1.11* (m, 4H, CH_2 [Pm]), relative integrals are given and the ratio of *α*:*β* is 1:4. * = coincident resonance

MS *m/z* 588 (M^+) (with an isotopic envelope spanning *m/z* 583-592), 511 (M-Ph), 434 (M- 2Ph)

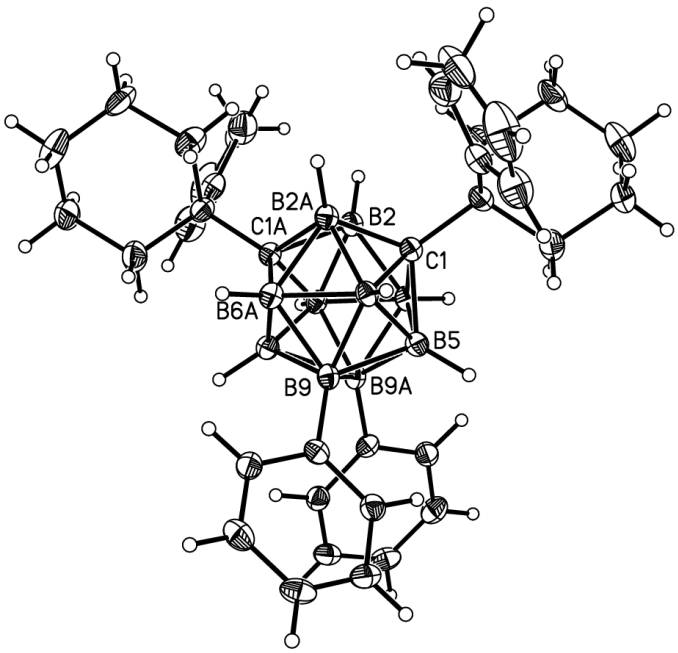

6.24 Synthesis of 9,10-Me_2-1,7-$(CPmFc)_2$-1,7-*closo*-$C_2B_{10}H_8$ (16a)

9,10-Me_2-1,7-{$CPm(C_5H_5)$}$_2$-1,7-*closo*-$C_2B_{10}H_8$ (0.7 g, 1.5 mmol) was dissolved in 20 ml dry THF and treated with *n*-BuLi (2.5 M in hexanes, 1.3 ml, 3.2 mmol) at -78°C. The pale yellow solution was stirred for 30 mins at this temperature followed by stirring for a further 90 mins at room temperature. The solution was frozen at -196°C and NaCp (2.0 M in THF, 7.5 ml, 15.0 mmol) followed by anhydrous $FeCl_2$ (1.9 g, 15.0 mmol) were added. The mixture was allowed to warm to room temperature and stirred for 18 hours. This was followed by heating to reflux for 1 hour. The solvent was removed *in vacuo* and the residue was extracted into DCM then filtered through silica to give a dark orange solution. This was subjected to column chromatography, firstly eluting with 40-60 petroleum ether to remove any ferrocene followed by elution with 40-60 petroleum ether: DCM mixture (3:1) to afford, on evaporation of solvent, an orange solid. The product **16a** was further purified by preparative TLC in 40-60 petroleum ether: DCM mixture (3:1) with an R_f of 0.45.

Yield	0.160 g (15%)
$^{11}B\{^{1}H\}$ NMR	δ -2.9 {4B (2B-Me) + 2B)}, -12.5 (4B), -18.0 (2B)
^{1}H NMR	δ 4.12 (m, 4H, C_5H_4), 4.05 (s, 10H, Cp), 3.96 (m, 4H, C_5H_4), 2.10 (m, 4H, CH_2), 1.88 (m, 8H, CH_2), 1.57 (m, 6H, CH_2), 1.42 (m, 2H, CH_2), 0.10 (s, 6H, B-CH_3)
CHN	$C_{36}H_{52}B_{10}Fe_2$: calc. C 61.2%, H 7.70%; found C 60.7%, H 7.32%
MS	*m/z* 705 (M^+) (with an isotopic envelope spanning *m/z* 698-709)

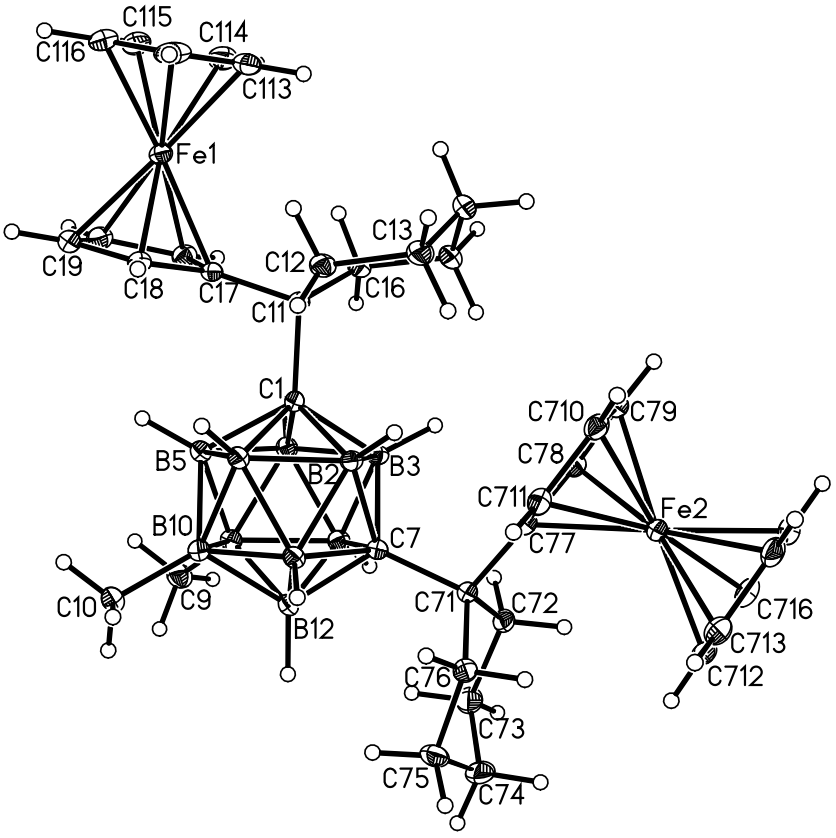

6.25 Deprotonation and Metallation of 9,10-Ph_2-1,7-{CPm(C_5H_5)}$_2$-1,7-*closo*-$C_2B_{10}H_8$

9,10-Ph_2-1,7-{CPm(C_5H_5)}$_2$-1,7-*closo*-$C_2B_{10}H_8$ (0.7 g, 1.19 mmol) was dissolved in 20 ml dry THF and treated with *n*-BuLi (2.5 M in hexanes, 1.0 ml, 2.5 mmol) at -78°C. The pale yellow solution was stirred for 30 mins at this temperature followed by stirring for a further 90 mins at room temperature. The solution was frozen at -196°C and NaCp (2.0 M in THF, 6.0 ml, 12.0 mmol) followed by anhydrous $FeCl_2$ (1.52 g, 12.0 mmol) were added. The mixture was allowed to warm to room temperature and stirred for 18 hours. This was followed with heating to reflux for 1 hour. The solvent was removed *in vacuo* and the residue was extracted into DCM then filtered through silica to give a dark orange solution. Removal of DCM afforded an orange solid, which when applied to a preparative TLC plate revealed ten orange bands with 60:40 DCM: petrol. The two most intense and highest yielding bands with R_f values of 0.45 and 0.56 were compounds **16b** and **16b'** respectively.

9,10-Ph_2-1-(CPmC_5H_5)-7-(CPmFc)-1,7-*closo*-$C_2B_{10}H_8$ (16b')

Yield 102 mg (12.1%)

$^{11}B\{^1H\}$ NMR δ -1.6 (2 × B-Me) -6.4 (2B), -12.2 (4B), -16.6 (2B)

^1H NMR major *β* isomer**,** δ 7.13* (m, 4H, C_6H_5), 7.10* (m, 6H, C_6H_5), 6.40 (m, 2H, C_5H_5), 6.04 (m, 1H, C_5H_5), 4.17* (m, 2H, C_5H_4), 4.11* (s, 5H, Cp), 4.08* (m, 2H, C_5H_4), 3.03 (d, 2H, CH_2, [C_5H_5]), 2.28* (br. m, 2H, [Pm]), 1.95-2.12* (br. m, 6H, [Pm]), 1.58-1.78* (br. m, 4H, [Pm]), 1.34-1.53* (br. m, 6H, [Pm]), 1.00-1.10* (br. m, 2H, [Pm]). Minor *α* isomer, δ 7.13* (m, 5H, C_6H_5), 7.10* (m, 5H, C_6H_5), 6.47 (m, 1H, C_5H_5), 6.35 (m, 1H, C_5H_5), 6.20 (m, 1H, C_5H_5), 4.17* (m, 2H, C_5H_4), 4.11* (s, 5H, Cp), 4.08* (m, 2H, C_5H_4), 2.70-2.91 (br. d, 2H, CH_2 [C_5H_5]), 2.28* (br. m, 2H, [Pm]), 1.95-2.12* (br. m, 6H, [Pm]), 1.58-1.78* (br. m, 4H, [Pm]), 1.34-1.53* (br. m, 6H, [Pm]), 1.00-1.10* (br. m, 2H, [Pm]). Relative integrals given are internal and ratio of *α*:*β* is 1:3. * = coincident resonance.

CHN $C_{41}H_{52}B_{10}Fe$: calc. C 69.5%, H 7.39%; found C 70.0%, H 7.22%

MS *m/z* 709 (M^+) (with an isotopic envelope spanning *m/z* 702-713)

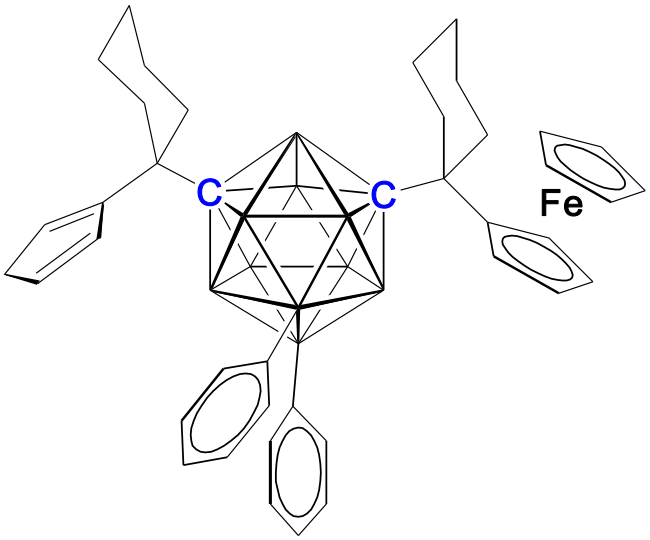

9,10-Ph_2-1,7-$(CPmFc)_2$-1,7-*closo*-$C_2B_{10}H_8$ (16b)

Yield	60 mg (6.1%)
$^{11}B\{^1H\}$ NMR	δ -1.6 (2 × B-Me), -6.0 (2B), -6.2 (4B), -16.0 (2B)
^1H NMR	δ 7.19 (m, 4H, C_6H_5), 7.08 (m, 6H, C_6H_5), 4.16 (m, 4H, C_5H_4), 4.10 (s, 10H, Cp), 4.05 (m, 4H, C_5H_4), 2.19-2.25 (br. m, 4H, CH_2[Pm]), 1.95 (br. m, 8H, CH_2[Pm]), 1.59-1.63 (br. m, 6H, CH_2[Pm]), 1.32-1.41 (br. m, 2H, CH_2[Pm])
CHN	$C_{46}H_{56}B_{10}Fe_2$: calc. C 66.7%, H 6.81%; found C 66.2%, H 6.62%
MS	*m/z* 829 (M^+) (with an isotopic envelope spanning *m/z* 822-834), 752 (M-Ph), 675 (M-2Ph)

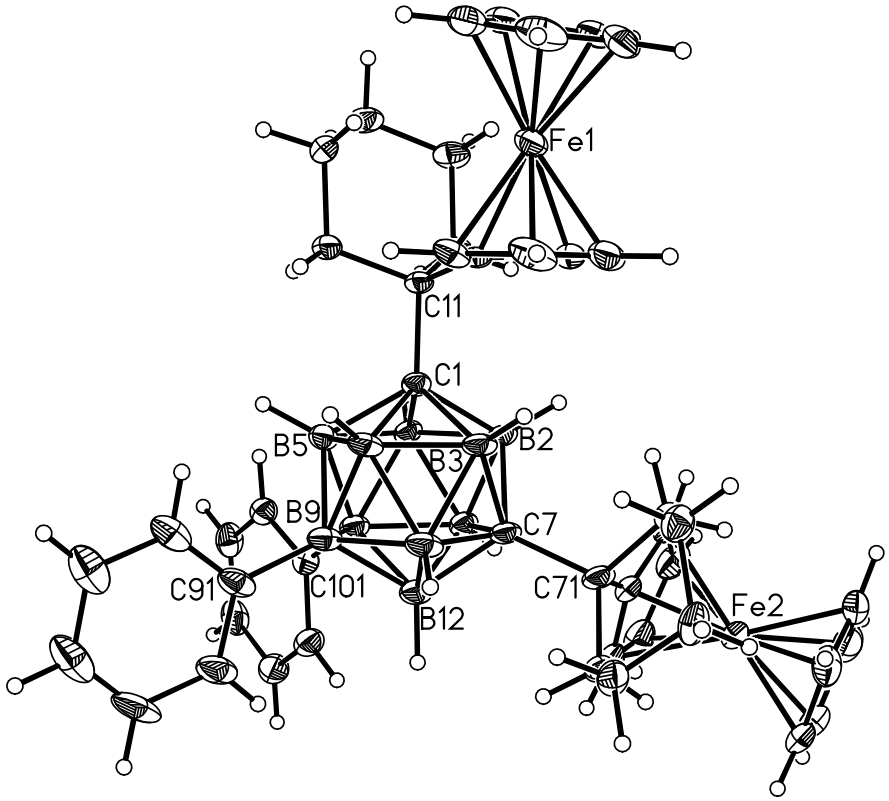

6.26 Reduction and Oxidation of 9,10-Me_2-1,7-$(CPmFc)_2$-1,7-*closo*-$C_2B_{10}H_8$

Small pieces of sodium metal (0.130 g, 5.6 mmol) were reacted with naphthalene (36 mg, 0.28 mmol, 2 equivalents relative to the carborane) in dry, degassed THF (20 ml) forming a dark green solution of sodium naphthalenide. This was added via cannula to an orange solution of 9,10-Me_2-1,7-$(CPmFc)_2$-1,7-*closo*-$C_2B_{10}H_8$ (100 mg, 0.14 mmol) in dry, degassed THF (20 ml). The dark green colour immediately decolourised (indicating reduction has occurred) leaving the initial orange colour of the carborane. A further two equivalents of naphthalenide were added and the same rapid decolourisation was observed. The solution was stirred in air for 20-30 mins to induce oxidation yielding a purple solution. The solvent was removed *in vacuo*. Preparative TLC in 8:3 petroleum ether: DCM mixture afforded two deep purple compounds **17a** (R_f 0.30) and **17b (**R_f 0.34).

The reaction was repeated with the addition of 8 equivalents of sodium naphthalenide added in 2-equivalent portions. The dark green colour decolourised as before after two and four equivalents. A further four equivalents of naphthalenide were added (as two two-equaivalent portions twenty minutes apart) which did not decolourise rapidly. After 30 minutes, a brown solution with some solid suspension remained.

The reaction was repeated using two molar equivalents of sodium naphthalenide and yielded only **17a** in 10% yield.

8,9-Me$_2$-1,2-(CPmFc)$_2$-1,2-*closo*-C$_2$B$_{10}$H$_8$ (17a)

Yield	11 mg (11%)
^{11}B{^{1}H} NMR	δ 10.9 (B-Me), 9.9 (B-Me), 0.2 (4B), -3.7 (2B), -14.00 (1B), -17.3 (1B)
^{1}H NMR	δ 4.20 (m, 4H, C$_5$*H*$_4$), 4.18 (m, 4H, C$_5$*H*$_4$), 4.09 (s, 10H, Cp), 2.57 (m, 4H, C*H*$_2$), 2.30 (m, 4H, C*H*$_2$), 2.20 (m, 2H, C*H*$_2$), 1.68 (m, 6H, C*H*$_2$), 1.53 (m, 4H, C*H*$_2$), 0.29 (s, 3H, B-C*H*$_3$), 0.01 (s, 3H, B-C*H*$_3$)
CHN	C$_{36}$H$_{52}$B$_{10}$Fe$_2$: calc. C 61.4%, H 7.44%; found C 60.1%, H 7.13%
MS	*m/z* 705 (M$^+$) (with an isotopic envelope spanning *m/z* 698-709), 439 (M-CPmFc)

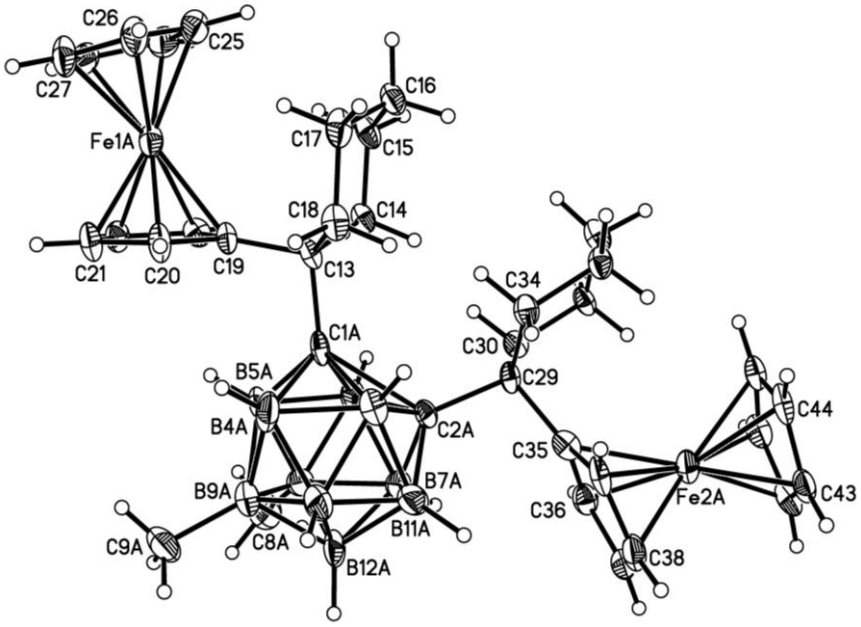

9,12-Me$_2$-1,2-(CPmFc)$_2$-1,2-*closo*-C$_2$B$_{10}$H$_8$ (17b)

Yield	7 mg (7%)
CHN	$C_{36}H_{52}B_{10}Fe_2$: calc. C 61.4%, H 7.44%; found C 59.3%, H 7.35%
^{11}B{^{1}H} NMR	δ 8.2 (2B-Me), 2.6 (2B), -3.2 (4B), -15.1 (2B)
^{1}H NMR	δ 4.21 (m, 8H, 2 x C_5H_4), 4.10 (s, 10H, Cp), 2.52 (m, 6H, CH_2), 2.18-2.34 (br. m, 8H, CH_2), 1.58 (m, 6H, CH_2), 0.01 (s, 6H, B-CH_3)
MS	*m/z* 705 (M^+) (with an isotopic envelope spanning *m/z* 698-709), 439 (M-CPmFc)

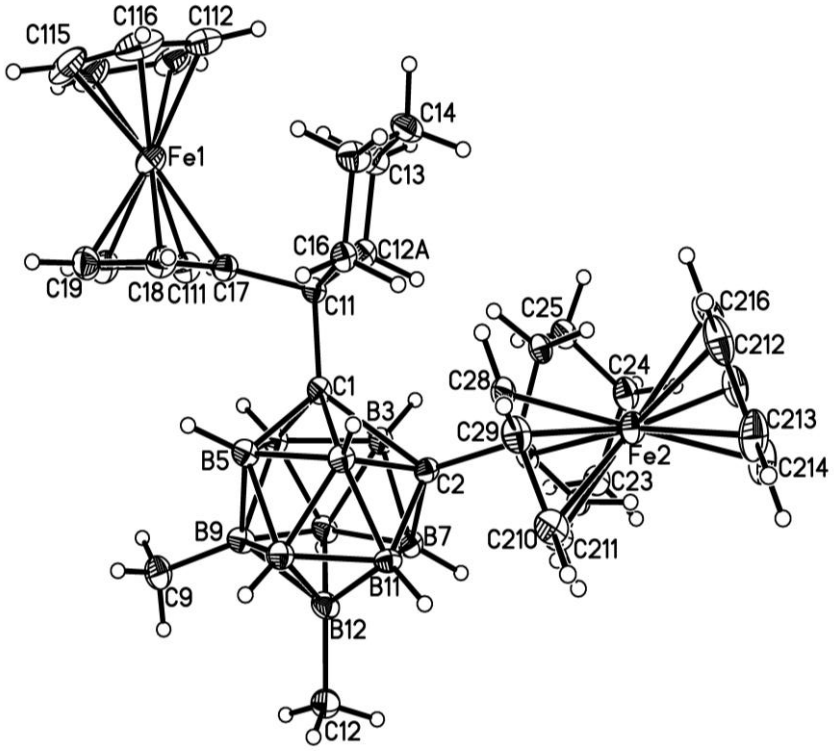

6.27 Isomerisation of 8,9-Me_2-1,2-$(CPmFc)_2$-1,2-*closo*-$C_2B_{10}H_8$

A solution of 8,9-Me_2-1,2-$(CPmFc)_2$-1,2-*closo*-$C_2B_{10}H_8$ (**17a**) (20 mg, 0.03 mmol) in dry toluene (20 ml) was heated to reflux for 20 hours. The toluene was removed *in vacuo*. Preparative TLC in 4:1 petroleum ether: DCM afforded 4 bands, one of which was unisomerised **17a** as identified by ^{1}H and ^{11}B NMR spectroscopies. An orange band with an R_f value of 0.45 was isolated (compound **18)**. An approximate X-ray crystal structure was determined that indicates the methyl positions are in the B(4) and B(9) positions. The remaining two compounds were not isolated but had R_f values consistent with the dissociation products, **12a** and **12b**.

4,9-Me_2-1,7-$(CPmFc)_2$-1,7-*closo*-$C_2B_{10}H_8$ (18)

Yield 12 mg (60%)

$^{11}B\{^{1}H\}$ NMR range of broad overlapping signals observed in the region δ -1.9 to -15.8

^{1}H NMR δ 4.18 (m, 4H, C_5H_4), 4.15 (m, 2H, C_5H_4), 4.10 (s, 10H, Cp), 3.98 (m, 2H, C_5H_4), 2.18-2.01 (br. m, 8H, CH_2), 1.79-1.80 (br. m, 6H, CH_2), 1.50-1.62 (br. m, 4H, CH_2), 1.28-1.33 (s, 2H, CH_2), 0.44 (s, 1H, B-CH_3), 0.10 (s, 1H, B-CH_3)

MS *m/z* 705 (M^+) (with an isotopic envelope spanning *m/z* 698-709)

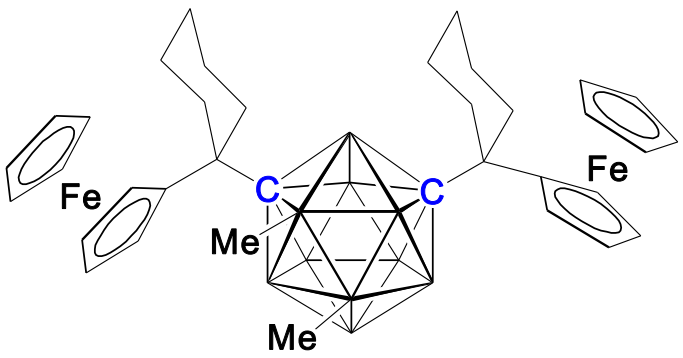

6.28 Isomerisation of 9,12-Me_2-1,2-$(CPmFc)_2$-1,2-*closo*-$C_2B_{10}H_8$

A solution of 9,12-Me_2-1,2-$(CPmFc)_2$-1,2-*closo*-$C_2B_{10}H_8$ (10 mg, 0.03 mmol) in dry toluene was heated to reflux for 20 hours affording a pale orange solution. The toluene was removed *in vacuo* and the residue applied to a preparative TLC plate yielding four bands upon chromamtography using a 4:1 petrol:DCM mixture as eluent. The four bands were purple starting material (2 mg), orange **16a** (4 mg) as identified by ^{1}H and ^{11}B NMR spectroscopies and the two associated decomposition products as identified by their comparable R_f values to **12a** and **12b**.

6.29 References

6.1 *Bruker AXS APEX2*, V1.0-8; Bruker-AXS, Madison, WI, USA, 2000.

6.2 *SHELXTL*, V6.10; Bruker-AXS, Madison, WI, USA, 2000.

6.3 *Mercury*, version 1.4.2, Cambridge Crystallographic Data Centre, Cambridge, UK, 2006.

6.4 O. V. Dolomanov, L. J. Bourhis, R. J. Gildea, J. A. K. Howard and H. Puschmann. "OLEX2: a complete structure solution, refinement and analysis program". *J. Appl. Cryst*. 2009, **42**, 339.

6.5 K. J. Stone and R. D. Little, *J. Org. Chem*., 1984, **49**, 1849.

6.6 Z. Zheng, W. Jiang, A. A. Zinn, C. B. Knobler and M. F. Hawthorne, *Inorg. Chem*., 1995, **34**, 2095.

6.7 M. A. Bennett, T. N. Huang, T. W. Matheson and A. K. Smith, *Inorg. Synth.*, 1982, **21**, 74.

6.8 E. Hong, Y. Kim and Y. Do, *Organometallics*, 1998, **17**, 2933.

Appendix A Crystal Data and Structure Refinements

Compound **1**
1,7-$(CMe_2OH)_2$-1,7-*closo*-$C_2B_{10}H_{10}$

Identification code	x81517
Empirical formula	$C_8H_{24}B_{10}O_2$
Formula weight	260.37
Temperature	100(2) K
Wavelength	0.71073 Å
Crystal system	Orthorhombic
Space group	Pbcn
Unit cell dimensions	a = 12.7085(13) Å; α= 90°. b = 19.925(2) Å; β= 90°. c = 11.5838(11) Å; γ = 90°.
Volume	2933.2(5) $Å^3$
Z	8
Density (calculated)	1.179 Mg/m^3
Absorption coefficient	0.065 mm^{-1}
F(000)	1104
Crystal size	0.60 x 0.38 x 0.10 mm^3
Theta range for data collection	2.59 to 25.66°.
Index ranges	-15<=h<=15, -24<=k<=24, -10<=l<=14
Reflections collected	31568
Independent reflections	2765 [R(int) = 0.0466]
Completeness to theta = 25.00°	99.9 %
Absorption correction	Semi-empirical from equivalents
Max. and min. transmission	0.994 and 0.835
Refinement method	Full-matrix least-squares on F^2
Data / restraints / parameters	2765 / 0 / 221
Goodness-of-fit on F^2	1.028
Final R indices [I>2sigma(I)]	R_1 = 0.0406, wR_2 = 0.1035
R indices (all data)	R_1 = 0.0583, wR_2 = 0.1164
Largest diff. peak and hole	0.346 and -0.263 e.$Å^{-3}$

Compound **2**
1-(CMe_2OH)-1,2-*closo*-$C_2B_{10}H_{11}$

Identification code	x81510
Empirical formula	$C_5H_{18}B_{10}O$
Formula weight	202.29
Temperature	100(2) K
Wavelength	0.71073 Å
Crystal system	Monoclinic
Space group	P2(1)/c
Unit cell dimensions	a = 12.2242(5) Å; α= 90°. b = 17.2749(7) Å; β= 110.619(2)°. c = 11.9613(17) Å; γ = 90°.
Volume	2364.09(17) $Å^3$
Z	8
Density (calculated)	1.137 Mg/m^3
Absorption coefficient	0.057 mm^{-1}
F(000)	848
Crystal size	0.78 x 0.32 x 0.20 mm^3
Theta range for data collection	2.17 to 27.69°.
Index ranges	-14<=h<=15, -22<=k<=22, -15<=l<=15
Reflections collected	47921
Independent reflections	5529 [R(int) = 0.0510]
Completeness to theta = 25.00°	100.0 %
Absorption correction	Semi-empirical from equivalents
Max. and min. transmission	0.989 and 0.860
Refinement method	Full-matrix least-squares on F^2
Data / restraints / parameters	5529 / 3 / 390
Goodness-of-fit on F^2	1.038
Final R indices [I>2sigma(I)]	R_1 = 0.0442, wR_2 = 0.1128
R indices (all data)	R_1 = 0.0627, wR_2 = 0.1254
Largest diff. peak and hole	0.384 and -0.450 e.$Å^{-3}$

Compound **4**
4-(*p*-cymene)-2,6-μ-(OCH_2CMe_2)-4,1,6-*closo*-$RuC_2B_{10}H_9$

Identification code	x81570_0m
Empirical formula	$C_{19.5}H_{39}B_{10}ORuCl$
Formula weight	534.12
Temperature	100.15 K
Wavelength	0.71073 Å
Crystal system	Monoclinic
Space group	Pc
Unit cell dimensions	a = 15.8008(14) Å; α= 90(7)°. b = 9.2588(8) Å; β= 99.344(3)°. c = 17.1210(13) Å; γ = 90°.
Volume	2471.5(4) $Å^3$
Z	4
Density (calculated)	1.435 Mg/m^3
Absorption coefficient	0.755 mm^{-1}
F(000)	1100.0
Crystal size	0.54 x 0.18 x 0.12 mm^3
Thata range for data collection	1.31 to 29.48°.
Index ranges	-21<=h<=21, -12<=k<=11, -23<=l<=21
Reflections collected	36952
Independent reflections	12840 [R(int) = 0.0464]
Completeness to theta = 25.00°	100.0 %
Absorption correction	Semi-empirical from equivalents
Max. and min. transmission	0.915 and 0.686
Refinement method	Full-matrix least-squares on F^2
Data / restraints / parameters	12840 / 98 / 658
Goodness-of-fit on F^2	1.055
Final R indices [I>2sigma(I)]	R_1 = 0.0505, wR_2 = 0.0932
R indices (all data)	R_1 = 0.0749, wR_2 = 0.1030
Largest diff. peak and hole	1.05 and -1.04 e.$Å^{-3}$
Flack parameter	0.55(6)

Compound **5b**
1,7-{CMe_2[3-(C_5H_4)-3,1,2-*closo*-$CoC_2B_9H_{11}$]}$_2$-1,7-*closo*-$C_2B_{10}H_{10}$

Identification code	x82804
Empirical formula	$C_{22}H_{52}B_{28}Co_2$
Formula weight	737.18
Temperature	100(2) K
Wavelength	0.71073 Å
Crystal system	Triclinic
Space group	P-1
Unit cell dimensions	a = 7.6090(16) Å; α= 82.267(7)°. b = 14.690(3) Å; β= 83.799(7)°. c = 16.786(4) Å; γ = 79.162(6)°.
Volume	1819.4(7) $Å^3$
Z	2
Density (calculated)	1.346 Mg/m^3
Absorption coefficient	0.933 mm^{-1}
F(000)	756
Crystal size	0.42 x 0.142 x 0.02 mm^3
Theta range for data collection	2.69 to 24.74°.
Index ranges	-8<=h<=8, -17<=k<=17, -19<=l<=19
Reflections collected	23699
Independent reflections	6090 [R(int) = 0.1216]
Completeness to theta = 24.74°	98.2 %
Absorption correction	Semi-empirical from equivalents
Max. and min. transmission	0.9816 and 0.6952
Refinement method	Full-matrix least-squares on F^2
Data / restraints / parameters	6090/ 0 / 474
Goodness-of-fit on F^2	0.958
Final R indices [I>2sigma(I)]	R_1 = 0.0577, wR_2 = 0.1119
R indices (all data)	R_1 = 0.1283, wR_2 = 0.1369
Largest diff. peak and hole	0.454 and -0.549 e.$Å^{-3}$

Compound **6a**

1-{CPm(C_5H_5)}-7-{CPm[3-(C_5H_4)-3,1,2-*closo*-$CoC_2B_9H_{11}$]}-1,7-*closo*-$C_2B_{10}H_{10}$

Identification code	x82841
Empirical formula	$C_{26}H_{50}B_{19}Co$
Formula weight	626.98
Temperature	100(2) K
Wavelength	0.71073 Å
Crystal system	Monoclinic
Space group	P2(1)/n
Unit cell dimensions	a = 19.353(3) Å; α= 90°. b = 8.0942(9) Å; β= 105.209(4)°. c = 21.593(3) Å; γ = 90°.
Volume	3264.1(7) $Å^3$
Z	4
Density (calculated)	1.276 Mg/m^3
Absorption coefficient	0.547 mm^{-1}
F(000)	1312
Crystal size	0.42 x 0.24 x 0.20 mm^3
Theta range for data collection	2.52 to 25.76°.
Index ranges	-23<=h<=23, -9<=k<=9, -26<=l<=26
Reflections collected	50820
Independent reflections	6213 [R(int) = 0.1135]
Completeness to theta = 25.00°	99.9 %
Absorption correction	Semi-empirical from equivalents
Max. and min. transmission	0.8984 and 0.8027
Refinement method	Full-matrix least-squares on F^2
Data / restraints / parameters	6213 / 3 / 415
Goodness-of-fit on F^2	1.001
Final R indices [I>2sigma(I)]	R_1 = 0.0505, wR_2 = 0.1112
R indices (all data)	R_1 = 0.0974, wR_2 = 0.1312
Largest diff. peak and hole	0.404 and -0.368 e.$Å^{-3}$

Compound **7a**

1,7-{CMe_2(C_5H_5)}$_2$-1,7-*closo*-$C_2B_{10}H_{10}$

Identification code	bjtaj3
Empirical formula	$C_{18}H_{32}B_{10}$
Formula weight	356.54
Temperature	160(2) K
Wavelength	0.71073 Å
Crystal system	Monoclinic
Space group	P2
Unit cell dimensions	a = 14.804(3) Å; α= 90°. b = 10.428(6) Å; β= 100.501(15)°. c = 27.942(11) Å; γ = 90°.
Volume	4241.3(17) $Å^3$
Z	8
Density (calculated)	1.117 Mg/m^3
Absorption coefficient	0.055 mm^{-1}
F(000)	1520
Crystal size	0.70 x 0.40 x 0.30 mm^3
Theta range for data collection	1.40 to 24.69°.
Index ranges	-17<=h<=17, -12<=k<=12, -32<=l<=32
Reflections collected	59225
Independent reflections	14242[R(int) = 0.1063]
Completeness to theta = 24.69°	99.0 %
Absorption correction	Semi-empirical from equivalents
Max. and min. transmission	0.9839 and 0.9740
Refinement method	Full-matrix least-squares on F^2
Data / restraints / parameters	14242 / 1 / 1025
Goodness-of-fit on F^2	1.014
Final R indices [I>2sigma(I)]	R_1 = 0.0671, wR_2 = 0.1423
R indices (all data)	R_1 = 0.1995, wR_2 = 0.1962
Largest diff. peak and hole	0.202 and -0.285 e.$Å^{-3}$

Compound **7b**

1,7-{CPm(C_5H_5)}$_2$-1,7-*closo*-$C_2B_{10}H_{10}$

Identification code	x82233_0m
Empirical formula	$C_{24}H_{40}B_{10}$
Formula weight	436.66
Temperature	100(2) K
Wavelength	0.71073 Å
Crystal system	Monoclinic
Space group	Cc
Unit cell dimensions	a = 21.315(4) Å; α= 90°. b = 8.1515(16) Å; β= 112.03(3)°. c = 15.649(3) Å; γ = 90°.
Volume	2520.6(9) $Å^3$
Z	4
Density (calculated)	1.151 Mg/m^3
Absorption coefficient	0.058 mm^{-1}
F(000)	936
Crystal size	0.82 x 0.75 x 0.08 mm^3
Theta range for data collection	2.70to 26.12°.
Index ranges	-26<=h<=26, -10<=k<=10, -19<=l<=13
Reflections collected	13998
Independent reflections	2424[R(int) = 0.0399]
Completeness to theta = 25.00°	97.5 %
Absorption correction	Semi-empirical from equivalents
Max. and min. transmission	0.9954 and 0.9538
Refinement method	Full-matrix least-squares on F^2
Data / restraints / parameters	2424 / 2 / 307
Goodness-of-fit on F^2	1.152
Final R indices [I>2sigma(I)]	R_1 = 0.0582, wR_2 = 0.1515
R indices (all data)	R_1 = 0.0643, wR_2 = 0.1568
Largest diff. peak and hole	0.500 and -0.234 e.$Å^{-3}$

Compound **7c**

1,7-{CPm(Me_4)(C_5H_5)}$_2$-1,7-*closo*-$C_2B_{10}H_{10}$

Identification code	x82702
Empirical formula	$C_{32}H_{56}B_{10}$
Formula weight	548.87
Temperature	100(2) K
Wavelength	0.71073 Å
Crystal system	Monoclinic
Space group	C2/c
Unit cell dimensions	a = 27.219(4) Å; α= 90°. b = 8.0365(11) Å; β= 102.449(6)°. c = 31.225(4) Å; γ = 90°.
Volume	6669.9(17) $Å^3$
Z	8
Density (calculated)	1.093 Mg/m^3
Absorption coefficient	0.056 mm^{-1}
F(000)	2384
Crystal size	0.58 x 0.30 x 0.14 mm^3
Theta range for data collection	2.65 to 24.72°.
Index ranges	-32<=h<=31, 0<=k<=9, 0<=l<=36
Reflections collected	43548
Independent reflections	5972 [R(int) = 0.1084]
Completeness to theta = 24.72°	96.0 %
Absorption correction	Semi-empirical from equivalents
Max. and min. transmission	0.9922 and 0.6873
Refinement method	Full-matrix least-squares on F^2
Data / restraints / parameters	5972 / 0 / 388
Goodness-of-fit on F^2	1.077
Final R indices [I>2sigma(I)]	R_1 = 0.0872, wR_2 = 0.2054
R indices (all data)	R_1 = 0.1451, wR_2 = 0.2345
Largest diff. peak and hole	0.340 and -0.398 e.$Å^{-3}$

Compound **8a**
1,7-$(CMe_2Fc)_2$-1,7-*closo*-$C_2B_{10}H_{10}$

Identification code	x81966_0m
Empirical formula	$C_{28}H_{40}B_{10}Fe_2$
Formula weight	596.40
Temperature	100(2) K
Wavelength	0.71073 Å
Crystal system	Triclinic
Space group	P-1
Unit cell dimensions	a = 10.187(2) Å; α= 96.618(8)°. b = 12.513(3) Å; β= 112.070(7)°. c = 13.387(2) Å; γ = 112.308(8)°.
Volume	1395.2(5) $Å^3$
Z	2
Density (calculated)	1.420 Mg/m^3
Absorption coefficient	1.060 mm^{-1}
F(000)	620
Crystal size	0.52 x 0.42 x 0.08 mm^3
Theta range for data collection	1.72 to 28.03°.
Index ranges	-13<=h<=13, -16<=k<=16, -16<=l<=17
Reflections collected	25611
Independent reflections	6521 [R(int) = 0.0533]
Completeness to theta = 25.00°	98.4 %
Absorption correction	Semi-empirical from equivalents
Max. and min. transmission	0.9200 and 0.6087
Refinement method	Full-matrix least-squares on F^2
Data / restraints / parameters	6521 / 0 / 365
Goodness-of-fit on F^2	1.018
Final R indices [I>2sigma(I)]	R_1 = 0.0411, wR_2 = 0.0893
R indices (all data)	R_1 = 0.0761, wR_2 = 0.1033
Largest diff. peak and hole	0.421and -0.485 e.$Å^{-3}$

Compound **8b**
1,7-$(CPmFc)_2$-1,7-*closo*-$C_2B_{10}H_{10}$

Identification code	x82290_0m
Empirical formula	$C_{34}H_{48}B_{10}Fe_2$
Formula weight	676.52
Temperature	100(2) K
Wavelength	0.71073 Å
Crystal system	Triclinic
Space group	P-1
Unit cell dimensions	a = 9.803(8) Å; α= 73.99(2)°. b = 12.947(10) Å; β= 78.525(15)°. c = 14.060(11) Å; γ = 70.027(18)°.
Volume	1601(2) $Å^3$
Z	2
Density (calculated)	1.403 Mg/m^3
Absorption coefficient	0.933 mm^{-1}
F(000)	708
Crystal size	0.52 x 0.30 x 0.08 mm^3
Theta range for data collection	2.43 to 28.11°.
Index ranges	-12<=h<=12, -11<=k<=17, -18<=l<=16
Reflections collected	11495
Independent reflections	7594 [R(int) = 0.0356]
Completeness to theta = 25.00°	98.2 %
Absorption correction	Semi-empirical from equivalents
Max. and min. transmission	0.9291 and 0.6427
Refinement method	Full-matrix least-squares on F^2
Data / restraints / parameters	7594 / 0 / 445
Goodness-of-fit on F^2	1.008
Final R indices [I>2sigma(I)]	R_1 = 0.0471, wR_2 = 0.0984
R indices (all data)	R_1 = 0.0804, wR_2 = 0.1132
Largest diff. peak and hole	0.466 and -0.422 e.$Å^{-3}$

Compound **9a**
1,2-$(CMe_2Fc)_2$-1,2-*closo*-$C_2B_{10}H_{10}$

Identification code	x82197_0m
Empirical formula	$C_{28}H_{40}B_{10}Fe_2$
Formula weight	596.40
Temperature	100(2) K
Wavelength	0.71073 Å
Crystal system	Monoclinic
Space group	P2(1)/n
Unit cell dimensions	a = 8.7366(14) Å; α= 90°. b = 16.920(3) Å; β= 100.783(7)°. c = 19.641(3) Å; γ = 90°.
Volume	2852.1(8) $Å^3$
Z	4
Density (calculated)	1.389 Mg/m^3
Absorption coefficient	1.037 mm^{-1}
F(000)	1240
Crystal size	0.60 x 0.48 x 0.20 mm^3
Theta range for data collection	2.41 to 32.63°.
Index ranges	-13<=h<=12, -22<=k<=24, -28<=l<=29
Reflections collected	71682
Independent reflections	9673[R(int) = 0.0462]
Completeness to theta = 25.00°	99.9 %
Absorption correction	Semi-empirical from equivalents
Max. and min. transmission	0.8195 and 0.728
Refinement method	Full-matrix least-squares on F^2
Data / restraints / parameters	9673 / 0 / 395
Goodness-of-fit on F^2	1.034
Final R indices [I>2sigma(I)]	R_1 = 0.0323, wR_2 = 0.0760
R indices (all data)	R_1 = 0.0458, wR_2 = 0.0824
Largest diff. peak and hole	0.6524 and -0.436 e.$Å^{-3}$

Compound **9b**
1,2-$(CPmFc)_2$-1,2-*closo*-$C_2B_{10}H_{10}$

Identification code	x82302_0m
Empirical formula	$C_{34}H_{48}B_{10}Fe_2$
Formula weight	676.52
Temperature	100(2) K
Wavelength	0.71073 Å
Crystal system	Monoclinic
Space group	P2(1)/n
Unit cell dimensions	a = 15.1029(17) Å; α= 90°. b = 15.4587(19) Å; β= 118.556(6)°. c = 15.6930(18) Å; γ = 90°.
Volume	3218.2(7) $Å^3$
Z	4
Density (calculated)	1.396Mg/m^3
Absorption coefficient	0.928 mm^{-1}
F(000)	1416
Crystal size	0.60 x 0.30 x 0.14 mm^3
Theta range for data collection	2.03 to 25.14°.
Index ranges	-18<=h<=18, -18<=k<=18, -18<=l<=18
Reflections collected	47044
Independent reflections	5648 [R(int) = 0.0855]
Completeness to theta = 25.00°	98.8 %
Absorption correction	Semi-empirical from equivalents
Max. and min. transmission	0.8810 and 0.5969
Refinement method	Full-matrix least-squares on F^2
Data / restraints / parameters	5648 / 0 / 415
Goodness-of-fit on F^2	1.053
Final R indices [I>2sigma(I)]	R_1 = 0.0492, wR_2 = 0.1275
R indices (all data)	R_1 = 0.0685, wR_2 = 0.1493
Largest diff. peak and hole	0.946 and -0.800 e.$Å^{-3}$

Compound **11**
1,2-$(CMe_2Fc)_2$-4-OH-1,2-*closo*-$C_2B_{10}H_9$

Identification code	x82228_0m
Empirical formula	$C_{28}H_{40}B_{10}Fe_2O$
Formula weight	612.40
Temperature	100(2) K
Wavelength	0.71073 Å
Crystal system	Monoclinic
Space group	P2(1)/n
Unit cell dimensions	a = 8.1417(17) Å; α= 90°.
	b = 17.864(4) Å; β= 100.168(10)°.
	c = 19.757(4) Å; γ = 90°.
Volume	2830.3(10) $Å^3$
Z	4
Density (calculated)	1.437 Mg/m^3
Absorption coefficient	1.049 mm^{-1}
F(000)	1272
Crystal size	0.54 x 0.50 x 0.18 mm^3
Theta range for data collection	1.55 to 29.73°.
Index ranges	-11<=h<=10, -24<=k<=21, -27<=l<=27
Reflections collected	46045
Independent reflections	7996 [R(int) = 0.0462]
Completeness to theta = 25.00°	100.0 %
Absorption correction	Semi-empirical from equivalents
Max. and min. transmission	0.8336 and 0.6011
Refinement method	Full-matrix least-squares on F^2
Data / restraints / parameters	7996 / 0 / 424
Goodness-of-fit on F^2	1.035
Final R indices [I>2sigma(I)]	R_1 = 0.0376, wR_2 = 0.0907
R indices (all data)	R_1 = 0.0849, wR_2 = 0.1229
Largest diff. peak and hole	0.501 and -0.519 e.$Å^{-3}$

Compound **12a**
1-(CPmFc)-1,2-*closo*-$C_2B_{10}H_{11}$

Identification code	x82407_0m
Empirical formula	$C_{18}H_{30}B_{10}Fe$
Formula weight	410.37
Temperature	100(2) K
Wavelength	0.71073 Å
Crystal system	Monoclinic
Space group	P2(1)/n
Unit cell dimensions	a = 9.6156(10) Å; α= 90°.
	b = 18.153(2) Å; β= 103.014(5)°.
	c = 11.9102(11) Å; γ = 90°.
Volume	202.5(4) $Å^3$
Z	4
Density (calculated)	1.346 Mg/m^3
Absorption coefficient	0.747 mm^{-1}
F(000)	856
Crystal size	0.62 x 0.48 x 0.30 mm^3
Theta range for data collection	2.45 to 36.54°.
Index ranges	-15<=h<=16, -30<=k<=30, -18<=l<=19
Reflections collected	60740
Independent reflections	9711 [R(int) = 0.0502]
Completeness to theta = 25.00°	99.7 %
Absorption correction	Semi-empirical from equivalents
Max. and min. transmission	0.8070 and 0.6546
Refinement method	Full-matrix least-squares on F^2
Data / restraints / parameters	9711 / 0 / 295
Goodness-of-fit on F^2	1.042
Final R indices [I>2sigma(I)]	R_1 = 0.0348, wR_2 = 0.0797
R indices (all data)	R_1 = 0.0505, wR_2 = 0.0854
Largest diff. peak and hole	0.518 and -0.514 e.$Å^{-3}$

Compound **14**
4-(*p*-cymene)-2,11-Me_2-4,1,6-*closo*-$RuC_2B_{10}H_{10}$

Identification code	x83148
Empirical formula	$C_{14}H_{30}B_{10}Ru$
Formula weight	407.55
Temperature	100(2) K
Wavelength	0.71073 Å
Crystal system	Monoclinic
Space group	P2(1)/n
Unit cell dimensions	a = 18.517(7) Å; α= 90°.
	b = 11.479(6) Å; β= 99.245(18)°.
	c = 18.806(7) Å; γ = 90°.
Volume	3946(3) $Å^3$
Z	8
Density (calculated)	1.372 Mg/m^3
Absorption coefficient	0.788 mm^{-1}
F(000)	1664
Crystal size	0.38 x 0.24 x 0.08 mm^3
Theta range for data collection	1.43 to 26.50°.
Index ranges	-23<=h<=22, 0<=k<=11, 0<=l<=23
Reflections collected	20534
Independent reflections	5912 [R(int) = 0.0713]
Completeness to theta = 25.00°	66.1 % (very weak diffraction)
Absorption correction	Semi-empirical from equivalents
Max. and min. transmission	0.9397 and 0.7539
Refinement method	Full-matrix least-squares on F^2
Data / restraints / parameters	5912/ 390 / 475
Goodness-of-fit on F^2	1.035
Final R indices [I>2sigma(I)]	R_1 = 0.0630, wR_2 = 0.1407
R indices (all data)	R_1 = 0.1343, wR_2 = 0.1750
Largest diff. peak and hole	1.004 and -0.841 e.$Å^{-3}$

Compound 1**5a**
9,10-Me_2-1,7-{CPm(C_5H_5)}$_2$-1,7-*closo*-$C_2B_{10}H_8$

Identification code	x82944
Empirical formula	$C_{26}H_{44}B_{10}$
Formula weight	464.71
Temperature	100(2) K
Wavelength	0.71073 Å
Crystal system	Monoclinic
Space group	C2/c
Unit cell dimensions	a = 14.5608(14) Å; α= 90°.
	b = 15.8539(16) Å; β= 100.075(4)°.
	c = 11.7712(12) Å; γ = 90°.
Volume	2675.4(5) $Å^3$
Z	4
Density (calculated)	1.154 Mg/m^3
Absorption coefficient	0.059 mm^{-1}
F(000)	1000
Crystal size	0.44 x 0.20 x 0.08 mm^3
Theta range for data collection	1.92 to 30.04°.
Index ranges	-20<=h<=18, -22<=k<=22, -16<=l<=16
Reflections collected	27158
Independent reflections	3869 [R(int) = 0.0332]
Completeness to theta = 25.00°	100.0 %
Absorption correction	Semi-empirical from equivalents
Max. and min. transmission	0.995 and 0.986
Refinement method	Full-matrix least-squares on F^2
Data / restraints / parameters	3896 / 0 / 164
Goodness-of-fit on F^2	1.049
Final R indices [I>2sigma(I)]	R_1 = 0.0487, wR_2 = 0.1390
R indices (all data)	R_1 = 0.0698, wR_2 = 0.1597
Largest diff. peak and hole	0.375 and -0.466 e.$Å^{-3}$

Compound 1**5b**
9,10-Ph_2-1,7-{CPm(C_5H_5)}$_2$-1,7-*closo*-$C_2B_{10}H_8$

Identification code	x83060
Empirical formula	$C_{36}H_{48}B_{10}$
Formula weight	588.84
Temperature	100(2) K
Wavelength	0.71073 Å
Crystal system	Monoclinic
Space group	C2/c
Unit cell dimensions	a = 15.214(4) Å; α= 90°. b = 18.538(5) Å; β= 123.120(8)°. c = 13.439(6) Å; γ = 90°.
Volume	3170.5(18) $Å^3$
Z	4
Density (calculated)	1.232 Mg/m^3
Absorption coefficient	0.064 mm^{-1}
F(000)	1256
Crystal size	0.34 x 0.24 x 0.12 mm^3
Theta range for data collection	2.85 to 25.14°.
Index ranges	-14<=h<=18, -22<=k<=0, -14<=l<=15
Reflections collected	67417
Independent reflections	2792 [R(int) = 0.0445]
Completeness to theta = 25.00°	98.9 %
Absorption correction	Semi-empirical from equivalents
Max. and min. transmission	0.992 and 0.866
Refinement method	Full-matrix least-squares on F^2
Data / restraints / parameters	2792 / 0 / 209
Goodness-of-fit on F^2	1.033
Final R indices [I>2sigma(I)]	R_1 = 0.0595, wR_2 = 0.1363
R indices (all data)	R_1 = 0.1089, wR_2 = 0.1612
Largest diff. peak and hole	0.341 and -0.237 e.$Å^{-3}$

Compound **16a**
9,10-Me_2-1,7-($CPmFc)_2$-1,7-*closo*-$C_2B_{10}H_8$

Identification code	x83042
Empirical formula	$C_{37}H_{53}B_{10}Cl_3Fe_2$
Formula weight	823.94
Temperature	100(2) K
Wavelength	0.71073 Å
Crystal system	Monoclinic
Space group	P2(1)/n
Unit cell dimensions	a = 11.4588(8) Å; α= 90°. b = 20.1918(13) Å; β= 94.816(4)°. c = 16.7858(11) Å; γ = 90°.
Volume	3869.8(4) $Å^3$
Z	4
Density (calculated)	1.414 Mg/m^3
Absorption coefficient	0.986 mm^{-1}
F(000)	1712
Crystal size	0.44 x 0.38 x 0.08 mm^3
Theta range for data collection	1.58 to 28.31°.
Index ranges	-15<=h<=15, -26<=k<=26, -22<=l<=22
Reflections collected	63782
Independent reflections	9550 [R(int) = 0.0407]
Completeness to theta = 25.00°	99.8 %
Absorption correction	Semi-empirical from equivalents
Max. and min. transmission	0.9253 and 0.6709
Refinement method	Full-matrix least-squares on F^2
Data / restraints / parameters	9550 / 0 / 499
Goodness-of-fit on F^2	0.984
Final R indices [I>2sigma(I)]	R_1 = 0.0310, wR_2 = 0.0746
R indices (all data)	R_1 = 0.0443, wR_2 = 0.0810
Largest diff. peak and hole	0.376 and -0.283 e.$Å^{-3}$

Compound **16b**
9,10-Ph_2-1,7-($CPmFc)_2$-1,7-*closo*-$C_2B_{10}H_8$

Identification code	3126m
Empirical formula	$C_{46}H_{56}B_{10}Fe_2$
Formula weight	828.71
Temperature	100(2) K
Wavelength	0.71073 Å
Crystal system	Monoclinic
Space group	C2/c
Unit cell dimensions	a = 44.566(2) Å; α= 90°. b = 11.2704(5) Å; β= 104.864(4)°. c = 16.6272(8) Å; γ = 90°.
Volume	8072.0(7) $Å^3$
Z	8
Density (calculated)	1.364 Mg/m^3
Absorption coefficient	0.754 mm^{-1}
F(000)	3472
Crystal size	0.42 x 0.26 x 0.08 mm^3
Theta range for data collection	2.17 to 27.69°.
Index ranges	-54<=h<=54, -13<=k<=13, -20<=l<=20
Reflections collected	57627
Independent reflections	8030 [R(int) = 0.0537]
Completeness to theta = 25.00°	100.0 %
Absorption correction	Semi-empirical from equivalents
Max. and min. transmission	0.9421 and 0.7424
Refinement method	Full-matrix least-squares on F^2
Data / restraints / parameters	8030 / 62 / 558
Goodness-of-fit on F^2	1.040
Final R indices [I>2sigma(I)]	R_1 = 0.0454, wR_2 = 0.1032
R indices (all data)	R_1 = 0.0700, wR_2 = 0.1145
Largest diff. peak and hole	1.210 and -1.211 e.$Å^{-3}$

Compound **17a**
8,9-Me_2-1,2-($CPmFc)_2$-1,2-*closo*-$C_2B_{10}H_8$

Identification code	x83089
Empirical formula	$C_{38.5}H_{58}B_{10}Fe_2$
Formula weight	740.65
Temperature	100(2) K
Wavelength	0.71073 Å
Crystal system	Triclinic
Space group	P-1
Unit cell dimensions	a = 14.768(2) Å; α= 83.801(6)°. b = 16.583(2) Å; β= 73.944(6)°. c = 17.018(2) Å; γ = 70.198(6)°.
Volume	3767.9(9) $Å^3$
Z	4
Density (calculated)	1.306 Mg/m^3
Absorption coefficient	0799mm^{-1}
F(000)	1564
Crystal size	0.24 x 0.16 x 0.10 mm^3
Theta range for data collection	1.31 to 25.93°.
Index ranges	-17<=h<=17, -19<=k<=20, 0<=l<=20
Reflections collected	120989
Independent reflections	13771 [R(int) = 0.1.074]
Completeness to theta = 25.00°	94.2 %
Absorption correction	Semi-empirical from equivalents
Max. and min. transmission	0.9244 and 0.8314
Refinement method	Full-matrix least-squares on F^2
Data / restraints / parameters	13771/ 0 / 917
Goodness-of-fit on F^2	0.980
Final R indices [I>2sigma(I)]	R_1 = 0.0931, wR_2 = 0.2123
R indices (all data)	R_1 = 0.2100, wR_2 = 0.2765
Largest diff. peak and hole	1.150 and -0.815 e.$Å^{-3}$

Compound **17b**
9,12-Me_2-1,2-$(CPmFc)_2$-1,2-*closo*-$C_2B_{10}H_8$

Identification code	x83086
Empirical formula	$C_{38.5}H_{57.5}B_{10}Fe_2$
Formula weight	740.15
Temperature	100(2) K
Wavelength	0.71073 Å
Crystal system	Triclinic
Space group	P-1
Unit cell dimensions	a = 11.3278(9) Å; α= 78.594(4)°.
	b = 13.0940(11) Å; β= 69.306(4)°.
	c = 14.0875(12) Å; γ = 71.366(4)°.
Volume	1843.8(3) $Å^3$
Z	2
Density (calculated)	1.333 Mg/m^3
Absorption coefficient	0.816 mm^{-1}
F(000)	781
Crystal size	0.38 x 0.12 x 0.04 mm^3
Theta range for data collection	2.22 to 26.05°.
Index ranges	-13<=h<=13, -16<=k<=15, -17<=l<=16
Reflections collected	21739
Independent reflections	7091 [R(int) = 0.0448]
Completeness to theta = 25.00°	99.4 %
Absorption correction	Semi-empirical from equivalents
Max. and min. transmission	0.9681 and 0.7467
Refinement method	Full-matrix least-squares on F^2
Data / restraints / parameters	7091 / 2 / 463
Goodness-of-fit on F^2	0.962
Final R indices [I>2sigma(I)]	R_1 = 0.0517, wR_2 = 0.1244
R indices (all data)	R_1 = 0.0852, wR_2 = 0.1443
Largest diff. peak and hole	0.856 and -0.475 e.$Å^{-3}$

Appendix B

Pictorial molecular representations

Brian Hutton, PhD Thesis,
Heriot-Watt University, 2014

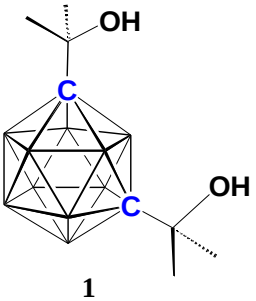

1

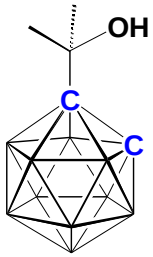

2

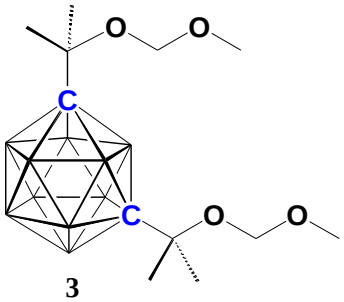

3

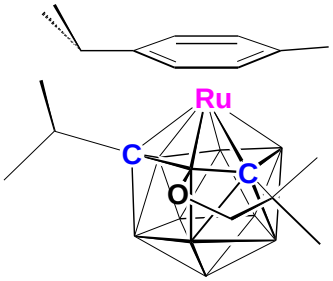

4

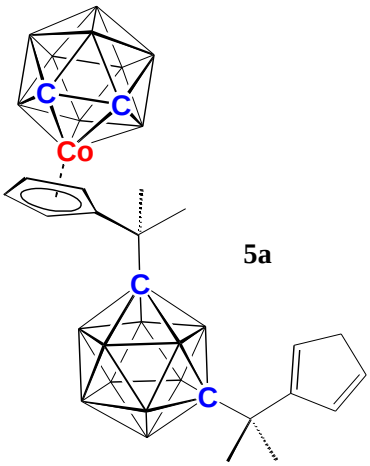

5a

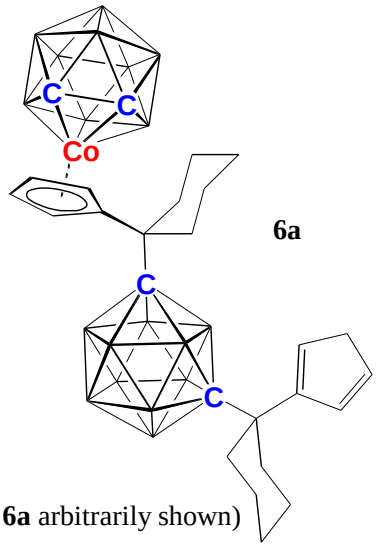

6a

(*β* form of **5a** and **6a** arbitrarily shown)

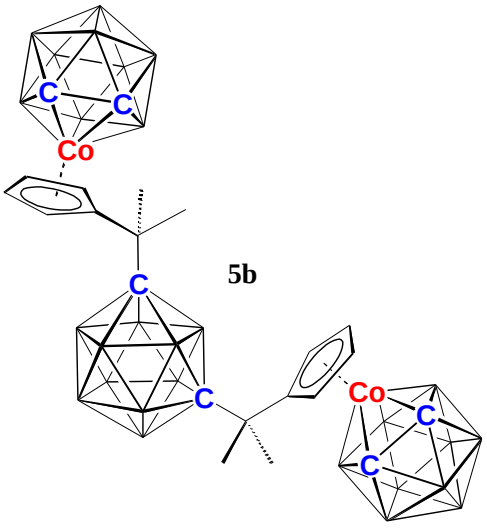

5b

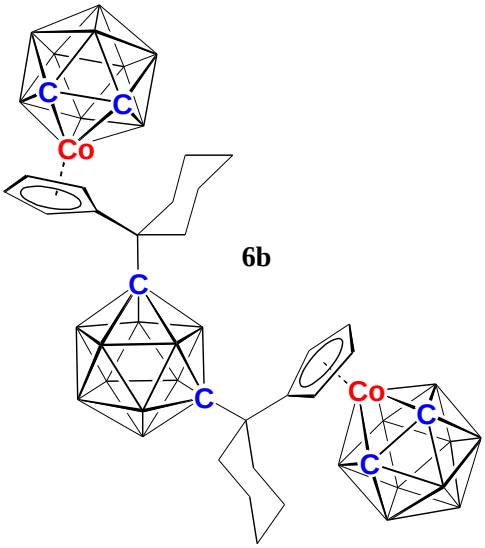

6b

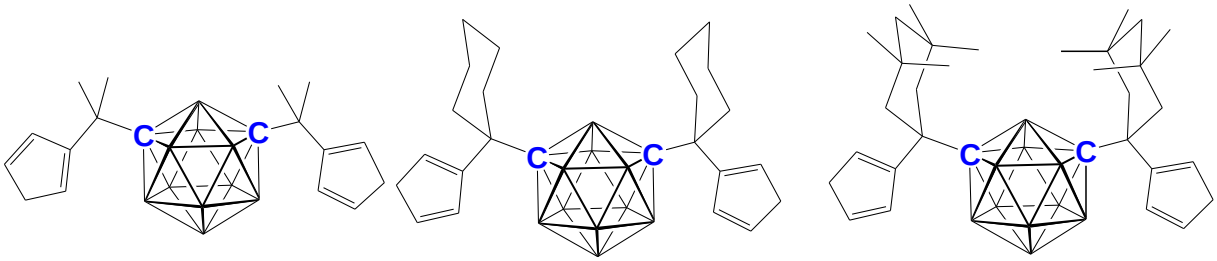

7a **7b** **7c**

(*ββ* form of **7a,b,c** arbitrarily shown)

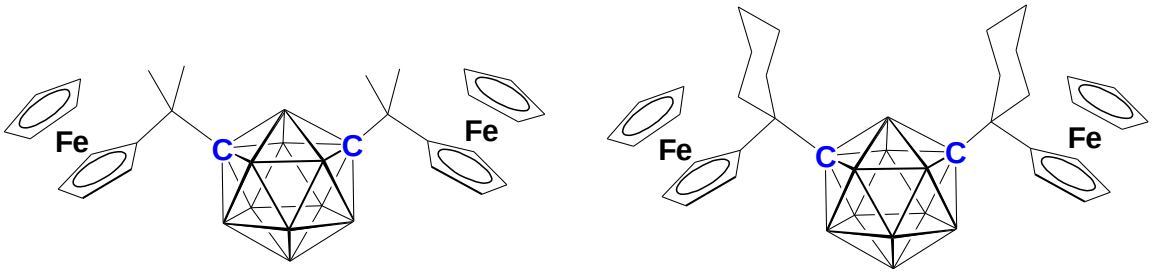

8a **8b**

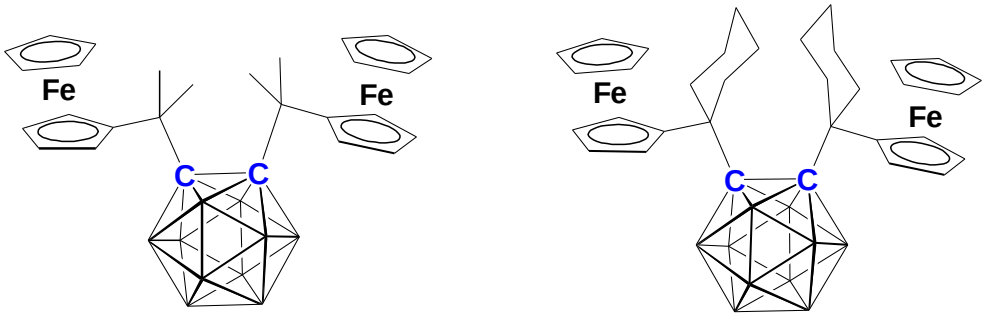

9a **9b**

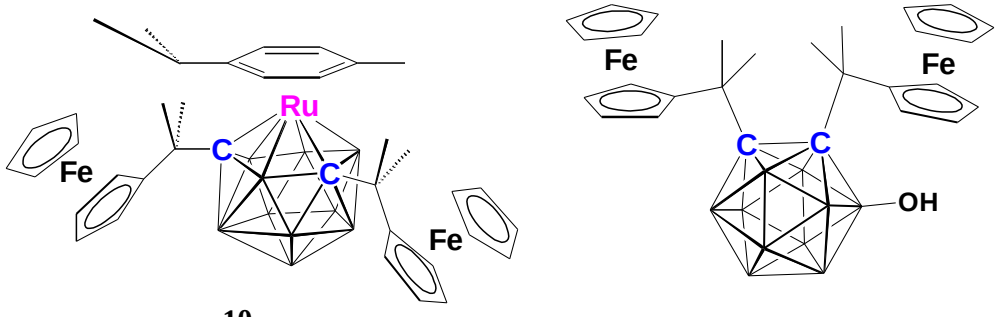

10 **11**

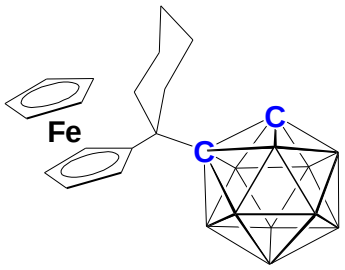

12a

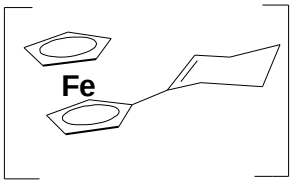

12b

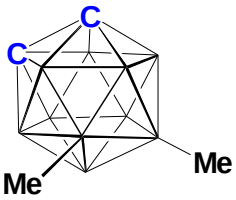

13a

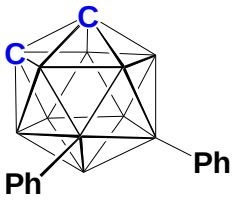

13b

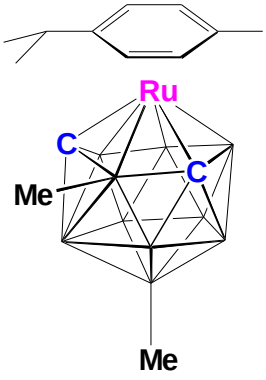

14

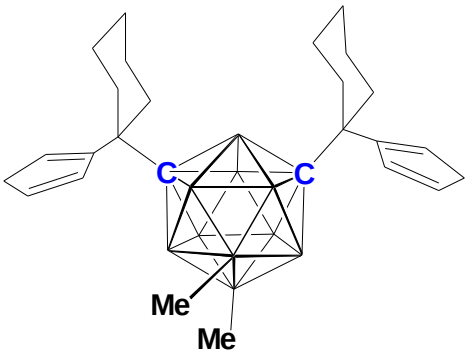

15a

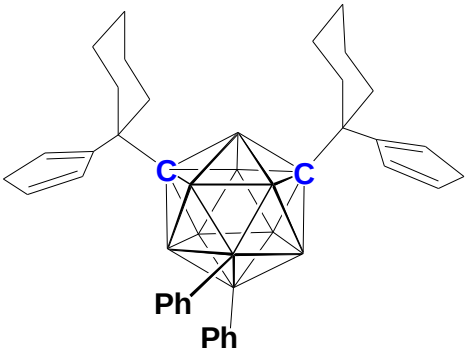

15b

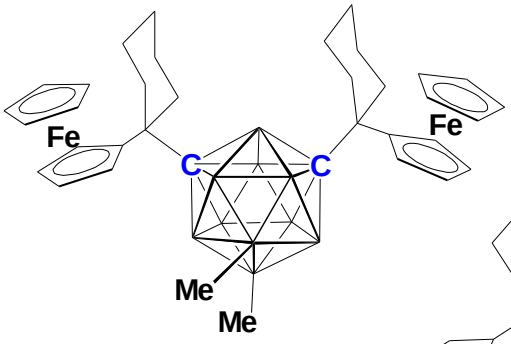

16a

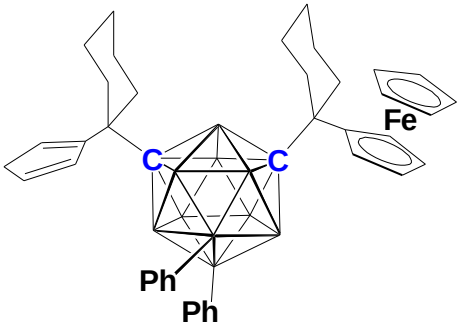

16b'

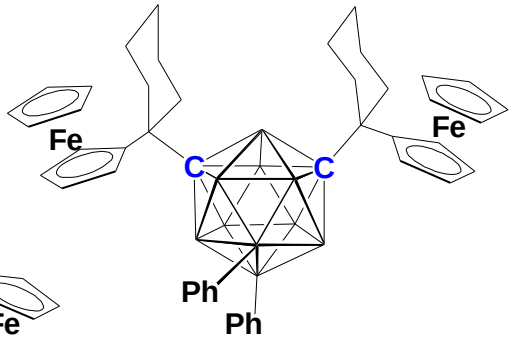

16b

(*ββ* form of **15a,b** and *β* form of **16b'** arbitrarily shown)

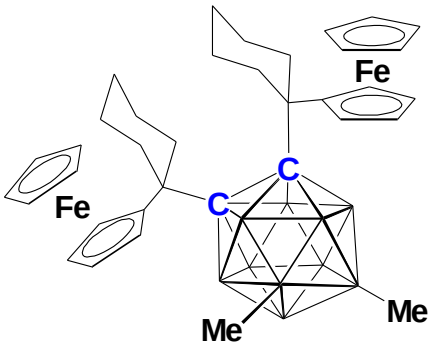

17a

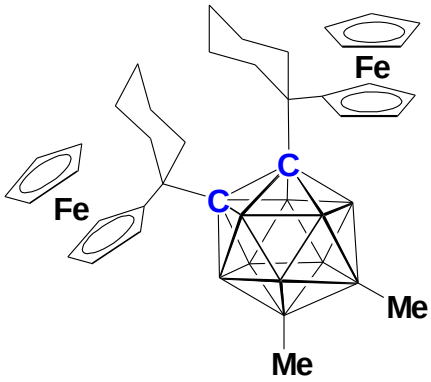

17b

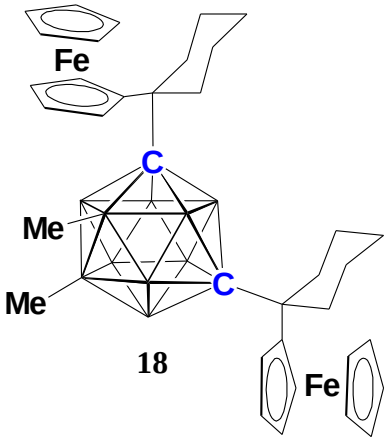

18

Unprecedented steric deformation of *ortho*-carborane†

Brian W. Hutton, Fraser MacIntosh, David Ellis, Fabien Herisse, Stuart A. Macgregor,* David McKay, Victoria Petrie-Armstrong, Georgina M. Rosair, Dmitry S. Perekalin, Hugo Tricas and Alan J. Welch*

Received (in Cambridge, UK) 25th June 2008, Accepted 15th August 2008
First published as an Advance Article on the web 19th September 2008
DOI: 10.1039/b810702e

The reduction and subsequent oxidation of *meta*-carboranes containing bulky groups attached to the cage C atoms affords sterically-crowded *ortho*-carboranes with unprecedentedly long C–C connectivities.

Although it has been appreciated for more than 45 years that *ortho*-carborane, 1,2-*closo*-$C_2B_{10}H_{12}$, has a distorted icosahedral geometry,[1] its accurate structure has been determined only relatively recently. In 1996 Davidson, Wade *et al.*[2] used the acidic nature of the carborane CH units to form a supramolecular dimer with hexamethylphosphoramide, locking the CH units in C–H···O hydrogen bonds and so overcoming the disorder that had frustrated previous attempts to obtain an accurate structure crystallographically; the two independent C–C distances measured at 150 K were 1.629(6) and 1.630(6) Å. Later, Rankin and co-workers[3] redetermined the gas phase structure of *ortho*-carborane by electron diffraction, improving on the accuracy of previous determinations[4] and affording C1–C2 1.624(8) Å, in excellent agreement with the results of a parallel computational study, 1.621 Å.

The C–C distance in *ortho*-carborane can be lengthened to *ca.* 1.8 Å by attaching bulky substituents to the cage C atoms,[5] or to nearly 1.9 Å by incorporating the cage C atoms in suitable exopolyhedral cycles.[6] Alternatively, the C–C distance can be extended *electronically* by π-donor substituents at one cage C atom to distances >2 Å,[7] but such species can be argued to have formal skeletal electron counts in excess of the $(2n + 2)$ (n = no. of vertices) normally associated with *closo* species[8] and so bear closer comparison with $(2n + 3)$ carborane radical anions[9] or $(2n + 4)$ *nido* dianions.[8] The electronic causes for long C–C distances in neutral and anionic *ortho*-carboranes as a function of various substituents have been explored computationally.[10] Herein we report unprecedented lengthening of the C1–C2 connectivity of *ortho*-carborane, to 2.15 Å, and related deformation of the carborane icosahedron by intramolecular steric crowding alone.

When *ortho*-carborane is doubly deprotonated and allowed to react with two equivalents of the substituted fulvene **1** (**a**, R = Me) the known,[11] singly-substituted, product 1-$CMe_2(C_5H_5)$-1,2-*closo*-$C_2B_{10}H_{11}$ is afforded on aqueous work-up, implying that the $CMe_2(C_5H_5)$ substituent is already too bulky to 1,2-disubstitute by this approach. However, double deprotonation of *meta*-carborane, 1,7-*closo*-$C_2B_{10}H_{12}$ (**I**), followed by treatment with two equivalents of **1** readily yields the disubstituted species 1,7-$\{CR_2(C_5H_5)\}_2$-1,7-*closo*-$C_2B_{10}H_{10}$ (**2a**, R = Me; **2b**, R_2 = Pm) (Pm = pentamethylene) on work-up (Scheme 1).‡ In **2** there are two isomeric forms of the cyclopentadienyl ring, with the CH_2 function α or β; by ^{1}H NMR spectroscopy the ratio α : β is 1 : 2 for **2a** and 2 : 9 for **2b**. Compounds **2** are converted to the corresponding bis-ferrocenyl species 1,7-$(CR_2Fc)_2$-1,7-*closo*-$C_2B_{10}H_{10}$ **3a** and **3b** {Fc = (η-C_5H_4)Fe(η-C_5H_5)} by standard means.

It is well established that 2e reduction of *meta*-carborane followed by reoxidation affords *ortho*-carborane.[12] Similarly, reduction (Na, THF) then reoxidation of compounds **3** produces the crowded substituted *ortho*-carboranes **4a** and **4b**. By this (indirect) method may be prepared *ortho*-carborane derivatives with substantially sterically demanding groups attached to the two cage carbon atoms that are not possible starting from *ortho*-carborane directly.

Crystallographic study§ of **4a** and **4b** reveals the extent of the steric crowding within. Molecules of **4a** have effective C_2 symmetry about an axis from the mid-point of C1–C2 to the mid-point of B9–B12, with the Me groups of the CMe_2Fc substituents interdigitated about this axis and the Fc units oriented away from both the C1/C2 region and the BH cage vertices. The C1–C2 distance is 1.9378(16) Å. In **4b** (Fig. 1) the CPmFc substituent on C2 has an orientation that corresponds to the CMe_2Fc substituent in **4a**, but the other CPmFc substituent (on C1) has rotated so that its Pm group is side-on to the Pm group on C21 not face-on (which presumably would be untenable). Nevertheless, the C1–C2 distance in **4b** is 2.156(4) Å, easily the longest such distance experimentally recorded for a true $(2n + 2)$ *ortho*-carborane derivative. Further evidence for the severe intramolecular crowding in **4b** is the presence of two H···H distances of 2 Å (H12B···H26B 1.995 Å, H12B···H22A 1.997 Å) and distortion of the Fc group on C211 as a result of the forced orientation of the adjacent Pm group; the C211–C215 ring is tilted at C211 (the C21–C211 bond meets the plane at 11.38°) and the two Cp rings on Fe2 subtend a dihedral angle of 11.65°.

As the cage carbon atoms C1 and C2 are progressively forced apart by steric crowding, the boron atoms to which they are both connected, B3 and B6, are pulled together, the B3···B6 separation reducing from 2.886 Å (average) in *ortho*-carborane,[2] to 2.756 Å in **4a** to 2.663 Å in **4b**. Concomitantly, a smaller,

Department of Chemistry, School of Engineering & Physical Sciences, Heriot–Watt University, Edinburgh, UK EH14 4AS.
E-mail: a.j.welch@hw.ac.uk, s.a.macgregor@hw.ac.uk;
Fax: +44 131 451 3180/+ 44 131 451 3180;
Tel: +44 131 451 3217/+44 131 451 8031

† Electronic supplementary information (ESI) available: Experimental procedures; views of all structures; computational details. CCDC 688279–688284. For ESI and crystallographic data in CIF or other electronic format see DOI: 10.1039/b810702e

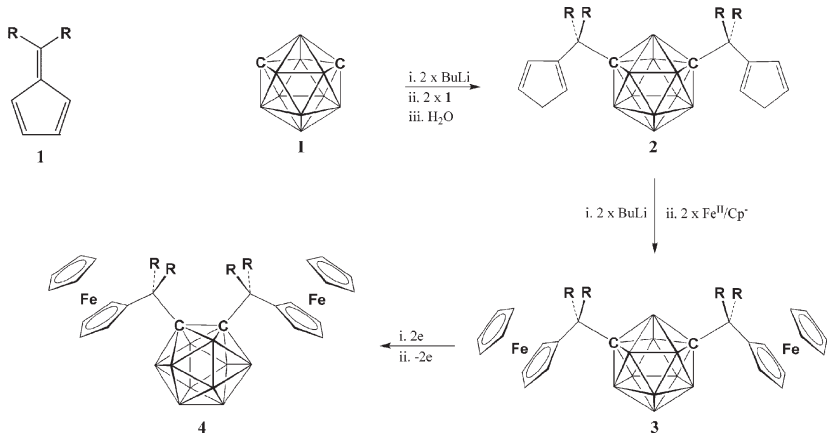

Scheme 1 Synthesis of compounds **2–4** (**a**, R = Me; **b**, R_2 = Pm). For **2** the β,β isomer of the C_5 ring is arbitrarily shown.

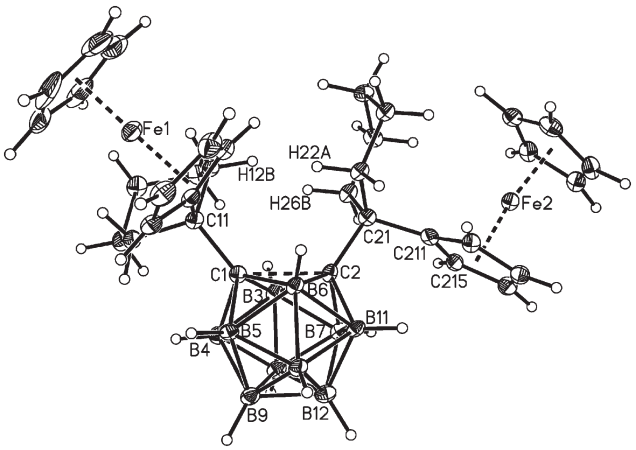

Fig. 1 Perspective view of compound **4b** (50% probability ellipsoids); C1–C2 2.156(4) Å.

second-order, effect is a lengthening of the B3–B8 and B6–B10 connectivities, from (averages¶) 1.766(8) Å in *ortho*-carborane,[2] to 1.794(3) Å in **4a** to 1.818(7) Å in **4b**, to become the longest B–B distances in the last.

Why do the *meta*-carborane derivatives **3** convert to the crowded *ortho*-carborane derivatives **4** on reduction and reoxidation? Why do they not simply reclose on oxidation to the less crowded (and thermodynamically preferred) original *meta*-carborane species? In Fig. 2 are presented the results of a DFT study‖ on the reoxidation of [7,9-*nido*-$C_2B_{10}H_{12}]^{2-}$, the product of 2e reduction of *ortho*- (and *meta*-) carborane. Two-electron oxidation of [7,9-*nido*-$C_2B_{10}H_{12}]^{2-}$ affords a basket-shaped intermediate 4.8 kcal mol^{-1} above the dianion. This intermediate (**INT**) isomerises to *ortho*-carborane *via* a transition state (**TS1**) with an activation energy of +9.2 kcal mol^{-1}, or, alternatively, isomerises to *meta*-carborane *via* an alternative transition state (**TS2**) with an activation energy of +16.7 kcal mol^{-1}. Clearly, therefore, oxidation of [7,9-*nido*-$C_2B_{10}H_{12}]^{2-}$ will preferentially afford *ortho*-carborane over *meta*-carborane. **INT** and **TS2** have been previously characterised by Brown and McKee[13] (*o-m*-INT and *o-m*-TS2, respectively, in ref. 13) in their computational study of the isomerisation of *ortho*- to *meta*-carborane by a non-TFR (TFR = triangular face rotation) pathway, but **TS1** has not previously been reported. It is significant that **TS1** in this

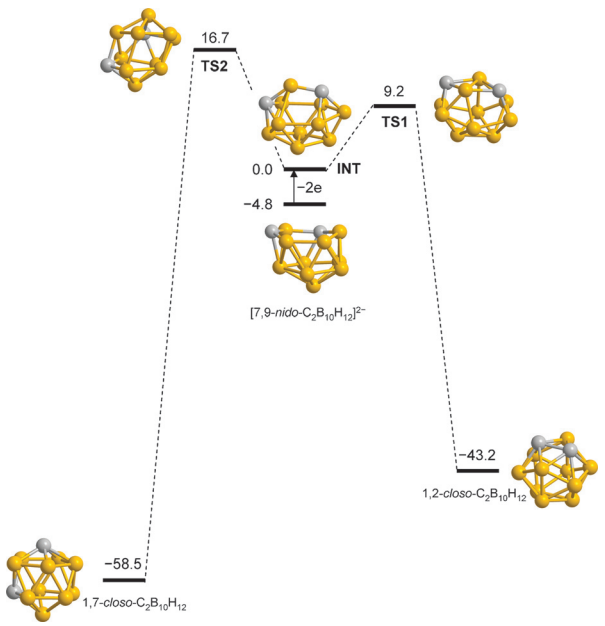

Fig. 2 Computational study of the 2e oxidation of [7,9-*nido*-$C_2B_{10}H_{12}]^2$. All energies in kcal mol^{-1}.

study is considerably more stable than *o-m*-TS1 in McKee's study, and thus that the profile from *ortho*- to *meta*-carborane in Fig. 2, with an overall activation energy of 59.9 kcal mol^{-1}, is computed to be more favourable than McKee's non-TFR pathway and comparable with his TFR route.

The deformation of the C1C2B3B6 diamond of *ortho*-carborane in the sterically crowded compounds **4** is reminiscent of that of the C1C2M3B6 unit in semi-pseudo-*closo*[14] and pseudo-*closo*[15] metallacarboranes which we and others first studied a decade or more ago, but this is the first time such a deformation has been described in carboranes. In pseudo-*closo* metallacarboranes there is a pronounced shift to high frequency of $\langle\delta(^{11}B)\rangle$, the weighted average ^{11}B chemical shift, compared to analogous undistorted species. A similar phenomenon is observed here. $\langle\delta(^{11}B)\rangle$ barely changes on metallation from **2a** to **3a** and **2b** to **3b**, lying between −11 and −12 ppm in all cases. However, as *meta* **3a** converts to *ortho* **4a** $\langle\delta(^{11}B)\rangle$ moves 4.3 ppm to high

frequency, and as *meta* **3b** converts to the even more distorted *ortho* **4b** the average shift is even greater, 6.5 ppm.

In conclusion, by utilising the fact that *meta*-carboranes can be converted to *ortho*-carboranes by successive reduction and reoxidation, we have prepared unprecedented, sterically-crowded, (2*n* + 2) skeletal electron *ortho*-carborane derivatives which relieve that crowding by severe structural deformation. We have previously proposed (derivatised) sterically crowded metallacarboranes as potential vehicles by which to study the mechanism(s) of isomerisation of carboranes experimentally, a possibility which relies on the ability of the crowded species to isomerise at relatively low temperatures. However, results so far[16] indicate only limited agreement between theoretical predictions (on carboranes) and experimental results (on metallacarboranes), possibly linked to the greater electronic complexity of metallacarboranes. It may be that our ability now to prepare severely crowded carboranes could revive interest in this area. In this context it is informative to note that *ortho*-carborane **4b** converts to *meta*-carborane **3b** in refluxing toluene.[17]

We thank the EPSRC for support.

Notes and references

‡ *Selected NMR spectroscopic data* ($CDCl_3$, 298 K): for **2a**: ^{1}H: Major (β) isomer; δ 6.42 (m, 1H, CH), 6.30 (m, 1H, CH), 6.23 (m, 1H, CH), 2.87 (m, 2H, CH_2), 1.31* (s, 6H, CH_3). Minor (α) isomer; δ 6.62, 1H, CH), 6.37 (m, 1H, CH), 6.05 (m, 1H, CH), 2.93 (m, 2H, CH_2), 1.31* (s, 6H, CH_3). Relative integrals given are internal and the ratio of α : β is 1 : 2. * = coincident resonance. $^{11}B\{^1H\}$: δ −6.4 (2B), −12.0 (6B), −14.2 (2B), $\langle\delta(^{11}B)\rangle$ −11.34.

For **2b**: ^{1}H: Major (β) isomer; δ 6.38 (m, 2H, CH), 6.03 (m, 1H, CH), 2.98 (br m, 2H, CH_2 [C_5H_5]), 2.08 (br d, 2H, CH_2 [Pm]), 1.45 (br m, 8H, CH_2 [Pm]). Minor (α) isomer; δ 6.47 (m, 1H, CH), 6.32 (m, 1H, CH), 6.18 (m, 1H, CH), 2.83 (br m, 2H, CH_2 [C_5H_5]), 1.90 (br d, 2H, CH_2 [Pm]), 1.03 (br m, 8H, CH_2 [Pm]). Relative integrals given are internal and the ratio of α : β is 2 : 9. $^{11}B\{^1H\}$: δ −6.6 (2B), −12.3 (6B), −14.7 (2B), $\langle\delta(^{11}B)\rangle$ −11.65.

For **3a**: ^{1}H: δ 4.15 (m, 4H, C_5H_4), 4.10 (s, 10H, Cp), 4.01 (m, 4H, C_5H_4), 1.38 (s, 12H, CH_3). $^{11}B\{^1H\}$: δ −6.7 (2B), −12.2 (6B), −14.1 (2B), $\langle\delta(^{11}B)\rangle$ −11.50.

For **3b**: ^{1}H: δ 4.15 (m, 4H, C_5H_4), 4.07 (s, 10H, Cp), 3.98 (m, 4H, C_5H_4), 2.17 (m, 4H, CH_2), 1.90 (m, 8H, CH_2), 1.59 (m, 6H, CH_2), 1.37 (m, 2H, CH_2). $^{11}B\{^1H\}$: δ −5.9 (2B), −12.4 (8B), $\langle\delta(^{11}B)\rangle$ −11.12.

For **4a**: ^{1}H: δ 4.24 (m, 4H, C_5H_4), 4.15 (m, 4H, C_5H_4), 4.12 (s, 10H, Cp), 1.87 (s, 12H, CH_3). $^{11}B\{^1H\}$: δ −2.6 (2B), −6.6 (4B), −7.9 (2B), −12.6 (2B), $\langle\delta(^{11}B)\rangle$ −7.25.

For **4b**: ^{1}H: δ 4.23 (m, 4H, C_5H_4), 4.19 (m, 4H, C_5H_4), 4.11 (s, 10H, Cp), 2.63 (m, 4H, CH_2), 2.33 (m, 4H, CH_2), 2.24 (m, 4H, CH_2), 1.73 (m, 6H, CH_2), 1.52 (m, 2H, CH_2). $^{11}B\{^1H\}$: δ −0.7 (4B), −3.7 (4B), −14.2 (2B), $\langle\delta(^{11}B)\rangle$ −4.61.

§ *Crystal data*: for **2a** (mixture of α,α; β,β and α,β isomers): $C_{18}H_{32}B_{10}$, *M* = 356.54, monoclinic, *P*2, *a* = 14.804(3), *b* = 10.428(3), *c* = 27.942(6) Å, β = 100.501(15)°, *V* = 4241.3(17) Å^3, *Z* = 8, D_c = 1.117 Mg m^{-3}, μ = 0.055 mm^{-1}, *F*(000) = 1520. θ_{max} = 24.69°. 7586/59 225 independent reflections (R_{int} = 0.1145), R_1 = 0.0621, wR_2 = 0.1403, *S* = 1.016 for data with $I > 2\sigma(I)$.

For **2b**: $C_{24}H_{40}B_{10}$ (β,β isomer), *M* = 436.66, monoclinic, *Cc*, *a* = 21.315(4), *b* = 8.1515(16), *c* = 15.649(3) Å, β = 112.03(3)°, *V* = 2520.6(9) Å^3, *Z* = 4, D_c = 1.151 Mg m^{-3}, μ = 0.058 mm^{-1}, *F*(000) = 936, θ_{max} = 26.12°. 2424/13998 reflections (R_{int} = 0.0399), R_1 = 0.0582, wR_2 = 0.1515, *S* = 1.152, $I > 2\sigma(I)$.

For **3a**: $C_{28}H_{40}B_{10}Fe_2$, *M* = 596.40, triclinic, *P* − 1, *a* = 10.187(2), *b* = 12.513(3), *c* = 13.387(2) Å, α = 96.618(8), β = 112.070(7), γ = 112.308(8)°, *V* = 1395.2(5) Å^3, *Z* = 2, D_c = 1.420 Mg m^{-3}, μ = 1.060 mm^{-1}, *F*(000) = 620, θ_{max} = 28.03°. 6521/25611 reflections (R_{int} = 0.0533), R_1 = 0.0411, wR_2 = 0.0893, *S* = 1.018, $I > 2\sigma(I)$.

For **3b**: $C_{34}H_{48}B_{10}Fe_2$, *M* = 676.52, triclinic, *P* − 1, *a* = 9.808(8), *b* = 12.947(10), *c* = 14.060(11) Å, α = 73.99(2), β = 78.525(15), γ = 70.027(18)°, *V* = 1601(2) Å^3, *Z* = 2, D_c = 1.403 Mg m^{-3}, μ = 0.933 mm^{-1}, *F*(000) = 708, θ_{max} = 28.11°. 7594/11459 reflections (R_{int} = 0.0356), R_1 = 0.0471, wR_2 = 0.0984, *S* = 1.008, $I > 2\sigma(I)$.

For **4a**: $C_{28}H_{40}B_{10}Fe_2$, *M* = 596.40, monoclinic, $P2_1/n$, *a* = 8.7366(14), *b* = 16.920(3), *c* = 19.641(3) Å, β = 100.783(7)°, *V* = 2852.1(8) Å^3, *Z* = 4, D_c = 1.389 Mg m^{-3}, μ = 1.037 mm^{-1}, *F*(000) = 1240, θ_{max} = 32.63°. 9673/71 682 reflections (R_{int} = 0.0462), R_1 = 0.0323, wR_2 = 0.0760, *S* = 1.034, $I > 2\sigma(I)$.

For **4b**: $C_{34}H_{48}B_{10}Fe_2$, *M* = 676.52, monoclinic, $P2_1/n$, *a* = 15.1029(17), *b* = 15.4587(19), *c* = 15.6930(18) Å, β = 118.556(6)°, *V* = 3218.2(7) Å^3, *Z* = 4, D_c = 1.396 Mg m^{-3}, μ = 0.928 mm^{-1}, *F*(000) = 1416, θ_{max} = 25.14°. 5648/47 044 reflections (R_{int} = 0.0885), R_1 = 0.0492, wR_2 = 0.1275, *S* = 1.053, $I > 2\sigma(I)$.

¶ E.s.d.'s of the mean of *N* independent observations given by the expression $\sigma^2 = (\sigma_1^2 + \sigma_2^2)$ if *N* = 2, or $\sigma^2 = \{\sum_{i=1}^{i=N}(\chi^i - \bar{\chi})^2\}/(N-1)$ where χ^i is the *i*th and $\bar{\chi}$ the mean value if $N > 2$.

‖ Calculations run with Gaussian 03 with the BP86 functional and 6-31G** basis sets. See ESI† for full details.†

1 T. L. Heying, J. W. Ager, Jr, S. L. Clark, D. J. Mangold, H. L. Goldstein, M. Hillman, R. J. Polak and J. W. Szymanski, *Inorg. Chem.*, 1963, **2**, 1089.

2 M. G. Davidson, T. G. Hibbert, J. A. K. Howard, A. Mackinnon and K. Wade, *Chem. Commun.*, 1996, 2285.

3 A. R. Turner, H. E. Robertson, K. B. Borisenko, D. W. H. Rankin and M. A. Fox, *Dalton Trans.*, 2005, 1310.

4 R. K. Bohn and M. D. Bohn, *Inorg. Chem.*, 1971, **10**, 350, and references therein.

5 *E.g.* Y.-J. Lee, S.-J. Kim, C.-H. Kang, J. Ko, S. O. Kang and P. J. Carroll, *Organometallics*, 1998, **17**, 1109.

6 (*a*) *E.g.* F. Teixidor, C. Viñas, J. Rius, C. Miravitlles and J. Casabó, *Inorg. Chem.*, 1990, **29**, 149; (*b*) D.-H. Kim, J. Ko, K. Park, S. Cho and S. O. Kang, *Organometallics*, 1999, **18**, 2738.

7 (*a*) D. A. Brown, W. Clegg, H. M. Colquhoun, J. A. Daniels, I. R. Stephenson and K. Wade, *J. Chem. Soc., Chem. Commun.*, 1987, 889; (*b*) T. D. Getman, C. B. Knobler and M. F. Hawthorne, *Inorg. Chem.*, 1992, **31**, 101; (*c*) K. Chui, H.-W. Li and Z. Xie, *Organometallics*, 2000, **19**, 5447; (*d*) L. A. Boyd, W. Clegg, R. C. B. Copley, M. G. Davidson, M. A. Fox, T. G. Hibbert, J. A. K. Howard, A. Mackinnon, R. J. Peace and K. Wade, *Dalton Trans.*, 2004, 2786.

8 K. Wade, *J. Chem. Soc. D*, 1971, 792.

9 M. A. Fox, C. Nervi, A. Crivello and P. J. Low, *Chem. Commun.*, 2007, 2372.

10 J. M. Oliva, N. L. Allan, P. v. R. Schleyer, C. Viñas and F. Teixidor, *J. Am. Chem. Soc.*, 2005, **127**, 13538.

11 E. Hong, Y. Kim and Y. Do, *Organometallics*, 1998, **17**, 2933.

12 (*a*) G. B. Dunks, R. J. Wiersema and M. F. Hawthorne, *J. Am. Chem. Soc.*, 1973, **95**, 3174; (*b*) L. I. Zakharkin, V. N. Kalinin and L. S. Podvisotskaya, *Bull. Acad. Sci. USSR, Div. Chem. Sci.*, 1966, 1444.

13 C. A. Brown and M. L. McKee, *J. Mol. Model.*, 2006, **12**, 653.

14 (*a*) *E.g.* Rh. Ll. Thomas and A. J. Welch, *J. Chem. Soc., Dalton Trans.*, 1997, 631; (*b*) F. Teixidor, C. Viñas, M. A. Flores, G. M. Rosair, A. J. Welch and A. S. Weller, *Inorg. Chem.*, 1998, **37**, 5394.

15 (*a*) *E.g.* Z. G. Lewis and A. J. Welch, *J. Organomet. Chem.*, 1992, **430**, C45; (*b*) P. T. Brain, M. Bühl, J. Cowie, Z. G. Lewis and A. J. Welch, *J. Chem. Soc., Dalton Trans.*, 1996, 231; (*c*) A. J. Welch and A. S. Weller, *Inorg. Chem.*, 1996, **35**, 4548; (*d*) A. J. Welch, Steric Effects in Metallacarboranes, , in *Metal Clusters in Chemistry*, ed. P. Braunstein, L. A. Oro and P. R. Raithby, Wiley-VCH, Weinheim Germany, 1999, p. 26; (*e*) F. Teixidor, M. A. Flores, C. Viñas, R. Sillanpää and R. Kivekäs, *J. Am. Chem. Soc.*, 2000, **122**, 1963; (*f*) A. V. Safronov, F. M. Dolgushin, P. V. Petrovskii and I. T. Chizhevsky, *Organometallics*, 2005, **24**, 2964; (*g*) L. S. Alekseev, F. M. Dolgushin, A. A. Korlyukov, I. A. Godovikov, E. V. Vorontsov and I. T. Chizhevsky, *Organometallics*, 2007, **26**, 3868.

16 (*a*) *E.g.* S. Robertson, D. Ellis, G. M. Rosair and A. J. Welch, *Appl. Organomet. Chem.*, 2003, **17**, 518; (*b*) S. Robertson, D. Ellis, G. M. Rosair and A. J. Welch, *J. Organomet. Chem.*, 2003, **680**, 286; (*c*) S. Robertson, R. M. Garrioch, D. Ellis, T. D. McGrath, B. E. Hodson, G. M. Rosair and A. J. Welch, *Inorg. Chim. Acta*, 2005, **358**, 1485.

17 B. W. Hutton and A. J. Welch, unpublished results.